AD NUMBER

AD891439

NEW LIMITATION CHANGE

TO

Approved for public release, distribution unlimited

FROM

Distribution authorized to U.S. Gov't. agencies only; Test and Evaluation; SEP 1971. Other requests shall be referred to Air Force Flight Dynamics Lab., AFSC, Wright-Patterson AFB OH 45433.

AUTHORITY

AFFDL ltr, 10 May 1976

AFFDL-TR-71-121
Volume II

SUPERSONIC INLET INVESTIGATION

Volume II. Air Induction System Dynamic Simulation Model

N.F. Amin
G.R. Hall

Northrop Corporation
Aircraft Division

TECHNICAL REPORT AFFDL-TR-71-121, Volume II
September 1971

AIR FORCE FLIGHT DYNAMICS LABORATORY
AIR FORCE SYSTEMS COMMAND
WRIGHT-PATTERSON AIR FORCE BASE, OHIO 45433

NOTICE

When Government drawings, specifications, or other data are used for any purpose other than in connection with a definitely related Government procurement operation, the United States Government thereby incurs no responsibility nor any obligation whatsoever, and the fact that the government may have formulated, furnished, or in any way supplied the said drawings, specifications, or other data, is not to be regarded by implication or otherwise as in any manner licensing the holder or any other person or corporation, or conveying any rights or permission to manufacture, use, or sell any patented invention that may in any way be related thereto.

Copies of this report should not be returned unless return is required by security considerations, contractual obligations, or notice on a specific document

AFFDL-TR-71-121
Volume II

SUPERSONIC INLET INVESTIGATION

Volume II. Air Induction System Dynamic Simulation Model

N.F. Amin
G.R. Hall

FOREWORD

This document was prepared by the Northrop Corporation, Aircraft Division, Hawthorne, California, under USAF Contract No. F33615-69-C-1699, "Supersonic Inlet Investigation," Project No. 1476, "Airframe Propulsion Compatibility for Advanced Tactical and Strategic Aircraft." The work under this contract was performed during the period 1 May 1969 to 1 May 1971.

The program was administered by the Air Force Flight Dynamics Laboratory, Internal Aerodynamics Branch, under the technical cognizance of Donald J. Stava, Project Monitor.

The contract effort conducted at Northrop Corporation, Aircraft Division, was under the direction of G.R. Hall, Program Manager, and T.W. Tsukahira, Principal Investigator. Major contributions to this program were made by Messrs. N.F. Amin, B.G. Franco, P.M. Parmar, W.F. Wong, and M. Yamada.

Special acknowledgement is given to F.K. Hube, L.M. Jenke of the Von Karman Gas Dynamics Facility; R.W. Butler of the Propulsion Wind Tunnel; and others on the staff of ARO, Inc. and AEDC, Tullahoma, Tennessee.

The final report prepared under the contract consists of three volumes. The title of each volume is shown below:

Volume I — Supersonic Inlet Investigation — Summary Report

Volume II — Supersonic Inlet Investigation — Air Induction System Dynamic Simulation Model

Volume III — Supersonic Inlet Investigation — Wind Tunnel Data Report

This technical report has been reviewed and is approved.

Philip P. Antonatos

PHILIP P. ANTONATOS
Chief, Flight Mechanics Division
Air Force Flight Dynamics Laboratory

ABSTRACT

A one-dimensional mathematical dynamic simulation model for predicting the transient behavior of air induction systems for advanced tactical aircraft operating in the supersonic portion of the flight spectrum is discussed. As a part of the simulation model, control system logic is included to provide control system design criteria necessary to maintain air induction system response to selected input disturbances within prescribed limits. The model is applicable to both external and mixed compression inlets operating at supersonic conditions. The "lumped parameter" concept is used in simulating the dynamic response of the subsonic duct downstream of the terminal shock, with the duct divided into three lumps. CDC 6600 digital computer programs have been generated for each of three sub-models (i.e., Standard, Buzz, and Hammershock models). Numerous sample simulation runs are presented and discussed in detail. Limited comparisons of simulation results to available test data show good agreement.

TABLE OF CONTENTS

TABLE OF CONTENTS (CONTINUED)

LIST OF ILLUSTRATIONS

LIST OF ILLUSTRATIONS (CONTINUED)

SYMBOLS AND ABBREVIATIONS

A	Duct or Effective flow area, (in^2)
A_{EX}	Effective flow area upstream of NS for subcritical mode ($X < X_c$) or duct area upstream of NS for critical/supercritical mode ($X \geq X_c$) during Buzz (Model 2), (in^2)
ΔA_{EX}	Separated boundary layer thickness during Buzz (Model 2), (in^2)
ΔA_{ET}	Throat area blockage during Buzz (Model 2), (in^2)
c	Speed of sound, (fps)
C, C'	Coefficients used in lumped volume temperature and pressure rate equations (see Appendix I for definition)
C_p	Constant pressure specific heat, $\left(\frac{ft\ lb}{lb\ ^oR}\right)$
E	Total energy of fluid, (ft. lb)
e	Internal energy per unit mass, $\left(\frac{ft\ lb}{lb}\right)$
F	Flow function, $\left(\frac{W\sqrt{T_T}}{AP_T}\right)$
g	Gravitational acceleration, $\left(32.2\ \frac{ft}{sec^2}\right)$
G	Control signal gain
H	Altitude, (ft)
h	Enthalpy, $\left(\frac{ft\ lb}{lb}\right)$
h_t	Perpendicular distance between cowl and final inlet ramp, (in)
I_1, I_2	Dynamic impedance constants used in the $\dot{W}_8$ and $\dot{W}_{14}$ calculation (see Appendix II)

SYMBOLS AND ABBREVIATIONS (CONTINUED)

J	Mechanical equivalent of heat, $\left(778 \frac{\text{ft lb}}{\text{BTU}}\right)$
K_{SP}	Spillage coefficient in Moeckel's Model for Shock Stand-off/ Spillage flow calculations (see Appendix III)
ℓ_1, ℓ_2	Lengths of two lumped volumes used in the $\dot{W}_8$ and $\dot{W}_{14}$ calculation (see Appendix II), (in)
L	Normal shock stand-off distance, (in)
M	Mach number of the flow, with respect to the duct
$\overline{M}$	Mach number of the flow, with respect to the normal shock
m	Air Mass, (lb)
N_F	Engine fan speed, (% rpm)
N_{FC}	Engine corrected fan speed, $\left(\frac{N_F}{\sqrt{\theta_2}}\right)$
P	Pressure, (psi)
$\dot{P}$	Pressure rate, (psi/sec)
R	Gas constant, $\left(53.35 \frac{\text{ft lb}}{\text{lb } ^\circ\text{R}}\right)$
S	Throat boundary layer slot length, (in)
T	Temperature, ($^\circ$R)
T_{TES}	Engine stall total temperature, ($^\circ$R)
$\dot{T}$	Temperature rate, ($^\circ$R/sec)
t	Time, (sec)
u	Flow velocity, (fps)
V, Vol	Lumped Volume, (in^3)
$\dot{W}$	Work, (ft lb)
W	Weight flow, (lbs/sec)
$\dot{W}$	Rate of change of weight flow, (lbs/sec^2)

SYMBOLS AND ABBREVIATIONS (CONTINUED)

W_{XSK}	Flow term associated with the motion of normal shock in the flow field. Negative when $\dot{X}$ is positive and vice versa.
X	Normal shock location, (in); Distance from inlet leading edge (in)
$\dot{X}$	Normal shock velocity, positive for downstream NS travel, negative for upstream NS travel
Z	Coefficient used in lumped volume temperature and pressure rate equations (see Appendix I for definition)
α	angle of attack
α_{R1}	2D inlet first ramp angle. Fixed at 10^{O}
α_{R2}	2D inlet second ramp angle
β	angle of sideslip
θ_2	$T_{T2}/518.69$
δ_2	$P_{T2}/14.696$
γ	Ratio of specific heats. Assumed equal to 1.4
ρ	Density, (lbs/ft^3)

Subscripts

B	Total bleed
BR	Ramp bleed
BY	Bypass properties
CAP	Maximum inlet capture properties
C	Engine corrected properties
c	Cowl station
ET	Effective conditions at the throat during Buzz (Model 2)
FWD	Forward flow properties
IC	Initial conditions
L	Flow properties behind the first inlet oblique shock

SYMBOLS AND ABBREVIATIONS (CONTINUED)

R	Flow properties behind the second inlet oblique shock
REF	Reference conditions
REV	Reverse flow properties
S	Static conditions
SCH	Scheduled value
SL	Downstream edge of throat bleed slot
SP	Subsonic Spillage
SU	Upstream edge of throat bleed slot
T	Total flow conditions or throat properties
XE	Conditions upstream of the NS for subcritical inlet operating mode ($X < X_c$)
XI	Conditions upstream of the NS for critical/supercritical inlet operating mode ($X \geq X_c$)
X	Conditions upstream of normal shock for all inlet operating modes
Y	Conditions downstream of normal shock for all inlet operating modes
0	Freestream conditions
STD	Standard ambient conditions
TBX	Throat bleed upstream of NS (NS within slot)
TBY	Throat bleed downstream of NS (NS within slot)
1	Properties within first half volume (used in calculating $\dot{W}_8$)
6	First lumped volume properties
8	First/second lumped volume interface
12	Second lumped volume properties
14	Second/third lumped volume interface
18	Third lumped volume properties

SYMBOLS AND ABBREVIATIONS (CONTINUED)

2	Diffuser exit properties; properties within second half volume (used in calculating $\dot{W}_{14}$)
2E	Engine properties at compressor entrance

Abbreviations

BL	Boundary Layer
2DE	2D External Compression
2DM	2D Mixed Compression
HS	Hammershock
M.S.	Model Scale
NS	Normal Shock
NAR	North American Rockwell Corporation
GE	General Electric Company

SECTION 1

INTRODUCTION

The basic requirement for any air induction system is to provide the engine with air at high pressure recovery and low pressure distortion at all flight conditions. The increased mission requirements for future highly maneuverable advanced supersonic tactical aircraft have made the task of designing air induction systems for these aircraft extremely complex. In addition to the steady state requirements for high efficiency at subsonic and supersonic cruise Mach numbers, the air induction systems for these aircraft must be designed to provide stable operation of the propulsion system during transient conditions resulting from rapid changes in engine thrust, flight altitude, and aircraft attitude during transonic and supersonic maneuvering. Thus, prediction of the transient response of air induction systems to externally or internally generated disturbances whose combined rates and amplitudes lead to non-equilibrium flow phenomena is highly desirable during preliminary design in order to provide early assessment of potential problems affecting propulsion system stability.

Reported herein is a one-dimensional mathematical dynamic simulation model for predicting the transient behavior of air induction systems for advanced tactical aircraft operating in the supersonic portion of the flight spectrum. As a part of the simulation model, control system logic is included to provide control system design criteria necessary to maintain air induction system response to selected input disturbances within prescribed limits. The model is applicable to both external and mixed compression inlets operating at supersonic conditions. The "lumped parameter" concept is used in simulating the dynamic response of the subsonic duct downstream of the terminal shock, with the duct divided into three lumps. The total dynamic simulation model consists of three sub-models designated as follows:

Model 1 – Standard Model

Model 2 – Buzz Model

Model 3 – Hammershock Model

The decks for these models were initially developed on Northrop's IBM 360 computer using IBM "Continuous Systems Modeling Program" (CSMP) language and have subsequently been converted to a similar language from CDC called "Continuous Systems Simulation Language (CSSL 3)" for use on the Air Force CDC 6600 system. A user's manual is available (Reference 1) for the CDC 6600 (CSSL 3) version of the dynamic simulation program. It describes the decks in detail and discusses the procedure for operating them.

The results presented herein begin with a brief review of input transients likely to be encountered by advanced tactical aircraft. Following this is a detailed description of the theoretical approach used in developing the simulation models, with separate derivations of key equations given in the appendices. Next, numerous sample simulation runs are presented and discussed in detail. Finally, hammershock simulation results are compared with available test data.

SECTION II

AIR INDUCTION SYSTEM TRANSIENTS

Transient disturbances contributing to propulsion system instability have been well documented by various sources (e.g., References 2 and 3). These disturbances may be generally categorized as follows:

1. External Disturbances – Transient disturbances originating external to the propulsion system such as wind gusts, clear air turbulence, passing aircraft wakes, aircraft maneuvering, hot gas ingestion due to missile and gun firing, etc.

2. Internal Disturbances – Transient disturbances that originate within the propulsion system such as sudden changes in engine airflow demand caused by throttle burst or chop, afterburner light-off or blowout, engine stall, etc.

The range in rates and amplitudes of input disturbances likely to be encountered by advanced tactical aircraft is wide. Of interest with respect to air induction dynamic simulation are those transients whose combined rates and amplitudes are sufficiently high to cause significant deviation in the instantaneous thermodynamic properties within the air induction system from the quasi-steady state properties associated with slower transients. For example, a typical engine throttle burst occurring over a period of a few seconds, while seemingly being a "transient" situation, is in fact essentially a quasi-steady state process with respect to the response of the air induction system. That is, at each instant in time during such a transient, the airflow within the induction system is in equilibrium with respect to the instantaneous engine demand.

On the other hand, more rapid input disturbances (some examples of which are shown in Figure 1) can cause significant deviations in the thermodynamic properties within the air induction system from steady state conditions. The magnitude of deviation from steady state is also a function of the length/volume characteristics of the air induction system. For these cases, non-equilibrium effects occur due to the

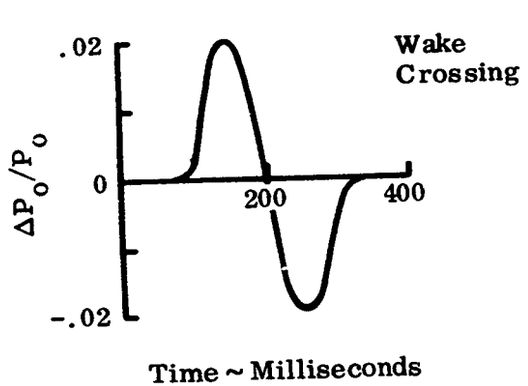

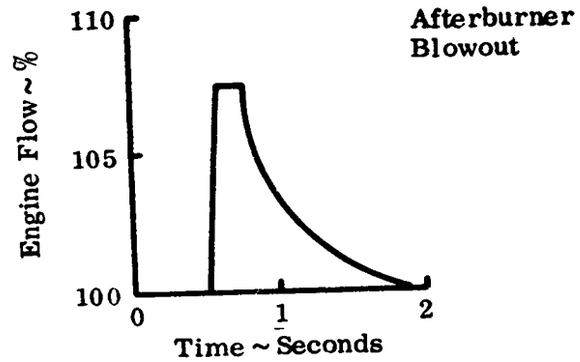

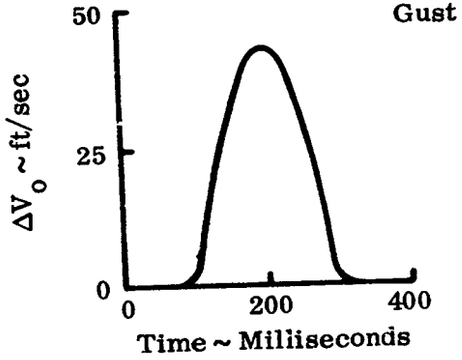

a. External Transients

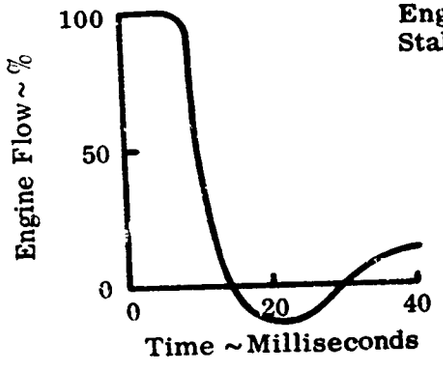

b. Internal Transients

Figure 1. Typical Air Induction System Input Transients

inertial and capacitance characteristics of air within the induction system. The result is an instantaneous imbalance of airflows and pressures within the duct over the duration of the input disturbance. This can lead to propulsion system instability due to exposure of the engine compressor face to rapid rates of pressure rise and decay and/or adverse instantaneous pressure distortion and turbulence patterns. It can also lead to excessive pressure levels within the duct (e.g., rapid cut-off of engine airflow can result in instantaneous duct pressure levels in excess of freestream stagnation pressure).

SECTION III

SIMULATION MODELS – THEORETICAL APPROACH

Dynamic mathematical models are currently available which simulate air induction system response to given input transients using various calculation approaches in modeling the portion of the subsonic duct downstream of the normal shock (NS). Reference 4 uses a Helmholtz resonator spring-mass concept when calculating conditions within the subsonic duct. Reference 5 uses the artificial viscosity technique in calculating the effect of large amplitude transients (i.e., compressor surge). Wasserbauer and Willoh (Reference 6) use a linearized small perturbation method to predict inlet response, while Marvin (Reference 2) uses the 'lumped parameter' concept in simulating air induction system response to various typical transients.

After a thorough technical review of the various available models and an assessment of their suitability for achieving the objectives of Contract F33615-69-C-1699, "Supersonic Inlet Investigation," the 'lumped parameter' concept developed in Reference 2 was selected, based on the merits of its thermodynamic formulation, and also because the range of models developed and the types of air induction systems simulated were the most suitable for achieving the contract objectives. This concept (which is explained in detail in this section) divides the subsonic duct into a number of lumped volumes. Models that treat the whole subsonic duct as a single lumped volume may be sufficiently accurate for fairly short air induction systems (podded or wing mounted turbofan installations), but their accuracy deteriorates for inlets which are long with respect to their equivalent flow diameters (fuselage integrated air induction systems typical of advanced tactical aircraft). For relatively long air induction systems, it becomes necessary to divide the subsonic duct into more than one lumped volume. Although simulation accuracy increases with increasing number of volume lumps used, practical considerations (computer storage and run time) limit the number to three or four. All the models reported herein divide the subsonic duct volume into three initially equal volumes.

This section outlines the theory and equations for three models, all based on the 'lumped parameter' concept for the subsonic duct downstream of the NS. Each model treats both mixed and external compression air induction systems at supersonic speeds. The three models are:

Model 1 – Three Lump Standard Model

Model 2 – Three Lump Buzz Model

Model 3 – Three Lump Hammershock Model

The 2D mixed compression (2DM) air induction system is used to illustrate Model 1, while the 2D external compression (2DE) air induction system is used to illustrate Models 2 and 3. Since only one air induction system is used to illustrate each model in detail, any key differences in the basic model after it has been adapted to the other air induction system are also described. Each theoretical model is divided into three segments – Input Data, Initial Conditions, and Dynamic Calculations. The Input Data segment supplies the others with all the information regarding inlet steady state operating conditions, inlet geometry and the engine inputs to the air induction system. The Initial Conditions segment calculates the steady state air induction system performance in order to supply the Dynamic segment with initial values of key simulation parameters which are required before the dynamic calculations can be initiated. The complete dynamic problem, including the response of the relevant control parameters to any input transient, is solved in the Dynamic segment. Block diagrams containing the structural statements required for each model are included. A detailed discussion of the lumped parameter concept and the theoretical approach used in formulating each model follows.

'LUMPED PARAMETER' CONCEPT

The application of this concept to the thermodynamic system can be explained with the help of an analogous electrical network with lumped parameters. The thermodynamic system and the corresponding electrical analogy are shown in Figure 2. Inertia (dynamic) and friction (steady state) forces, which are analogous to inductance and resistance in the electrical system, are 'lumped' and inserted between 'lumped volumes' with stored mass and energy, the latter being analogous to capacitance in the electrical circuit.

Thermodynamic System

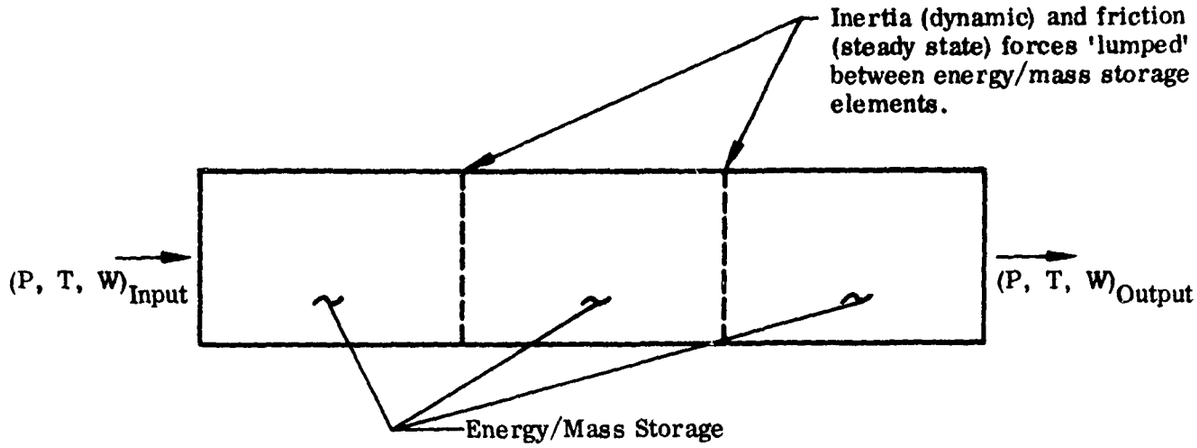

Electrical Analogy

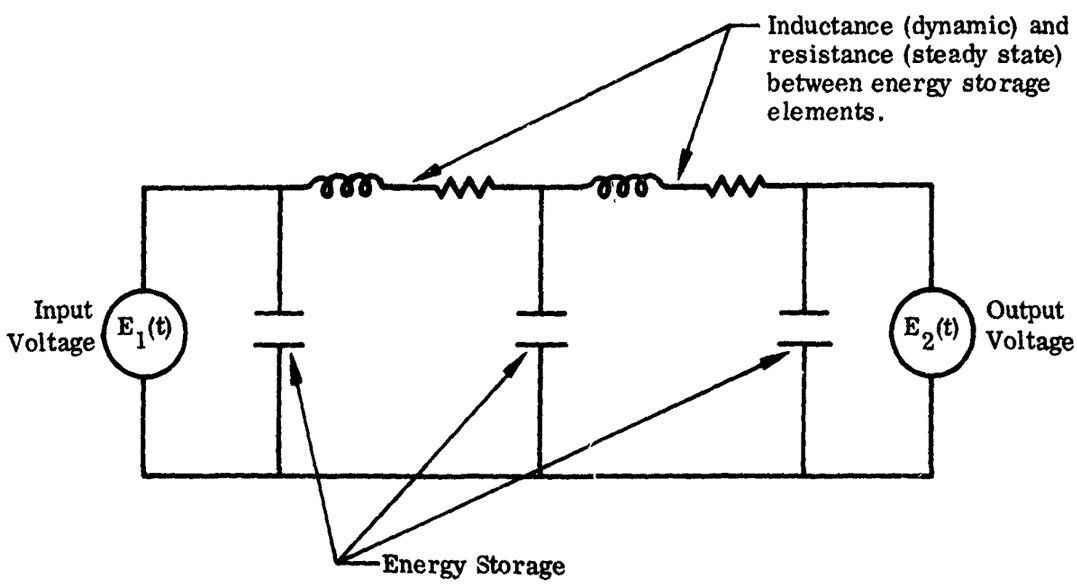

Figure 2. Electrical Analogy for 'Lumped Parameter' Thermodynamic System

The thermodynamic lumped parameter concept, as applied to supersonic air induction systems, is shown in Figure 3, using the 2DM inlet. The subsonic duct is first divided into three initially equal volumes, Vol_6, Vol_{12}, and Vol_{18}. The total pressures and temperatures within each of these volumes, during the simulation, are calculated using the equation of state in conjunction with the unsteady continuity and energy equations. Detailed derivation of the total pressure and temperature rate equations is presented in Appendix I. The volume of the first lump (Vol_6) changes with the movement of its upstream boundary (represented by the NS) under the influence of a transient. Boundaries of the remaining two volumes (Vol_{12} and Vol_{18}) are fixed. The model is limited to cases where the NS does not cross the fixed boundaries, since this situation could only arise when the bypass control malfunctions during an extremely severe transient, a rather unlikely occurrence for the cases of interest.

To calculate rate of change of flow rate ($\dot{W}_8$ and $\dot{W}_{14}$) at each of the two fixed boundaries, the subsonic duct is divided into two halves, each half containing a fixed boundary (Stations 8 and 14). The rate of change of flow rates at these boundaries are then determined by calculating the rate of change of momentum of each volume half due to the instantaneous net imbalanced force acting on it during the simulation. For this calculation both the volumes are frozen at their NS-at-throat value during the transient. The single fixed boundary for this calculation is located at the volumetric center of Vol_{12}. This derivation is presented in Appendix II.

MODEL 1 – THREE LUMP STANDARD MODEL

This model, as applied to the 2DM air induction system (Figure 3), is limited to simulating its response in the started mode. Bypass and throat area controls are provided to maintain the inlet in the started mode and, therefore, for transients severe enough to cause an unstart [excluding buzz (simulated by Model 2) and engine stall (simulated by Model 3)], the control system response may have to be modified to avoid the unstart.

This model, when adapted to the 2DE air induction system, includes an upstream supersonic model for simulating NS external movement on the ramp upstream of the cowl. A description of this upstream supersonic model for the 2DE inlet follows the

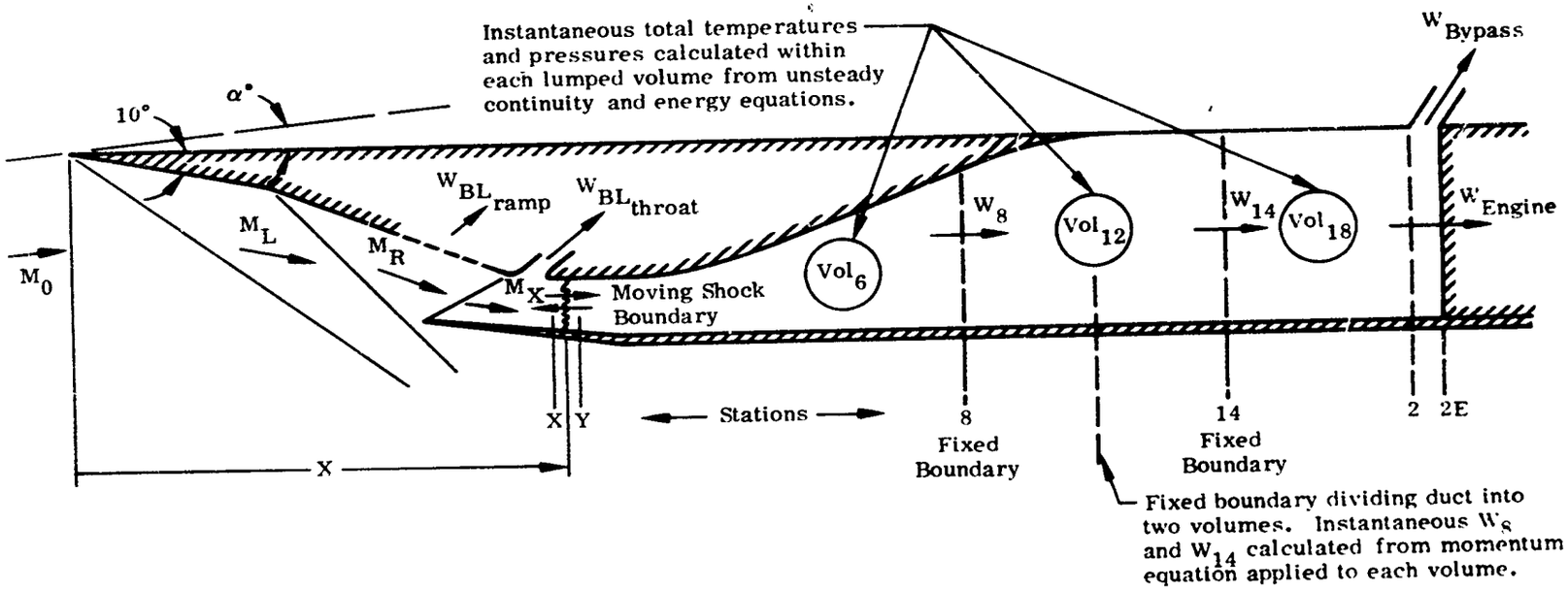

Figure 3. 2DM Air Induction System Schematic Illustrating Lumped Parameter Concept

detailed discussion of the theoretical approach in formulating the 2DM air induction system. Model 1 is capable of calculating system dynamic response to both external and internal transients. However, in discussing the theoretical approach, an internal transient (rapid changes in engine flow demand) has been used as an example.

Dynamic Calculations

The block diagram for the dynamic calculations is presented on Sheets 1 to 4, Figure 4. In the program, the NS motion ($\dot{X}$) during a transient (external or internal), with respect to the duct, is calculated using the equation

$$\dot{x} = C_x \left(M_x - \bar{M}_x \right) \tag{1}$$

where

$$C_x = \sqrt{\gamma g R T_{Sx}}$$

M_X = the Mach number of the flow, with respect to the duct, upstream of the NS

and $\bar{M}_X$ = the Mach number of the flow, with respect to the NS, upstream of the NS

$$= \sqrt{\frac{\gamma+1}{\gamma}\left(\frac{P_{SY}}{P_{SX}}\right) + \frac{\gamma-1}{2\gamma}} \tag{2}$$

$\dot{X}$ may be positive or negative, depending on whether the NS is travelling in the downstream or upstream direction, respectively. The NS is assumed to be without inertia or thickness. Instantaneous static pressures P_{SX} and P_{SY} across the NS [Equation (2)] are calculated independently from the upstream and downstream flow properties as follows:

Properties Upstream of the NS. The instantaneous value of P_{SX} is obtained by first calculating the flow function F_X upstream of the NS.

$$F_x = \frac{W_x \sqrt{T_{Tx}}}{A_x P_{Tx}} \tag{3}$$

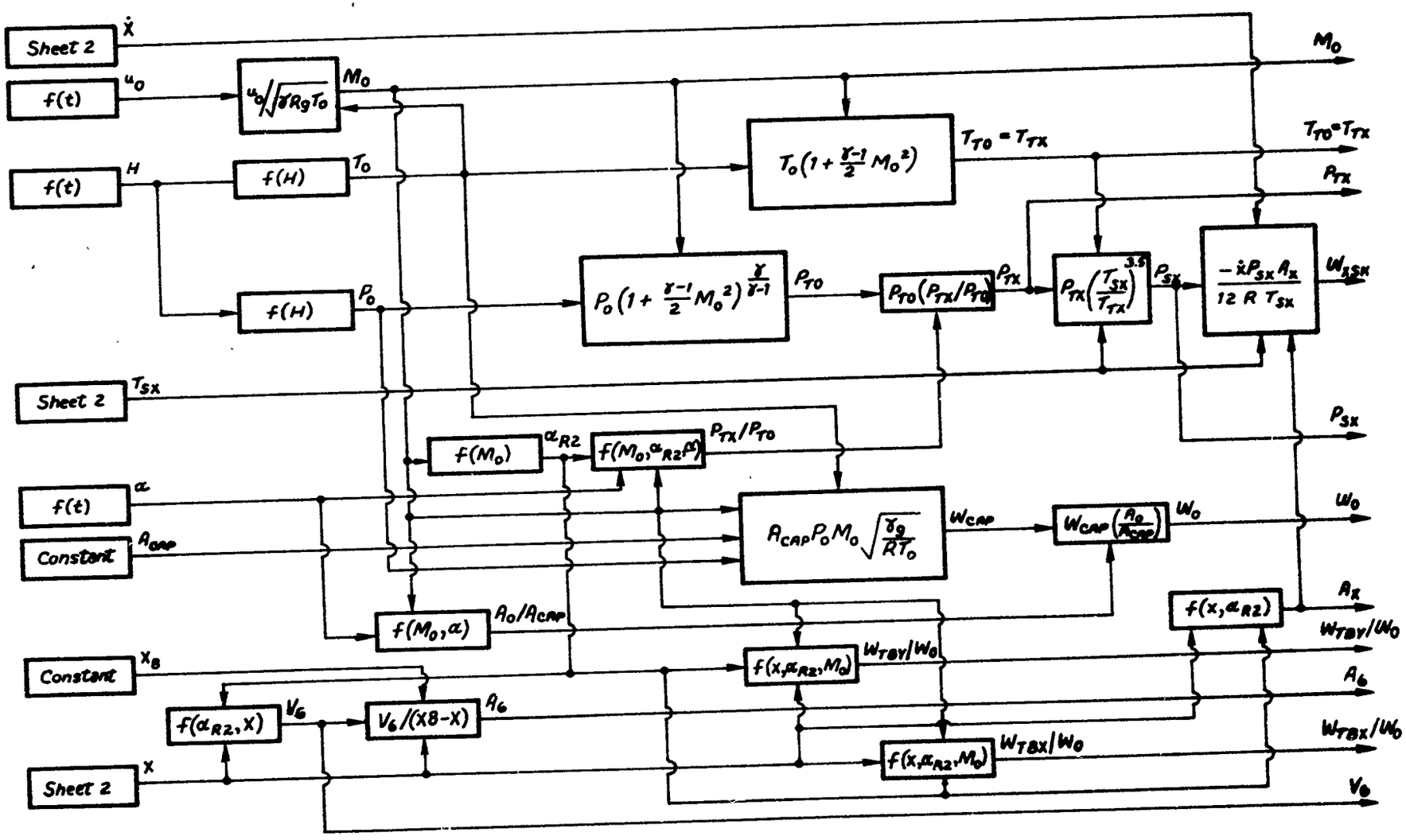

Figure 4. Model 1 - 2DM Three Lump Standard Model Block Diagram - Dynamic Section: Sheet 1 of 4

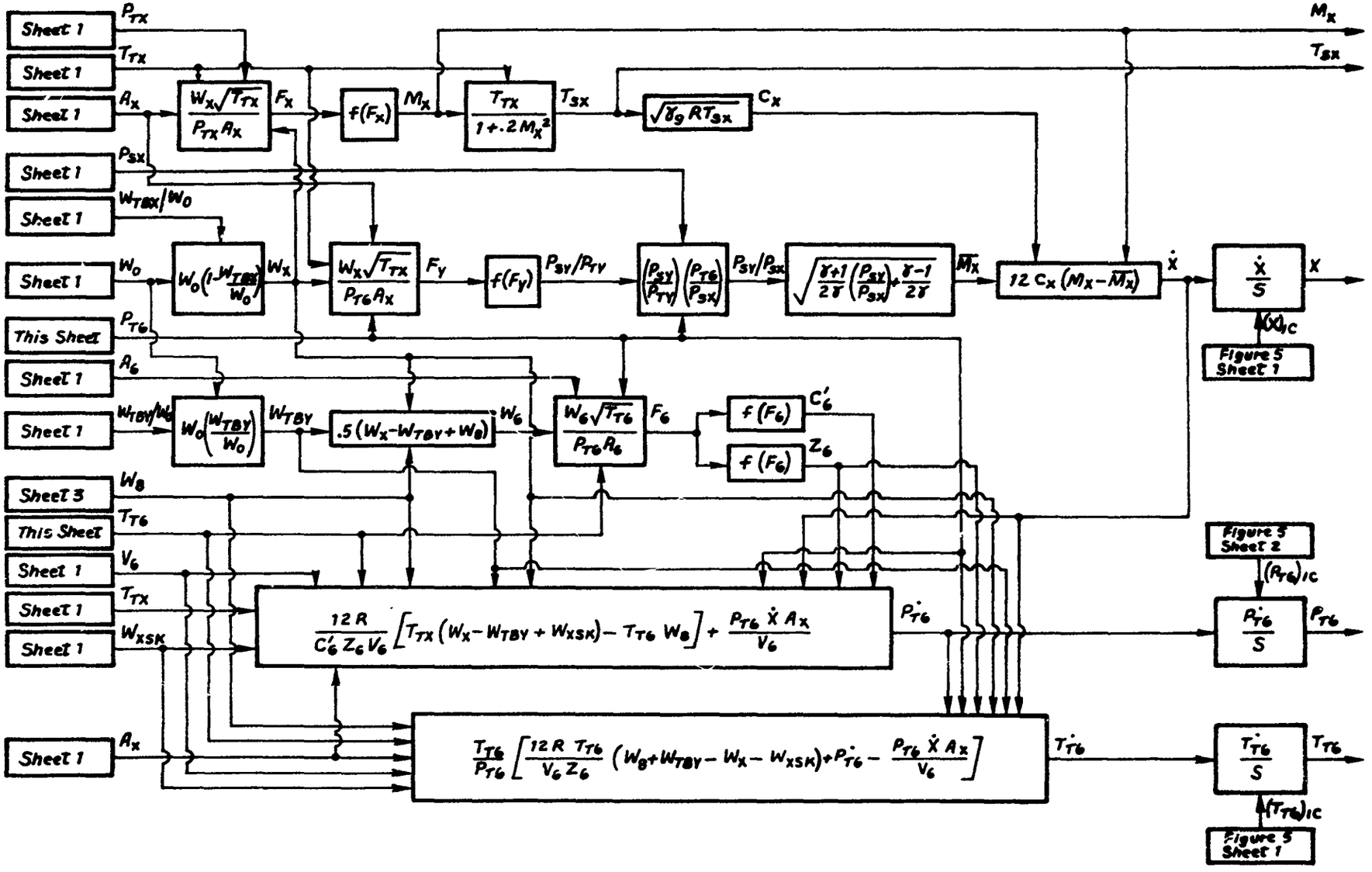

Figure 4 Continued: Sheet 2 of 4

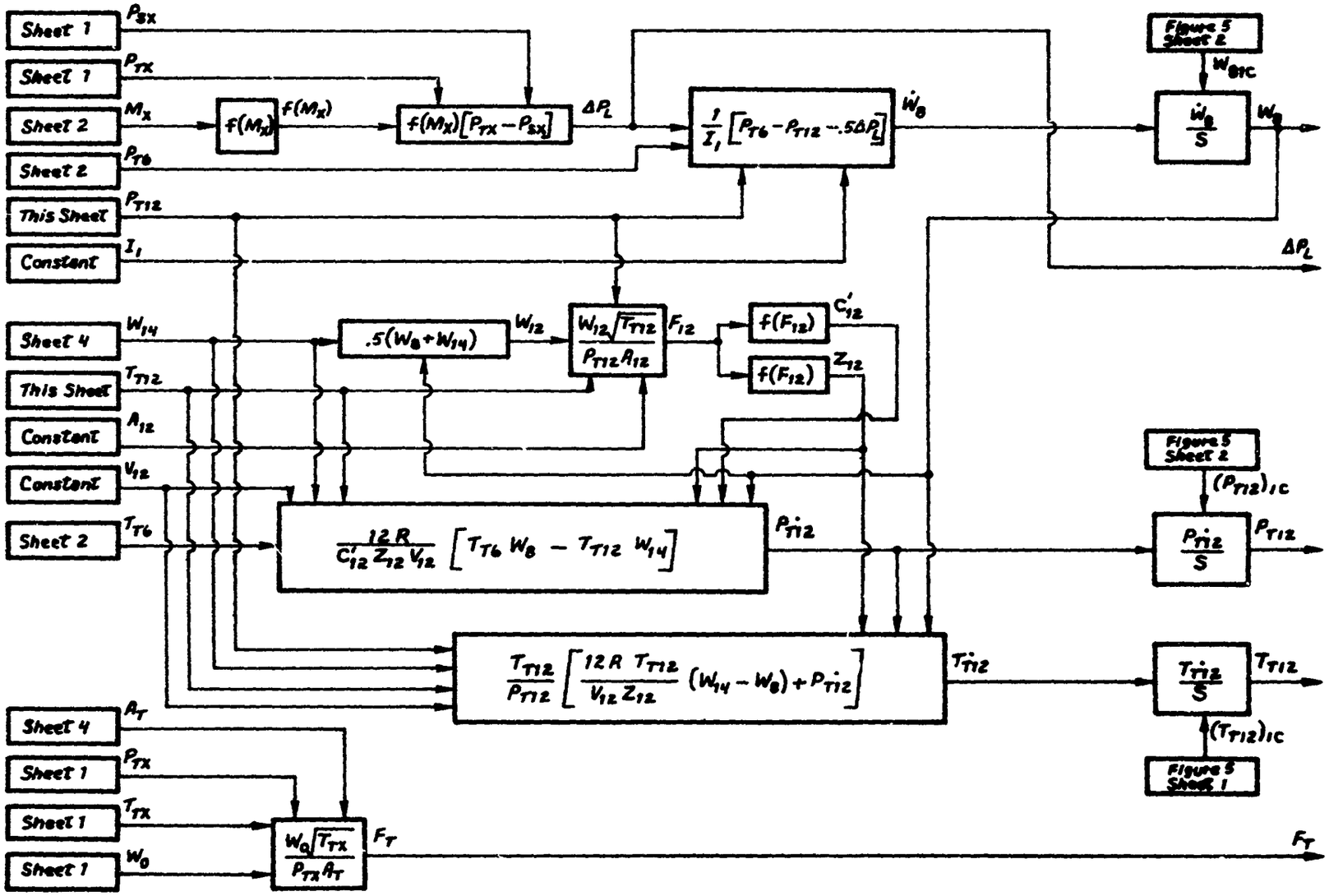

Figure 4 Continued: Sheet 3 of 4

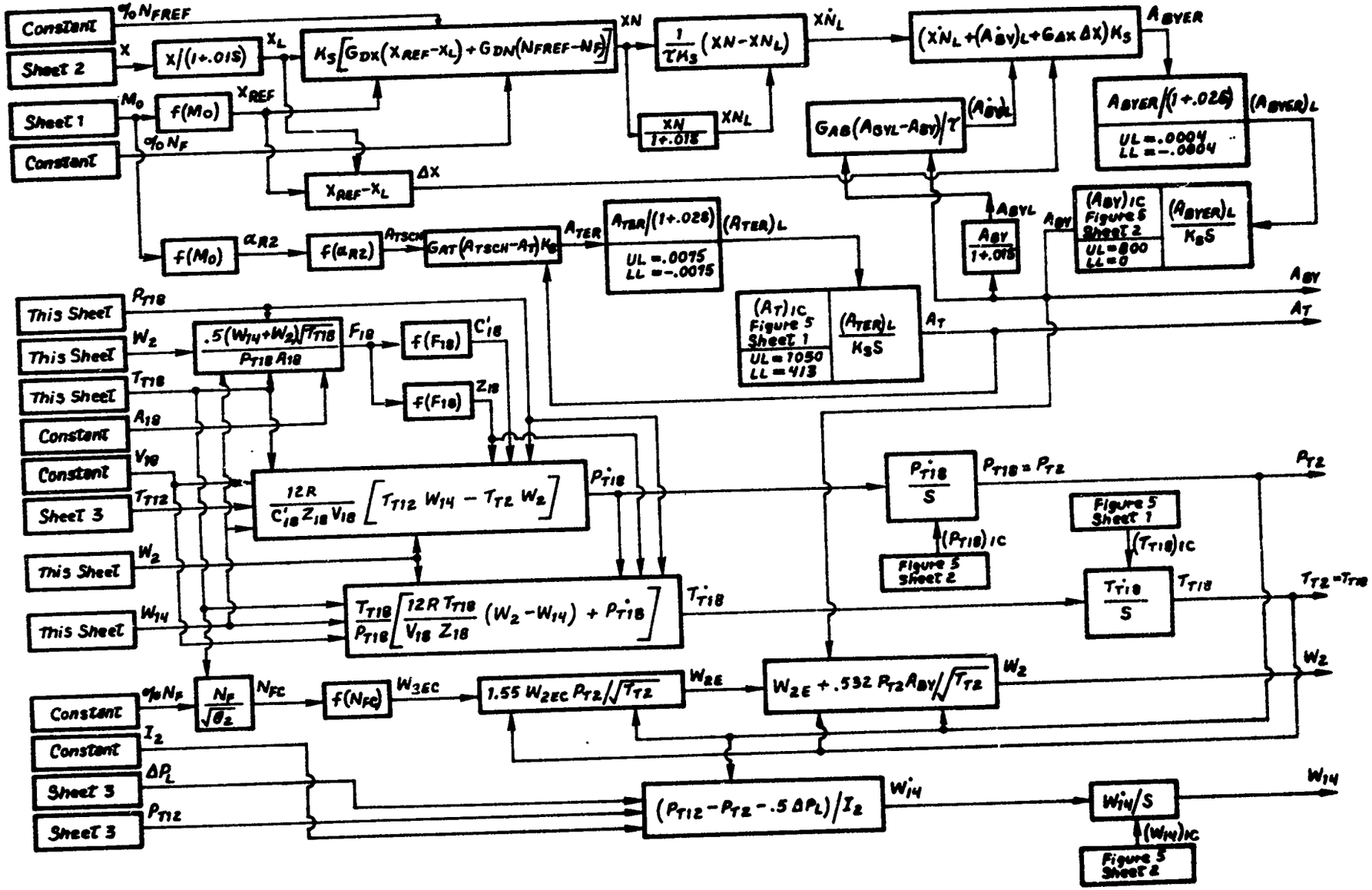

Figure 4 Concluded: Sheet 4 of 4

where A_X is the local duct area upstream of the NS.

M_X is then obtained using this value of flow function and the input curve,

$$M_x = f(F_x) \tag{4}$$

Knowing M_X, T_{SX} and P_{SX} can then be calculated as follows,

$$T_{sx} = T_{Tx} \Big/ \left(1 + \frac{\gamma-1}{2} M_x^2\right) \tag{5}$$

$$P_{Sx} = P_{Tx} \left(\frac{T_{sx}}{T_{Tx}}\right)^{\frac{\gamma}{\gamma-1}} \tag{6}$$

Properties Downstream of the NS. The response of the subsonic duct volume (and hence, the instantaneous value of P_{SY}) to rapid changes in flow (W_2) at the compressor face is calculated by first computing the rate of change of total pressure and temperature within each of the three volume lumps, Vol_{18}, Vol_{12}, and Vol_6, starting from the compressor face. Thus, within Vol_{18}, the total pressure and temperature rate equations (see Appendix I for derivation) can be written as

$$\dot{P}_{T2} = \dot{P}_{T1B} = \frac{12\,R}{C'_{1B}\,Z_{1B}\,V_{1B}} \left(T_{T12}\,W_{14} - T_{T2}\,W_2\right) \tag{7}$$

$$\dot{T}_{T2} = \dot{T}_{T1B} = \frac{T_{T1B}}{P_{T1B}} \left[\frac{12\,R\,T_{T1B}}{V_{1B}\,Z_{1B}} \left(W_2 - W_{14}\right) + \dot{P}_{T1B}\right] \tag{8}$$

Inflow at each of the two fixed boundaries is computed by integrating the rate of change of flow ($\dot{W}_8$ and $\dot{W}_{14}$). Thus, at the fixed boundary station 14, the inflow W_{14} into Vol_{18} changes at the rate

$$\dot{W}_{14} = \frac{1}{I_2}\left(P_{T12} - P_{T2} - 0.5\,\Delta P_L\right) \tag{9}$$

where I_2 is the dynamic impedance constant (derived in Appendix II)

and
$$\begin{aligned}\Delta P_L &= K_M\left(P_{TX} - P_{SX}\right)\\ &= 0.026\left(P_{TX} - P_{SX}\right)\end{aligned} \tag{10}$$

K_M is an empirical subsonic diffuser pressure loss factor which is a function of M_X. The value of .026 selected for this factor by Reference 2 in their simulation models is also used here.

Similarly, within Vol_{12}, $\dot{P}_{T12}$ and $\dot{T}_{T12}$ are obtained from equations

$$\dot{P}_{T12} = \frac{12\,R}{c'_{12}\,z_{12}\,V_{12}}\left(T_{T6}\,W_8 - T_{T12}\,W_{14}\right) \tag{11}$$

$$\dot{T}_{T12} = \frac{T_{T12}}{P_{T12}}\left[\frac{12\,R\,T_{T12}}{V_{12}\,z_{12}}\left(W_{14} - W_8\right) + \dot{P}_{T12}\right] \tag{12}$$

where, at the fixed boundary station 8, the inflow W_8 into Vol_{12} changes at the rate

$$\dot{W}_8 = \frac{1}{I_1}\left(P_{T6} - P_{T12} - 0.5\,\Delta P_L\right) \tag{13}$$

The total pressure and temperature rate equations for Vol_6 include the effect of the moving upstream boundary, represented by the NS, so that

$$\dot{P}_{T6} = \frac{12\,R}{c'_6\,z_6\,V_6}\left[T_{TX}\left(W_X - W_{TBY} + W_{XSK}\right) - T_{T6}\,W_8\right] + \frac{P_{T6}\,A_X\,\dot{X}}{V_6} \tag{14}$$

$$\dot{T}_{T6} = \frac{T_{T6}}{P_{T6}}\left[\frac{12\,R\,T_{T6}}{V_6\,z_6}\left(W_8 + W_{TBY} - W_X - W_{XSK}\right) + \dot{P}_{T6} - \frac{P_{T6}\,A_X\,\dot{X}}{V_6}\right] \tag{15}$$

Inflow into Vol_6, where the upstream boundary represented by the NS is moving, can be visualized to consist of two parts:

(a) Inflow W_X with respect to the duct

(b) Inflow swept by the upstream boundary area A_X, moving at velocity $\dot{X}$ relative to the duct, through air at density ρ_{SX}, which is equal to $\rho_{SX}\,A_X\,\dot{X}$.

Thus, inflow with respect to the normal shock

$$= W_X - \rho_{SX} A_X \dot{X}$$

$$= W_X + W_{XSK}$$

where, by definition,

$$W_{XSK} \equiv -\rho_{SX} A_X \dot{X} = -\frac{P_{SX} A_X \dot{X}}{R\ T_{SX}} \tag{16}$$

and is negative for positive $\dot{X}$ (downstream NS movement) and vice-versa.

The total-to-static pressure and temperature ratio terms C' and Z (defined in Appendix I) are obtained by entering the input data tables C'_6 and Z_6, repeatedly with the following flow functions based on the instantaneous mean flow rates within each volume lump.

$$F_6 = \frac{0.5\,(W_X - W_{TBY} + W_8)\sqrt{T_{T6}}}{A_6\ P_{T6}} \tag{17}$$

$$F_{12} = \frac{0.5\,(W_8 + W_{14})\sqrt{T_{T12}}}{A_{12}\ P_{T12}} \tag{18}$$

$$F_{18} = \frac{0.5\,(W_{14} + W_2)\sqrt{T_{T18}}}{A_{18}\ P_{T18}} \tag{19}$$

Using P_{T6} (obtained by integrating Equation 14), P_{SY} is next calculated as follows. The flow function F_Y may be written as

$$F_Y = \frac{W_X \sqrt{T_{TX}}}{A_X\ P_{T6}} \tag{20}$$

P_{SY}/P_{TY} is next obtained using this value of flow function and the input curve

$$\frac{P_{SY}}{P_{TY}} = f(F_Y) \tag{21}$$

From this ratio, P_{SY} is given by

$$P_{SY} = \left(\frac{P_{SY}}{P_{TY}}\right) P_{T6} \tag{22}$$

The instantaneous values of P_{SX} and P_{SY} (obtained from Equations 6 and 22, respectively) are then used in Equation (2) to obtain $\bar{M}_X$ for calculating the normal shock (NS) velocity $\dot{X}$ [Equation (1)].

Air Induction System Controls: Control logic is provided in this model to prevent two types of unstarts associated with mixed compression inlets: Choked throat unstart and the unstart caused by disgorgement of the NS resulting from reduction in engine demand. Choked throat unstart occurs when the throat cannot pass the flow being supplied by the inlet, resulting in an unstable normal shock appearing just upstream of the throat (in addition to the NS located downstream) which is immediately disgorged to allow subsonic spillage of the excess air. Choked throat unstart can be caused by (a) increase in the throat flow function towards the choked value due to reduction in M_0, (b) reduction in throat area, and (c) increase in the flow being supplied to the inlet due to increase in angle of attack. Thus, during this type of an unstart, two normal shocks can instantaneously exist in the induction system, although the choked throat unstart will probably also cause the supercritical NS (i.e., the terminal shock) to move rapidly upstream, overtake, and ultimately coalesce with the unstable normal shock originating at the throat before the latter reaches the cowl lip. In the program, a variable area bypass is used to control the terminal shock motion and the inlet throat area is programmed to open if the throat tends to choke. The control logic flow is presented in Figure 4, Sheet 4.

Bypass Area Control: The basic bypass area control error function consists of the following four error signals:

$$G_{\Delta X}\,\Delta X + G_{DX}\,\dot{\Delta X} + G_{DN}\,\dot{\Delta N}_F + G_{AB}\,\dot{A}_{BY} \tag{23}$$

where, $G_{\Delta X}\,\Delta X$ is the proportional signal on shock position deviation $\Delta X = (X_{REF} - X)$

$G_{DX}\,\dot{\Delta X}$ is the derivative signal on shock position deviation, ΔX

and $G_{DN}\,\Delta\dot{N}_F$ is the derivative signal on engine fan speed deviation $\Delta N_F = (N_{FREF} - N_F)$. Since the engine fan speed directly effects the engine flow demand, this is essentially an engine flow (W_{2E}) derivative signal.

$G_{AB}\,\dot{A}_{BY}$ is the derivative signal on bypass area, A_{BY}, and

$G_{\Delta X}$, G_{DX}, G_{DN} and G_{AB} are the gains associated with the signals defined above.

Also,

$\Delta\dot{X}$ is the derivative lag on shock position deviation, ΔX,

$\Delta\dot{N}_F$ is the derivative lag on engine fan speed deviation, ΔN_F, and

$\dot{A}_{BY}$ is the derivative lag on bypass area, A_{BY}.

Each of the above four error signals provide an overall bypass area error signal which is a function not only of the position error ($X_{REF} - X$), but also of the rate at which the deviation of X and N_F occurs from their respective reference values, and the rate at which A_{BY} opens or closes.

A derivative lag is a derivative of the lagged input and is obtained by subtracting the lagged input from the input and dividing the result by the time constant τ. Thus, using Laplace transforms

$$\frac{1}{\tau}\left(Z - \frac{Z}{1+\tau S}\right) = \frac{Z S}{1+\tau S} \qquad (24)$$

The expression on the RHS in the above equation is the derivative of the lagged input $\frac{Z}{1+\tau S}$ as defined by the theorem on Laplace transforms of derivatives (Reference 7).

Each of the derivative signals in the error function (23) is calculated in the model as follows, assuming a practical value, in terms of controls hardware response, of .01 for the time constant.

The derivative signal on shock position deviation (ΔX) is

$$G_{DX}\,\Delta\dot{X} = G_{DX}\left(\Delta X - \frac{\Delta X}{1+.01S}\right)\frac{1}{.01} \qquad (25)$$

Note that ΔX is negative for downstream movement of the normal shock. This essentially means that the signal will tend to increase the negative portion of the total error in the bypass logic if the rate of deviation increases as the NS moves downstream, thus tending to close the bypass at a faster rate to reduce the deivation.

Similarly, the derivative signal on engine fan speed deviation (ΔN_F) is

$$G_{DN}\ \dot{\Delta N}_F = G_{DN}\left(\Delta N_F - \frac{\Delta N_F}{1 + .01S}\right)\frac{1}{.01}. \tag{26}$$

If the fan speed increases beyond N_{FREF}, the engine instantaneously demands more flow and the NS again tends to move downstream. With ΔN_F negative, an error signal similar to ΔX is input to drive the NS back towards the throat.

The A_{BY} derivative signal is

$$G_{AB}\ \dot{A_{BY}} = G_{AB}\left(\frac{A_{BY}}{1 + .01S} - A_{BY}\right)\frac{1}{.01}. \tag{27}$$

This is a damping input on the closing/opening rate of A_{BY} itself to avoid large overshoots. The derivative input [i.e., the expression in brackets in equation (27)] is deliberately reversed to allow for a positive error when A_{BY} closes, (thus damping the overall negative error) and, correspondingly, a negative error when it opens.

Throat Area Control: The throat area control logic sets up an error function ($A_{TSCH} - A_T$) for any deviation of the actual throat area (A_T) from the scheduled value (A_{TSCH}) and tries to hold the scheduled value by reducing the error. Thus, in trying to hold the scheduled value, the control not only accomplishes the task of avoiding a choked throat unstart but also tries to maintain inlet performance as close to optimum as possible during a transient.

Initial Conditions

This segment supplies the dynamic segment with the initial values of the following parameters, calculated from the input data, which are required before the dynamic calculations can be initiated: $(X)_{IC}$, $(P_{T6})_{IC}$, $(P_{T12})_{IC}$, $(P_{T18})_{IC}$, $(T_{T6})_{IC}$, $(T_{T12})_{IC}$, $(T_{T18})_{IC}$, $(W_8)_{IC}$, $(W_{14})_{IC}$, $(A_{BY})_{IC}$, $(A_T)_{IC}$.

This is achieved by calculating the air induction system steady state performance at the given operating condition as shown in the block diagram (Figure 5). The NS initial condition $(X)_{IC}$ is obtained from the free stream Mach number using the input data table $X_{REF} = f(M_0)$. The initial values of various flow rates $[(W_0)_{IC}, (W_X)_{IC}, (W_{TBY})_{IC}]$, areas $[(A_X)_{IC}, (A_T)_{IC}]$ and the NS upstream total temperature $(T_{TX})_{IC}$ are calculated next, using the input data tables as shown in Sheet 1. These are then used as inputs in Sheet 2 to calculate properties behind the NS. $(P_{T6})_{IC}$ is obtained from the total pressure drop corresponding to the NS upstream Mach number, $(M_X)_{IC}$. The initial total pressures $(P_{T12})_{IC}$ and $(P_{T18})_{IC}$ are then obtained as follows.

$$(P_{T12})_{IC} = (P_{T6})_{IC} - 0.5\,(\Delta P_L)_{IC} \tag{28}$$

$$(P_{T18})_{IC} = (P_{T2})_{IC} = (P_{T12})_{IC} - 0.5\,(\Delta P_L)_{IC} \tag{29}$$

where

$$(\Delta P_L)_{IC} = 0.026\left[(P_{TX})_{IC} - (P_{SX})_{IC}\right].$$

The total temperatures throughout the air induction system are initially constant and equal to the initial freestream total temperature $(T_{T0})_{IC}$ since the flow process is assumed to be adiabatic.

At the initial condition, the bypass area is sized such that the NS is located at the desired supercritical location as follows:

$$(W_2)_{IC} = (W_{14})_{IC} = (W_8)_{IC} = (W_x)_{IC} - (W_{TBY})_{IC} \tag{30}$$

$$(A_{BY})_{IC} = \frac{\left[(W_2)_{IC} - (W_{2E})_{IC}\right]\sqrt{(T_{T2})_{IC}}}{0.5318\ (P_{T2})_{IC}}. \tag{31}$$

The bypass area is assumed to be choked during the entire simulation run.

Input Data

Input data required for the 2DM air induction system dynamic simulation is presented in Table I. The functional relations are shown for each input variable along with the figure in which it is presented. The overall data is input into the program

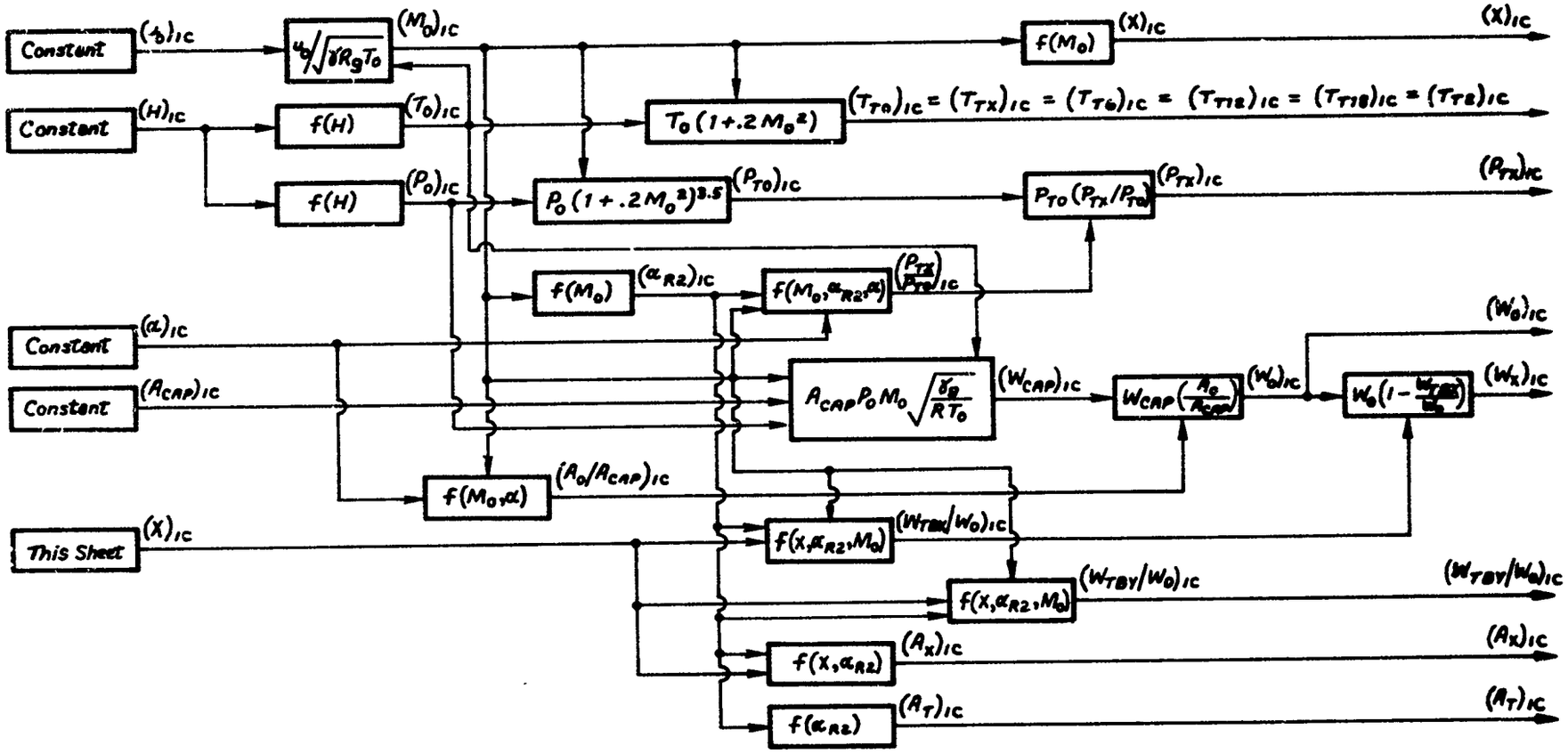

Figure 5. Model 1 - 2DM Three Lump Standard Model Block Diagram - Initial Conditions: Sheet 1 of 2

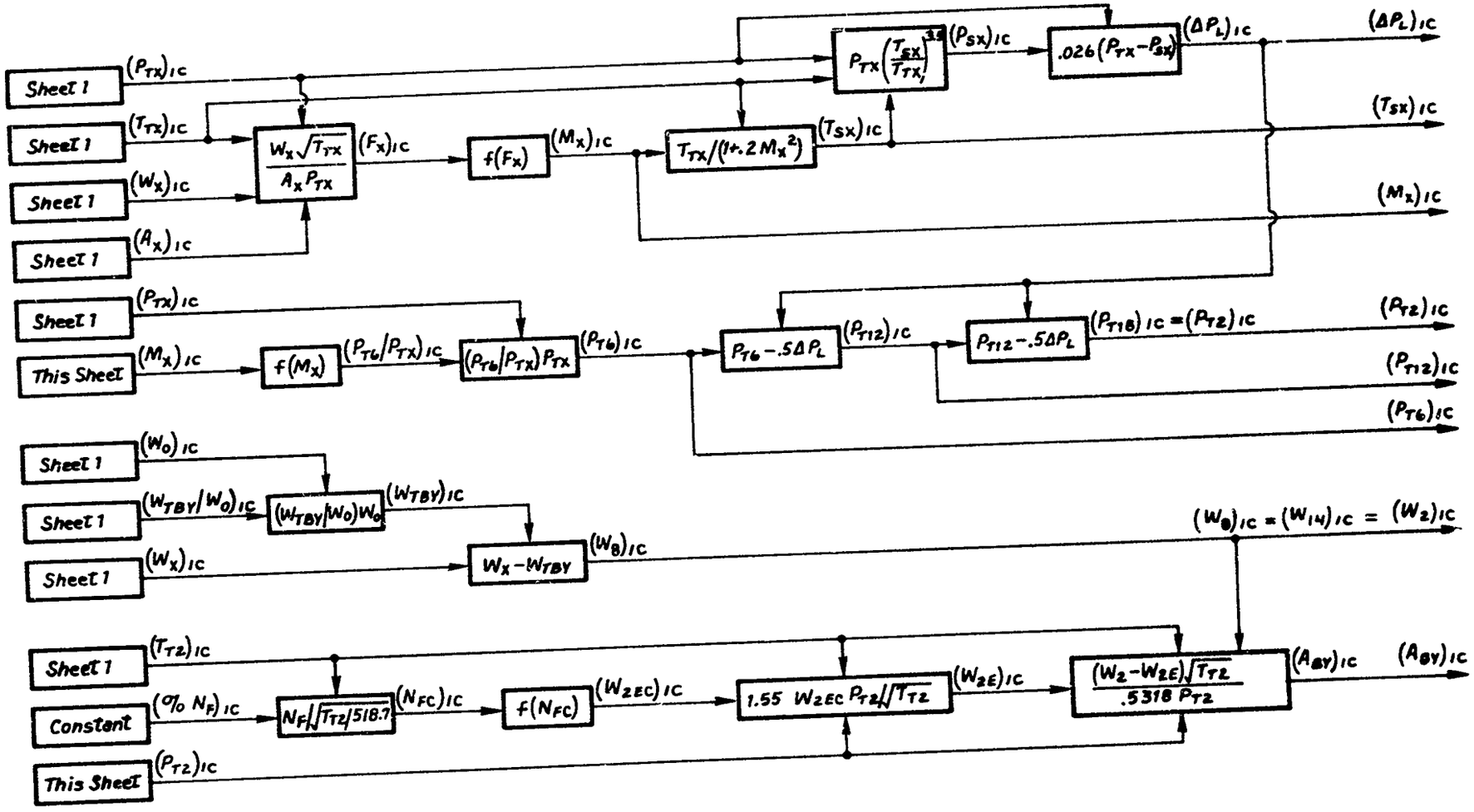

Figure 5 Concluded: Sheet 2 of 2

TABLE I. MODEL 1 - 2DM THREE LUMP STANDARD MODEL INPUT DATA

INPUT PARAMETER	FUNCTIONAL RELATION	FIGURE NO.
Inlet Key Operating and Geometric Parameters		
α^*	f(t) or constant	-
β	constant	-
H^*	f(t) or constant	-
u_0^*	f(t) or constant	-
A_{CAP}	constant	-
P_{0STD}	f(H)	-
T_{0STD}	f(H)	-
M_L	$f(M_0, \alpha)$	13(a)
M_R	$f(M_L, \alpha_{R2})$	13(b)
P_{TL}/P_{T0}	$f(M_0, \alpha)$	13(c)
P_{TR}/P_{TL}	$f(M_L, \alpha_{R2})$	13(d)
A_0/A_{CAP}	$f(M_0, \alpha)$	13(e)
α_{R2}	$f(M_0)$	13(f)
A_X	$f(X, \alpha_{R2})$	13(k)
A_{TSCH}	$f(\alpha_{R2})$	13(g)
W_{BR}/W_0	$f(M_L)$	13(i)
W_{BX}/W_0	$f(M_L, X)$	13(i)
W_{BY}/W_0	$f(M_L, X)$	13(i)
X_{SU}	$f(\alpha_{R2})$	13(j)
X_{SL}	$f(\alpha_{R2})$	13(j)
X_{REF}	$f(\alpha_{R2})$	13(h)
P_{SY}/P_{TY}	$f(F_Y)$	13(p)
M_{XI}	$f(F_{XI} \cdot \sqrt{R})$	13(n)
Scale	Constant	-

TABLE I. MODEL 1 - 2DM THREE LUMP STANDARD MODEL INPUT DATA
(Continued)

INPUT PARAMETER	FUNCTIONAL RELATION	FIGURE NO.
Lumped Volume Parameters		
$(P_{T6}/P_{TX})_{IC}$	$f(M_X)$	13(o)
A_{12}	constant	-
A_{18}	constant	-
X_8	constant	-
Vol_6	$f(\alpha_{R2}, X)$	13(l)
Vol_{12}	constant	-
Vol_{18}	constant	-
I_1	constant	-
I_2	constant	-
Z_6, Z_{12}, Z_{18}	$f(F_6), f(F_{12}), f(F_{18})$	13(r)
C'_6, C'_{12}, C'_{18}	$f(F_6), f(F_{12}), f(F_{18})$	13(q)
Engine Parameters		
N_F^*	f(t) or constant	-
W_{2EC}^*	$f(N_F/\sqrt{\theta_2})$ or constant	13(m)

*These parameters define specific input transients. One or more of these is input as a function of time for a particular simulation run, the others being constant.

either as a constant or as one or two dimensional tabulated data. Parameters marked with an asterisk define specific input transients. Any one or more of these may be input as a function of time for a particular simulation run, the others remaining constant. This concludes the discussion on Model 1 as applied to the 2DM air induction system. The key difference in this model, when it is used for the 2DE air induction system, is the model for simulating NS travel on the inlet ramp. This is discussed below.

Standard Supersonic/Subsonic Upstream Model

For the 2DE air induction system, a model is required to simulate NS travel on the ramp when the inlet is operating subcritically. The approach is shown schematically in Figure 6. Figure 6(a) shows the NS within the cowl when the inlet operates supercritically at an off-design Mach number and, hence, with only supersonic spillage ($W_{CAP} - W_0$). The inflows and outflows from the first lumped control volume, Vol_6, when the inlet operates subcritically, are shown in Figure 6(b). The subsonic spillage W_{SP} required to calculate the flow entering the inlet ($W_0 - W_{SP}$) is obtained from Moeckel's continuity model. This model defines the relationship between shock stand-off distance (L) and the subsonic spillage and is explained in detail in Appendix III.

MODEL 2 — THREE LUMP BUZZ MODEL

A number of theories are available in literature which attempt to explain the rather complex unsteady phenomena called inlet "buzz" (References 8 and 9). Inlet buzz generally occurs at subcritical operation when the inlet mass flow ratio falls below a certain level causing large excursions of the normal shock (NS) fore and aft along the inlet compression surfaces at a high frequency. The resulting large periodic total temperature/pressure variations, and the associated dynamic distortion at the compressor face, can lead to engine stall.

The analytical model described herein does not attempt to predict conditions at which buzz occurs. Rather, its function is to indicate the buzz intensity (i.e., frequency, NS excursion distance, P_{T2} and T_{T2} amplitudes, etc.), once it has been triggered at a particular inlet operating condition. The buzz concept adopted for this model, and the theoretical approach used in simulating it, is discussed below using the 2DE air induction system. The same model applies to the 2DM air induction system except for the added internal NS travel from the throat to the cowl defined as the 'unstart' portion of the transient.

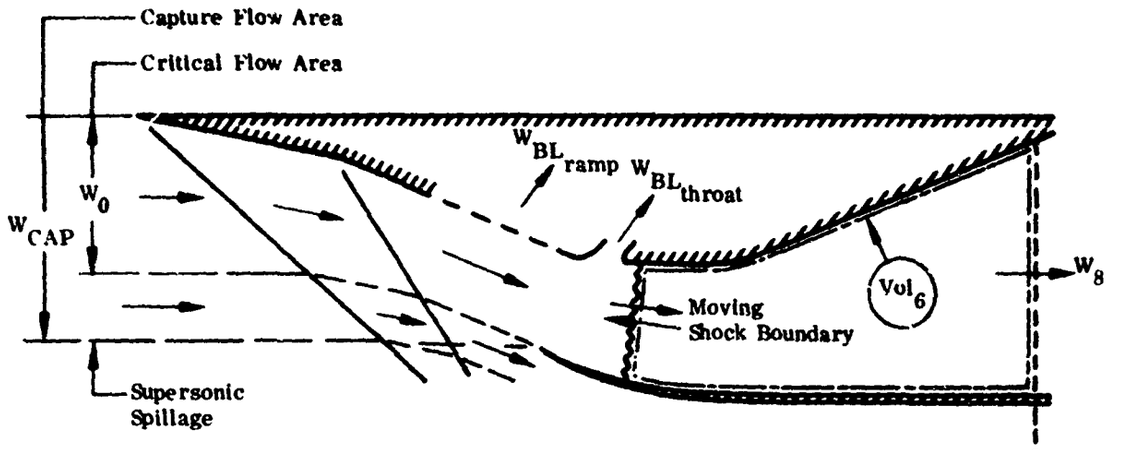

(a) Supercritical Operation

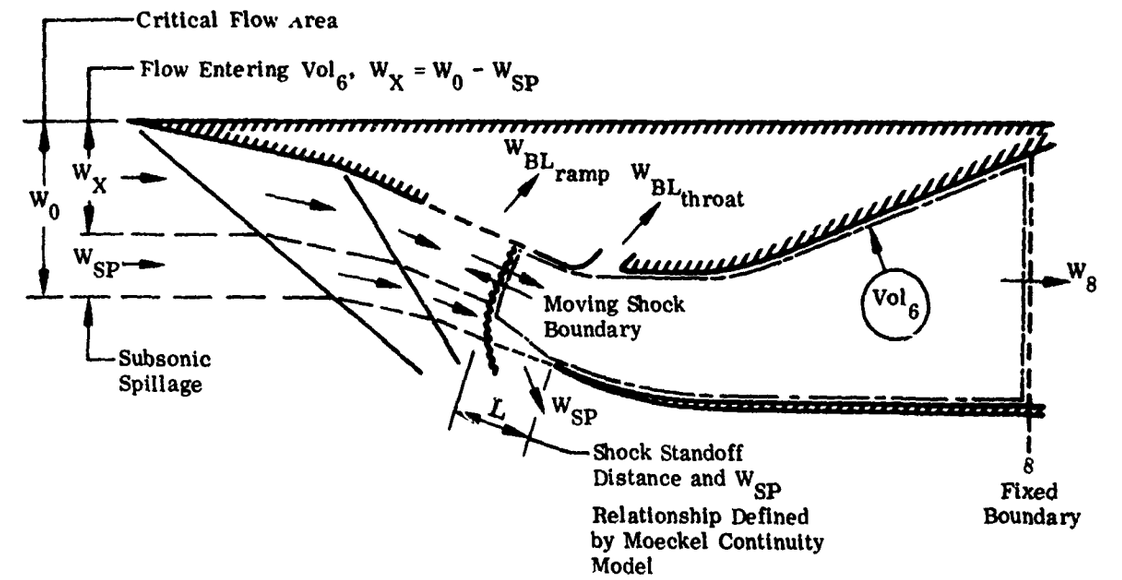

(b) Subcritical Operation

Figure 6. Model 1 - Standard Supersonic/Subsonic Upstream Model

The Buzz Concept

The theory for buzz adopted here focuses on the massive boundary layer separation due to the normal shock-boundary layer interaction on the inlet compression surfaces as the source of instability (Reference 2). The criteria for normal shock induced boundary layer separation is presented in Reference 10. It states that separation occurs when the static pressure across the NS rises to approximately 1.89. This static pressure rise requires that the Mach number entering the shock be 1.33 or above.

The buzz concept is shown schematically in Figure 7. The turbulent separated boundary layer region contains relatively low energy air compared to that outside the boundary layer. This low energy turbulent separated boundary layer zone tends to act like a wedge superimposed on the inlet compression surface, thus throttling the flow entering the inlet and causing significant quantities of the high energy air to spill subsonically outside the cowl.

Figure 7(a) schematically shows first lumped control volume (Vol_6), and the inflow and outflow through the boundaries. The upstream boundary is the NS which extends up to the critical flow streamline. The inflow (W_X) is compressed somewhat by the separated boundary layer as it enters the NS through the effective area A_{EX}, which is the geometric area (A_x) less the separated boundary layer area (ΔA_{EX}). This inflow includes the subsonic spillage flow (W_{SP}). The control volume includes both the high and the low energy streams, with the latter merely acting as a throttling agent, allowing only the throttled throat flow W_{ET} to exit (or enter, if reverse flow conditions exist) through the fixed boundary at Station 8. The remaining outflows from the volume are the ramp and throat bleeds and the subsonic spillage between the NS and the cowl.

The key parameters selected for simulating inlet buzz are the effective throat area ratio A_{ET}/A_T, and the total pressure ratio P_{T12}/P_{T0} (Figure 7(b) and (c)). As the NS travels upstream, separation increases significantly, causing massive throttling when the NS reaches the first ramp. Figure 7(b) shows that the effective throat area ratio, A_{ET}/A_T, decreases to 0.3 for the 2DE inlet operating at Mach 2.5, due to throat throttling as the NS travels upstream from the cowl. The decrease in A_{ET}/A_T is based on throat blockage levels used in Reference 11, which compares XB-70 flight test data with simulation predictions of inlet unstart and buzz.

The throttling of flow due to massive boundary layer separation during the buzz cycle causes significant instantaneous flow imbalance within the subsonic duct. That

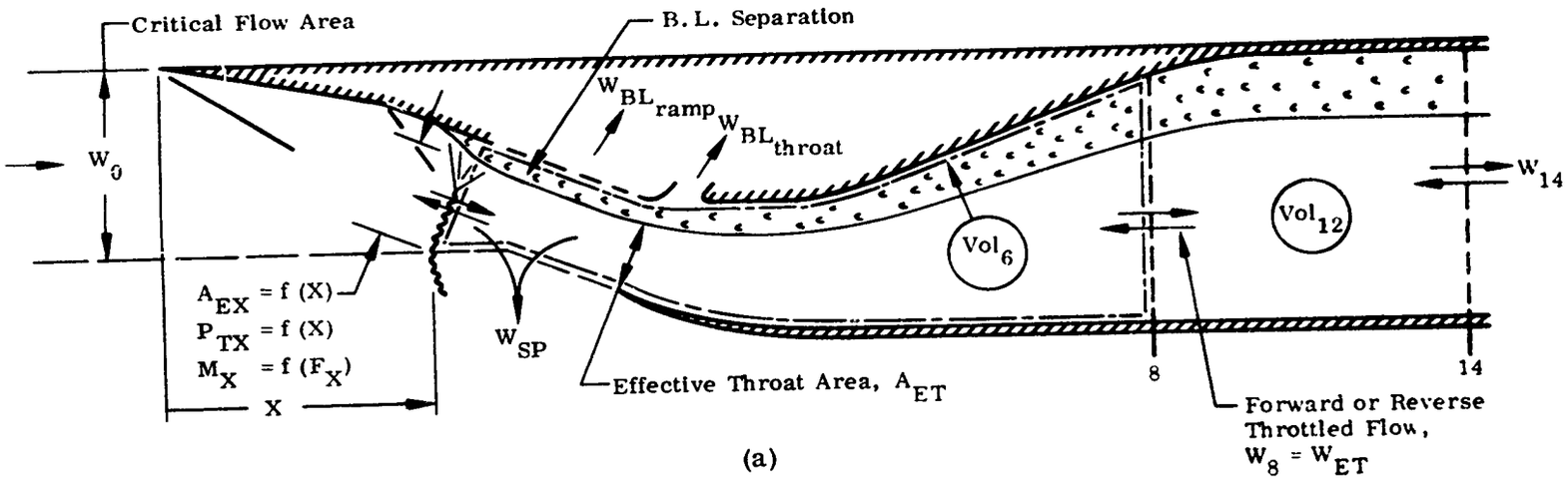

(a)

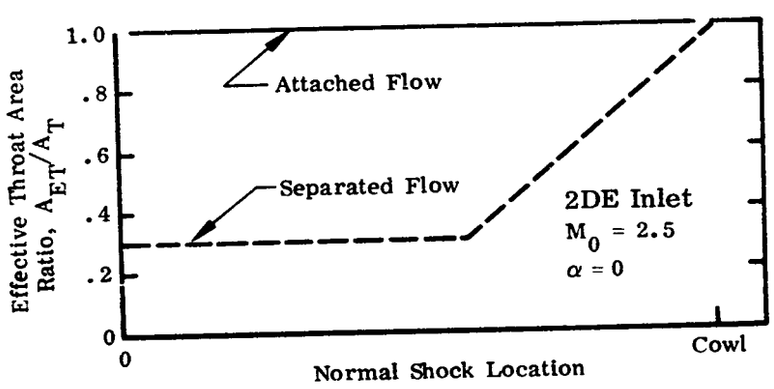

(b)

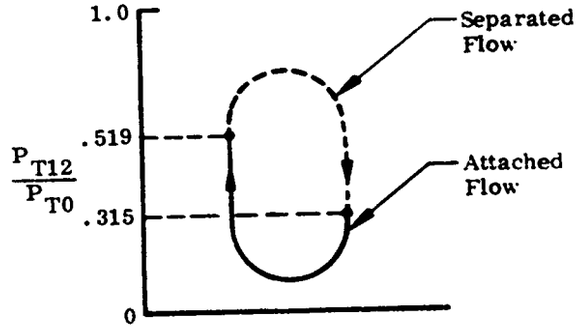

(c)

Figure 7. Model 2 - Supersonic/Subsonic Upstream Model for Simulating Inlet Buzz

is, during the separated flow portion of the buzz cycle, inflow to the subsonic duct is drastically reduced while the engine demand remains unchanged, resulting in a sharp reduction in pressure throughout the duct. As the pressure drops below a critical value (specifically when $P_{T12}/P_{T0} \leq .315$), reattachment of the flow occurs, thus increasing the throat flow area and the subsonic duct pressure level. As the pressure rises above a critical level (specifically, when $P_{T12}/P_{T0} > .519$), separation of the boundary layer is reinitiated. The reattachment/separation critical values of .315 and .519, respectively, were established in Reference 2.

Dynamic Calculations

The overall calculation procedure for the buzz condition is the same as for Model 1. That is, the NS velocity $\dot{X}$ is obtained from the instantaneous static pressures P_{SX} and P_{SY} calculated independently from the flow properties upstream and downstream of the NS. However, this model differs in the method used to calculate

(a) properties upstream of the NS, and

(b) properties within the first lumped volume (Vol_6).

Also, additional logic has been added for

(a) simulating buzz using a boundary layer separation/reattachment model, with on/off and hysteresis characteristics, that is controlled by key buzz parameters, and

(b) calculating dynamic conditions downstream of the NS for buzz severe enough to cause flow reversal within the subsonic diffuser.

A block diagram of the equations used in formulating the buzz model is presented in Figure 8, Sheets 1 to 6. The key differences and additions mentioned above are next discussed with the help of this block diagram.

Properties Upstream of the NS. The instantaneous static pressure P_{SX} is obtained by first calculating the appropriate NS upstream Mach number (M_X) by entering the input data curve

$$M_X = f(F_X) \tag{32}$$

with the corresponding value of the flow function (F_X) defined as

$$F_X = \frac{W_X \sqrt{T_{TX}}}{A_{EX} P_{TX}} \tag{33}$$

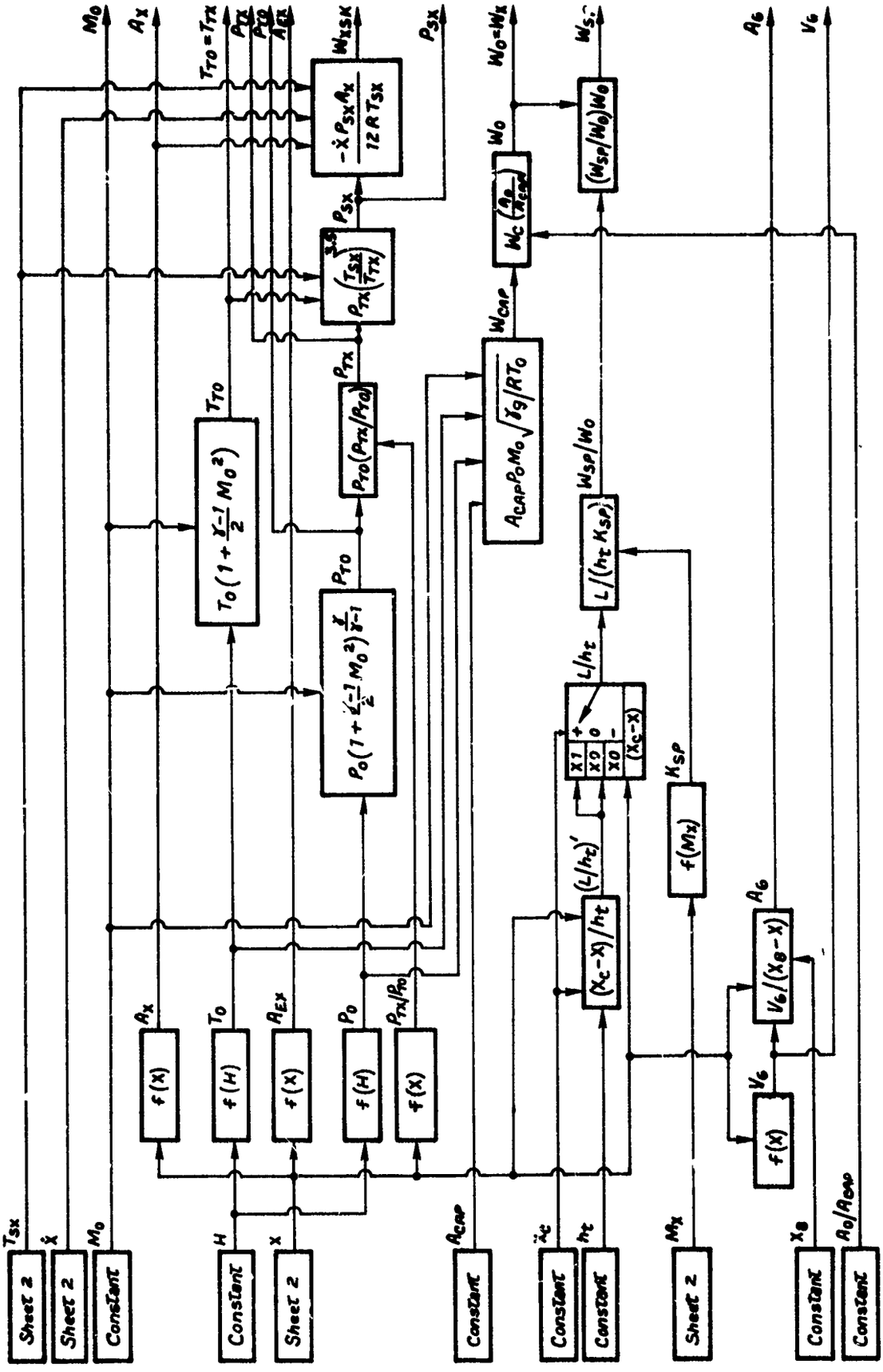

Figure 8. Model 2 – 2DE Three Lump Buzz Model Block Diagram – Dynamic Section: Sheet 1 of 6

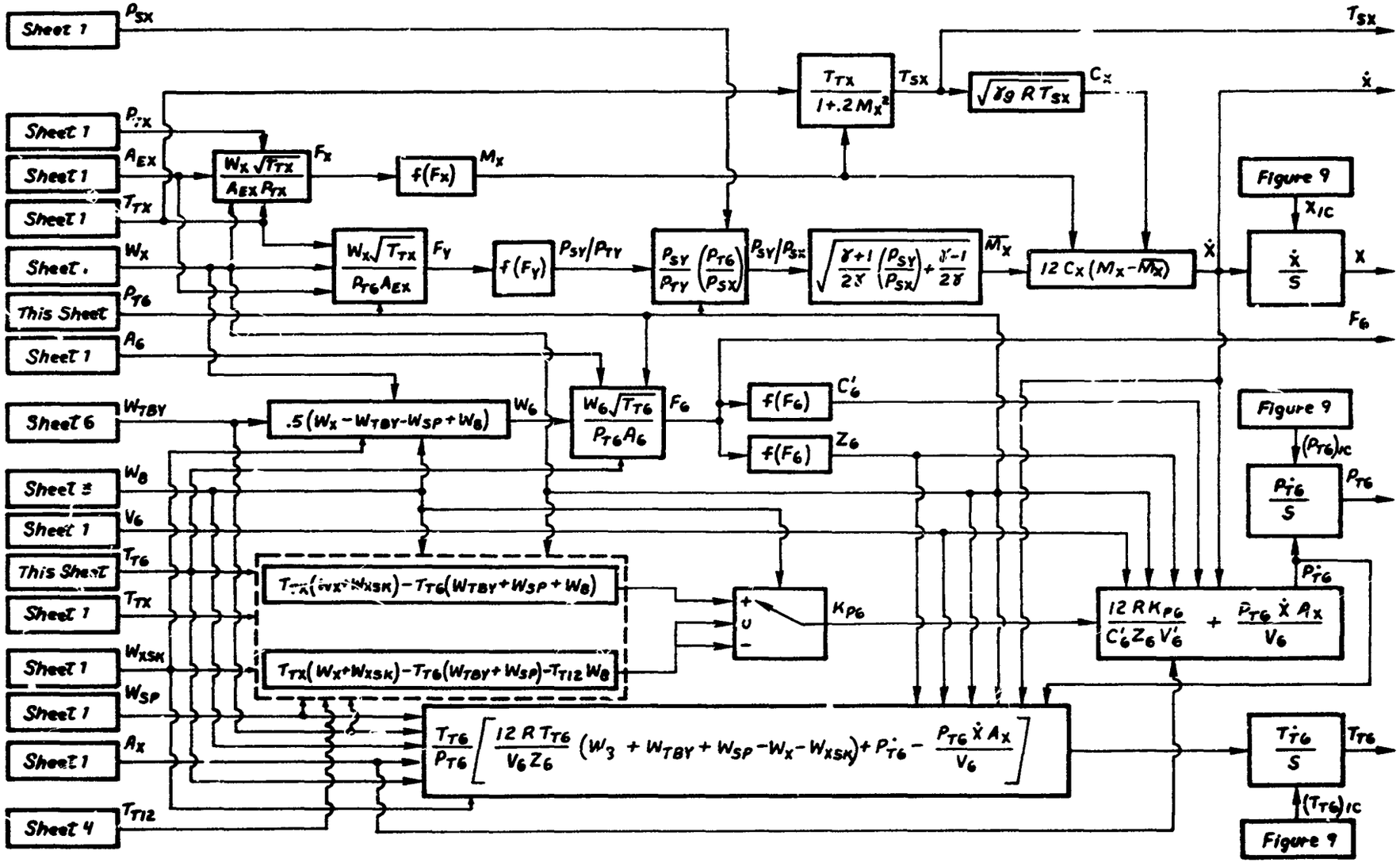

Figure 8 Continued: Sheet 2 of 6

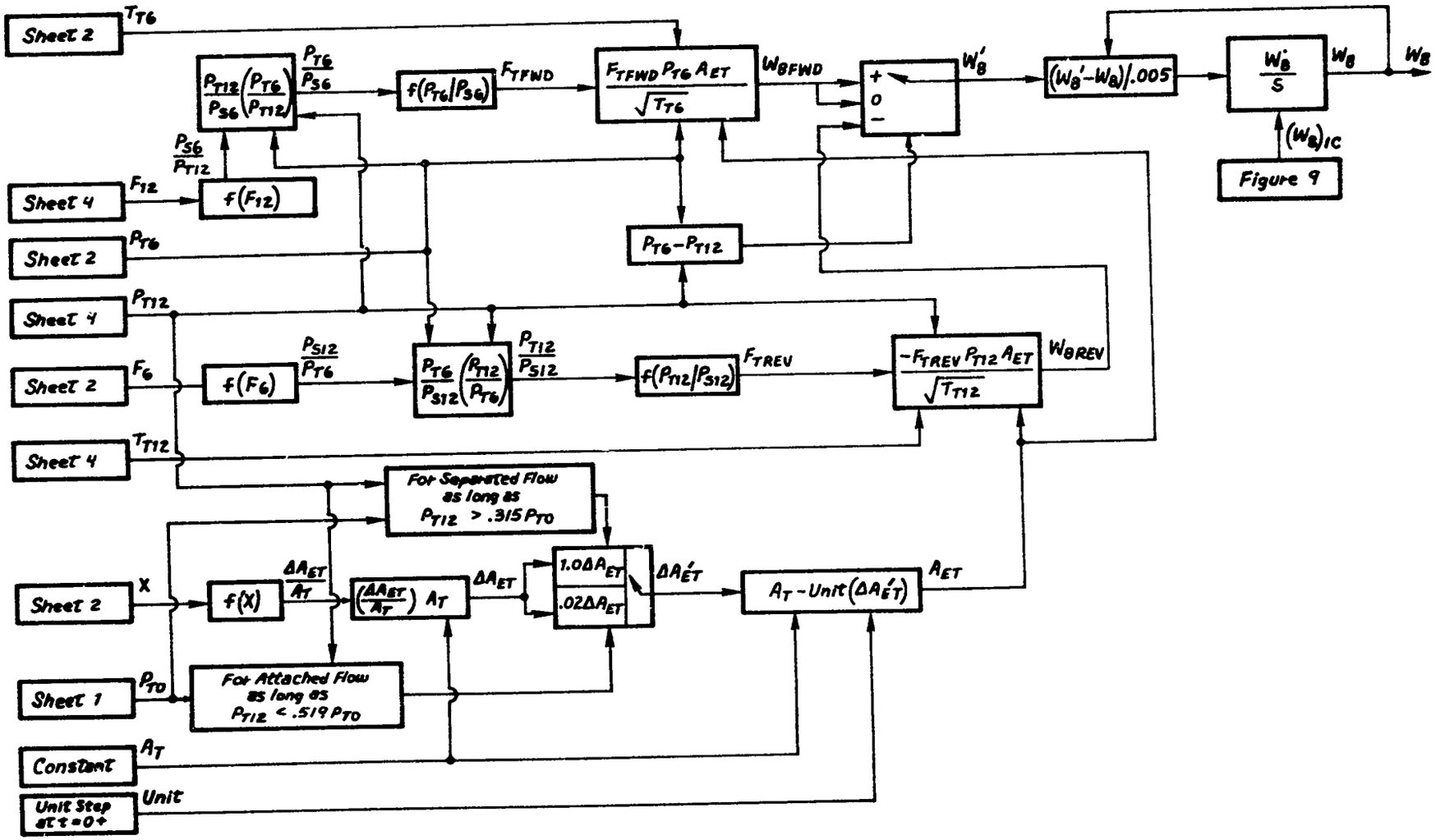

Figure 8 Continued: Sheet 3 of 6

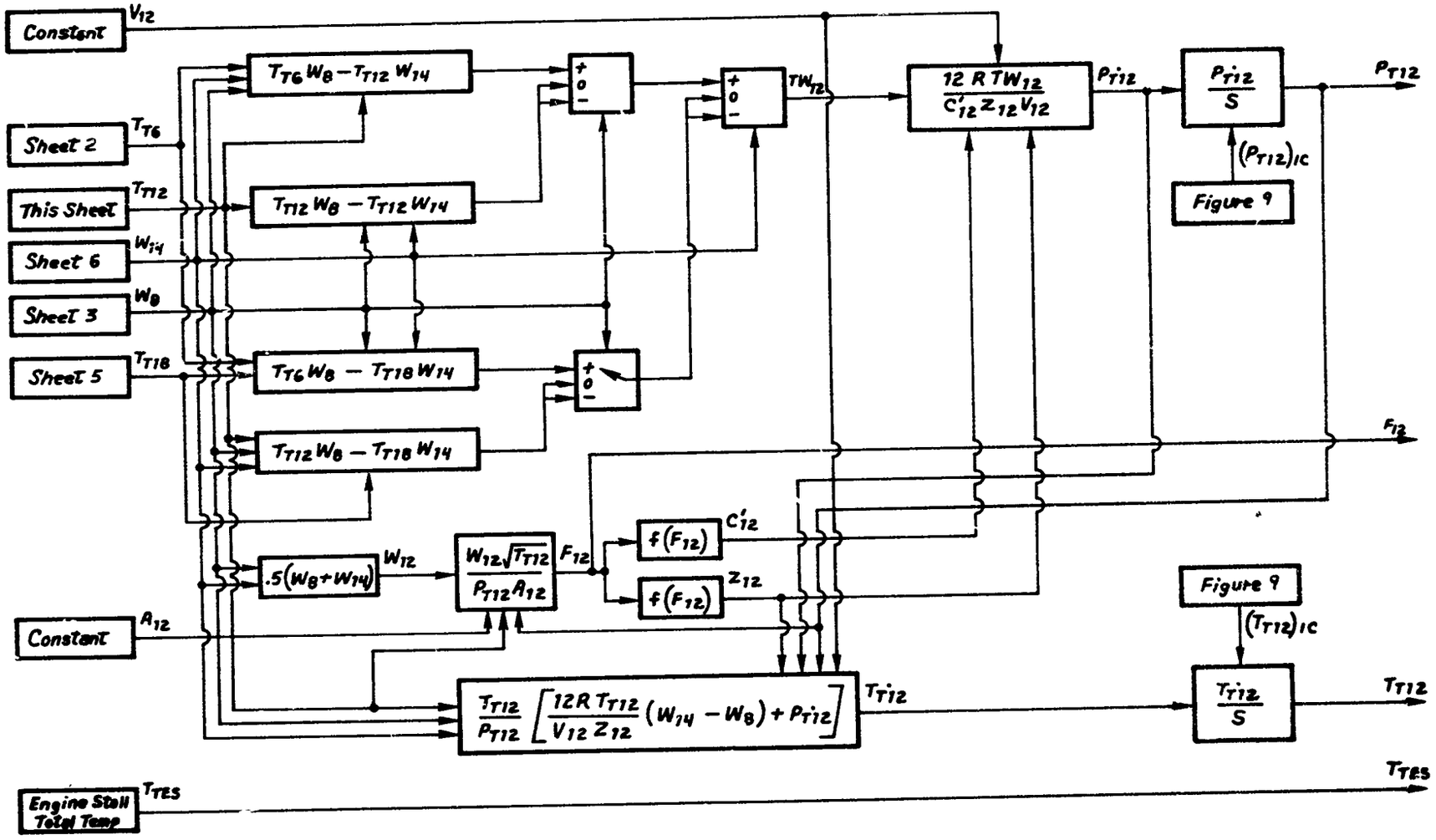

Figure 8 Continued: Sheet 4 of 6

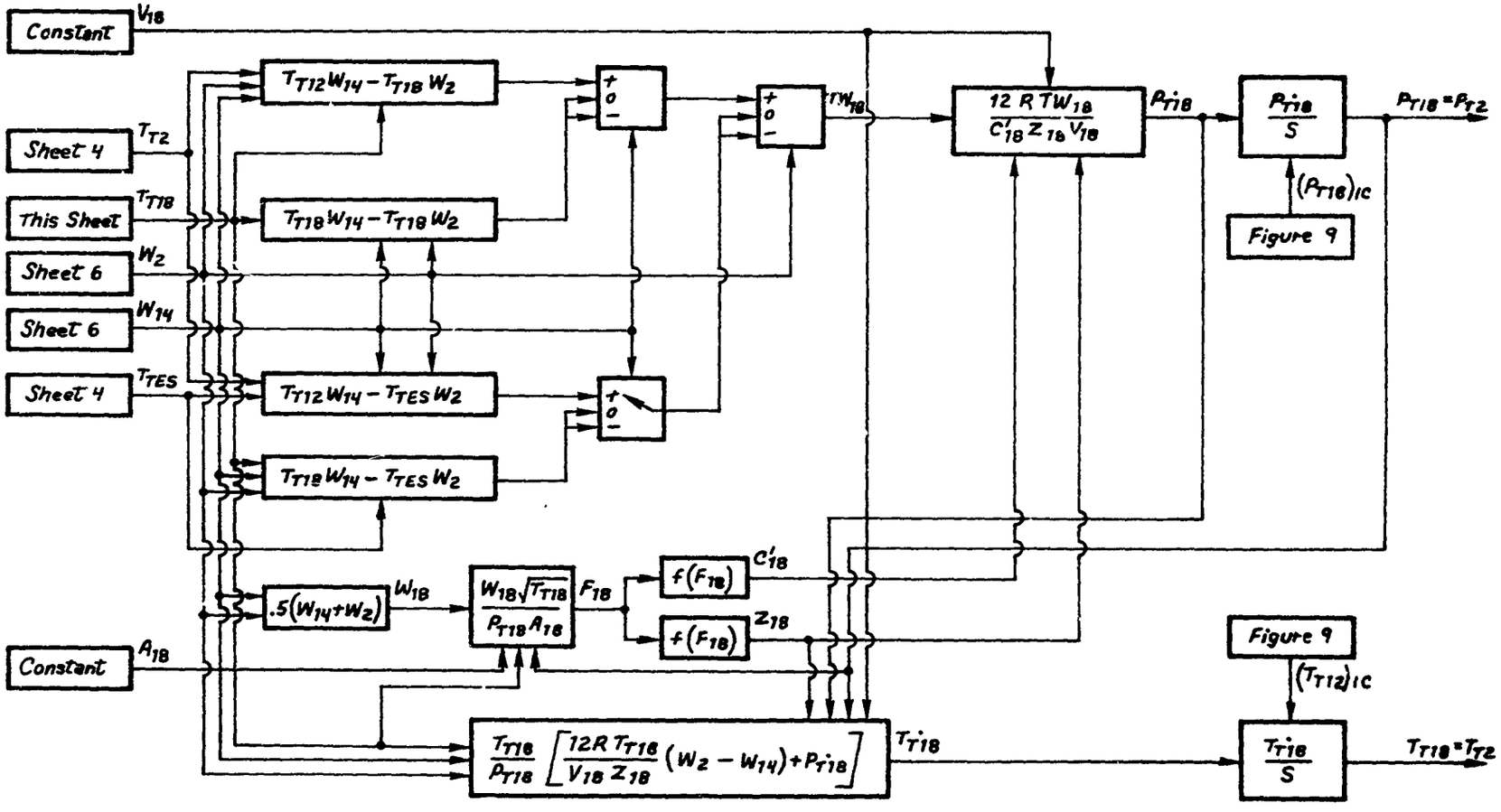

Figure 8 Continued: Sheet 5 of 6

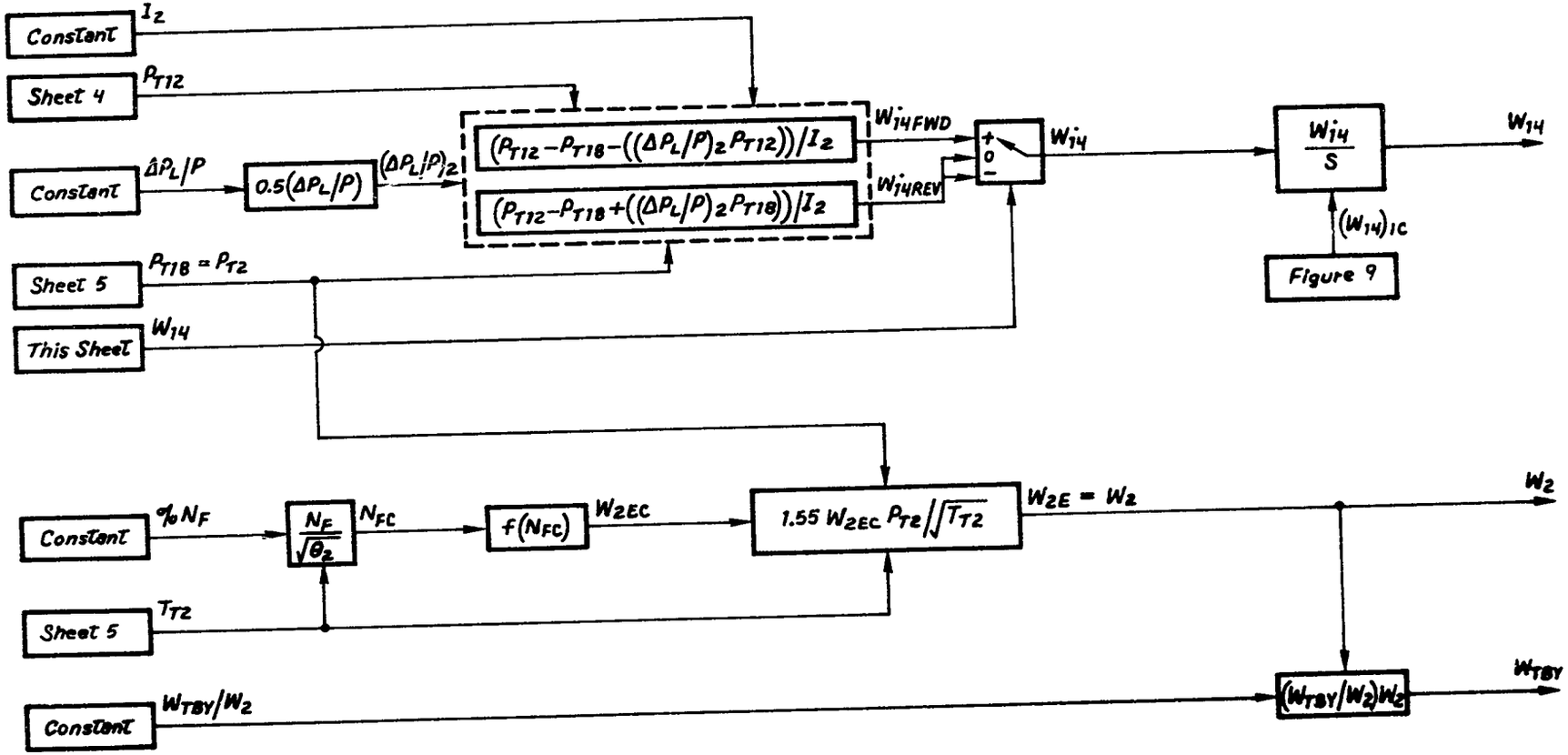

Figure 8 Concluded: Sheet 6 of 6

The effective flow area A_{EX}, upstream of the NS, is obtained by entering the input data curve

$$A_{EX} = f(X) \tag{34}$$

with the corresponding instantaneous value of X. This curve defines the effective flow area upstream of the NS for subcritical inlet operation (NS outside the cowl, $X < X_c$) and the duct cross-sectional area upstream of the NS for critical/supercritical inlet operation when the NS is inside the cowl ($X \geq X_c$).

For adiabatic flow the total temperature upstream of the NS (T_{TX}) is equal to the freestream total temperature T_{T0}. This temperature and M_X are used to calculate the corresponding static temperature

$$T_{SX} = T_{TX} / \left(1 + \frac{\gamma - 1}{2} M_X^2\right) \tag{35}$$

P_{SX} is then calculated from the relationship

$$P_{SX} = P_{TC} \left(\frac{P_{TX}}{P_{TC}}\right) \left(\frac{T_{SX}}{T_{TX}}\right)^{\frac{\gamma}{\gamma - 1}} \tag{36}$$

where the total pressure ratio P_{TX}/P_{T0} is obtained by entering the input data curve $P_{TX}/P_{T0} = f(X)$, with the corresponding instantaneous value of X.

Properties Downstream of the NS. Before discussing the response of the subsonic duct volume to the buzz transient, it is appropriate to examine the throat throttling logic that simulates the buzz transient (Figure 8, Sheet 3). In calculating the throttled throat flow, it is assumed that the instantaneous flow (W_8) exiting (for forward flow) or entering (for reverse flow) Vol_6 at Station 8 is equal to the instantaneous throttled throat flow, W_{ET}. Secondly, the lumped properties at Station 8 are used in calculating W_8. This is permissible since the 'lumped parameter' concept assumes that properties within the lumped volume Vol_6, and hence, the throat properties, are instantaneously equal to the property values at the exit Station 8. The rate of change of throttled throat flow ($\dot{W}_8$) is calculated next as follows.

Calculation of $\dot{W}_8$. The throat blockage, (ΔA_{ET}), is first calculated by entering the input data table

$$\frac{\Delta A_{ET}}{A_T} = f(X) \tag{37}$$

with the corresponding instantaneous value of X. Then,

$$\Delta A_{ET} = \left(\frac{\Delta A_{ET}}{A_T} \right) A_T \tag{38}$$

Now, referring to Figure 7(c), the flow once separated remains separated as long as P_{T12}/P_{T0} is above .315 and, therefore, for separated flow the full value of the blockage (ΔA_{ET}) is used

$$\Delta A_{ET}' = 1.0\ \Delta A_{ET} \tag{39}$$

When P_{T12}/P_{T0} drops below .315, attachment occurs and flow remains attached until the pressure ratio rises above .519. During this period when flow is attached, blockage is assumed to be two percent of its separated flow value, so that for attached flow

$$\Delta A_{ET}' = 0.02\ \Delta A_{ET} \tag{40}$$

Hence, the effective throat area, at any instant, can be calculated by using the appropriate $\Delta A_{ET}'$ for either separated or attached flow in the equation

$$A_{ET} = A_T - \Delta A_{ET}' \tag{41}$$

The throat throttling flow functions for both forward flow (F_{TFWD}) and reverse flow (F_{TREV}) are next calculated by entering the input data curve [$F_T = f(P_T/P_S)$] with the corresponding value of the appropriate total-to-static pressure ratio at Station 8. The procedure is discussed below.

For forward flow, the total-to-static pressure ratio in Vol_6 (P_{T6}/P_{S6}) is used to calculate F_{TFWD} as follows.

The input data curve

$$\frac{P_{SC}}{P_{T12}} = f(F_{12}) \tag{42}$$

includes the front half of the duct steady state friction losses within the steady state pressure recovery term, P_{T12}/P_{T6}. During simulation, the above input curve is entered with the corresponding mean flow function for Vol_{12},

$$F_{12} = \frac{0.5\,(W_8 + W_{14})\sqrt{T_{T12}}}{A_{12}\ P_{T12}} \tag{43}$$

to obtain the instantaneous P_{S6}/P_{T12} value. This ratio and the instantaneous total pressures P_{T6} and P_{T12} are used to obtain the instantaneous total-to-static pressure ratio

$$\frac{P_{T6}}{P_{S6}} = \left(\frac{P_{T6}}{P_{T12}}\right)\left(\frac{P_{T12}}{P_{S6}}\right). \tag{44}$$

Then the input data curve $[F_T = f(P_T/P_S]$ is entered with the pressure ratio P_{T6}/P_{S6} to obtain

$$F_{TFWD} = f\left(\frac{P_{T6}}{P_{S6}}\right). \tag{45}$$

Similarly, for reverse flow, the same curve $[F_T = f(P_T/P_S]$ is entered again with the pressure ratio P_{T12}/P_{S12} to obtain

$$F_{TREV} = f\left(\frac{P_{T12}}{P_{S12}}\right). \tag{46}$$

Then, for forward flow, the throttled throat flow is

$$W_8' = (F_{TFWD}\ P_{T6}\ A_{ET})/\sqrt{T_{T6}} \quad \text{if} \quad (P_{T6} - P_{T12}) \geq 0 \tag{47}$$

and for reverse flow, it is

$$W_8' = (F_{TREV}\ P_{T12}\ A_{ET})/\sqrt{T_{T12}} \quad \text{if} \quad (P_{T6} - P_{T12}) < 0. \tag{48}$$

Finally, $\dot{W}_8$ is obtained by imposing a lag on the appropriate W_8', using a typical value of .005 for the time constant τ_{W8}.

$$\dot{W}_8 = (W_8' - W_8)/\tau_{W8} \tag{49}$$

$$= (W_8' - W_8)/.005 \tag{50}$$

Calculation of the Instantaneous P_{SY}. The response of the subsonic lumped volume Vol_6 (and hence, the instantaneous value to P_{SY}) to the throttling of the flow at the fixed boundary exit Station 8 is calculated using the P_{T6} and T_{T6} rate equations.

For forward flow, W_8 is greater than zero and exits Vol_6 at the instantaneous total temperature T_{T6}, so that

$$\dot{P}_{T6} = \frac{12\,R}{C_6' Z_6 V_6}\left[T_{TX}(W_X + W_{XSK}) - T_{T6}(W_{TBY} + W_{SP} + W_8)\right] + \frac{P_{T6} A_X \dot{X}}{V_6}. \tag{51}$$

For reverse flow, W_8 is less than zero and enters Vol_6 at the instantaneous total temperature T_{T12}, so that

$$\dot{P}_{T6} = \frac{12R}{c_6' z_6 V_6}\left[T_{Tx}(W_x + W_{xsk}) - T_{T6}(W_{TBy} + W_{SP}) - T_{T12}W_8\right] + \frac{P_{T6}A_x\dot{X}}{V_6} \quad (52)$$

The appropriate value of $\dot{P}_{T6}$ corresponding to forward or reverse throttled flow direction (W_8 is positive or negative, respectively) is selected through program logic (see Figure 8, Sheet 2).

For both forward and reverse flow,

$$\dot{T}_{T6} = \frac{T_{T6}}{P_{T6}}\left[\frac{12RT_{T6}}{V_6 z_6}\left(W_8 + W_{TBy} + W_{SP} - W_x - W_{xsk}\right) + \dot{P}_{T6} - \frac{P_{T6}A_x\dot{X}}{V_6}\right]. \quad (53)$$

Note that the inflow (W_X) through the NS (Vol_6 upstream boundary) includes the subsonic flow spillage (W_{SP}) when the NS is upstream of the cowl. Moeckel's model (Appendix III) has been incorporated into the buzz model to calculate this spillage flow during the simulation. The NS standoff distance L is known, at any instant, during the dynamic calculations

$$\frac{L}{h_t} = \frac{X_c - X}{h_t} \qquad \text{for} \quad x < x_c$$
$$= 0 \qquad \text{for} \quad x \geq x_c . \quad (54)$$

The spillage coefficient, K_{SP}, corresponding to the NS upstream Mach number M_X, is obtained from Moeckel's curve

$$K_{SP} = f(M_x). \quad (55)$$

From this, the corresponding spillage is

$$W_{SP} = \frac{W_c L}{h_t K_{SP}}. \quad (56)$$

where W_0 is the critical inlet flow.

Using P_{T6} (obtained from Equation 51 or 52) P_{SY}, $\overline{M}_X$ and finally $\dot{X}$ are calculated as already explained for Model 1. The detailed procedure is shown in Figure 8, Sheet 2.

Vol$_{12}$ and Vol$_{18}$ Instantaneous Total Conditions. The instantaneous total pressures and temperatures within the volumes Vol_{12} and Vol_{18} are obtained by numerically integrating the corresponding rate equations. In Vol_{12}, since forward or reverse flows can occur at both the fixed boundary Stations 8 and 14,

any one of four combinations of forward/reverse flows canexist at any instant. Matching of these flows with the appropriate instantaneous total temperatures, at each fixed boundary, leads to the following four total pressure rate equations:

If W_8 and $W_{14} > 0$,

$$\dot{P}_{T12} = \frac{12\,R}{C'_{12}\,Z_{12}\,V_{12}} \left[T_{TC}\,W_8 - T_{T12}\,W_{14} \right] \tag{57}$$

If $W_8 > 0$ and $W_{14} < 0$

$$\dot{P}_{T12} = \frac{12\,R}{C'_{12}\,Z_{12}\,V_{12}} \left[T_{TC}\,W_8 - T_{T18}\,W_{14} \right] \tag{58}$$

If $W_8 < 0$ and $W_{14} > 0$

$$\dot{P}_{T12} = \frac{12\,R}{C'_{12}\,Z_{12}\,V_{12}} \left[T_{T12}\,W_8 - T_{T12}\,W_{14} \right] \tag{59}$$

If $W_8 < 0$ and $W_{14} < 0$

$$\dot{P}_{T12} = \frac{12\,R}{C'_{12}\,Z_{12}\,V_{12}} \left[T_{T12}\,W_8 - T_{T18}\,W_{14} \right] \tag{60}$$

The appropriate value of $\dot{P}_{T12}$ corresponding to the instantaneous W_8 and W_{14} flow directions is selected through program logic (see Figure 8, Sheet 4).

For both forward and reverse flows,

$$\dot{T}_{T12} = \frac{T_{T12}}{P_{T12}} \left[\frac{12\,R\,T_{T12}}{V_{12}\,Z_{12}} \left(W_{14} - W_8 \right) + \dot{P}_{T12} \right] \tag{61}$$

The calculation procedure for obtaining the total pressure and temperature rates within Vol_{18}, for forward and reverse flows at the two boundary stations 14 and 2, is similar to that discussed above for Vol_{12} and is shown in Figure 8, Sheet 5. An option is provided in program logic for calculating P_{T18} with reverse flow at the compressor face ($W_2 < 0$; i.e., during severe engine stall). An appropriate matching value of engine stall total temperature (T_{TES}) is required as input for simulating such a transient.

Calculation of $\dot{W}_{14}$. The forward ($\dot{W}_{14FWD}$) and reverse ($\dot{W}_{14REV}$) rates of change of flow rates at the second fixed boundary (Station 14) are calculated by applying the momentum equation to the half duct volume containing the second fixed boundary.

The two equations are

$$\dot{W}_{14FWD} = \frac{1}{I_2}\left[P_{T12} - P_{T18} - 0.5\left(\frac{\Delta P_L}{P_T}\right)P_{T12}\right] \quad (62)$$

$$\dot{W}_{14REV} = \frac{1}{I_2}\left[P_{T12} - P_{T18} + 0.5\left(\frac{\Delta P_L}{P_T}\right)P_{T18}\right] \quad (63)$$

where $\Delta P_L/P_T$ is the subsonic diffuser total pressure loss due to friction, and is assumed to be constant.

Note that for reverse flow, the frictional force acts in the upstream direction. Hence, the change in sign for the third expression in brackets in Equation (63).

Thus,

$$\begin{aligned} \dot{W}_{14} &= \dot{W}_{14FWD} \quad \text{if} \quad W_{14} > 0 \\ &= \dot{W}_{14REV} \quad \text{if} \quad W_{14} < 0 \end{aligned} \quad (64)$$

Initial Conditions

The initial values of the following parameters are supplied by this segment to the dynamic segment before dynamic calculations are initiated. $(X)_{IC}$, $(P_{T6})_{IC}$, $(P_{T12})_{IC}$, $(T_{T6})_{IC}$, $(T_{T12})_{IC}$, $(T_{T18})_{IC}$, $(W_8)_{IC}$, $(W_{14})_{IC}$.

The calculations are shown in Figure 9, and are self-explanatory. With no bypass, all the excess flow is spilled subsonically at the cowl lip with the NS located at the proper initial stand-off distance from the cowl to allow for the required spillage.

Input Data

The key input parameters required for the 2DE air induction system buzz simulation are presented in Table II. This model does not require any input transients. Buzz is triggered through internal program logic as explained in the dynamic segment.

MODEL 3 – THREE LUMP HAMMERSHOCK MODEL

Rapid cutoff of engine demand, usually due to compressor stall, causes an extreme instantaneous flow imbalance within the diffuser. With the diffuser outflow drastically reduced and the inflow unaffected, the instantaneous excess of inflow over outflow causes a sharp increase in pressure near the compressor face. With the diffuser exit blocked, this local pressure wave increases in strength and propagates upstream as a shock front or hammershock (HS). The pressure buildup within the duct is relieved through subsonic spillage when the hammershock exits from the duct at the

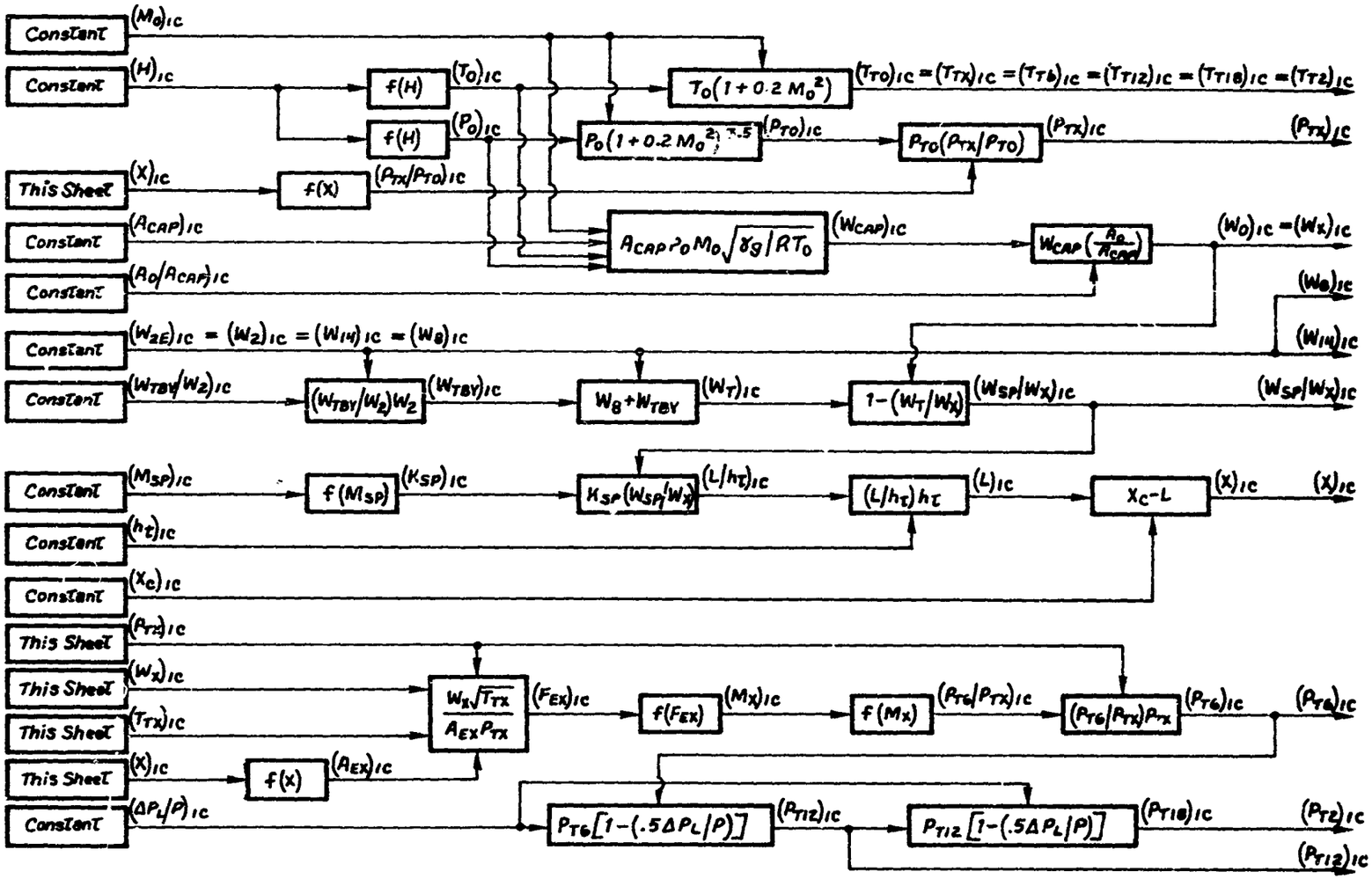

Figure 9. Model 2 - 2DE Three Lump Buzz Model Block Diagram - Initial Conditions

TABLE II. MODEL 2 - 2DE THREE LUMP BUZZ MODEL INPUT DATA

INPUT PARAMETER	FUNCTIONAL RELATION	FIGURE NO.
Inlet Key Operating and Geometric Parameters		
α	constant	-
β	constant	-
H	constant	-
M_0	constant	-
A_{CAP}	constant	-
A_0/A_{CAP}	constant	-
α_{R2}	constant	-
W_B/W_2	constant	-
$\Delta P_L/P$	constant	-
$(M_{SP})_{IC}$	constant	-
P_{0STD}	f(H)	-
T_{0STD}	f(H)	-
P_{TX}/P_{T0}	f(X)	22(a)
$\Delta A_{ET}/A_T$	f(X)	22(d)
A_X	f(X)	22(c)
A_{EX}	f(X)	22(c)
K_{SP}	$f(M_{XE})$	16(e)
M_{XI}	$f(F_X \cdot \sqrt{R})$	13(n)
P_{SY}/P_{TY}	$f(F_Y)$	13(p)
Scale	constant	-

TABLE II. MODEL 2 - 2DE THREE LUMP BUZZ MODEL INPUT DATA
(Continued)

INPUT PARAMETER	FUNCTIONAL RELATION	FIGURE NO.
Lumped Volume Parameters		
$(P_{T6}/P_{TX})_{IC}$	$f(M_X)$	13(o)
A_{12}	constant	-
A_{18}	constant	-
X_8	constant	-
Vol_6	f(X)	22(b)
Vol_{12}	constant	-
Vol_{18}	constant	-
I_2	constant	-
P_{S6}/P_{T12}	$f(F_{12})$	16(f)
F_T	$f(P_{T6}/P_{S6})$	16(g)
Z_6, Z_{12}, Z_{18}	$f(F_6)$, $f(F_{12})$, $f(F_{18})$	13(r)
C'_6, C'_{12}, C'_{18}	$f(F_6)$, $f(F_{12})$, $f(F_{18})$	13(q)
Engine Parameters		
N_F	constant	-
$(W_{2E})_{IC}$	constant	-
W_{2EC}	$f(N_F/\sqrt{\theta_2})$	13(m)

cowl. For severe hammershocks, flow reversal occurs within the duct, resulting in reverse flow spillage at the cowl. Knowledge of the pressure level behind the hammershock is important when designing subsonic diffusers since it can be considerably higher than freestream total pressure. The theoretical approach to hammershock simulation used in this model is discussed below.

Dynamic Calculations

The only key area in which this model differs significantly from Model 2 is in the approach used to simulate NS travel upstream along the ramp during a hammershock. Detailed discussion of the upstream hammershock model is included in the general review of the overall simulation approach that follows.

The three-lump "lumped parameter" approach provides an approximate simulation of the actual response of the system to a sudden cutoff in engine demand. The total pressures within each of the three lumped volumes are calculated using the same approach as discussed in detail under the dynamic section for Model 1. When outflow from Vol_{18} is suddenly cut off, the instantaneous flow imbalance across the lumped volume (Vol_{18}) causes its pressure P_{T2} and total temperature T_{T2} to rise. Instantaneous outflows at each of the two fixed boundaries (Stations 14 and 8) are computed by integrating the rates of change of flows ($\dot{W}_{14}$ and $\dot{W}_{8}$). Since these rates are a function of the pressure levels across the fixed boundaries, the rise in pressure in Vol_{18} reduces instantaneous outflow (W_{14}) from Vol_{12}, thereby producing an instantaneous flow imbalance across Vol_{12}, and increasing its pressure P_{T12}. Instantaneous outflow from the fixed boundary at Station 8 is similarly reduced by the rise in P_{T12}, resulting in an increase in Vol_6 pressure P_{T6}. The normal shock is unaffected by the sudden cutoff in engine demand until the rise in P_{T6} forces it to start traveling rapidly upstream.

Figure 10(a) shows the NS located downstream of the first ramp. The Vol_6 upstream boundary is the NS which extends to the critical flow streamline. The inflow (W_X) based on A_X, includes the subsonic spillage, W_{SP}. During the period the NS is downstream of the leading edge (i.e., $X > 0$), the critical flow areas A_X and P_{TX}/P_{T0} are obtained from input data curves as a function of X. The variation in P_{TX}/P_{T0} as the NS travels from the cowl to the inlet leading edge is obtained by preselecting the three known pressure ratio values for NS at (1) inlet leading edge ($P_{TX}/P_{T0} = 1$), (2) end of first inlet ramp, and (3) end of second inlet ramp, from the inlet input data at the given flight conditions. Linear variation in P_{TX}/P_{T0} is assumed between these

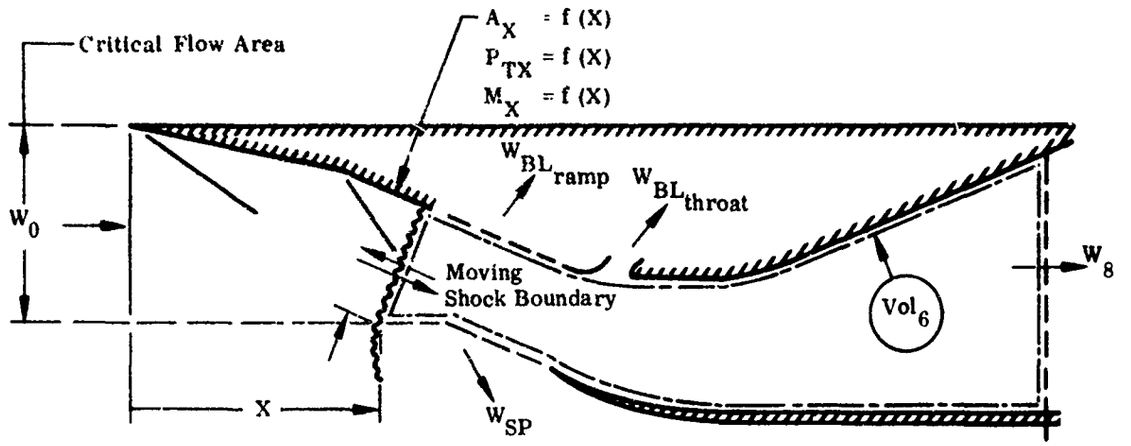

(a) Normal Shock Downstream of First Ramp

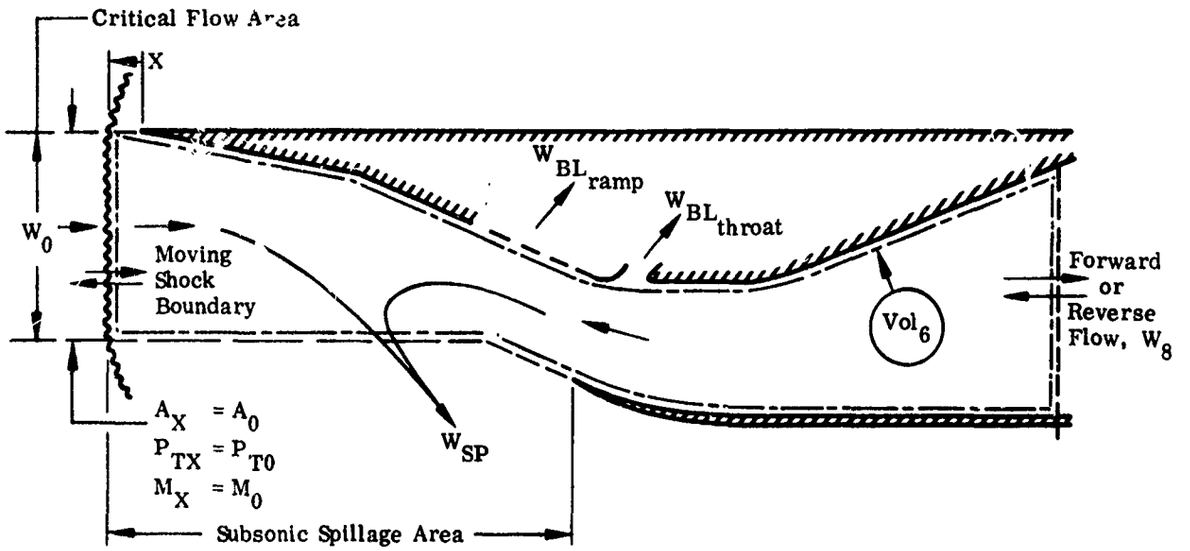

(b) Normal Shock Upstream of First Ramp

Figure 10. Model 3 - Supersonic/Subsonic Upstream Model for Simulating Hammershock

three values. The effective external Mach number M_{XE} upstream of the NS is obtained from the corresponding flow function $F_X\left[\left(W\sqrt{T_T}/P_T A\right)_X\right]$. For severe hammershocks, flow reversal occurs within the subsonic duct, usually before the NS reaches the inlet leading edge.

In simulating the normal shock travel upstream along the ramp, it is assumed that there is no massive boundary layer separation (i.e., $A_{EX} = A_X$). This is acceptable as a simplifying assumption, since for a hammershock transient, the primary interest is in the peak pressures and temperatures experienced within the subsonic duct rather than the accurate evaluation of the extent of the normal shock travel on the inlet ramp.

Figure 10(b) schematically shows the instantaneous inflow and outflow through Vol_6 when the NS is upstream of the inlet leading edge ($X \leq 0$). During simulation, as long as $X \leq 0$, the inflow into the NS is assumed to be at freestream operating conditions (i.e., $A_X = A_0$; $M_{XE} = M_0$; $P_{TX}/P_{T0} = 1$). As the NS travels upstream from the initial near-the-cowl position, the instantaneous inflow into Vol_6 can increase significantly due to flow reversal at Station 8. The instantaneous imbalance between this inflow and the outflow (i.e., spillage plus bleed flows) increases P_{T6}, until the point at which the outflow becomes instantaneously greater than inflow due to the continuing increase in spillage flow. At this point, P_{T6} starts to reduce, thus relieving the pressure buildup within the duct.

The overall procedure for calculating normal shock (NS) velocity $\hat{X}$ is the same as for Models 1 and 2. A block diagram of the equations used in formulating the hammershock model is presented in Figure 11. The procedure for calculating reverse flows at the two fixed boundaries within the subsonic duct (Stations 8 and 14) is the same as that used for W_{14} calculation in Model 2. Option is included in program logic (Figure 11, Sheet 5) to calculate P_{T18} for hammershocks severe enough to involve reverse flow at the compressor face ($W_2 < 0$). An appropriate value of the engine stall total temperature (T_{TES}) is required as input when simulating such a transient.

Initial Conditions and Input Data

The calculation sheet for the initial conditions is presented in Figure 12 and is self-explanatory. Input data are presented in Table III.

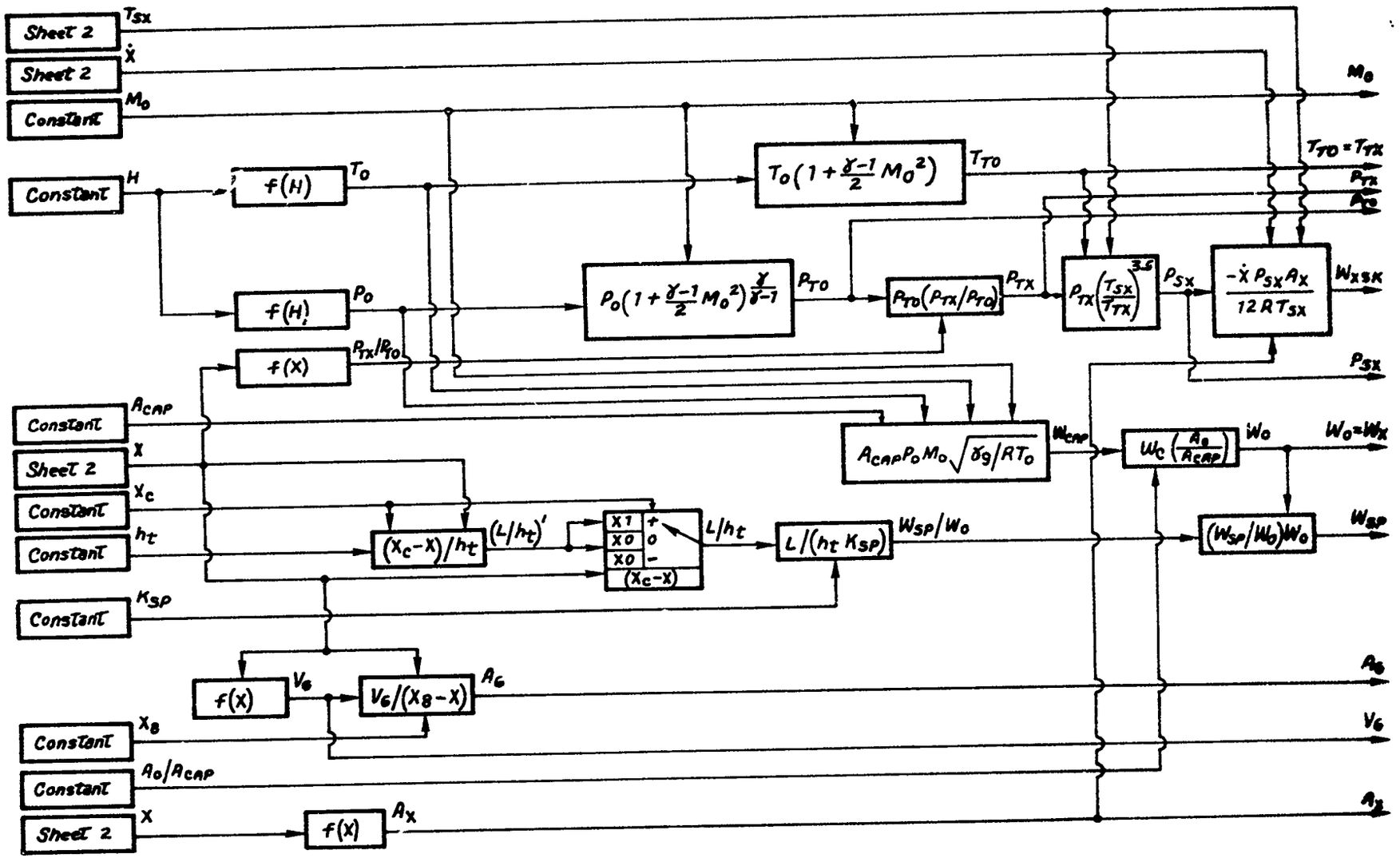

Figure 11. Model 3 - 2DE Three Lump Hammershock Model Block Diagram - Dynamic Section: Sheet 1 of 6

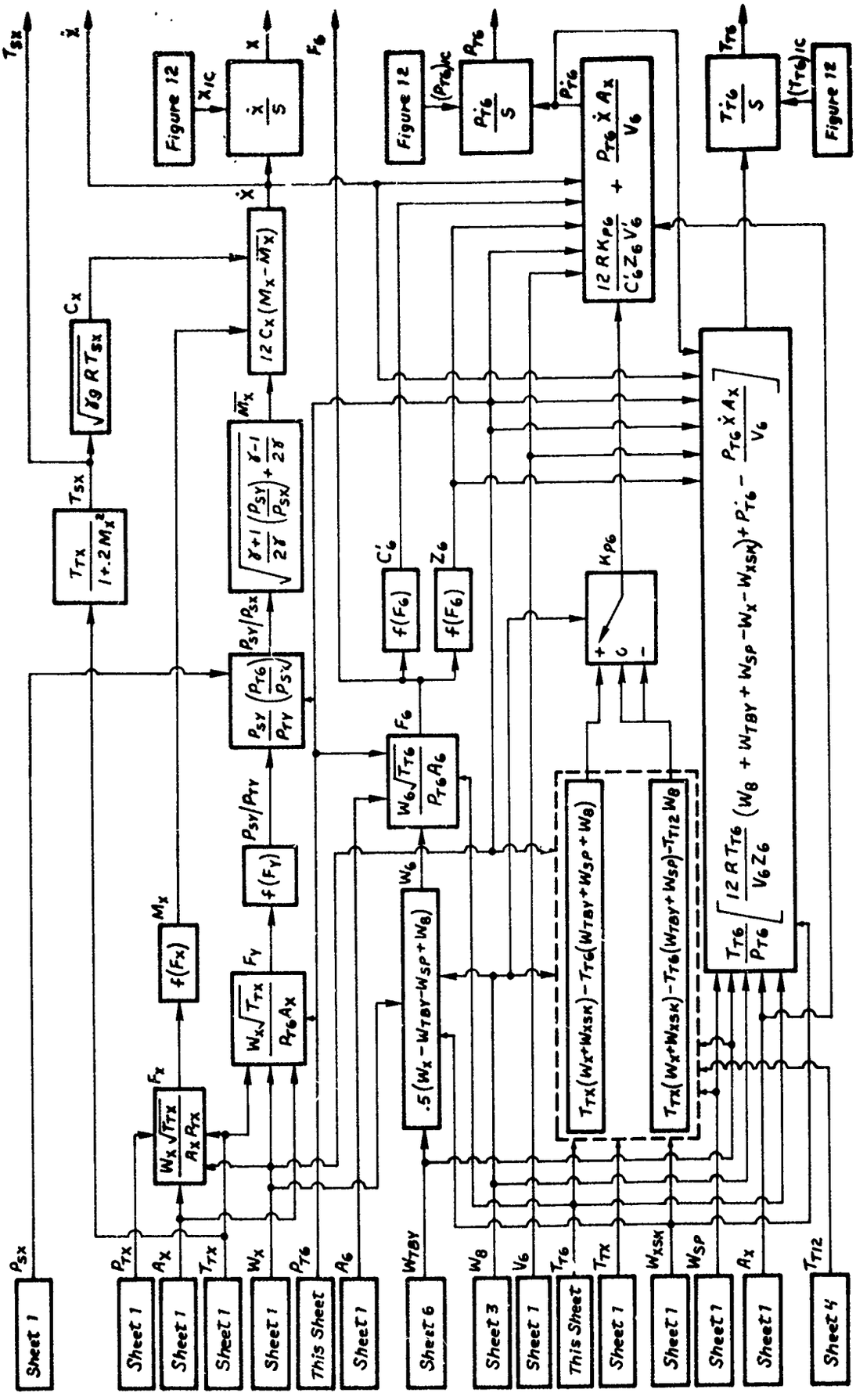

Figure 11 Continued: Sheet 2 of 6

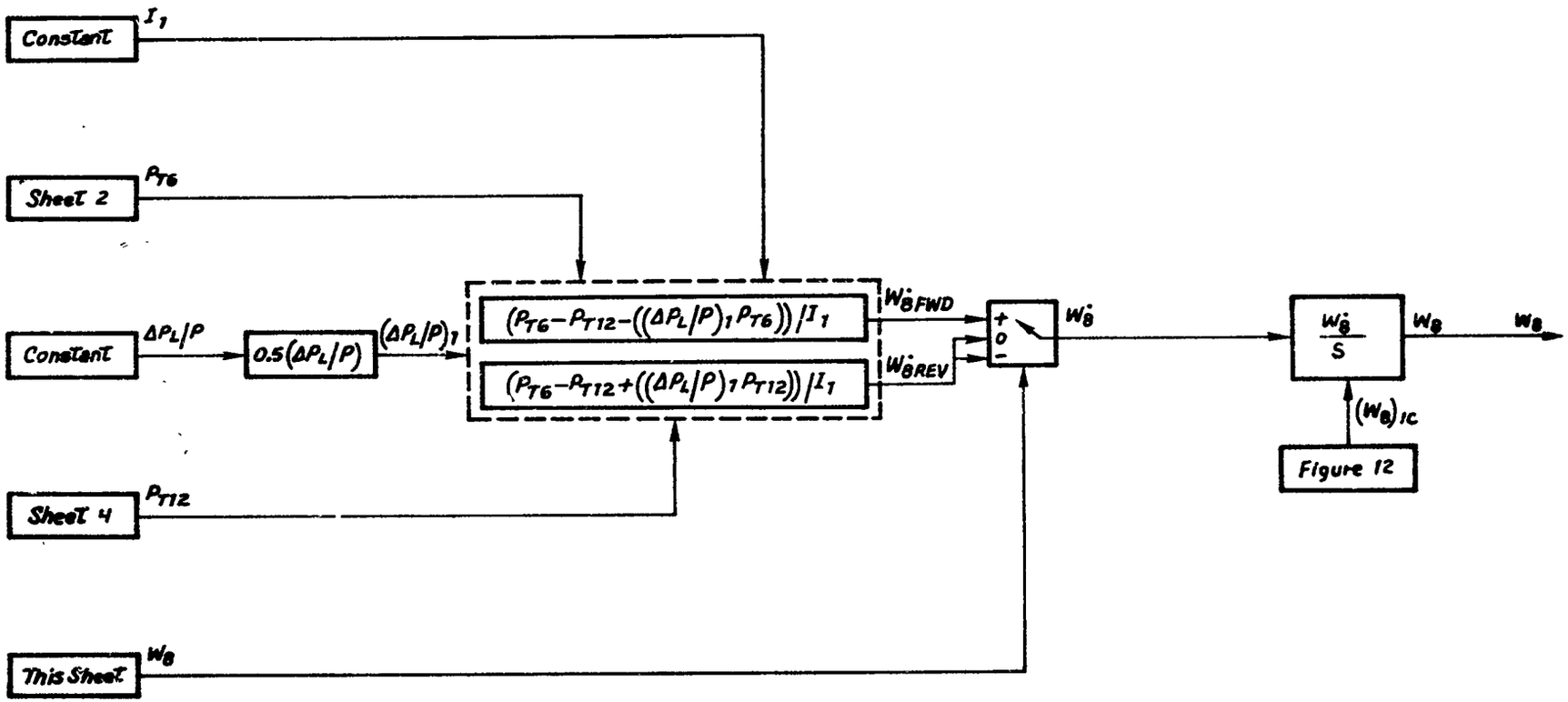

Figure 11 Continued: Sheet 3 of 6

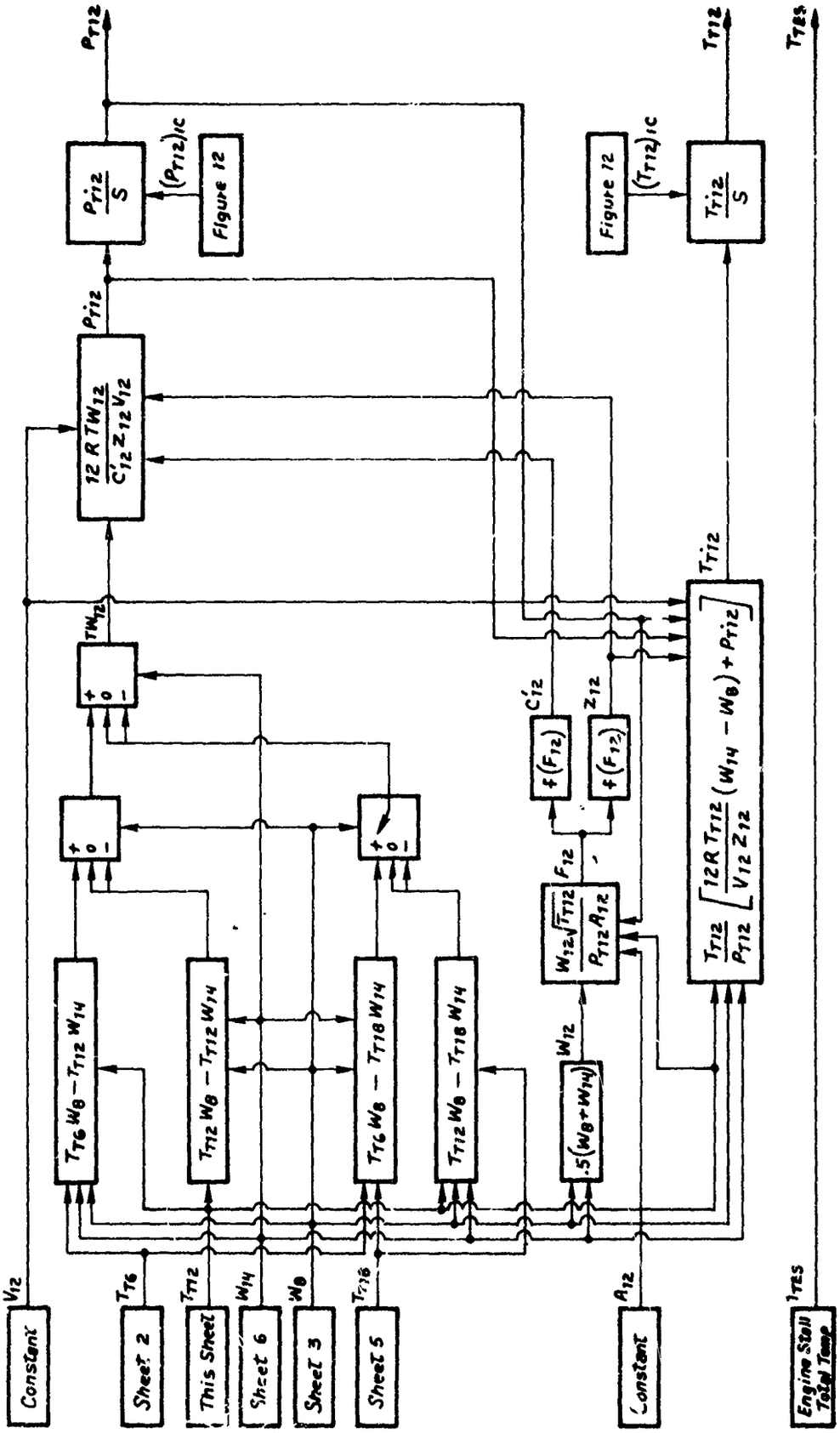

Figure 11 Continued: Sheet 4 of 6

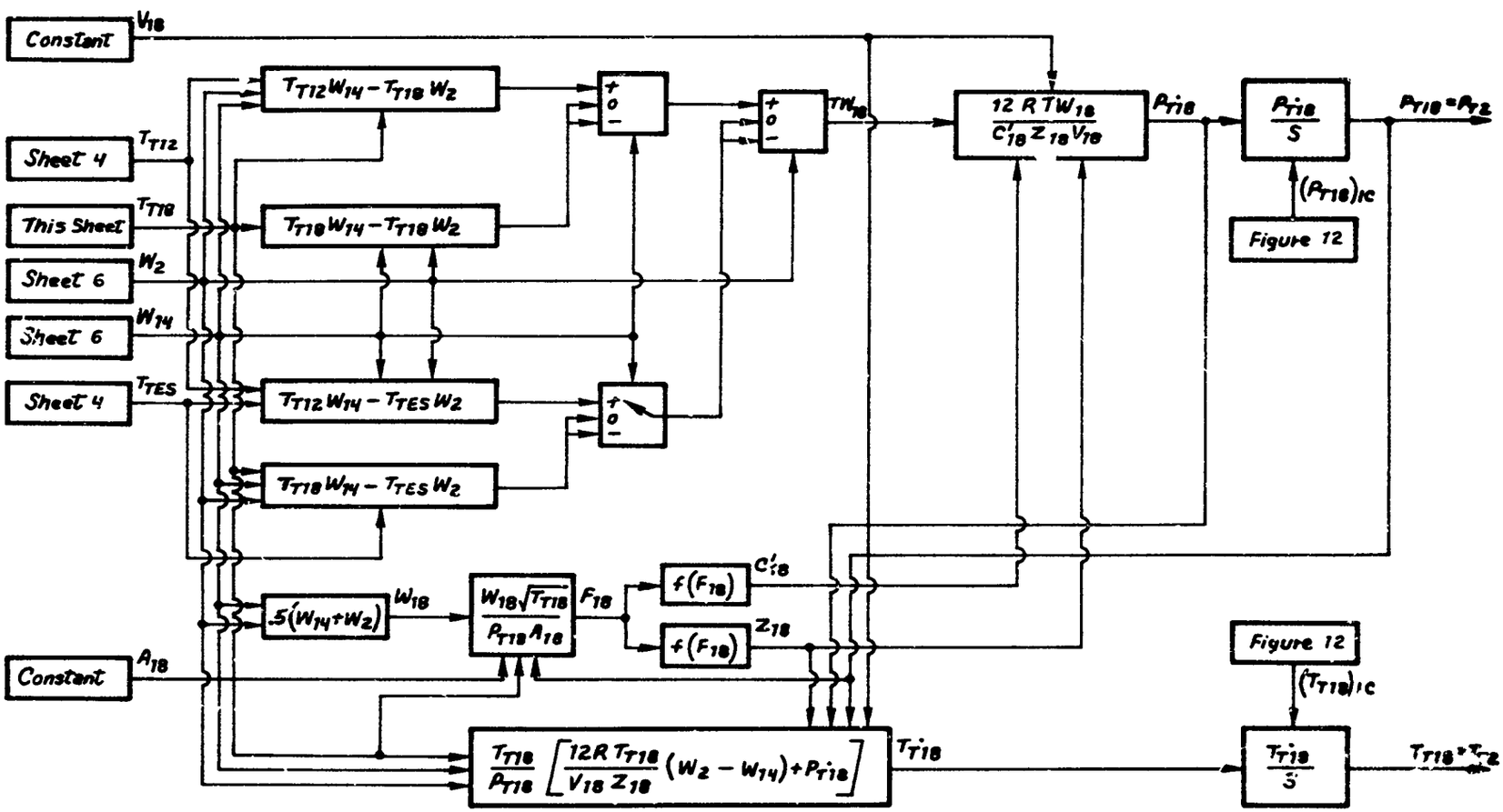

Figure 11 Continued: Sheet 5 of 6

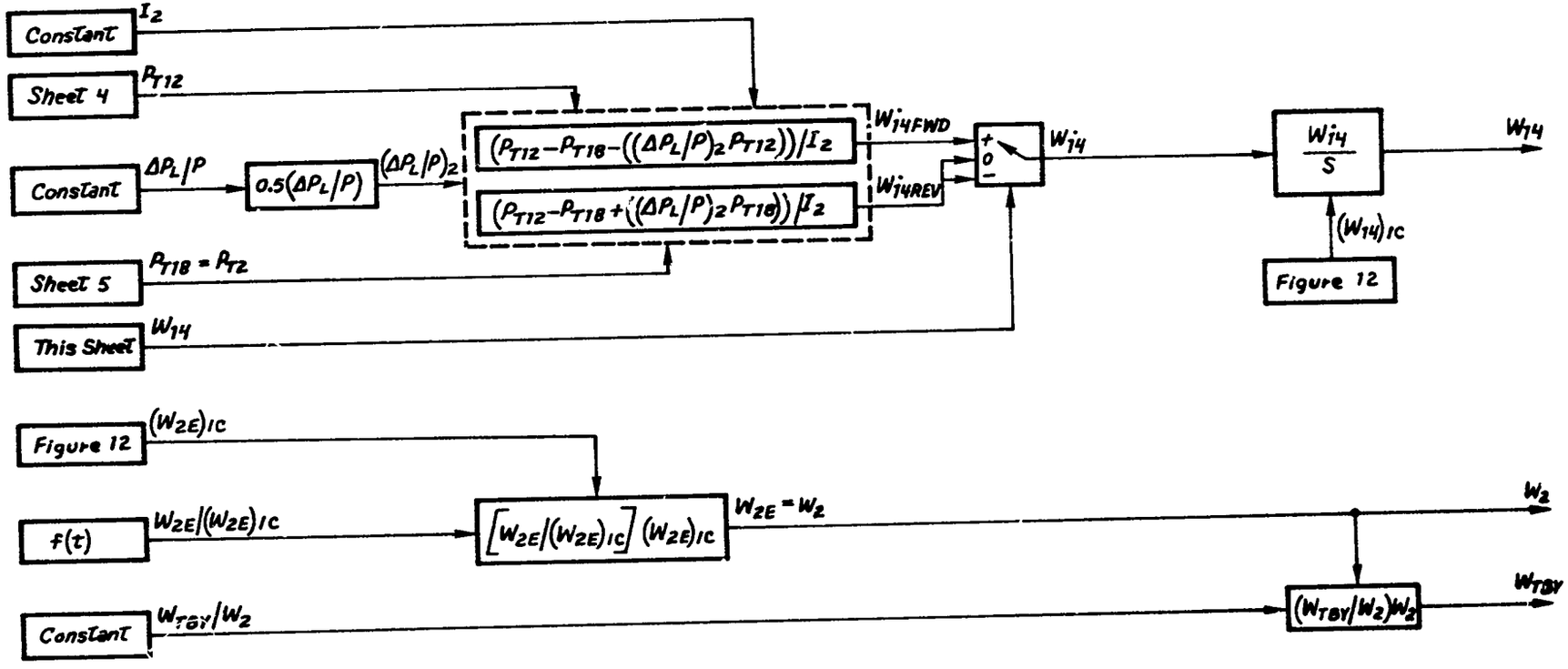

Figure 11 Concluded: Sheet 6 of 6

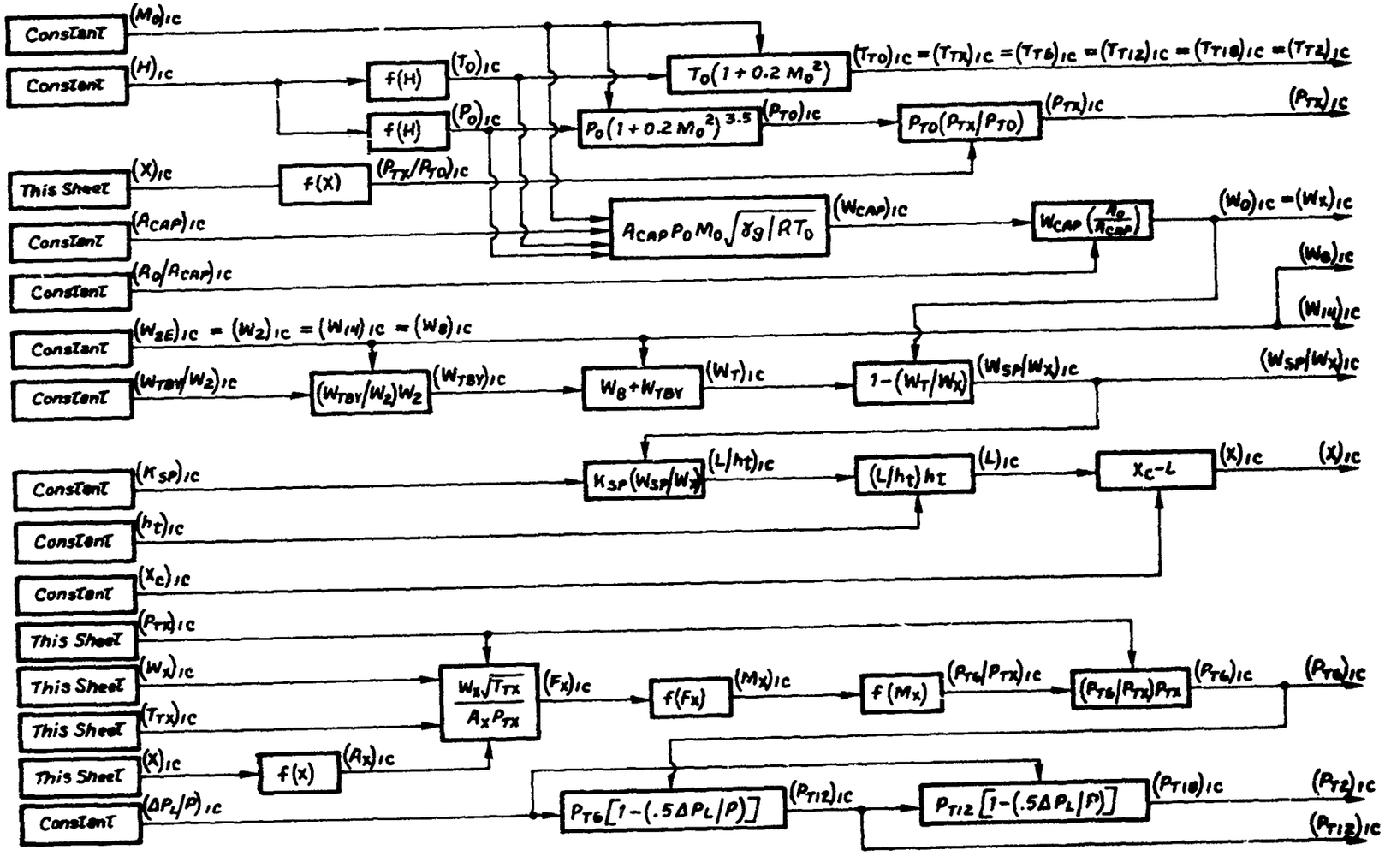

Figure 12. Model 3 - 2DE Three Lump Hammershock Model Block Diagram - Initial Conditions

TABLE III. MODEL 3 - 2DE THREE LUMP HAMMERSHOCK MODEL INPUT DATA

INPUT PARAMETER	FUNCTIONAL RELATION	FIGURE NO.
Inlet Key Operating and Geometric Parameters		
α	constant	-
β	constant	-
H	constant	-
M_0	constant	-
A_{CAP}	constant	-
A_0/A_{CAP}	constant	-
α_{R2}	constant	-
W_B/W_2	constant	-
$\Delta P_L/P$	constant	-
K_{SP}	constant	-
$(W_{RATE}/W_{2E})^*$	f(t)	24(a)
P_{TX}/P_{T0}	f(X)	22(a)
A_X	f(X)	22(c)
M_{XI}	$f(F_X \cdot \sqrt{R})$	13(n)
T_{0STD}	f(H)	-
P_{0STD}	f(H)	-
P_{SY}/P_{TY}	$f(F_Y)$	13(p)
Scale	constant	-
Lumped Volume Parameters		
$(P_{T6}/P_{TX})_{IC}$	$f(M_X)$	13(o)
A_{12}	constant	-
A_{18}	constant	-
X_8	constant	-
Vol_6	f(X)	22(b)
Vol_{12}	constant	-
Vol_{18}	constant	-
I_1	constant	-
I_2	constant	-
Z_6, Z_{12}, Z_{18}	$f(F_6)$, $f(F_{12})$, $f(F_{18})$	13(r)
C'_6, C'_{12}, C'_{18}	$f(F_6)$, $f(F_{12})$, $f(F_{18})$	13(q)
Engine Parameters		
$(W_{2E})_{IC}$	constant	-

*The hammershock input transient profile

SECTION IV

SIMULATION RUNS

Typical external and internal transients, important with respect to advanced fighter aircraft air induction systems, vary considerably in the rates, total amplitudes and the total time spans over which they act. In selecting the transients for the simulation runs, an attempt has been made to cover a wide range of input transients. This section describes the dynamic response of the full scale 2DM and 2DE air induction systems to the following set of typical transients.

2DM air induction system:	Gust
	Throttle Burst
	Buzz
	Hammershock
2DE air induction system:	Afterburner Blowout
	Angle of Attack
	Buzz
	Hammershock

The output data presented was plotted automatically at the end of each simulation run using IBM 360 on-line plotting capability.

2DM AIR INDUCTION SYSTEM

Input data for the program, developed for the 2DM air induction system model described in detail in Volume I of this report, are presented in Figure 13. Since the full-scale air induction system is to be simulated in the program, multipliers are used throughout the program to scale up the 1/10 scale model data of Figure 13. Only those figures requiring an explanation are discussed below.

Discussion of Input Data

In the triple oblique shock 2D mixed compression inlet, the local (M_L) and ramp (M_R) Mach numbers are obtained from Figures 13(a) and 13(b), respectively. M_L is presented as a function of M_0 and $(\alpha + \alpha_{R1})$ [where the first ramp angle

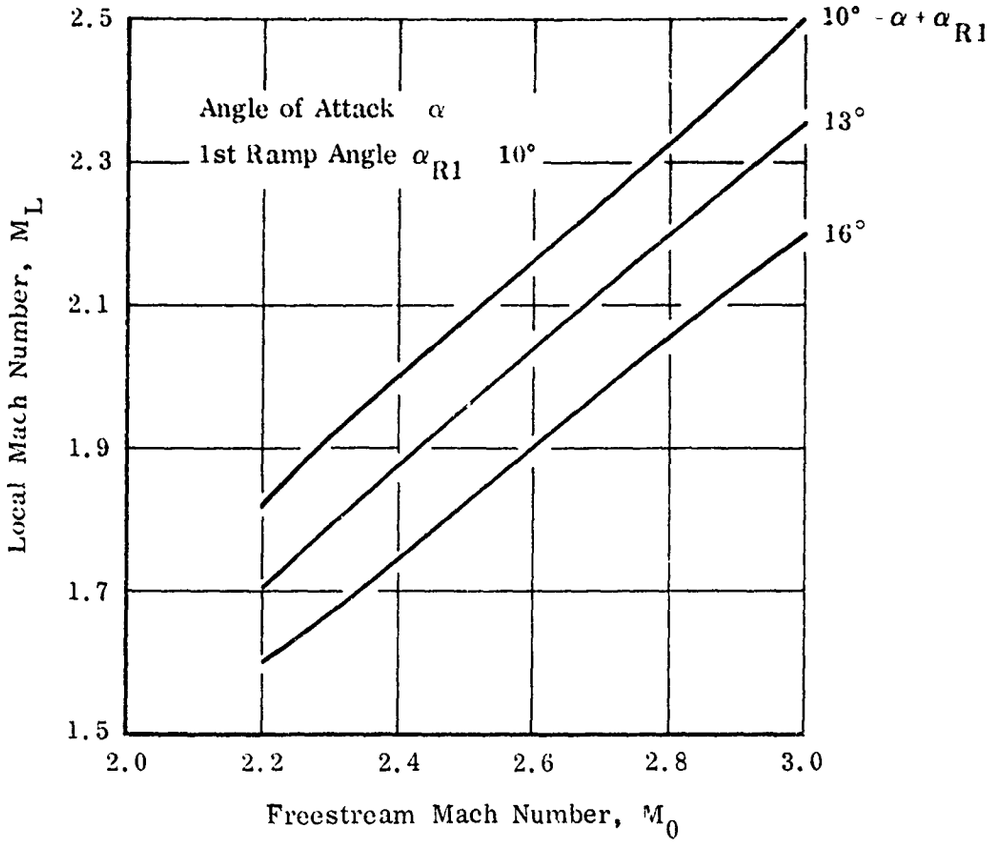

(a) $M_L = f(M_0, \alpha)$

Figure 13. 2DM Air Induction System Input Data

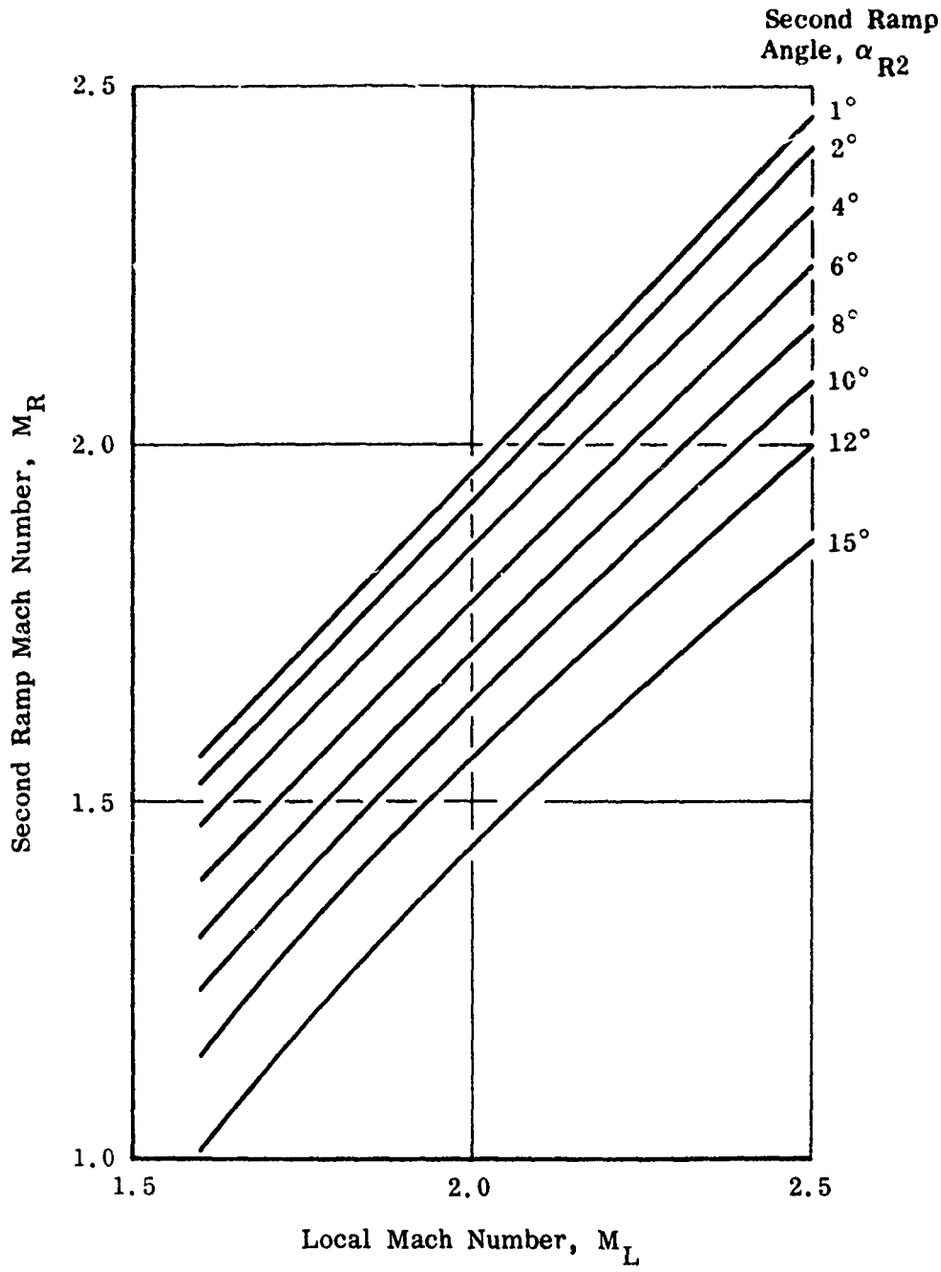

(b) $M_R = f(M_L, \alpha_{R2})$

Figure 13 Continued

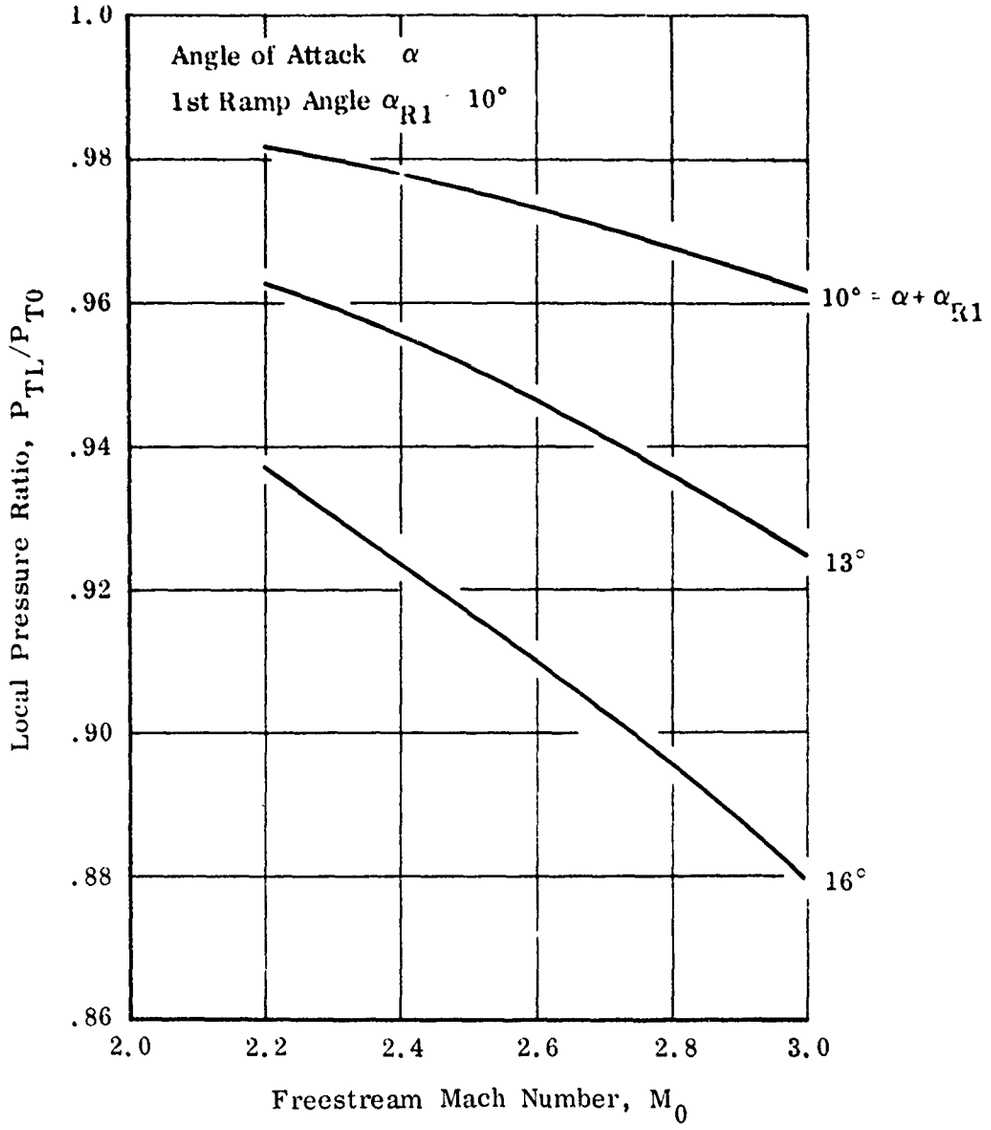

(c) $P_{TL}/P_{T0} = f(M_0, \alpha)$

Figure 13 Continued

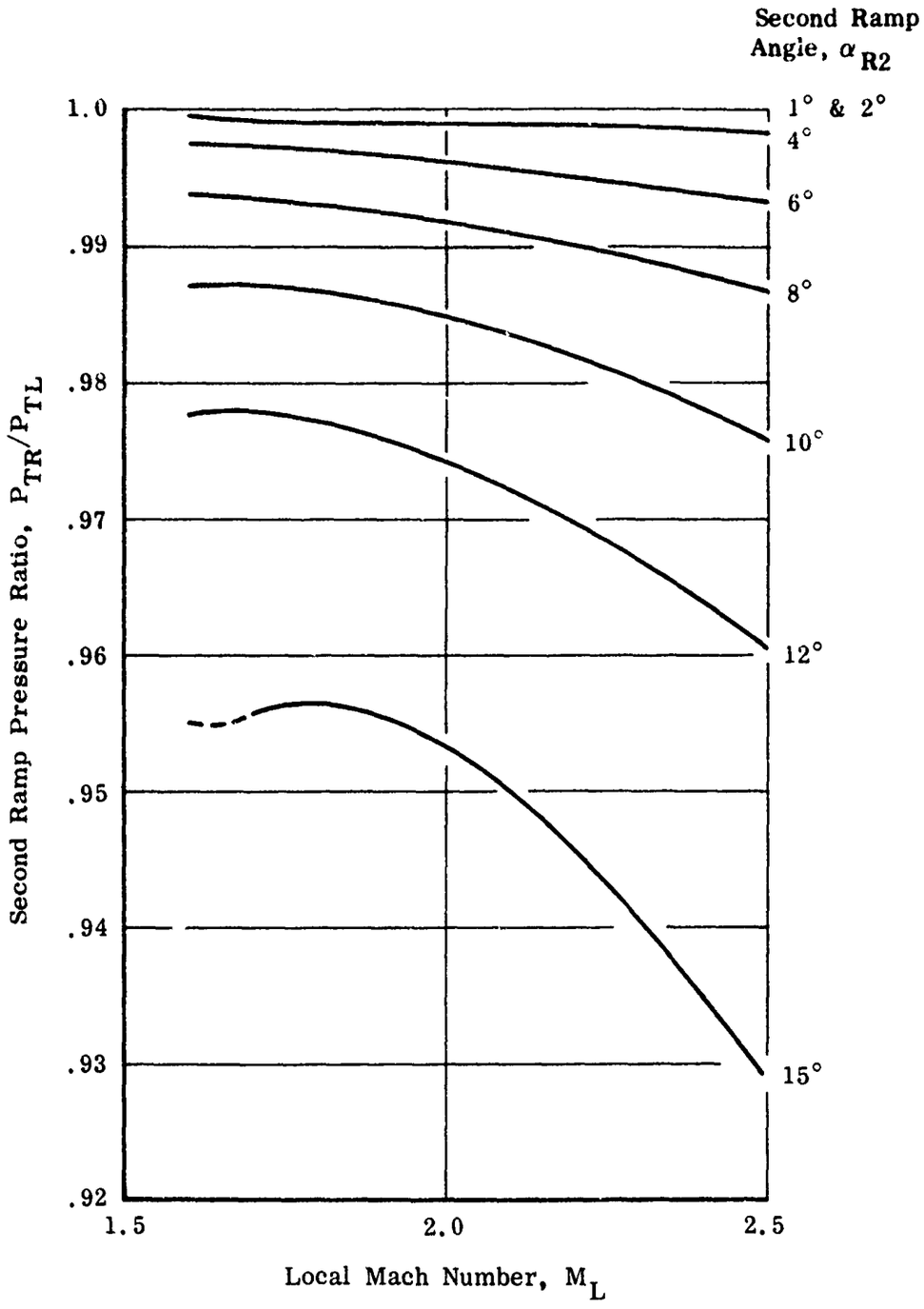

(d) $P_{TR}/P_{TL} = f(M_L, \alpha_{R2})$

Figure 13 Continued

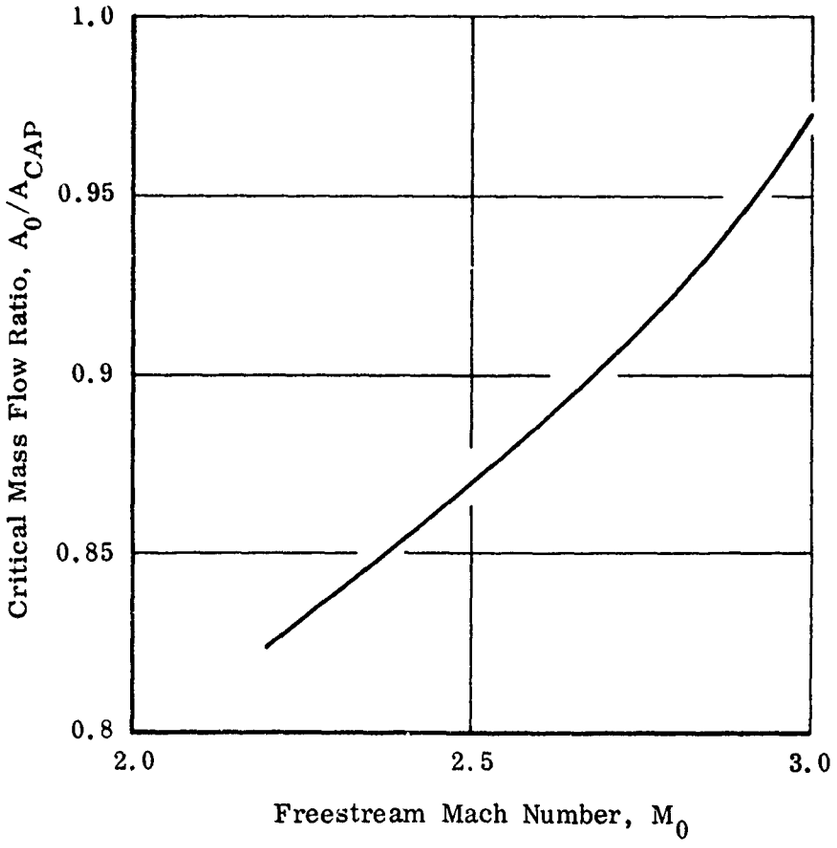

(e) $A_0/A_{CAP} = f(M_0)$

Figure 13 Continued

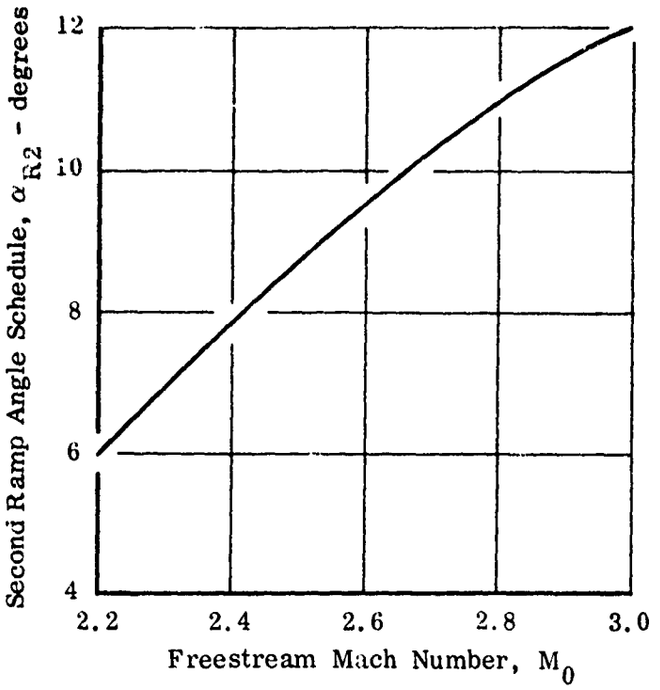

(f) $\alpha_{R2} = f(M_0)$

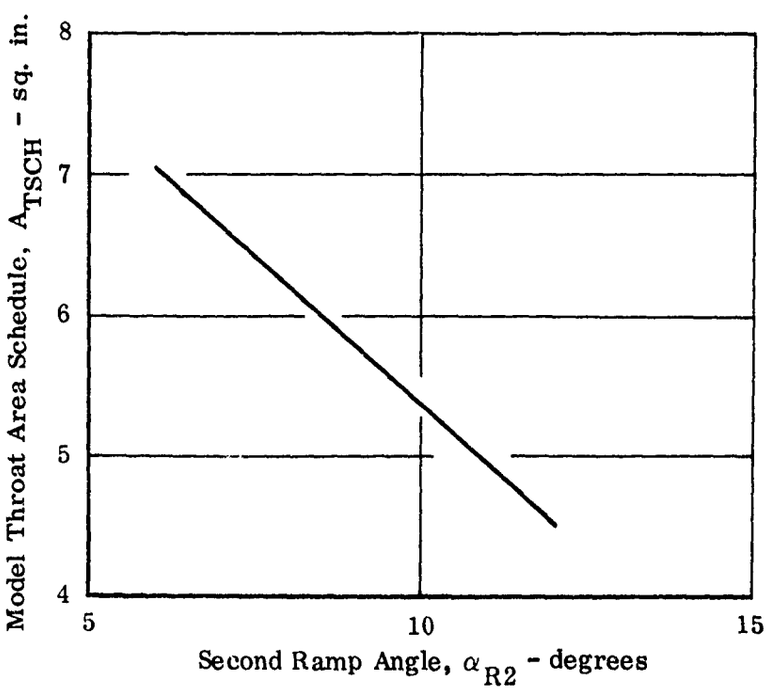

(g) $A_{TSCH} = f(\alpha_{R2})$

Figure 13 Continued

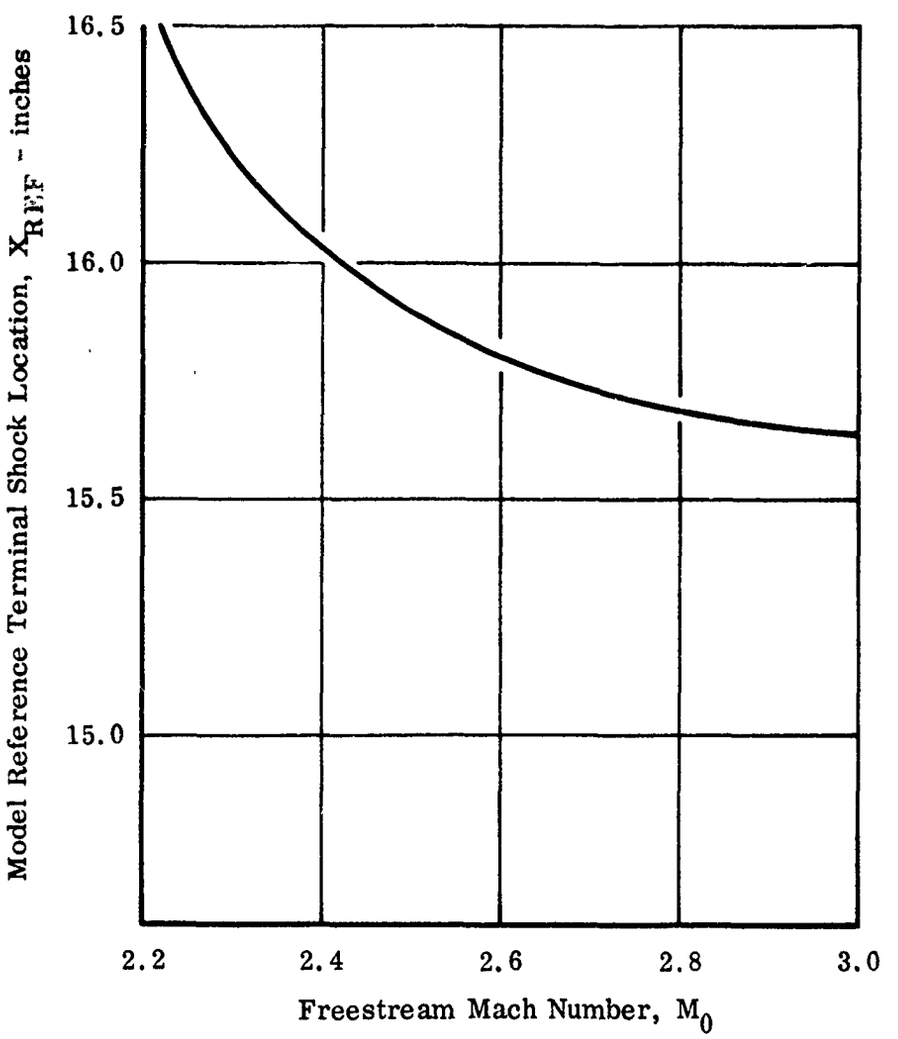

(h) $X_{REF} = f(M_0)$

Figure 13 Continued

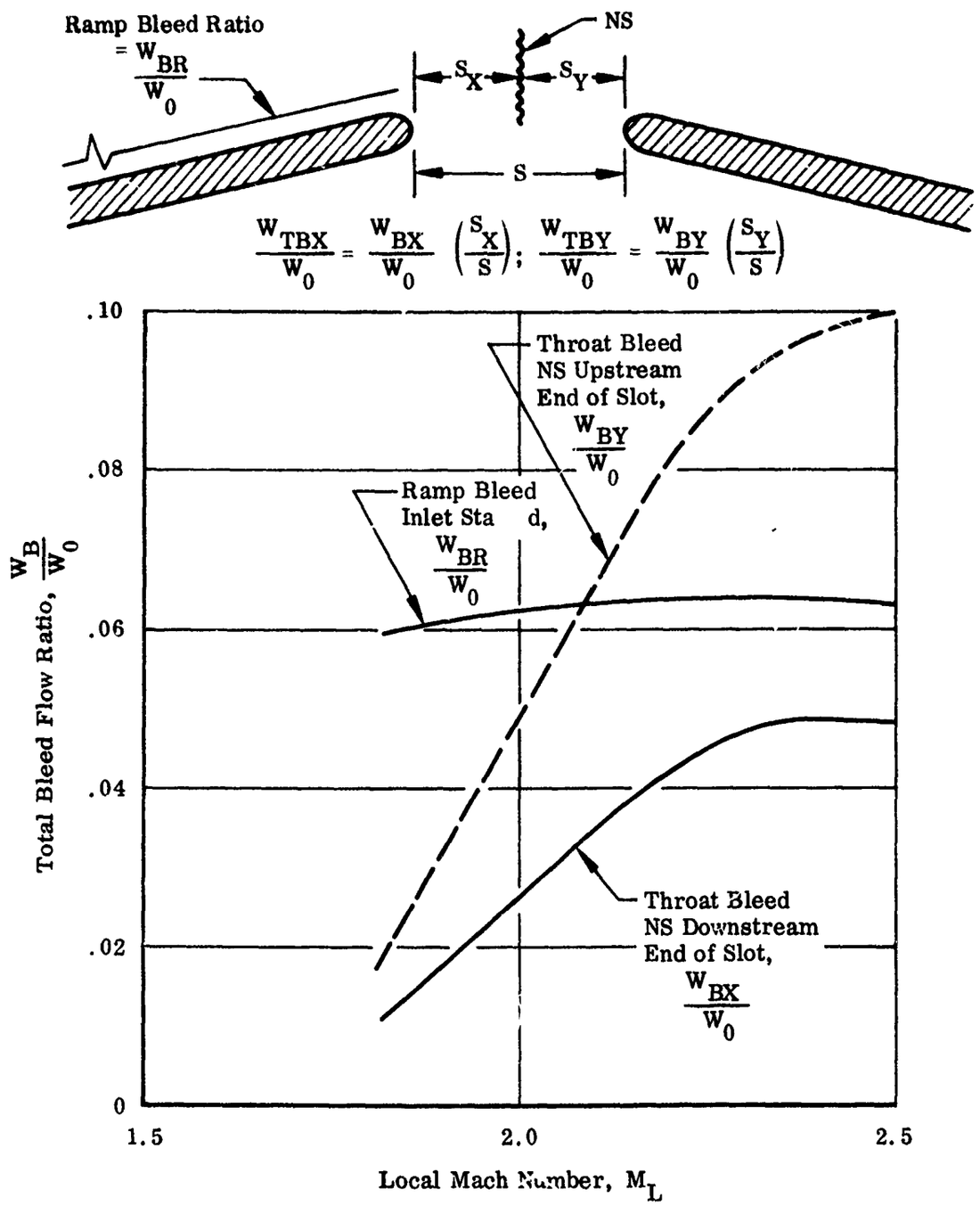

(i) $\frac{W_B}{W_0} = f(M_L)$

Figure 13 Continued

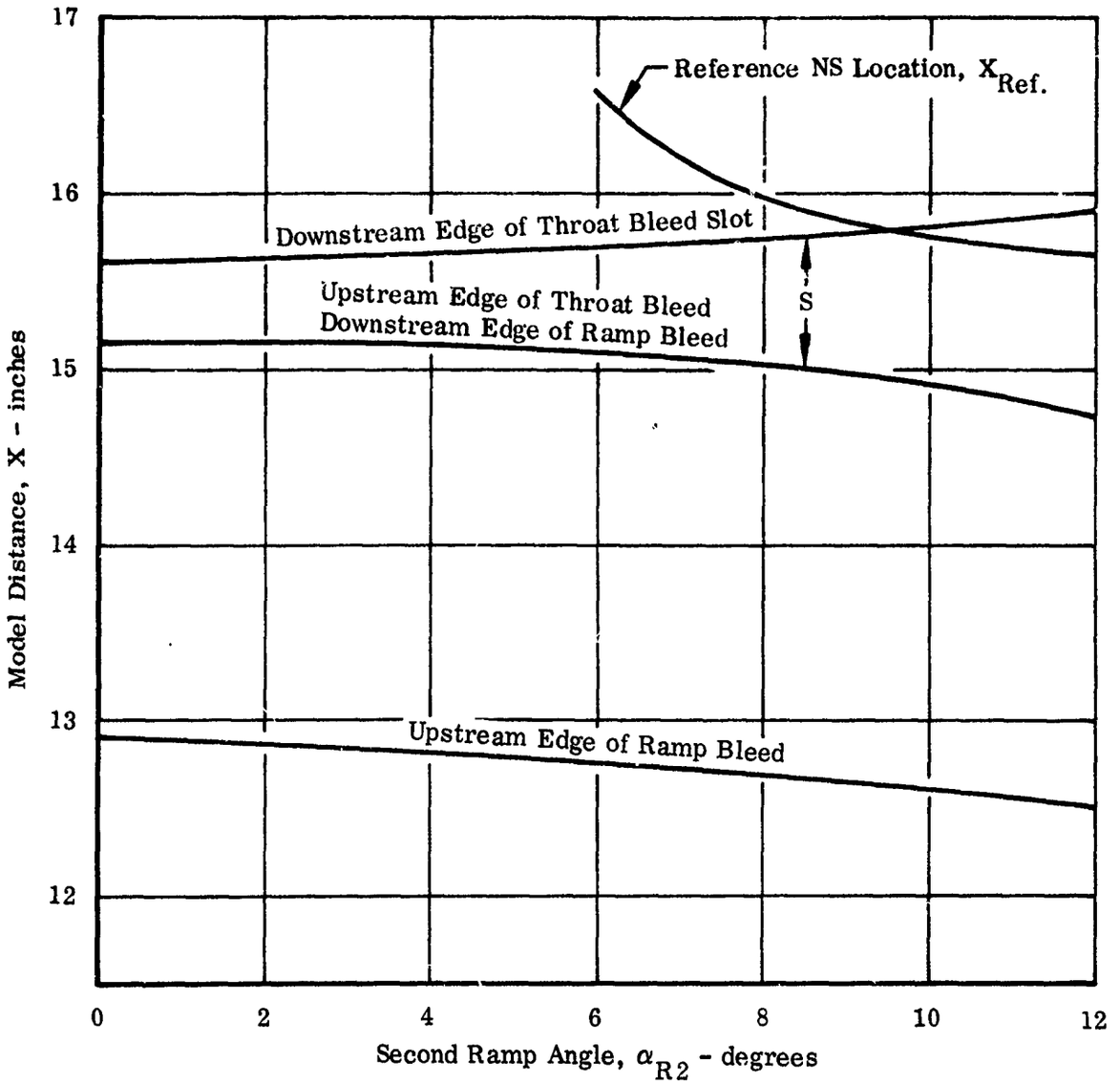

(j) $S = f(\alpha_{R2})$

Figure 13 Continued

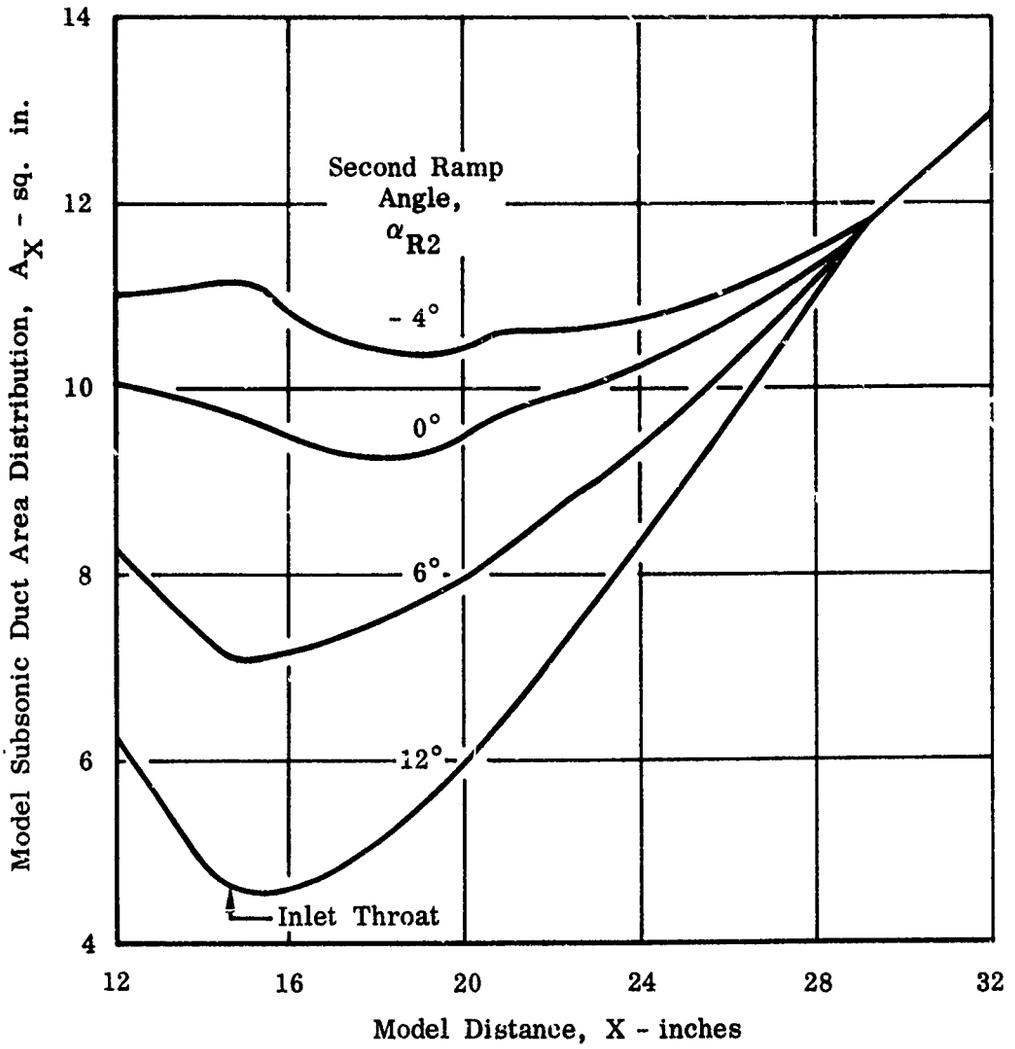

(k) $A_X = f(X, \alpha_{R2})$

Figure 13 Continued

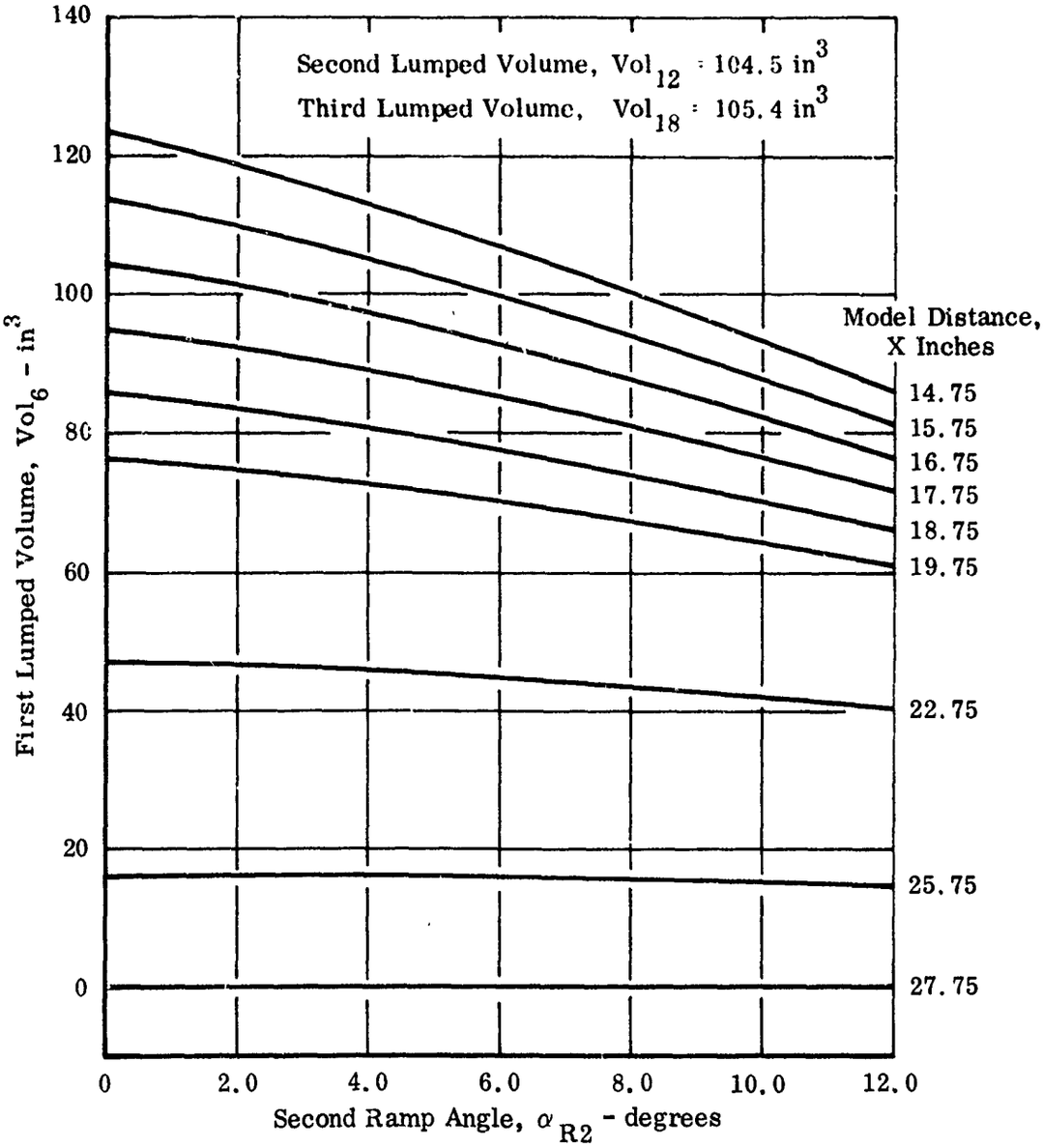

(l) $Vol_6 = f(\alpha_{R2}, X)$

Figure 13 Continued

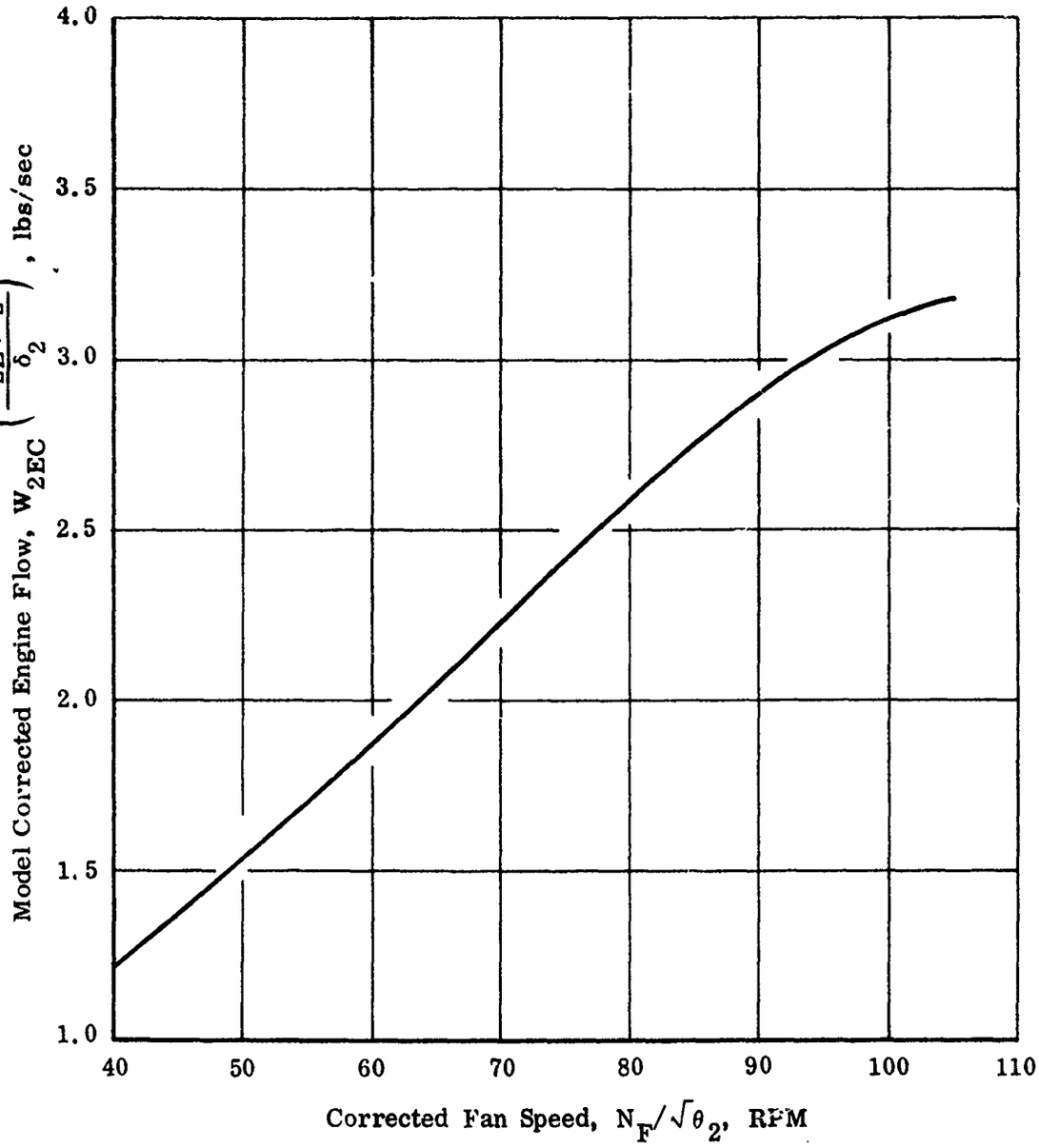

(m) $W_{2EC} = f\ (N_F/\sqrt{\theta_2})$

Figure 13 Continued

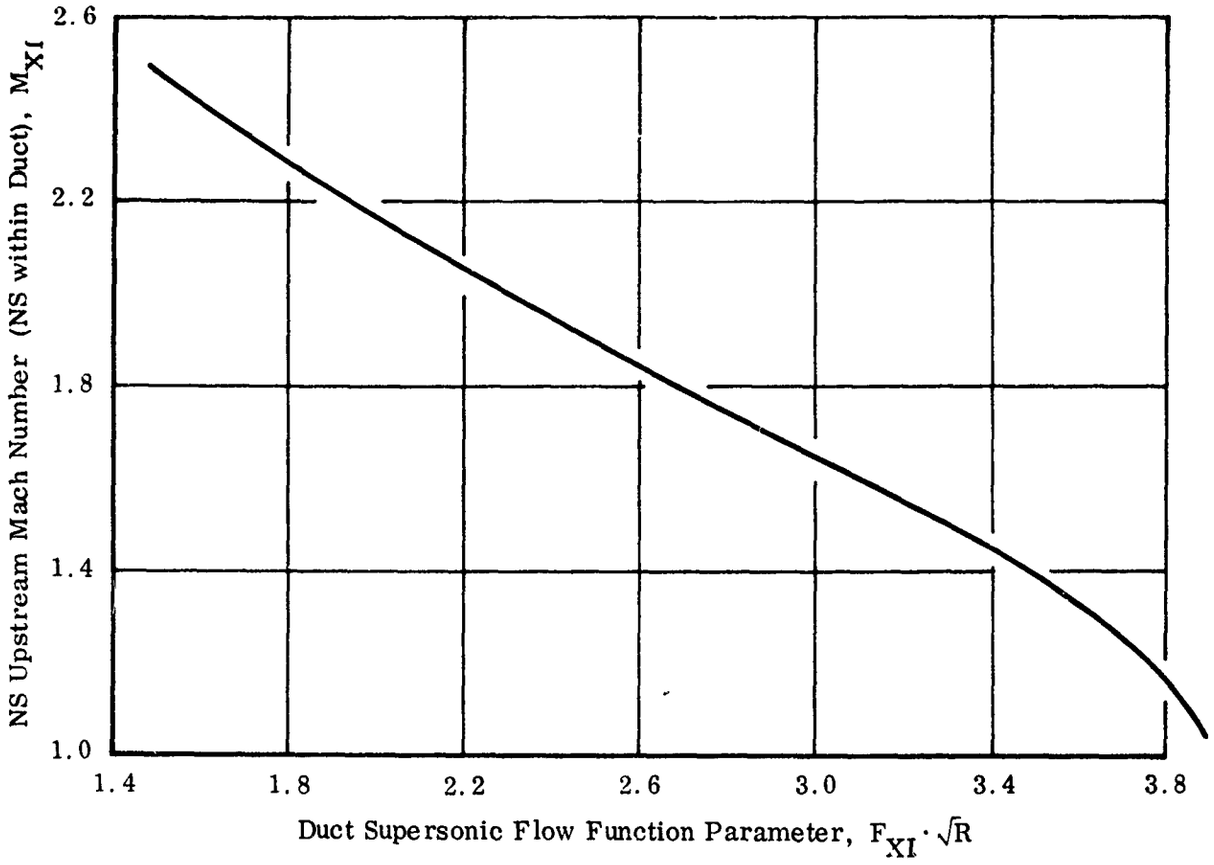

(n) $M_{XI} = f\ (F_{XI} \cdot \sqrt{R})$

Figure 13 Continued

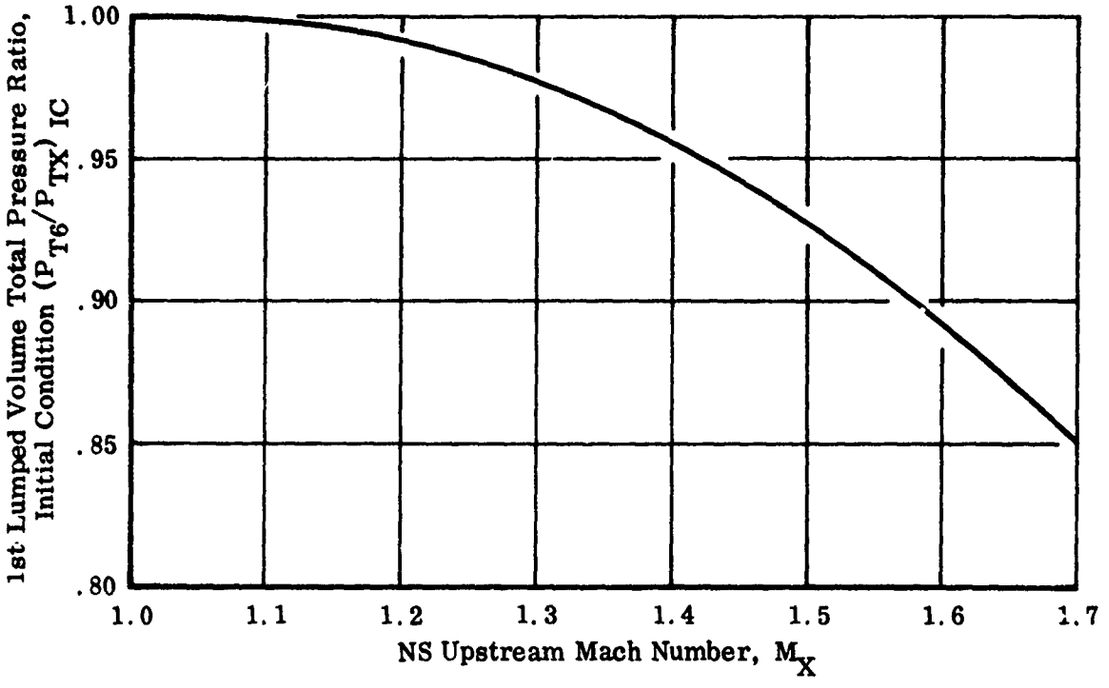

$$(o)\ \left(\frac{P_{T6}}{P_{TX}}\right)_{IC} = f(M_X)$$

Figure 13 Continued

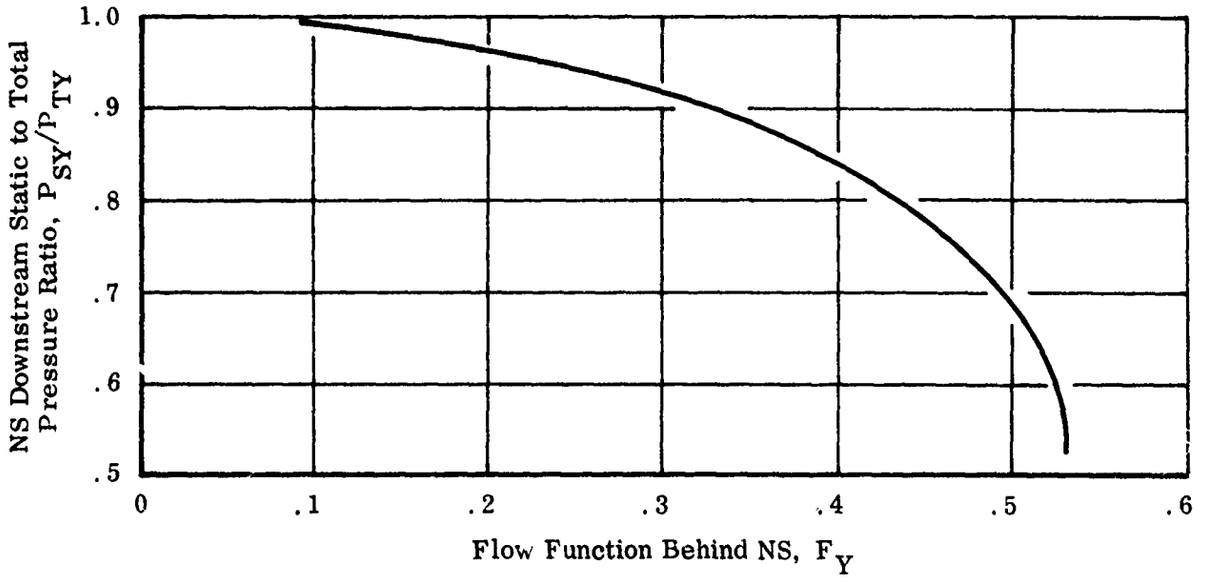

$$(p)\ \left(\frac{P_{SY}}{P_{TY}}\right) = f\ (F_Y)$$

Figure 13 Continued

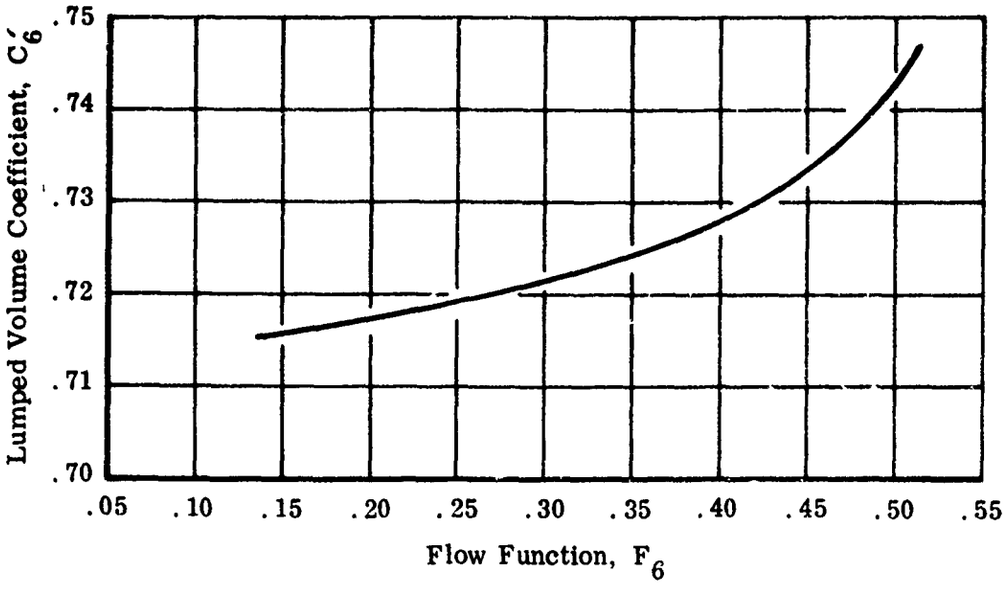

(q) $C_6' = f(F_6)$

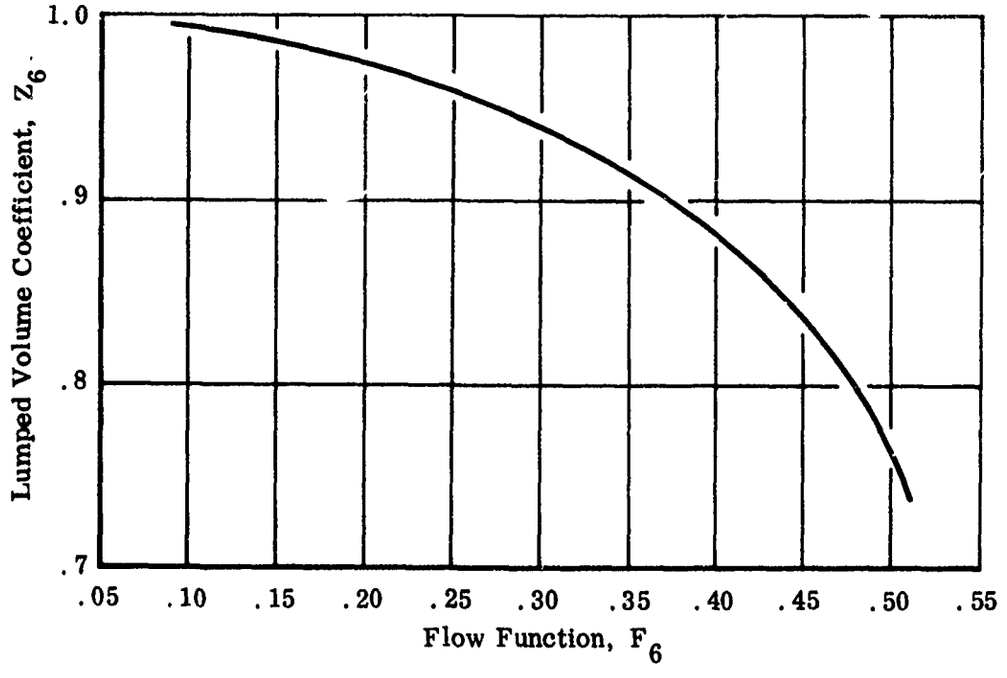

(r) $Z_6 = f(F_6)$

Figure 13 Concluded

α_{R1} is fixed at 10° | and M_R is presented as a function of the second ramp angle α_{R2} and M_L. The Mach number M_X behind the third oblique shock generated by the cowl lip is calculated from Figure 13(b) by entering it with the cowl ramp angle with respect to local flow (α_{R2} + 3°) and the corresponding Mach number M_R. The total pressure recovery P_{TX}/P_{T0} is obtained similarly in three steps by entering Figure 13(c) to obtain P_{TL}/P_{T0} and entering Figure 13(d) to obtain P_{TR}/P_{TL} and P_{TX}/P_{TR}.

The critical mass flow ratio (A_0/A_{CAP}) is presented in Figure 13(e) as a function of M_0 and is used to calculate the critical flow (W_0) entering the inlet during mixed mode operation.

Figure 13(f) shows the second ramp angle schedule α_{R2} as a function of M_0. This schedule is followed to maintain inlet operation at optimum performance as M_0 increases. The geometric throat area schedule is obtained from the α_{R2} schedule and is shown in Figure 13(g). The desired NS location as a function of M_0 is presented in Figure 13(h). The NS should be as close to the throat as possible yet with enough tolerance to avoid being disgorged due to a mild transient.

Figure 13(i) gives the total bleed flow ratio W_B/W_0 as a function of M_L for (a) ramp bleed inlet started, (b) throat bleed with NS located upstream end of slot, and (c) throat bleed with NS located downstream end of slot. Since (b) and (c) specify the total bleed flow when the NS is located at the two ends of the slot, at any intermediate NS position, the upstream (W_{TBX}) and downstream (W_{TBY}) bleed flows are computed as shown in the sketch in Figure 13(i).

The effect of second ramp movement on the boundary layer bleed slot geometry is shown in Figure 13(j). The slot increases in length(S) as α_{R2} increases, with the ramp bleed length staying relatively constant. The NS reference position, with respect to the slot, is superimposed on the figure in the α_{R2} range (6 degrees to 12 degrees) for inlet mixed mode operation.

Figures 13(k) and 13 (l) show the subsonic duct area and volume (Vol_6) distribution as a function of α_{R2} and X. Vol_{12} and Vol_{18} are assumed to be constant since their boundaries are fixed. Engine corrected flow (W_{2EC}) as a function of corrected fan speed ($N_F/\sqrt{\theta_2}$) is presented in Figure 13(m) for the model inlet.

Gust Transient (Model 1, Deck 1)

The following example is used to simulate the dynamic response of the full scale 2DM air induction system to a gust transient.

Transient:	A typical gust (changes in freestream velocity) initiated at 0.2 second and lasting for 0.2 second
Mach Number:	3.0
Altitude:	61,000 feet
Angle of Attack:	0

Control logic is provided in this example for two types of unstarts: choked throat unstart and the unstart caused by disgorgement of the normal shock (NS) when the latter reaches the unstable position just upstream of the throat. The inlet throat area (A_T) is programmed to open if the throat tends to choke and a variable area bypass is used to control NS motion. At the initial condition, the bypass area is sized such that the NS is located at the desired supercritical location.

Discussion of Output Data. Output data for this transient are presented in Figure 14. The imposed gust transient is represented by reduction in velocity starting at 0.2 second and lasting until 0.4 second [(Figure 14(a)]. The freestream static pressure (P_0) is held constant during the simulation. Hence, this transient essentially involves perturbation in freestream total pressure (P_{T0}) corresponding to the reduction in M_0 as shown in the same figure. The run is continued to 0.7 second to obtain complete convergence to initial conditions. As discussed before, two independent types of unstarts can occur when a gust transient is imposed on the 2DM air induction system. The NS unstart is prevented by the bypass area (A_{BY}) control and the choked throat unstart is prevented by the throat area (A_T) control. These are discussed separately below.

The effect of the gust transient on the NS position, and the action of the bypass area A_{BY} to prevent unstarting, is discussed first using Figures 14(b) and 14(c). Initially, the NS is located [Figure 14(b)] 8.7 inches downstream of the throat. Reduction in M_0 at 0.2 second reduces the NS upstream Mach number (M_X) along with a corresponding reduction in total pressure. This reduction in M_X and total pressure causes the NS to move upstream to a smaller area (A_X). Figure 14(c) shows that the bypass starts to open in response to the upstream movement of the NS, thus increasing the bypass outflow to the point where its effect becomes strong enough to change the direction of NS movement. This change in direction occurs at 0.275 second when X = 154.5 inches, thus indicating that an unstart has been avoided since

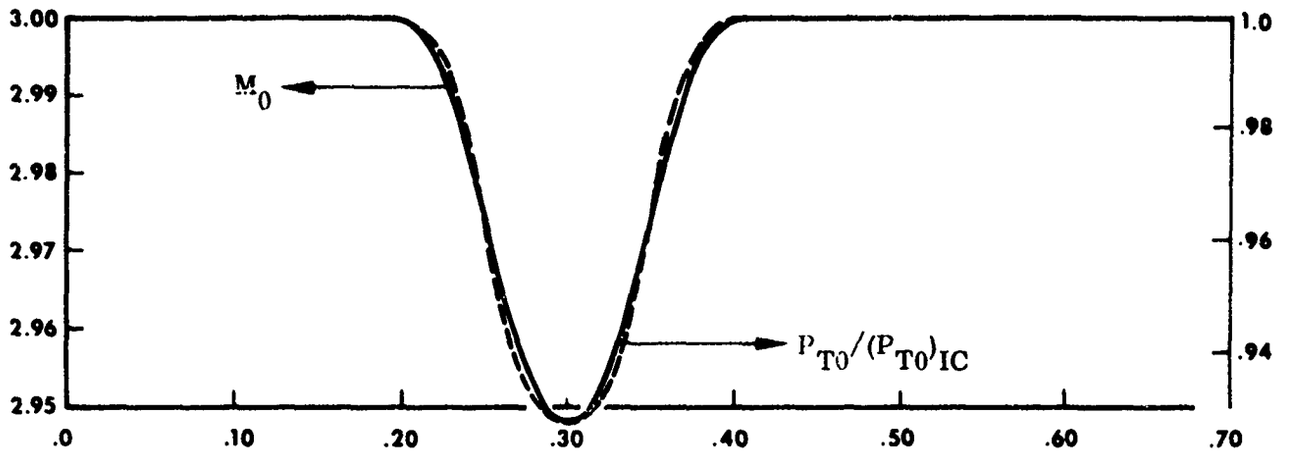

(a) Input Transient, M_0 vs Time with Corresponding $P_{T0}/(P_{T0})_{IC}$ vs Time

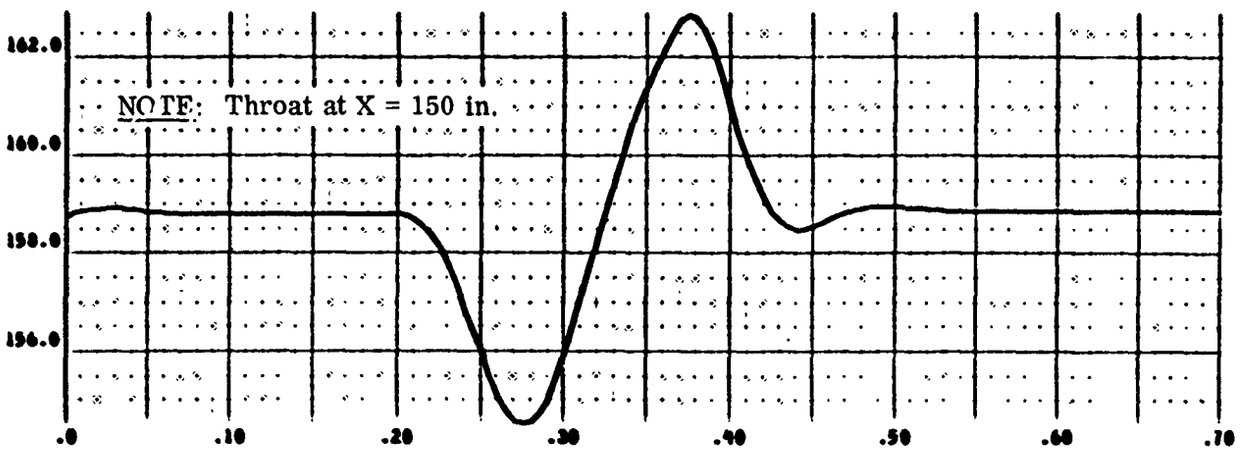

(b) X (in) vs Time

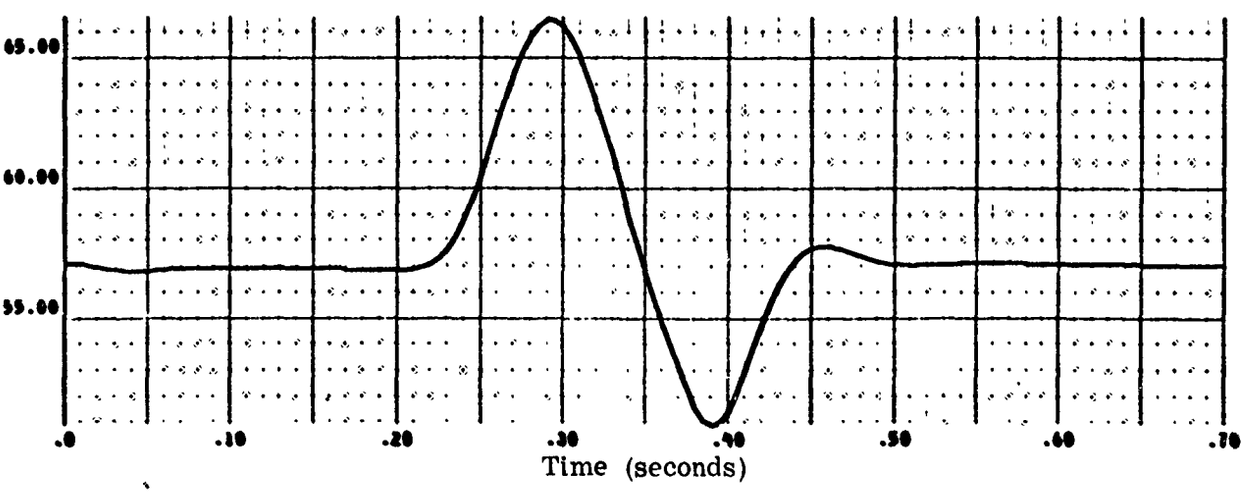

(c) A_{BY} (in^2) vs Time

Figure 14. 2DM Air Induction System Output Data - Gust Transient (Model 1, Deck 1); $M_0 = 3.0$; H = 61000 ft; $\alpha = 0$

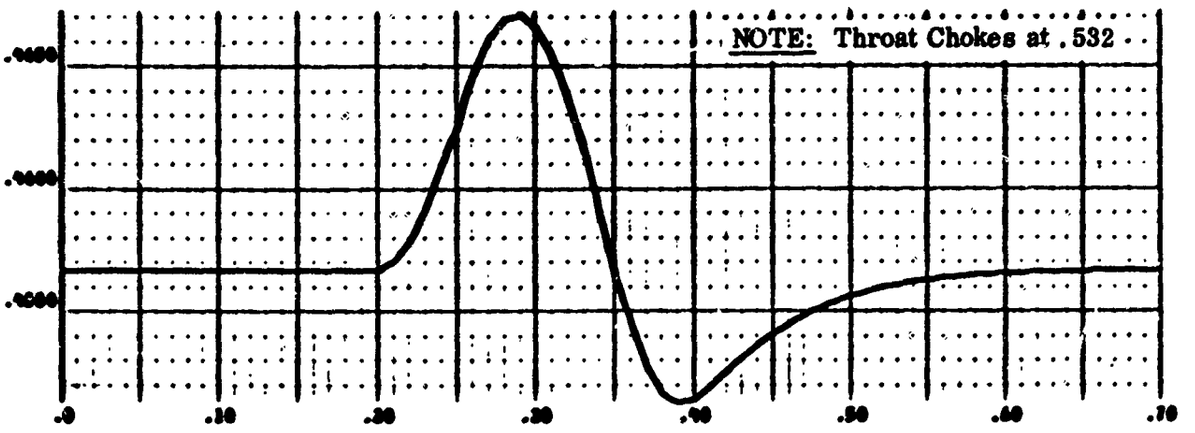

(d) F_T vs Time

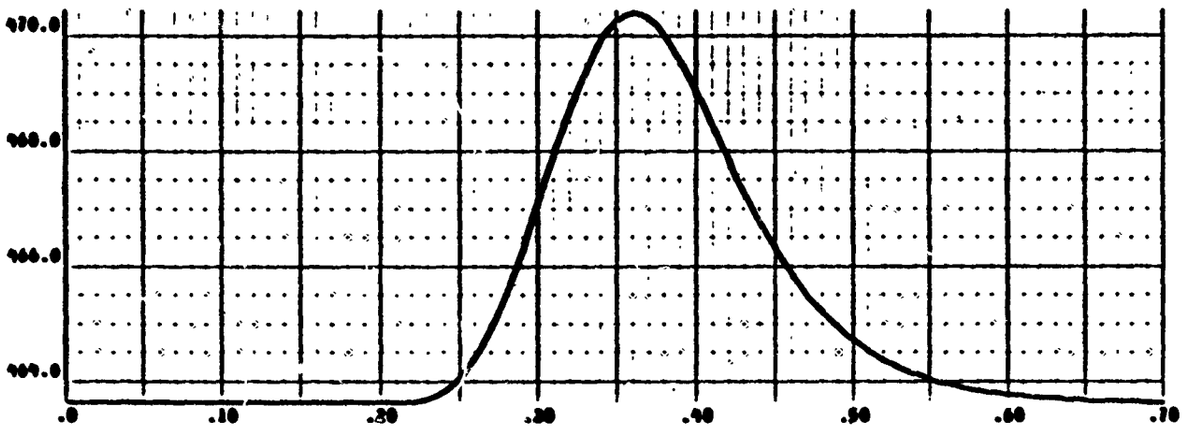

(e) A_T (in^2) vs Time

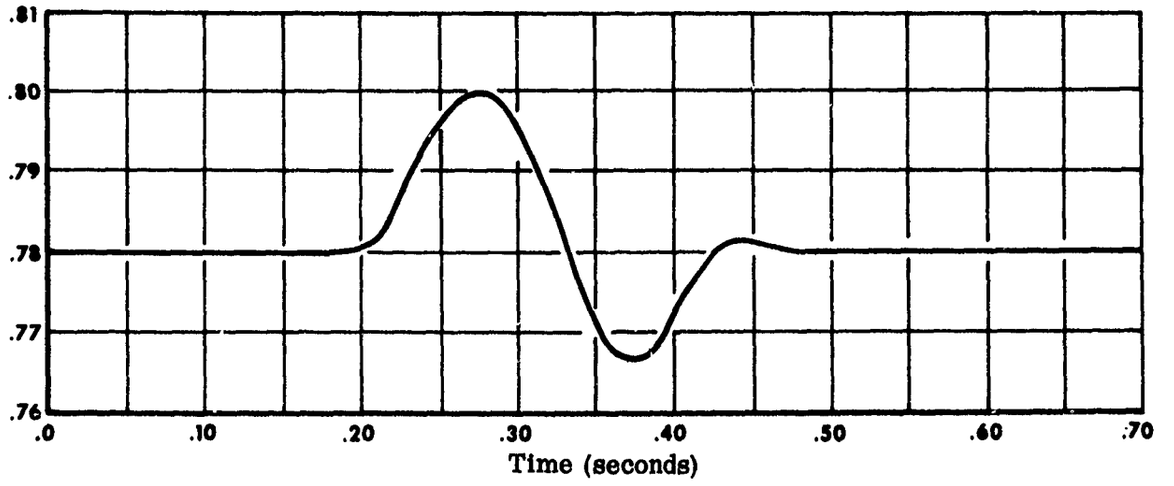

(f) P_{T2}/P_{T0} vs Time

Figure 14 Concluded

the NS is still downstream of the throat (X_T 150 inches). Having accomplished its task, the bypass then starts to close and since the NS is still moving under the influence of the transient, both X and A_{BY} tend to overshoot their initial locations. However, once the gust is over (at 0.4 second) the initial values are reached very rapidly. The bypass control logic error signal is a function not only of the position error (X_{REF}-X), but also of the rate at which the deviation from X_{REF} occurs and also the rate at which the A_{BY} opens or closes.

The throat area (A_T) response to avoid choked throat unstarting is now discussed using Figures 14(d) and 14(e). Reduction in M_0 causes a corresponding reduction in the total pressure. The result is that the throat flow function F_T ($W_T\sqrt{T_{TX}}/A_T P_{TX}$), initially corresponding to a throat Mach number of 1.5, tends to increase towards the choking value (0.532). The throat area control is programmed to try and hold the input throat area schedule A_{TSCH} [(Figure 13(g)]. Since this A_{TSCH} defines the desired F_T as a function of M_0, any deviation from this desired value introduces an error signal (A_{TSCH} -A_T) into the system which activates the throat area control. In this particular example, F_T increases and A_T [Figure 14(e)] responds by opening until F_T returns to its initial value at 0.35 secord. Its task accomplished, A_T then returns to its own initial value.

Figure 14(f) shows the instantaneous pressure recovery, P_{T2}/P_{T0}, during the transient. As the NS moves upstream during the initial phase of the transient (from 0.2 to 0.3 second), the total pressure loss across the progressively weakening NS decreases, hence, improving the overall instantaneous total pressure recovery. As mentioned previously, however, the absolute value of P_{T2} is reduced from the initial condition throughout the transient due to the overriding reduction in P_{T0}. A peak value of P_{T2}/P_{T0} = 0.8 is reached at 0.275 second before the recovery starts to drop again during the second phase of the transient (because the NS changes direction under bypass control) reaching a minimum value of 0.767 at 0.375 second before returning to its initial value.

Throttle Burst Transient (Model 1, Deck 1)

The following example is used to simulate the dynamic response of the full scale 2DM air induction system to a throttle burst transient.

Transient:	Throttle burst input as a ramp signature with percent fan speed increase from 56.5 to 75.5 in a time period of 1.5 seconds

Mach Number:	2.5
Altitude:	61,000 feet
Angle of Attack:	0

Discussion of Output Data. A ramp signature for the percent engine fan speed (N_F) which starts at 0.5 second and lasts for 1.5 seconds is input to simulate the throttle burst [Figure 15(a)]. The effect of this change in speed can be seen in the increase in engine flow demand W_{2E} [Figure 15(b)] during the transient. The effect of the transient can best be seen by observing its effect on the NS position X [Figure 15(e)].

Engine flow can be increased either at a high rate or a low rate. The effect of increasing the engine demand at a high rate is that the flow entering the lumped volume does not instantaneously match the demand at the lumped volume exit. The resulting instantaneous excess of outflow over inflow results in a rapid pressure drop in the lumped volumes and, hence, initially rapid downstream movement of the NS if not compensated for with a rapid response bypass control system. On the other hand, increasing engine demand at a low rate (nearly steady state) has the effect of merely relocating the NS progressively in a new equilibrium position. The effect that dominates NS movement during a transient is, therefore, established by the rate of the input transient. In this example, the input transient is at a relatively low rate with respect to the dynamic response of the air induction system and, therefore, the primary effect is a nearly steady state downstream movement of NS. The downstream movement of the NS, in turn, increases the NS strength and, hence, the total pressure loss across it as it travels downstream. This drop in P_{T2} is presented in Figure 15(d).

At 0.5 second when the transient is initiated, the NS is located just downstream of the throat [at 161 inches, Figure 15(e)] and starts to travel downstream under the influence of the transient. At the same time A_{BY} starts to close [Figure 15(f)] in an effort to return the NS to the throat. The NS, however, continues to travel downstream up to 171 inches because the influence of the input transient is greater than the influence of the closure of A_{BY} during the time period of the input transient. A more rapid closure of A_{BY} would reduce the maximum downstream excursion of the NS. After the input transient is over, the NS rapidly returns to its initial position which is the equilibrium position corresponding to the final value of A_{BY}.

The instantaneous imbalance between inflow [W_8, Figure 15(g)] and outflow [W_{14}, Figure 15(h)] for Vol_{12}, and similarly between inflow (W_{14}) and outflow [W_2, Figure 15(i)] for Vol_{18}, is practically negligible, indicating that the transient

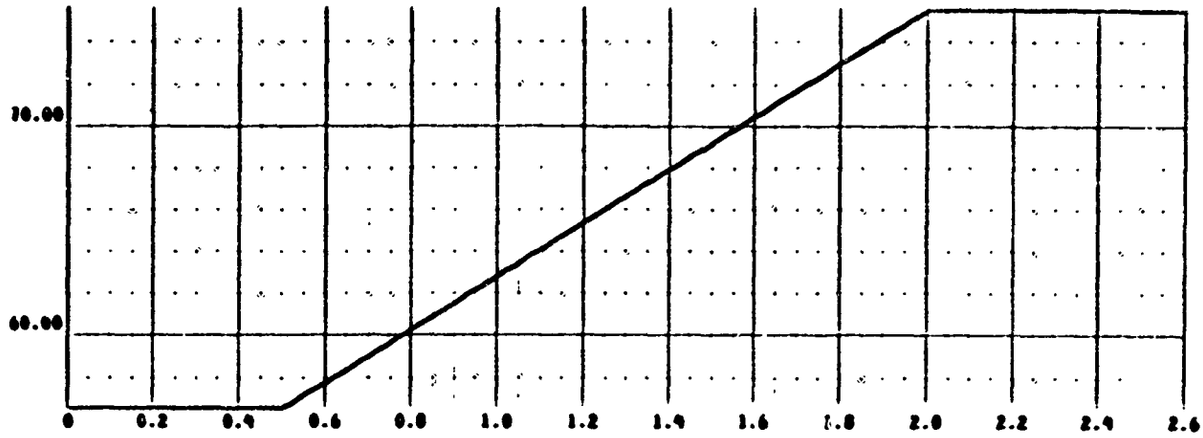

(a) Input Transient, N_F (%rpm) vs Time

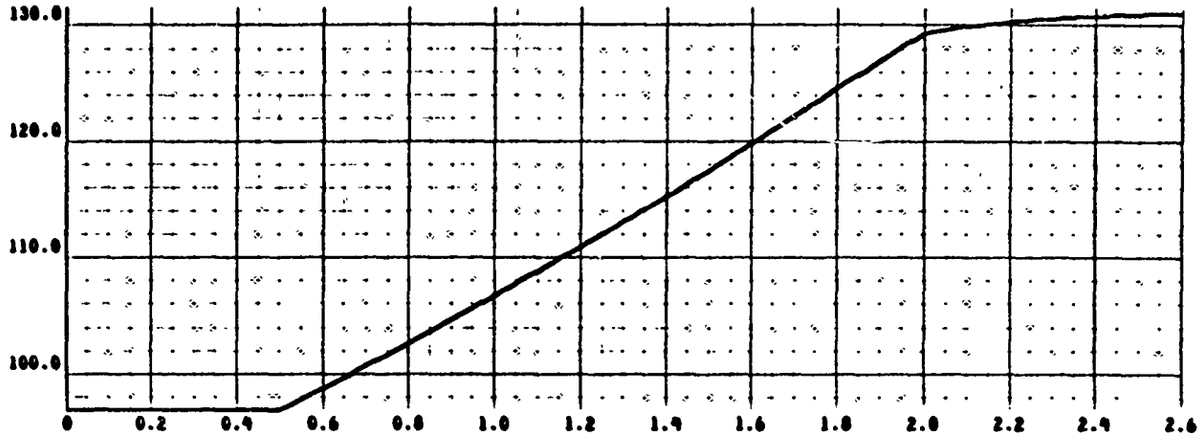

(b) W_{2E} (lbs/sec) vs Time

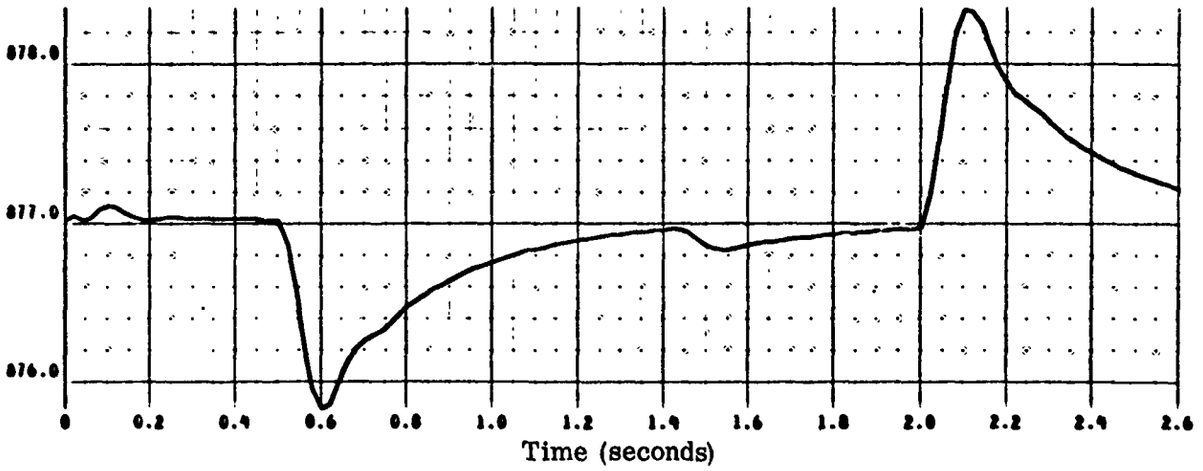

(c) T_{T2} (^{O}R) vs Time

Figure 15. 2DM Air Induction System Output Data - Throttle Burst (Model 1, Deck 1); $M_0 = 2.5$; H = 61000 ft; $\alpha = 0$

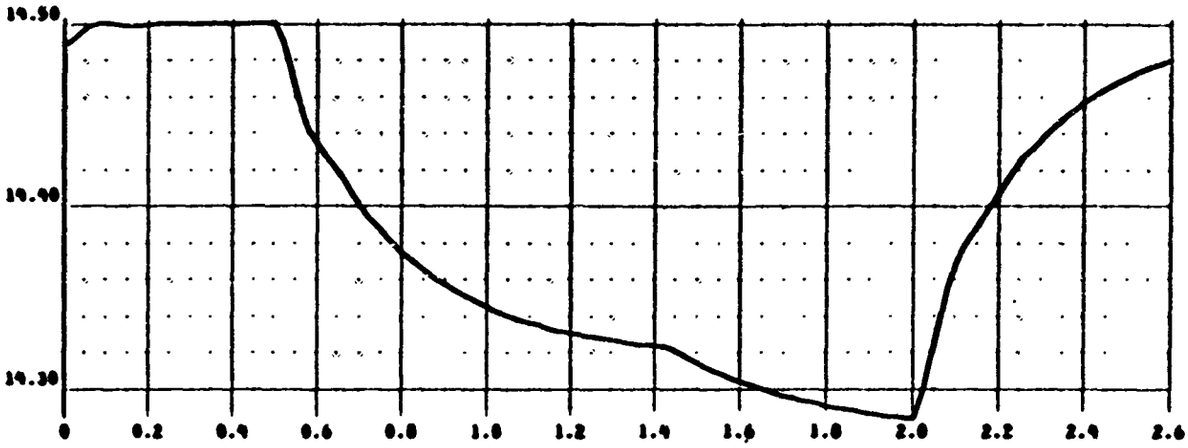

(d) P_{T2} (psi) vs Time

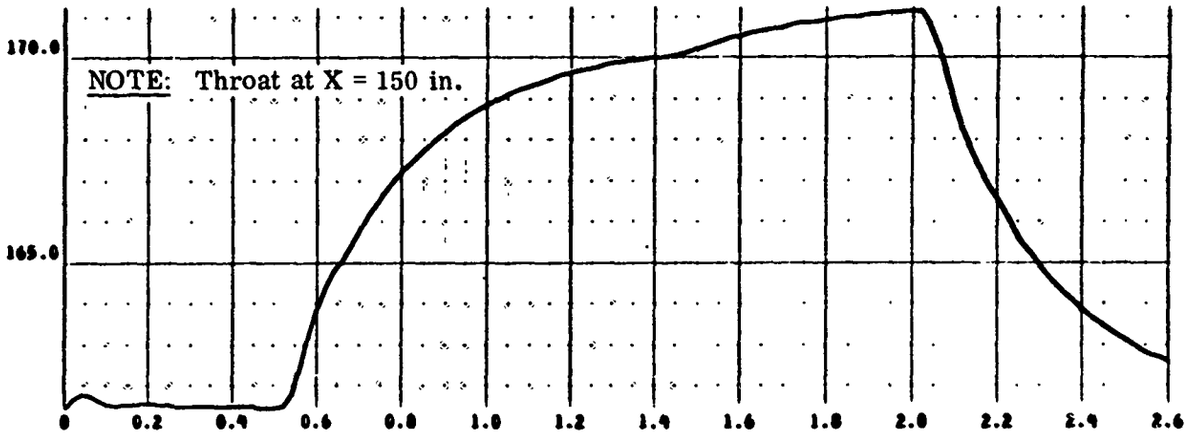

(e) X (in) vs Time

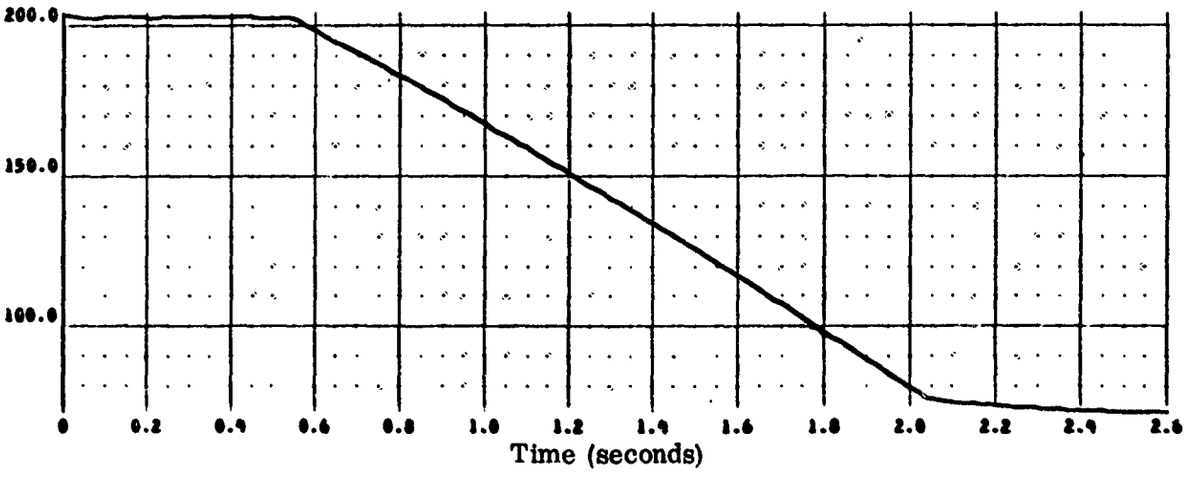

(f) A_{BY} (in^2) vs Time

Figure 15 Continued

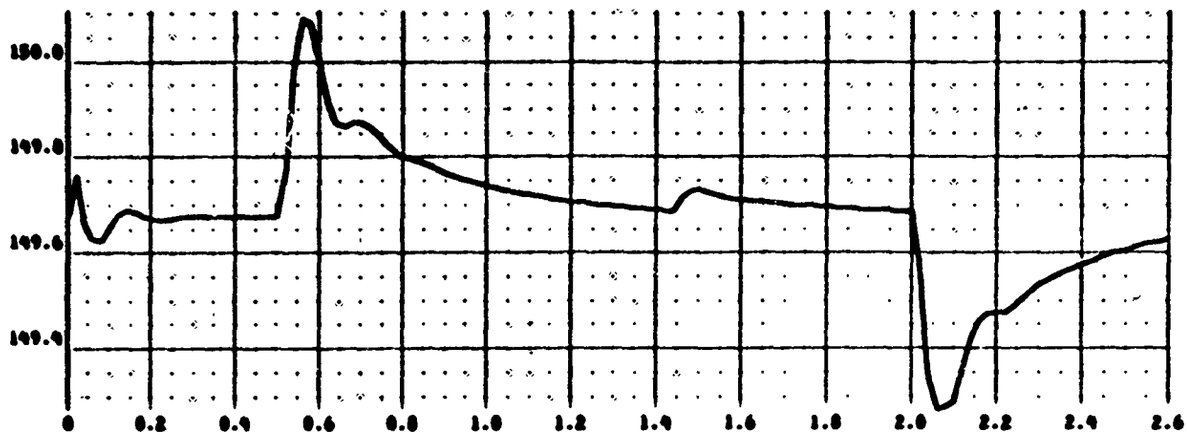

(g) W_8 (lbs/sec) bs Time

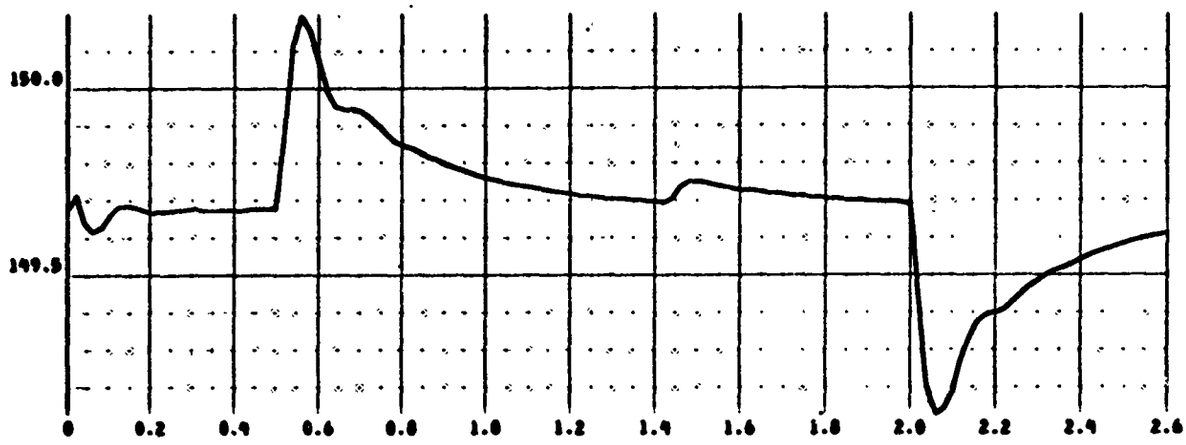

(h) W_{14} (lbs/sec) vs Time

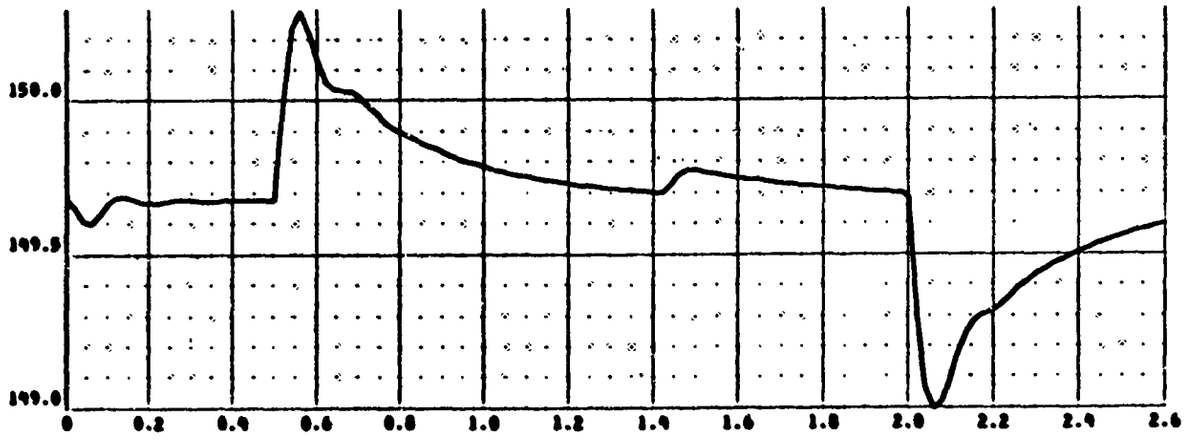

(i) W_2 (lbs/sec) vs Time

Figure 15 Concluded

is slow enough to be nearly steady state. The amplitude of the maximum instantaneous change for the three flows W_8, W_{14}, and W_2 from their initial values is also not significant. This is because the relatively slow increase in engine flow demand is met by a corresponding decrease in bypass area at nearly the same rate, with minimal dynamic fluctuations within the subsonic duct.

Buzz Transient (Model 2, Deck 3)

The following example is used to simulate a buzz transient of the full scale 2DM air induction system.

Transient:	Buzz
Mach Number:	3.0
Altitude:	70,000 feet
Angle of Attack:	0

Buzz is initiated by triggering separation through program logic with the NS located just upstream of the throat at the initial condition. The bypass area sized for this NS location is then frozen for the duration of the run by inputting zero bypass gain in the control logic.

Discussion of Input Data. Additional input data curves, for the buzz model (Model 2), are presented in Figure 16. These data are required for this model in addition to the basic input data presented for the Standard model (Figure 13).

The total pressure recovery upstream of the NS, P_{TX}/P_{T0}, is presented as a function of NS location X in Figure 16(a). During severe buzz the NS can have large excursions extending nearly to the tip of the inlet and resulting in a noticeable variation of P_{TX}/P_{T0}. Values of P_{TX}/P_{T0} are preselected from inlet input data when the NS is at (1) the inlet leading edge, (2) end of first ramp, (3) the cowl, and (4) the throat at the given flight conditions. Linear variation in P_{TX}/P_{T0} is assumed between these values.

Vol_6 is presented as a function of X in Figure 16(b). It is based on A_X, the latter being the critical flow cross-sectional area when the NS is external to the cowl ($X<X_c$) and the duct area when the NS is inside the inlet ($X \geq X_c$).

Figure 16(c) shows A_X and A_{EX} as a function of X. It can be seen that the area of separated flow (A_{EX}) increases rapidly as the NS moves upstream during the buzz cycle (as discussed previously in Section III, the flow is fully attached during downstream

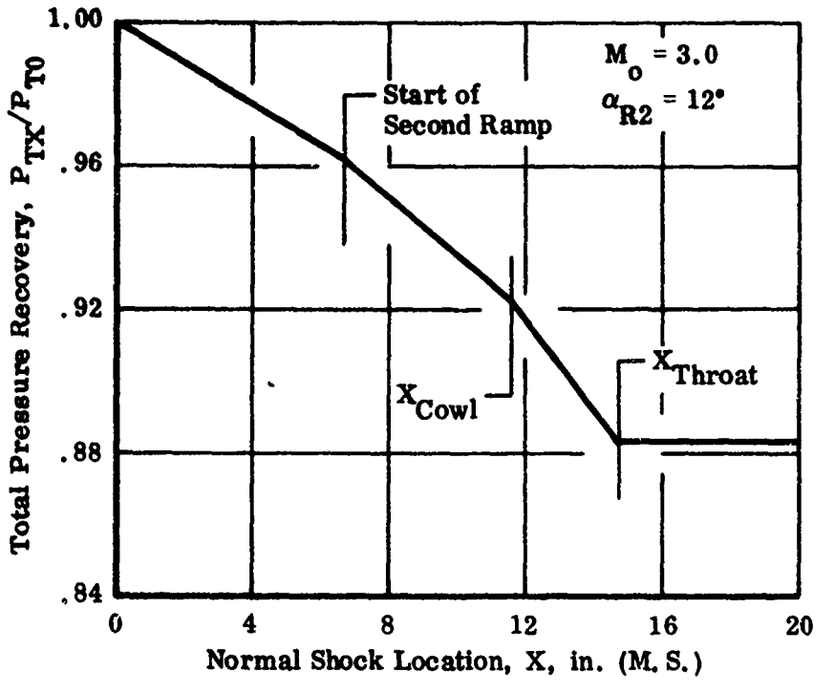

(a) $P_{TX}/P_{T0} = f(X)$

Figure 16. 2DM Air Induction System Additional Input Data for Buzz Model

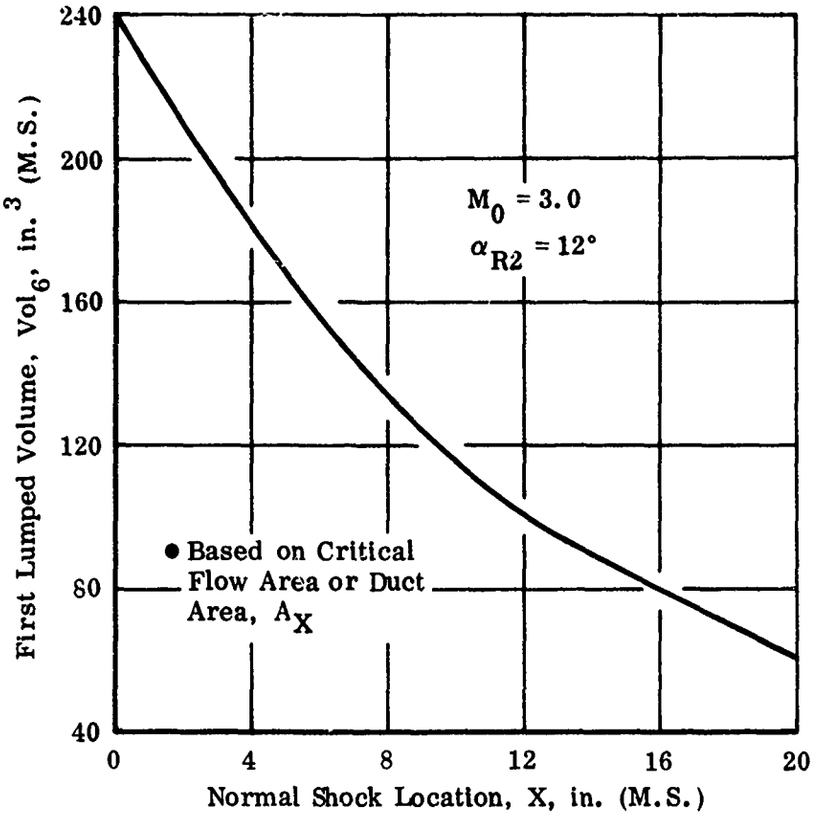

(b) $Vol_6 = f(X)$

Figure 16 Continued

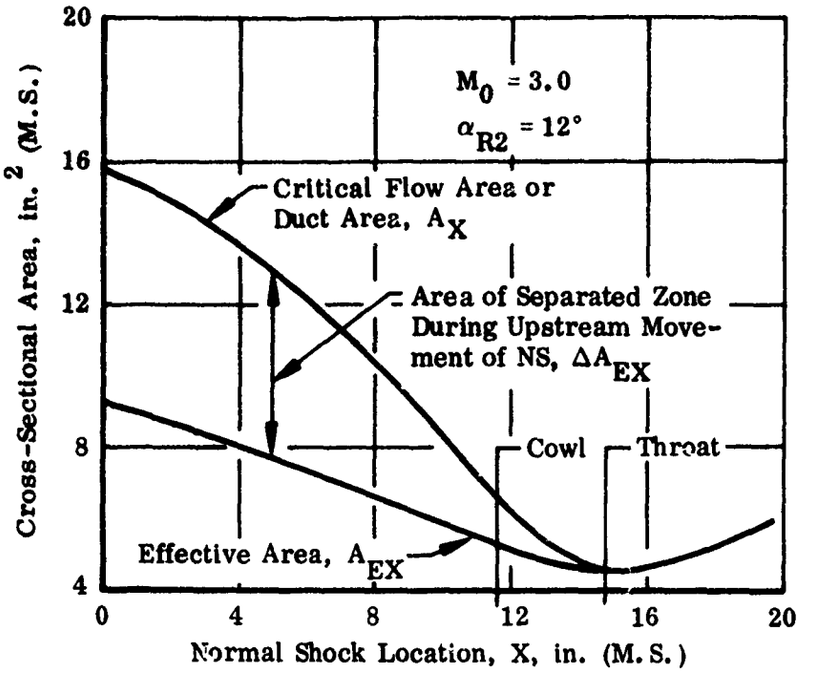

(c) Various Flow Areas as Function of X

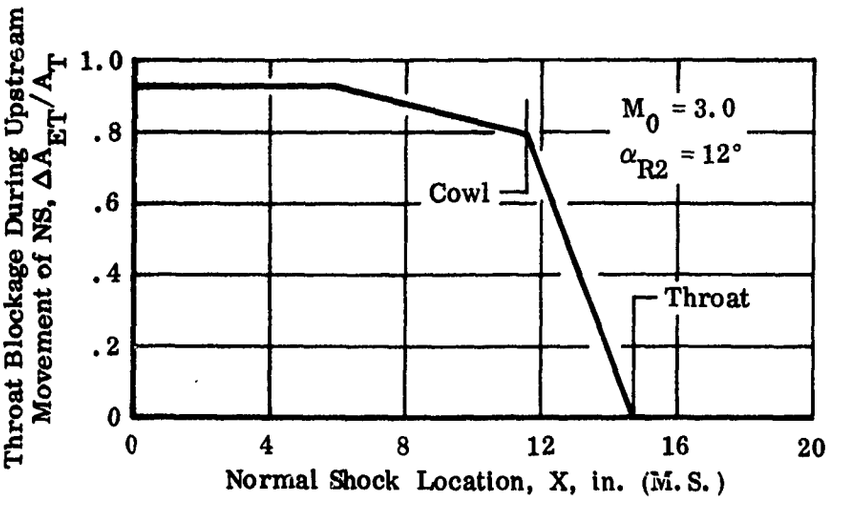

(d) $\Delta A_{ET}/A_T = f(X)$

Figure 16 Continued

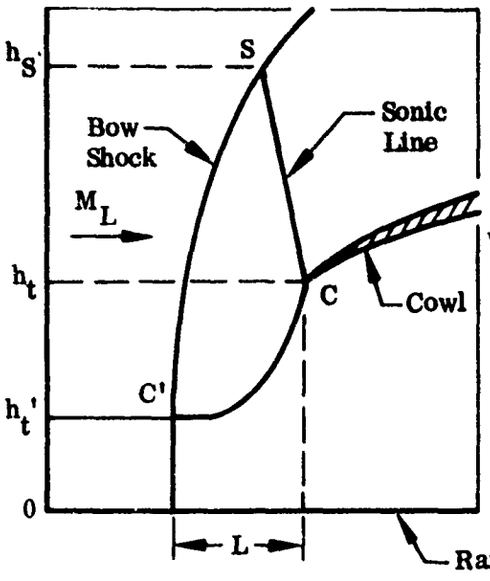

$$\frac{L}{h_t} = K_{SP}\left(1 - \frac{h_t'}{h_t}\right) = K_{SP}\,\frac{W_{SP}}{W_0}$$

where L = NS Stand-Off Distance, in.

h_t = Height, Ramp to Inlet Cowl, in.

W_{SP} = Inlet Subsonic Spillage, lb/sec.

W_0 = Inlet Critical Mass Flow, lb/sec.

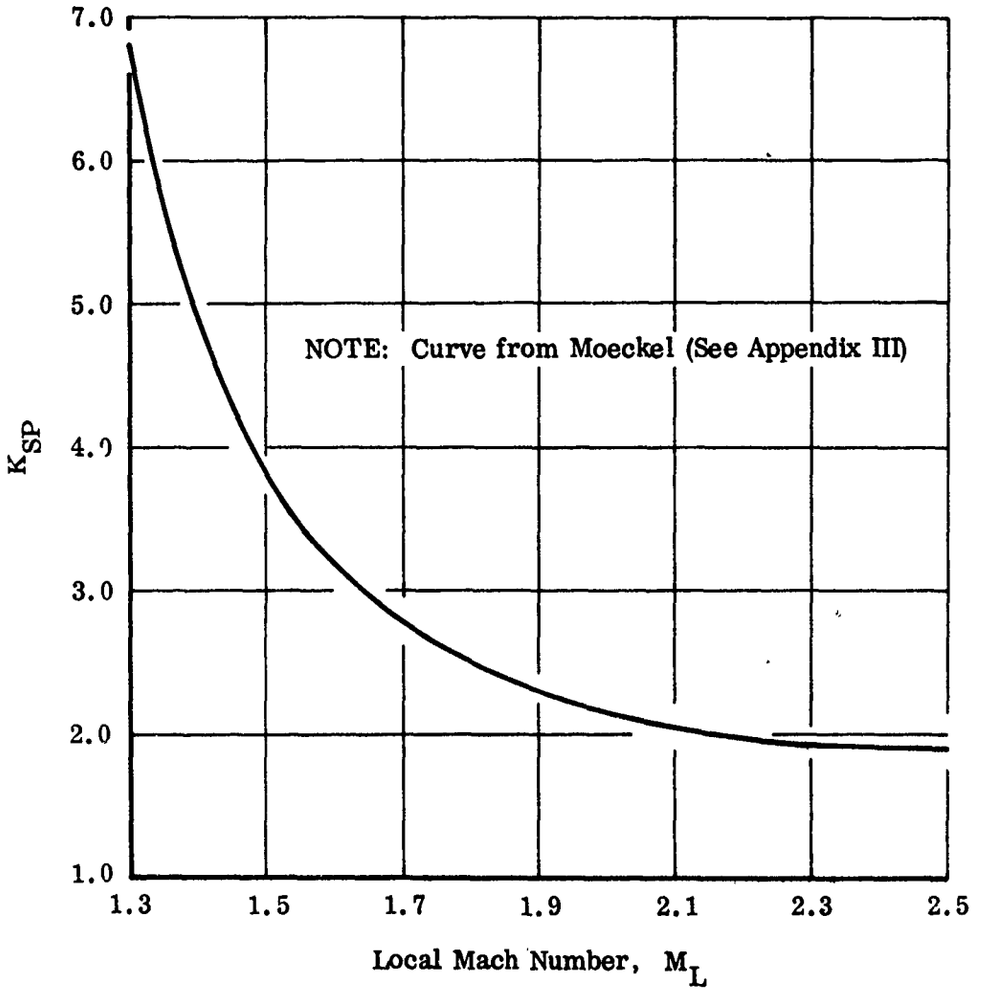

(e) Curve for Calculating L or W_{SP} Using Moeckel's Model

Figure 16 Continued

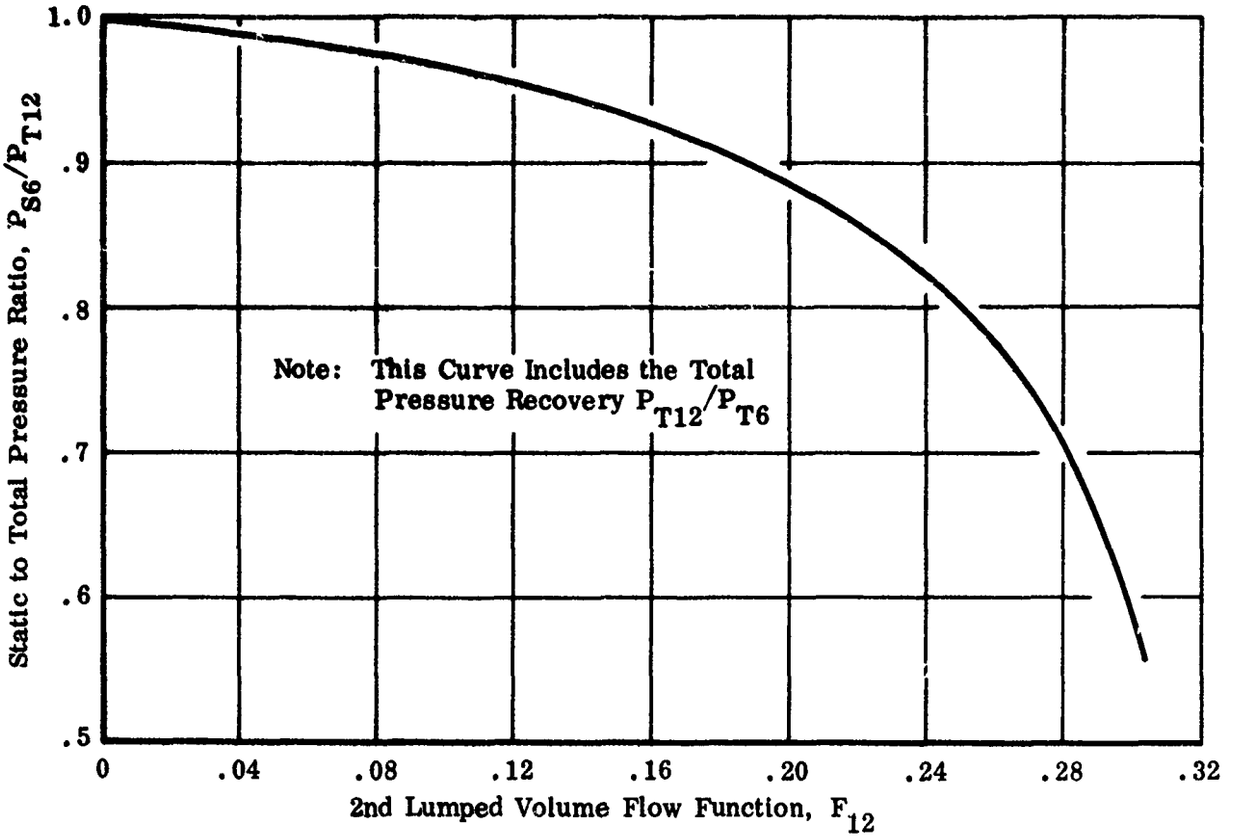

(f) $P_{S6}/P_{T12} = f(F_{12})$

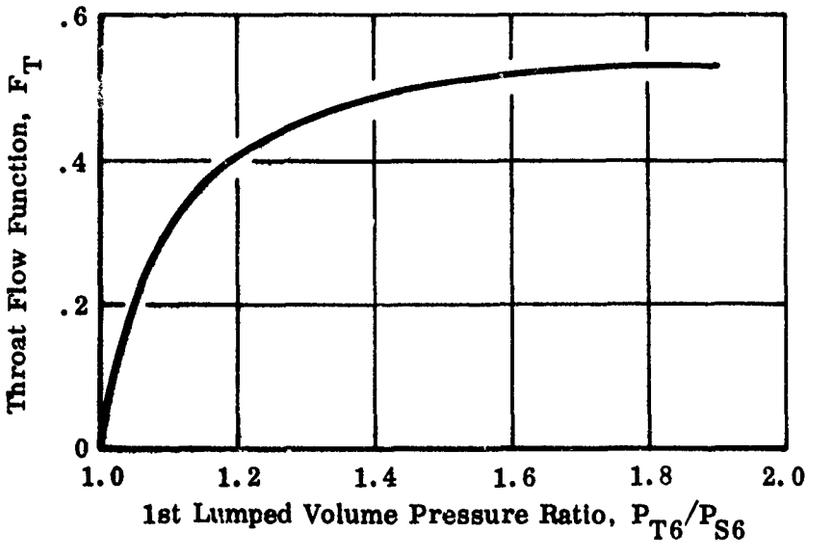

(g) $F_T = P_{T6}/P_{S6}$

Figure 16 Concluded

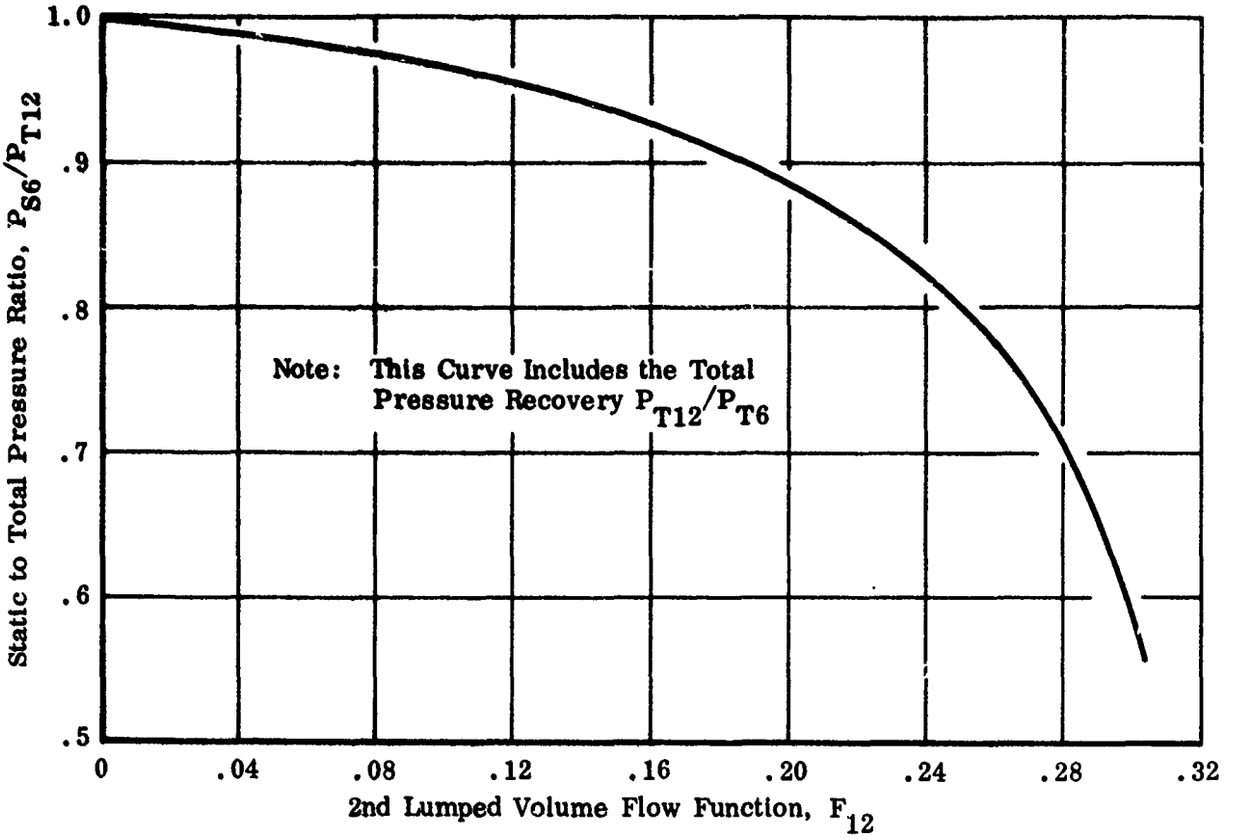

(f) $P_{S6}/P_{T12} = f(F_{12})$

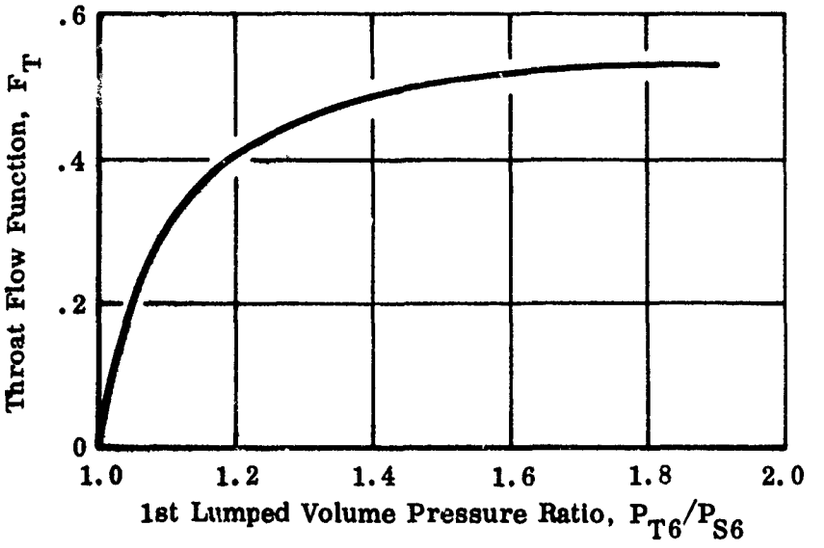

(g) $F_T = P_{T6}/P_{S6}$

Figure 16 Concluded

movement of the NS). Figure 16(d) shows the throat area blockage ratio $\Delta A_{ET}/A_T$ as a function of X. Flow is assumed to be attached when the NS is downstream of the throat. After an unstart is triggered, blockage increases rapidly until the NS reaches the cowl. It continues to increase at a reduced rate until the NS reaches the first ramp, beyond which a constant value of 0.93 is used. This maximum value of 0.93 is based on XB-70 simulation input data used in Reference 11 which compares XB-70 flight test data with simulation predictions of inlet unstart and buzz. Spillage flow W_{SP} is obtained using Moeckel's equation [Figure 16(e)].

Figures 16(f) and 16(g) are used to calculate the throttled throat flow W_{ET} ($=W_8$). Figure 16(f) shows P_{S6}/P_{T12} ratio as a function of the second lumped volume flow function F_{12}. The pressure ratio includes the steady state friction loss for the first half of the subsonic duct.

Discussion of Output Data. The output data for the buzz transient are presented in Figure 17. The run is terminated at 0.36 second after simulating two buzz cycles. There are no controls imposed on NS movement during the run.

When buzz is triggered through program logic at the beginning of the simulation run, the NS starts to move rapidly upstream from the initial location just upstream of the throat [Figure 17(a)]. The dominating effect during the unstart mode is the throat throttling as the NS moves upstream. As the geometric throat area A_T is throttled [Figure 17(b)] the throat flow W_{ET} ($=W_8$) is reduced [Figure 17(d)] and induces an instantaneous two-way flow imbalance, which increases P_{T6} [Figure 17(g)] since outflow ($W_8 + W_{TBY}$) is instantaneously less than inflow (W_X) and simultaneously decreases P_{T12} since outflow W_{14} [Figure 17(e)] is instantaneously greater than inflow W_8. As the NS is disgorged from the cowl at 0.018 second, the inlet starts spilling, the throttling rate drops [Figure 17(b)] and the accelerating NS increases the rate of change of Vol_6. With the Vol_6 flow imbalance now reversed [outflow ($W_8 + W_{TBY} + W_{SP}$) instantaneously greater than inflow (W_X)] and Vol_6 expanding rapidly, P_{T6} starts to drop. It should be noted that although W_8 continues to decrease because of throttling, the rapid increase in W_{SP} more than offsets this, thus increasing the instantaneous net outflow from Vol_6 to a level greater than W_X.

Instantaneous static pressure ratios across the NS, P_{SX} and P_{SY} (which are themselves functions of the corresponding instantaneous total pressures across the NS, P_{TX} and P_{T6} respectively) control the NS fluctuations on the ramp. Figure 17(a)

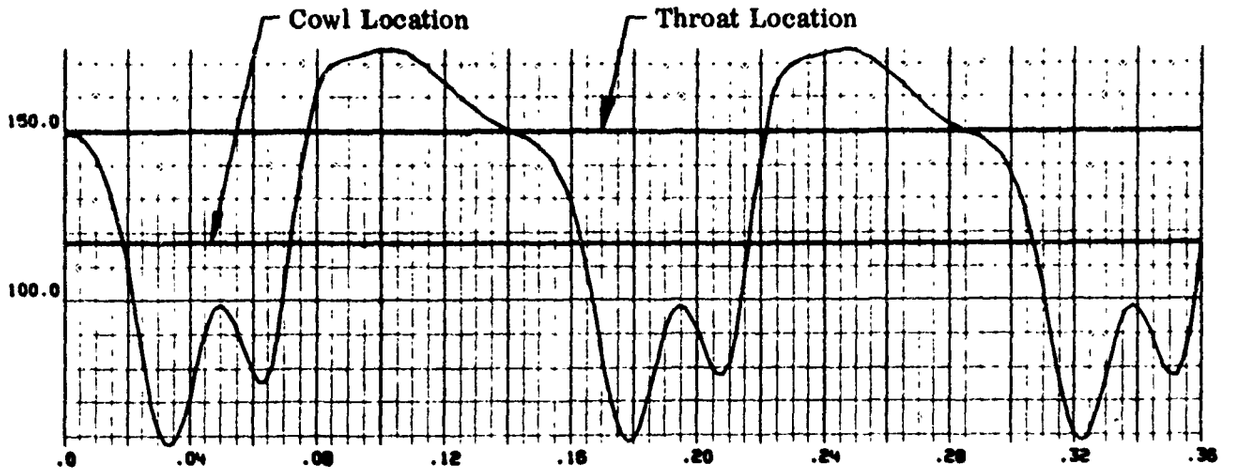

(a) X (in) vs Time

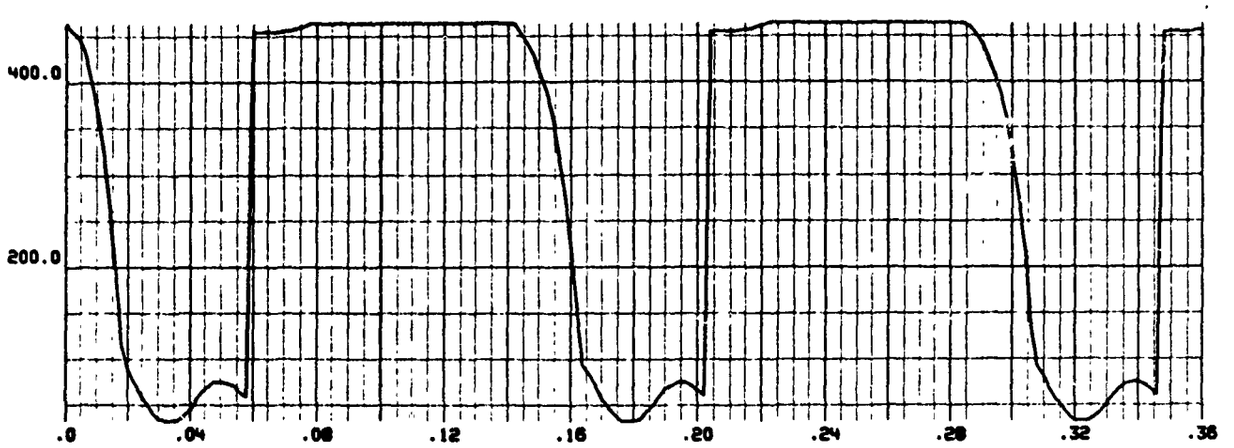

(b) A_{ET} (in^2) vs Time

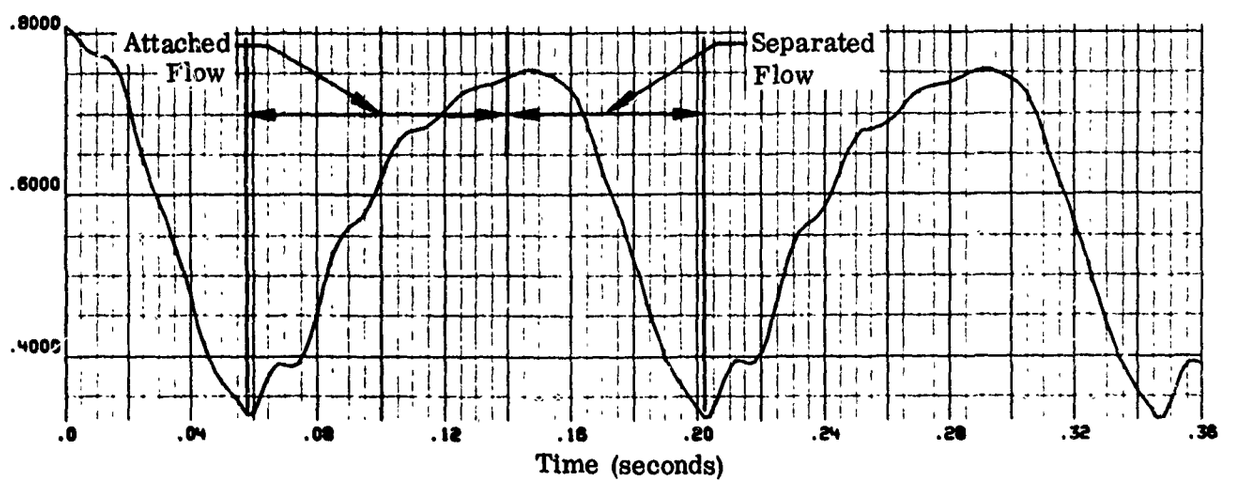

(c) P_{T12}/P_{T0} vs Time

Figure 17. 2DM Air Induction System Output Data - Buzz Transient (Model 2, Deck 3) $M_0 = 3$; H = 70000 ft; $\alpha = 0$

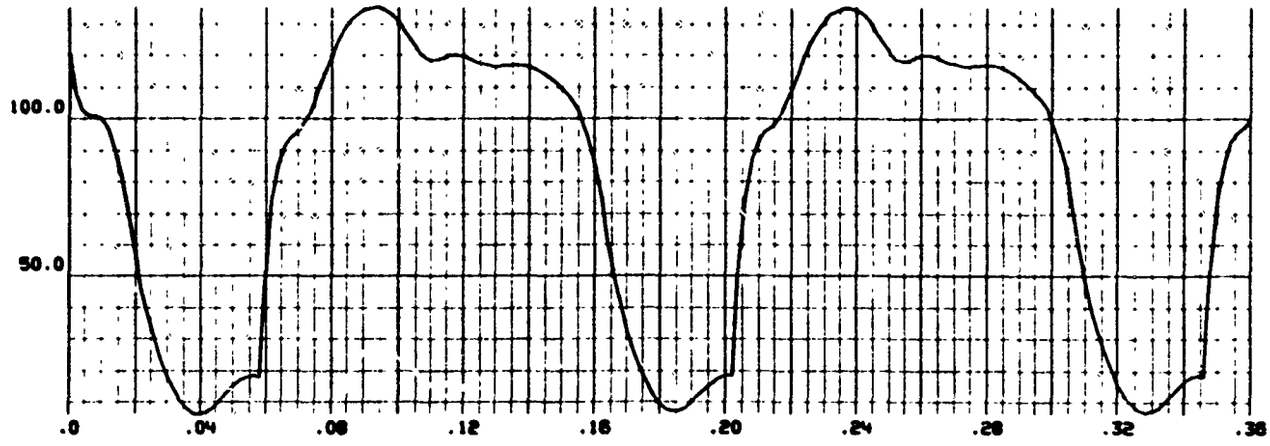

(d) W_8 (ft/sec) vs Time

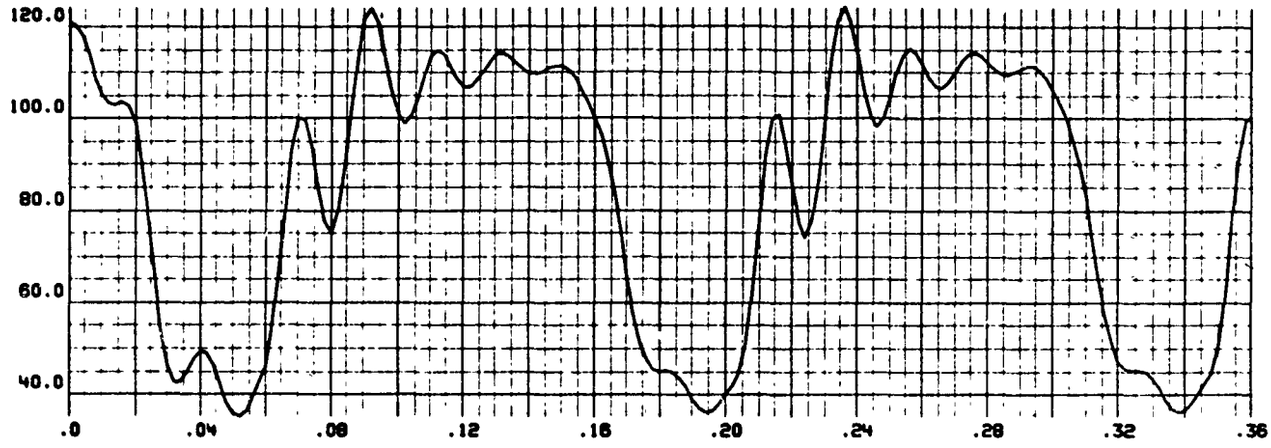

(e) W_{14} (ft/sec) vs Time

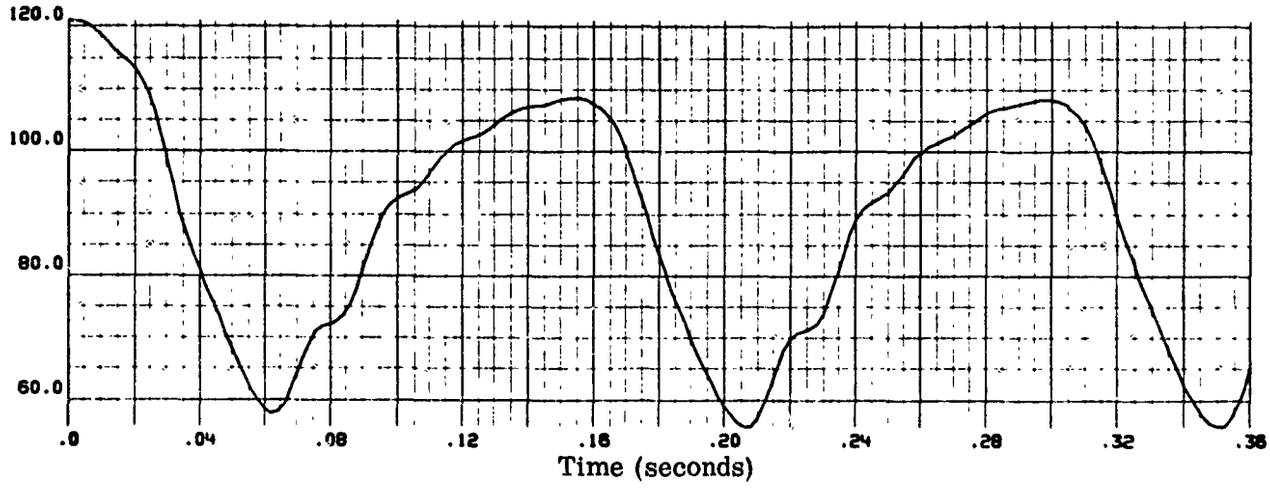

(f) W_2 (ft/sec) vs Time

Figure 17 Continued

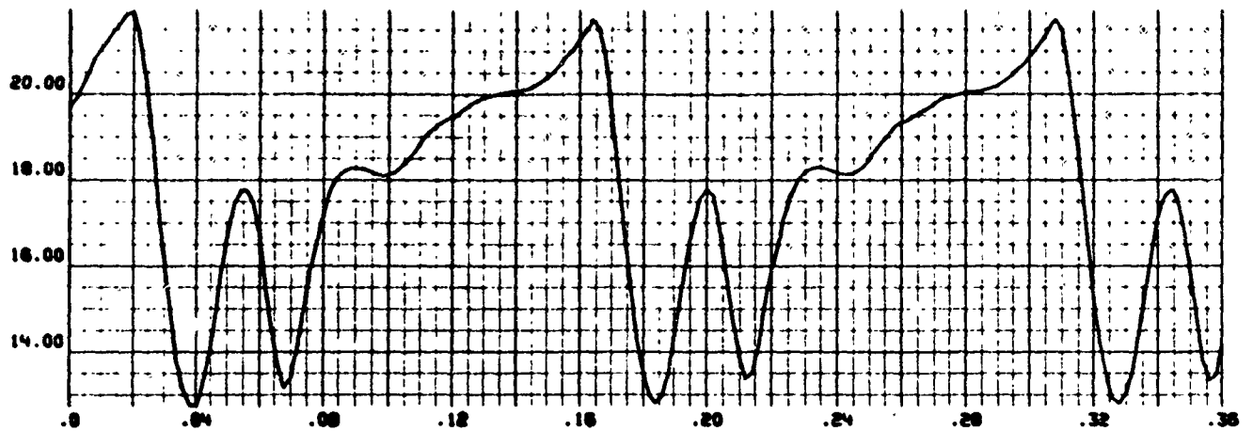

(g) P_{T6} (psi) vs Time

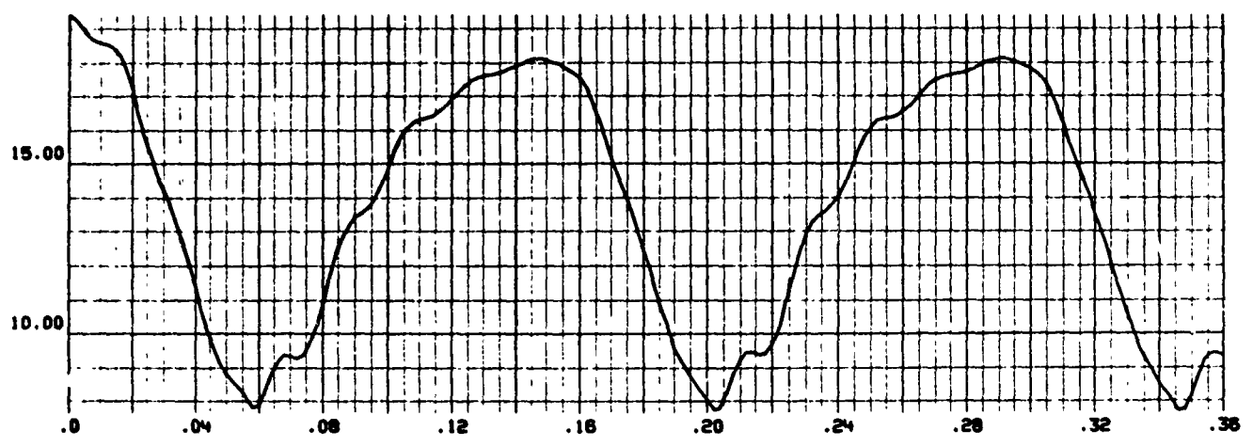

(h) P_{T12} (psi) vs Time

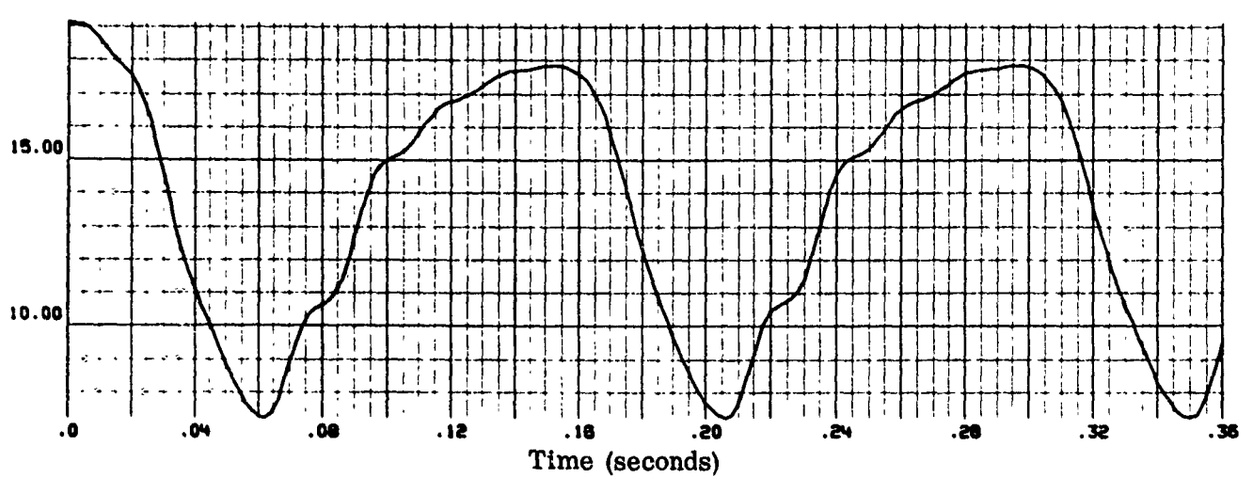

(i) P_{T2} (psi) vs Time

Figure 17 Continued

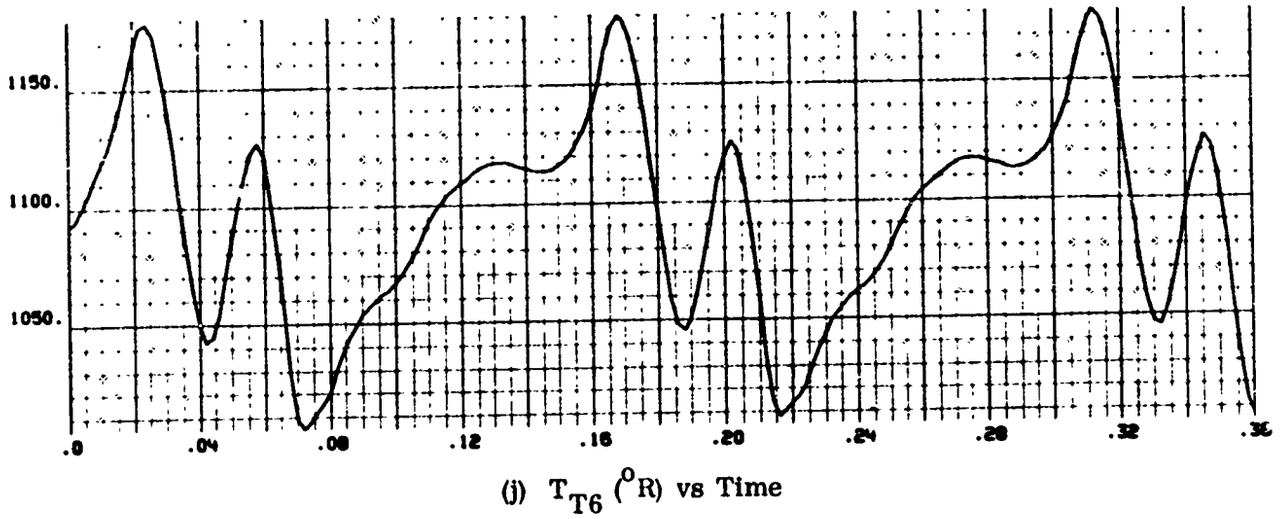

(j) T_{T6} (^{O}R) vs Time

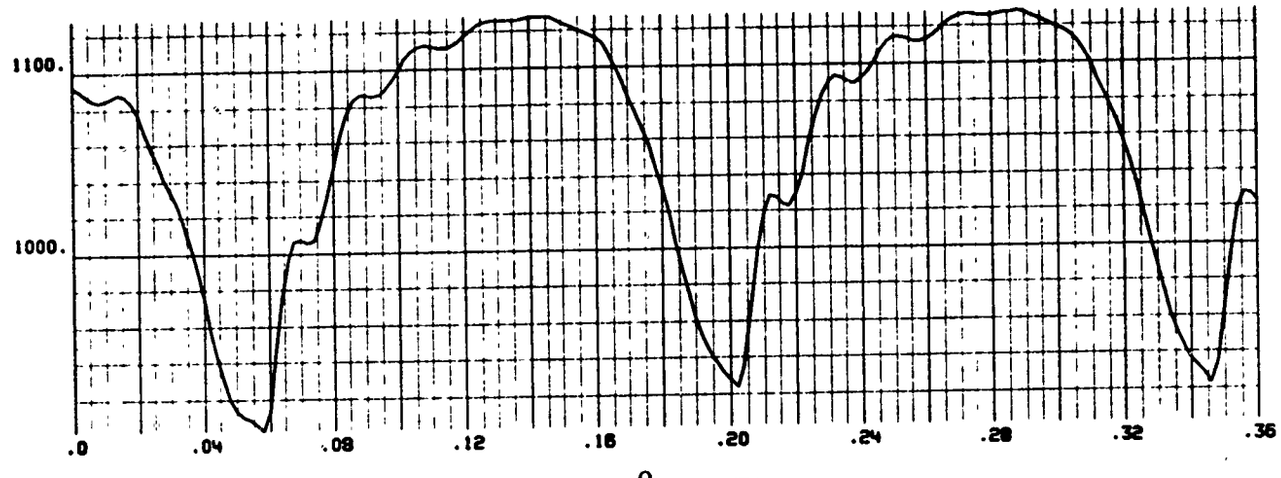

(k) T_{T12} (^{O}R) vs Time

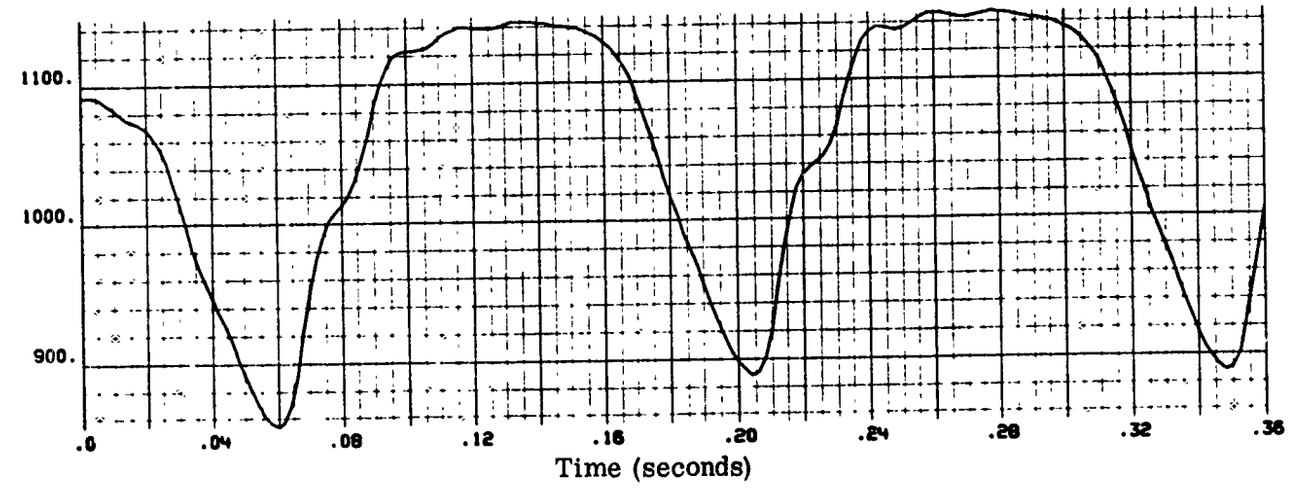

(l) T_{T2} (^{O}R) vs Time

Figure 17 Concluded

shows that the NS fluctuates once between 0.035 and 0.06 second before attachment occurs and triggers the second half of the buzz cycle. The duration of time the flow stays either attached or separated is indicated on the figure.

At 0.06 second the key buzz parameter P_{T12}/P_{T0} [Figure 17(c)] reaches the value of 0.315 when reattachment instantaneously occurs. With no throttling, outflow from Vol_6 rushes into Vol_{12} which is at a much lower pressure P_{T12} [Figure 17(h)], thereby causing a sucking effect on the NS, which reenters the inlet and surges to a highly supercritical position (X = 170 inches at t = 0.09). It reverses itself at this point and travels upstream until it again crosses the throat, thus initiating another buzz cycle. The reason why separation is not retriggered at $P_{T12}/P_{T0} = 0.519$ [see Figures 7(c) and 17(c)] is because at that time (0.084 second), the NS is downstream of the throat and the flow is assumed to be attached.

The buzz frequencies for the full-scale and model inlets are 7 and 70 cps respectively. The total pressures and temperatures at the compressor face during the buzz cycle are presented in Figures 17(i) and 17(l), respectively. The high rate of change of these properties and the large amplitudes (11 psi for P_{T2}, 250°R for T_{T2}), associated with severe buzz conditions, are the primary reasons for causing compressor stall. The pressure and the temperature variations increase the dynamic distortion at the compressor face to intolerable levels and drastically reduce the compressor stall margin.

Hammershock Transient (Model 3, Deck 5)

The dynamic response of the full scale 2DM air induction system to a hammershock transient has been studied at the following conditions.

Transient:	100 percent airflow cutoff in 0.01 second
Mach Number:	3.0
Altitude:	70,000 feet
Angle of Attack:	0

No additional input data are required to simulate a hammershock transient. At the initial condition, the bypass area is sized such that the NS is located at the desired supercritical location and then frozen at this value for the duration of the run. The bypass control logic is not included in this model.

Discussion of Output Data. The output data are presented in Figure 18. The input transient [Figure 18(a)] simulates engine stall by cutting off engine airflow (W_{2E}) within ten milliseconds. Thus, the air induction system continues to vent a small amount of airflow [W_2, Figure 18(f)] through the bypass area even after engine demand is reduced to zero.

At 0.01 second, as the Vol_{18} outflow W_2 starts to reduce at a rapid rate, the inflow W_{14} [Figure 18(e)] is initially unaffected, resulting in an instantaneous imbalance across the volume, which increases its pressure P_{T2} [Figure 18(i)]. At this time P_{T12} [Figure 18(h)] and P_{T6} [Figure 18(g)] are essentially unaffected. As P_{T2} continues to rise, W_{14} starts to reduce (at 0.013 second) since its rate of change is a function of the total pressures across the fixed boundary (Station 14). This reduction in Vol_{12} outflow now causes an instantaneous flow imbalance across Vol_{12} and starts to increase P_{T12} at 0.015 second. Similarly, a reduction in Vol_6 outflow W_8 [Figure 18(d)] at 0.02 second starts increasing P_{T6} three milliseconds later. P_{T2} continues to increase until 0.04 second [Figure 18(i)] and then starts to reduce rapidly when the Vol_6 instantaneous outflow becomes greater than inflow due to the continuously increasing subsonic spillage as the NS moves upstream of the cowl. Note that the subsonic duct experiences pressures greater than freestream stagnation pressure [Figure 18(c)]and that, due to the adiabatic compression of the air within the duct to pressure levels above the equilibrium recovery level, instantaneous temperature levels are significantly greater than freestream stagnation temperature.

2DE AIR INDUCTION SYSTEM

Input data for the program, developed from the 2DE 1/8 scale wind tunnel model described in Volume I of this report, are presented in Figure 19. Multipliers are used within the program to scale the inlet up to full scale. Only those figures requiring an explanation are discussed below.

Discussion of Input Data

Figure 19(a) is obtained from shock tables and gives the Mach number behind the first oblique shock (M_L) as a function of M_0 and ($\alpha + \alpha_{R1}$) where the first ramp angle α_{R1} is fixed at 10 degrees. A lower limit is defined for the supersonic model (dotted line) since below this line the flow is subsonic on the second ramp due to detachment of the second ramp oblique shock for the given M_L and the corresponding scheduled second ramp angle (α_{R2}).

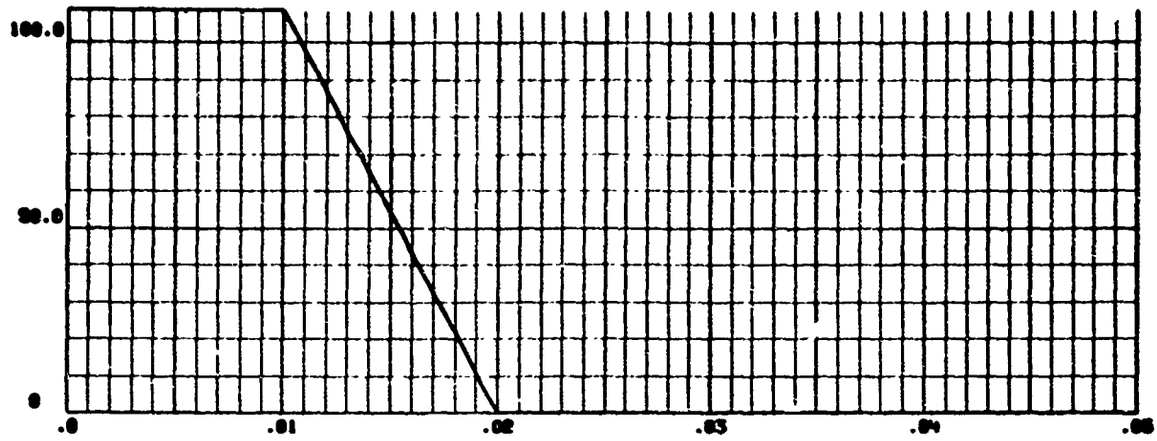

(a) Input Transient, W_{2E} (lbs/sec) vs Time

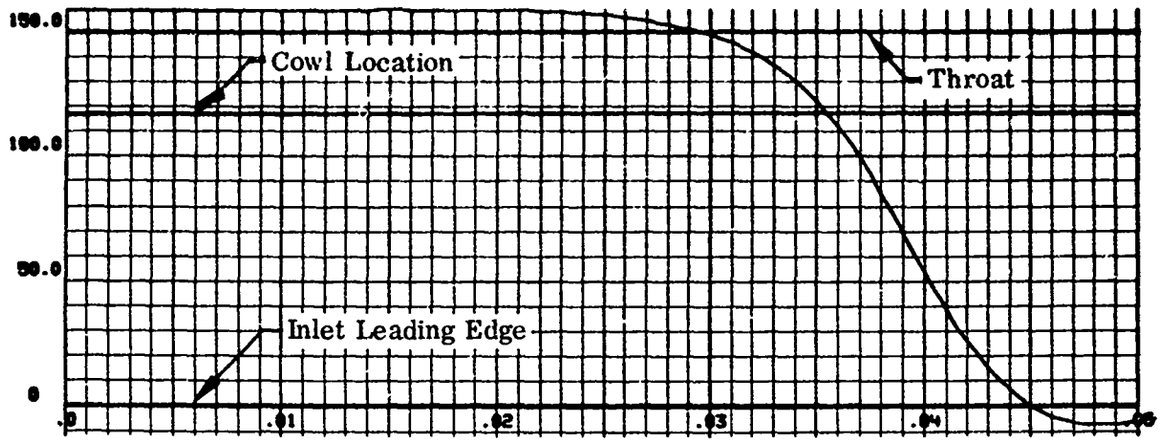

(b) X (in) vs Time

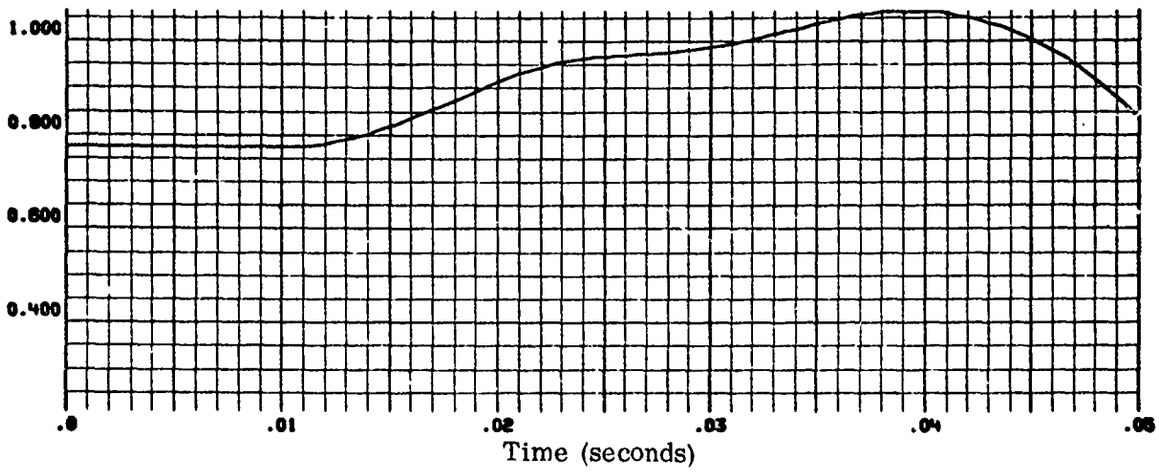

(c) P_{T2}/P_{T0} vs Time

Figure 18. 2DM Air Induction System Output Data - Hammershock Transient (Model 3, Deck 5) $M_0 = 3$; H = 70000 ft; $\alpha = 0$

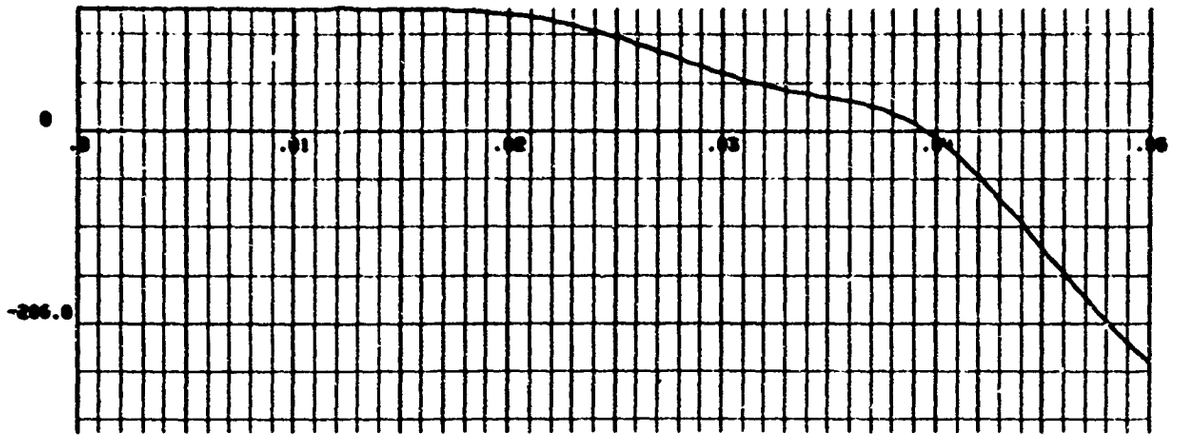

(d) W_8 (lbs/sec) vs Time

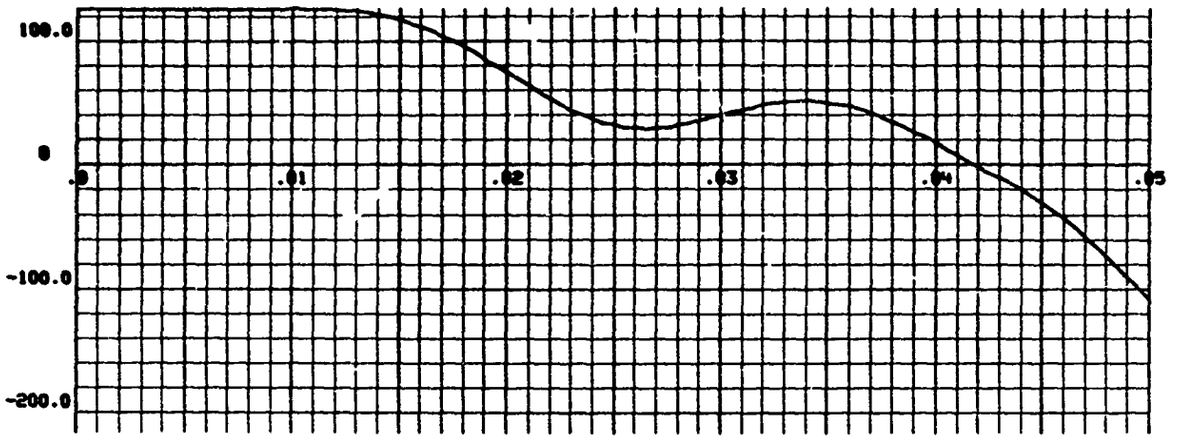

(e) W_{14} (lbs/sec) vs Time

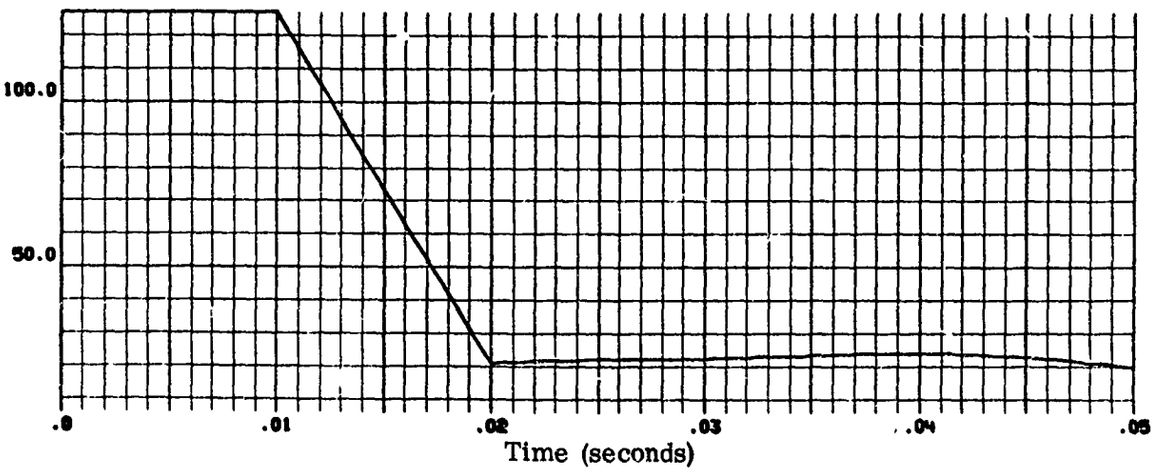

(f) W_2 (lbs/sec) vs Time

Figure 18 Continued

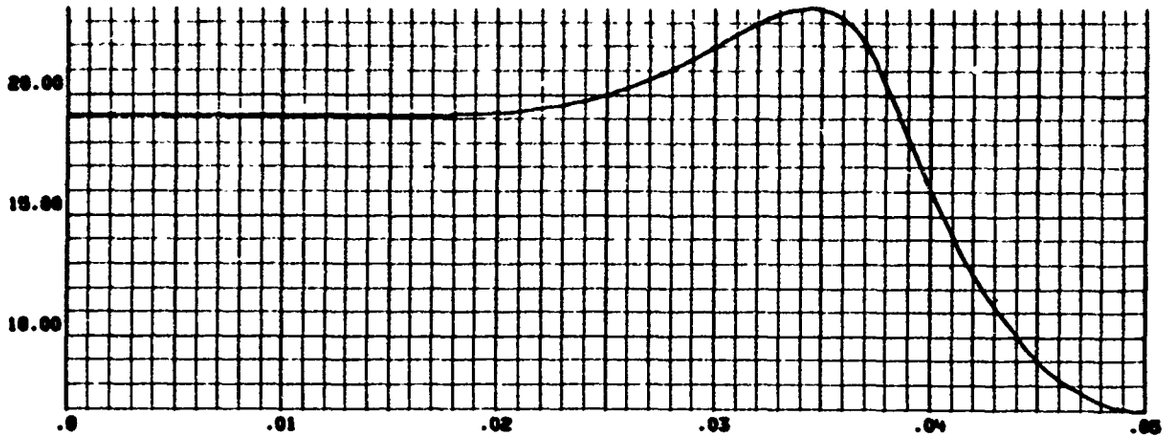

(g) P_{T6} (psi) vs Time

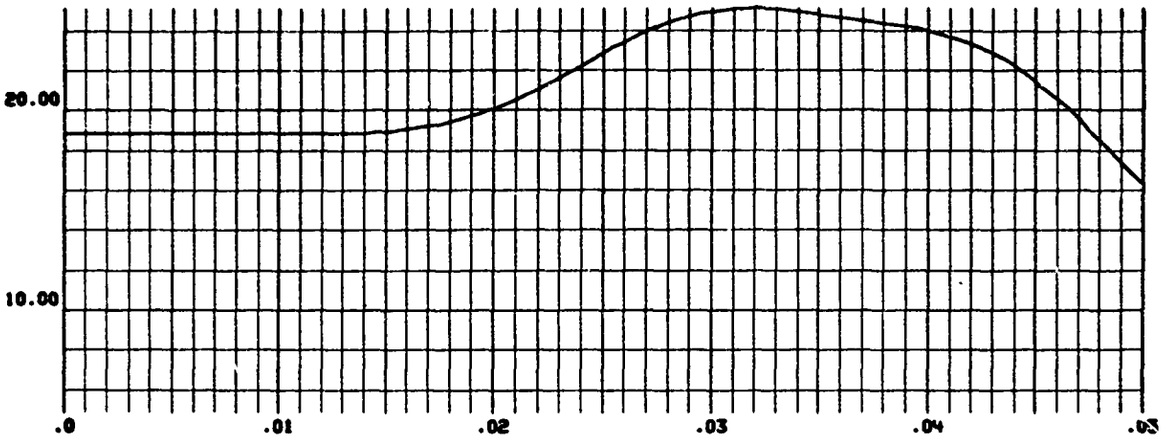

(h) P_{T12} (psi) vs Time

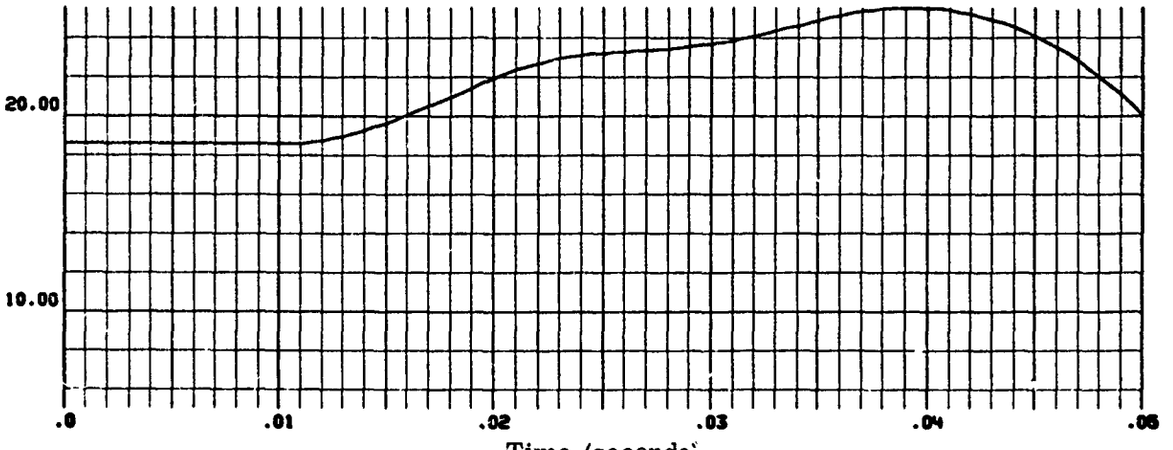

(i) P_{T2} (psi) vs Time

Figure 18 Continued

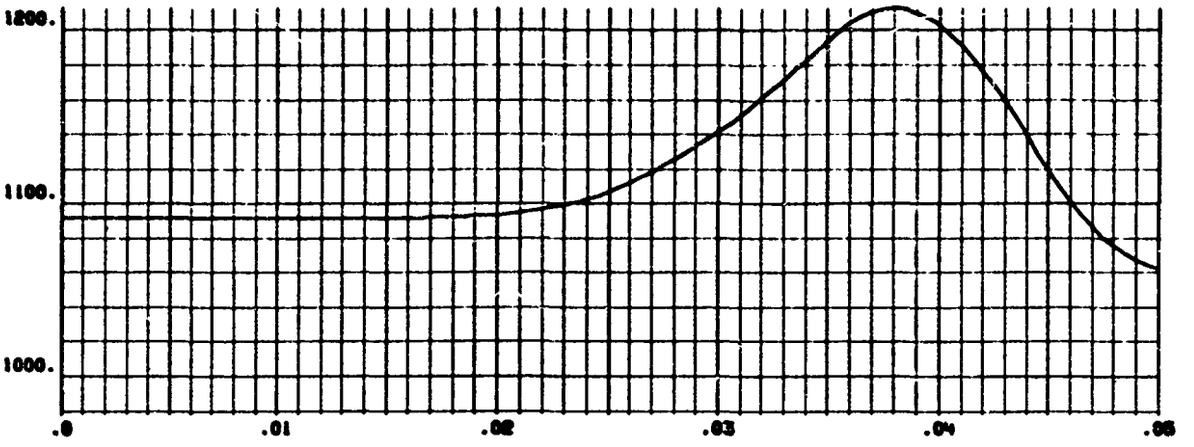

(j) T_{T6} (^{O}R) vs Time

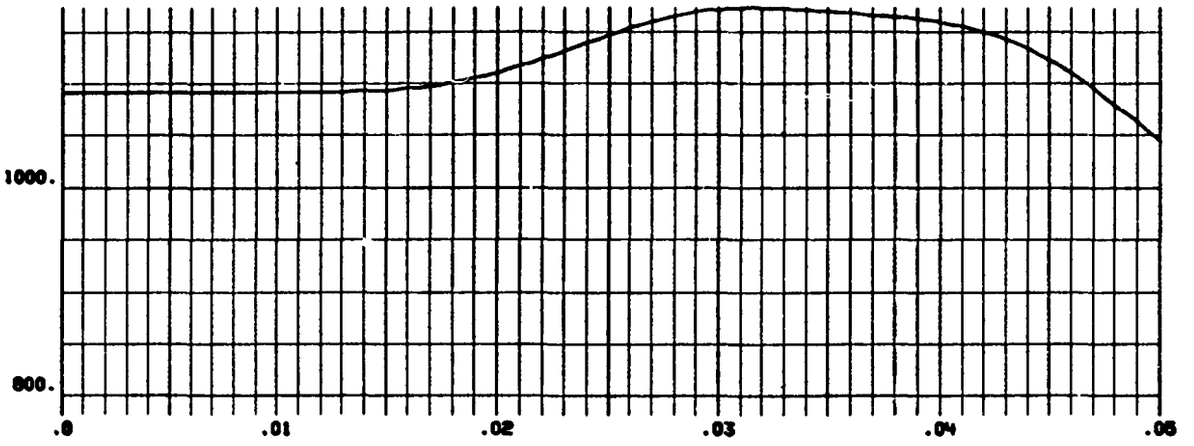

(k) T_{T12} (^{O}R) vs Time

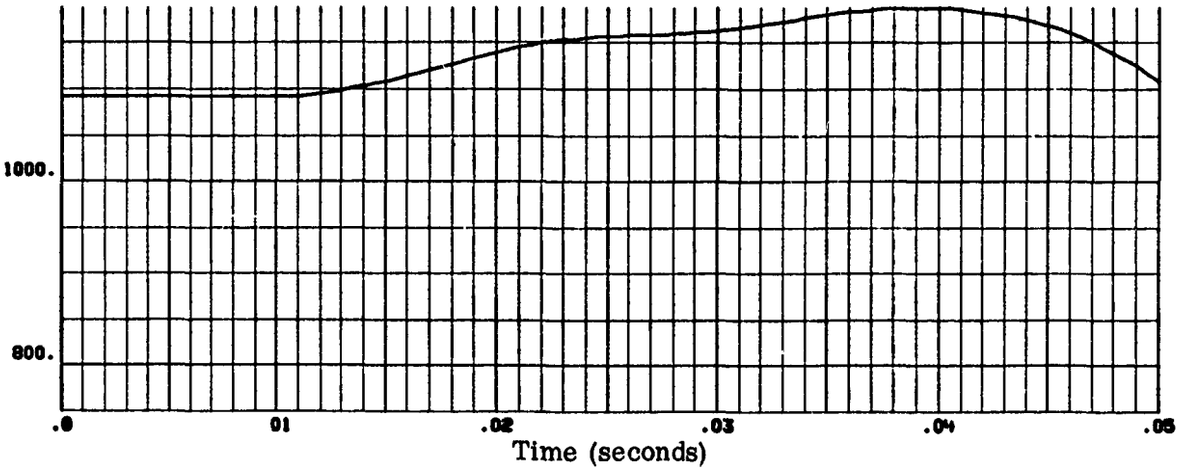

(l) T_{T2} (^{O}R) vs Time

Figure 18 Concluded

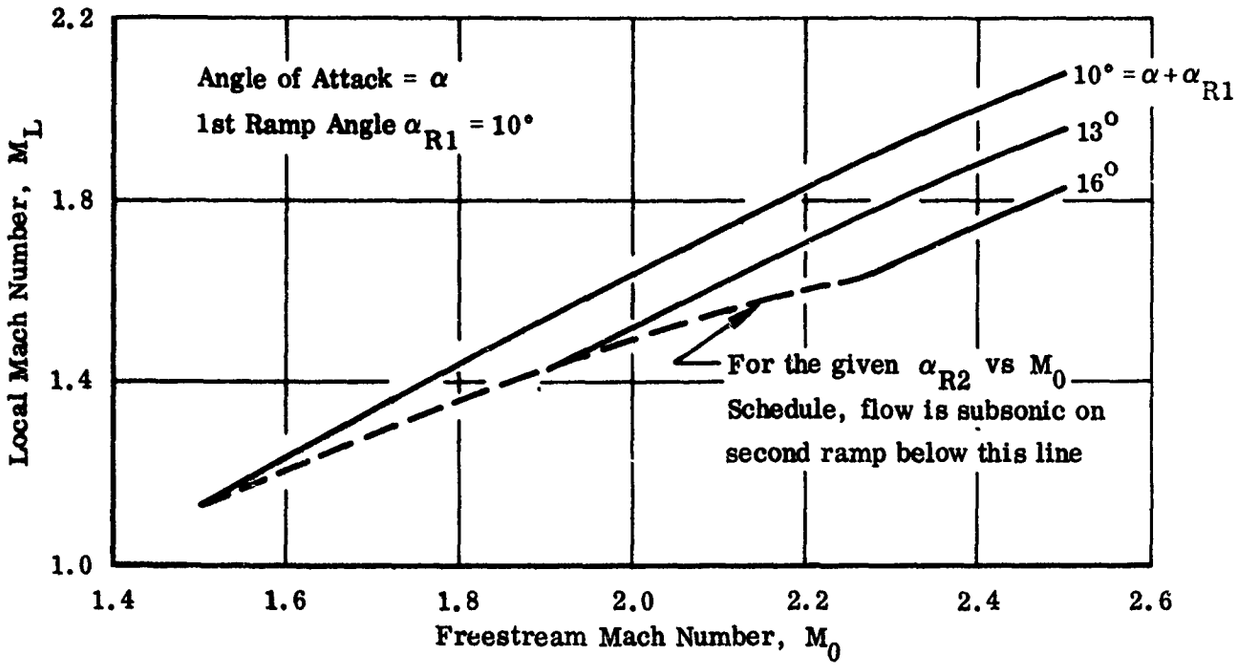

(a) $M_L = f(M_0, \alpha)$

Figure 19. 2DE Air Induction System Input Data

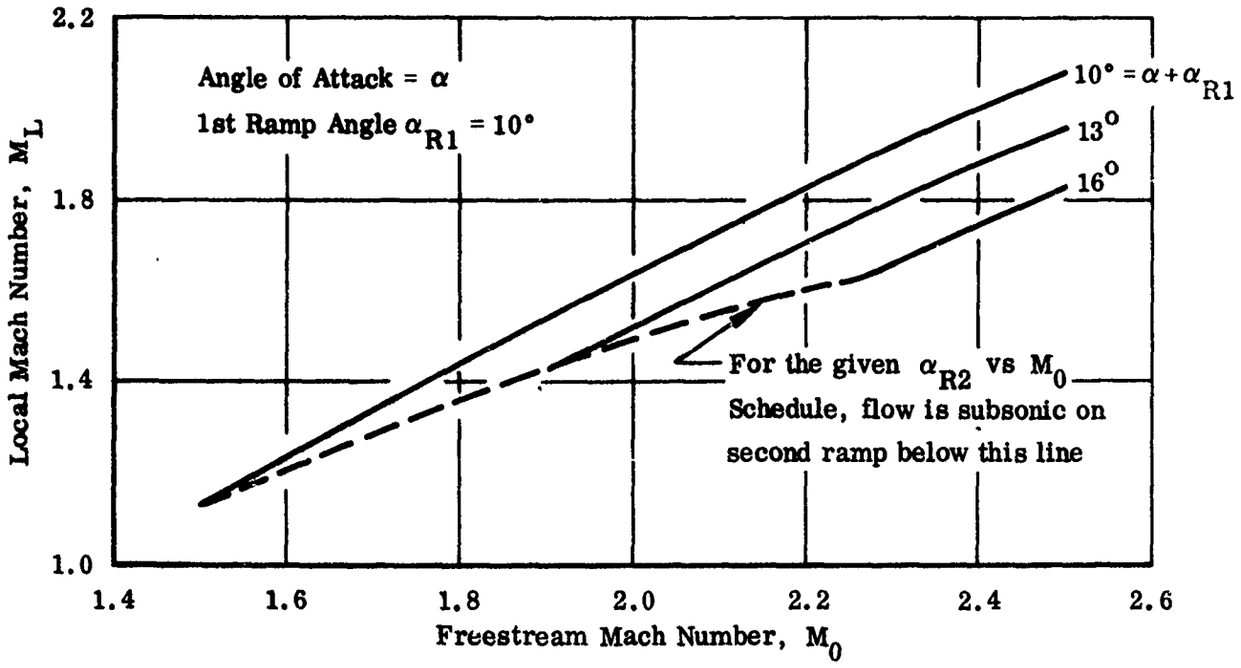

(a) $M_L = f(M_0, \alpha)$

Figure 19. 2DE Air Induction System Input Data

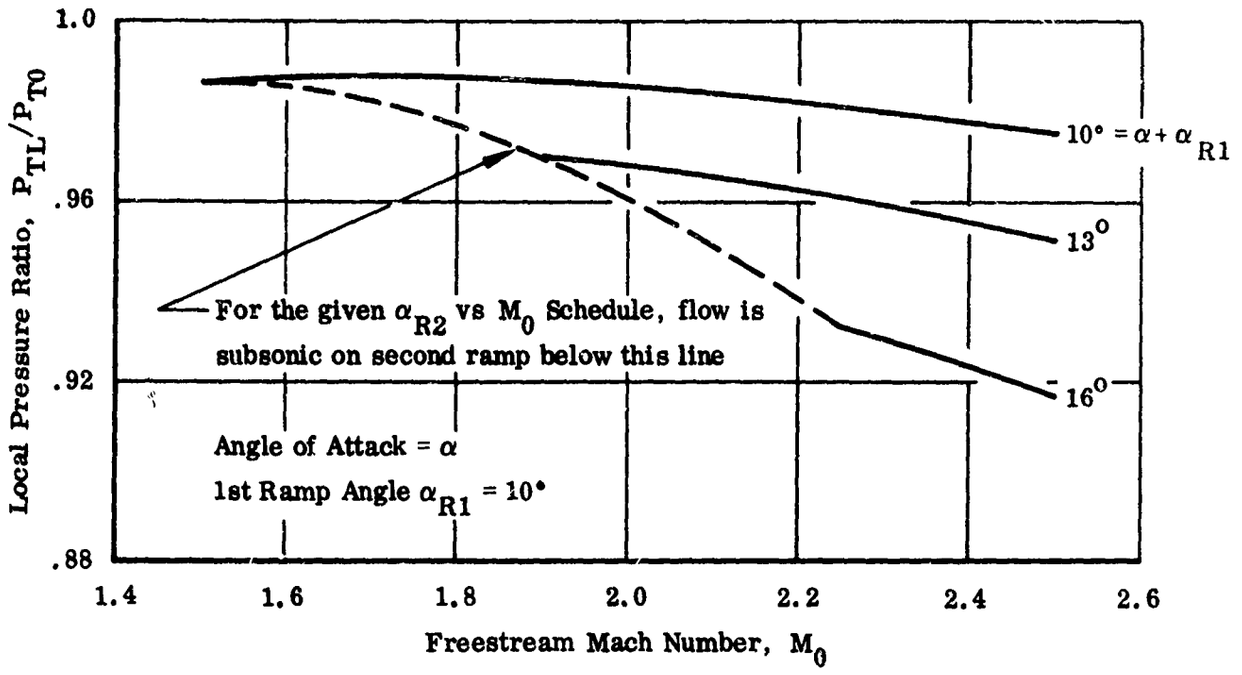

(c) $P_{TL}/P_{T0} = f(M_0, \alpha)$

Figure 19 Continued

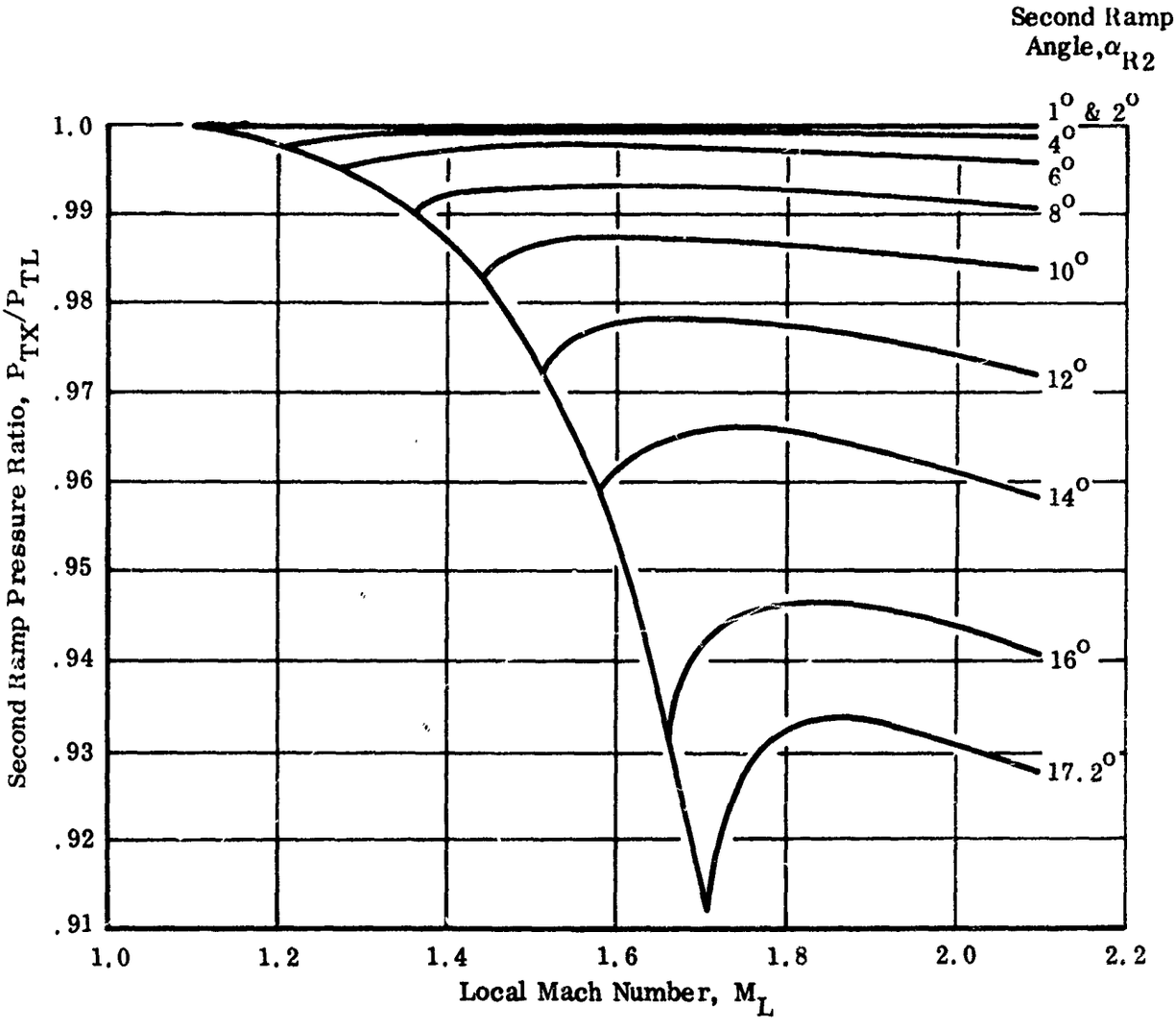

(d) $P_{TX}/P_{TL} = f(M_L, \alpha_{R2})$

Figure 19 Continued

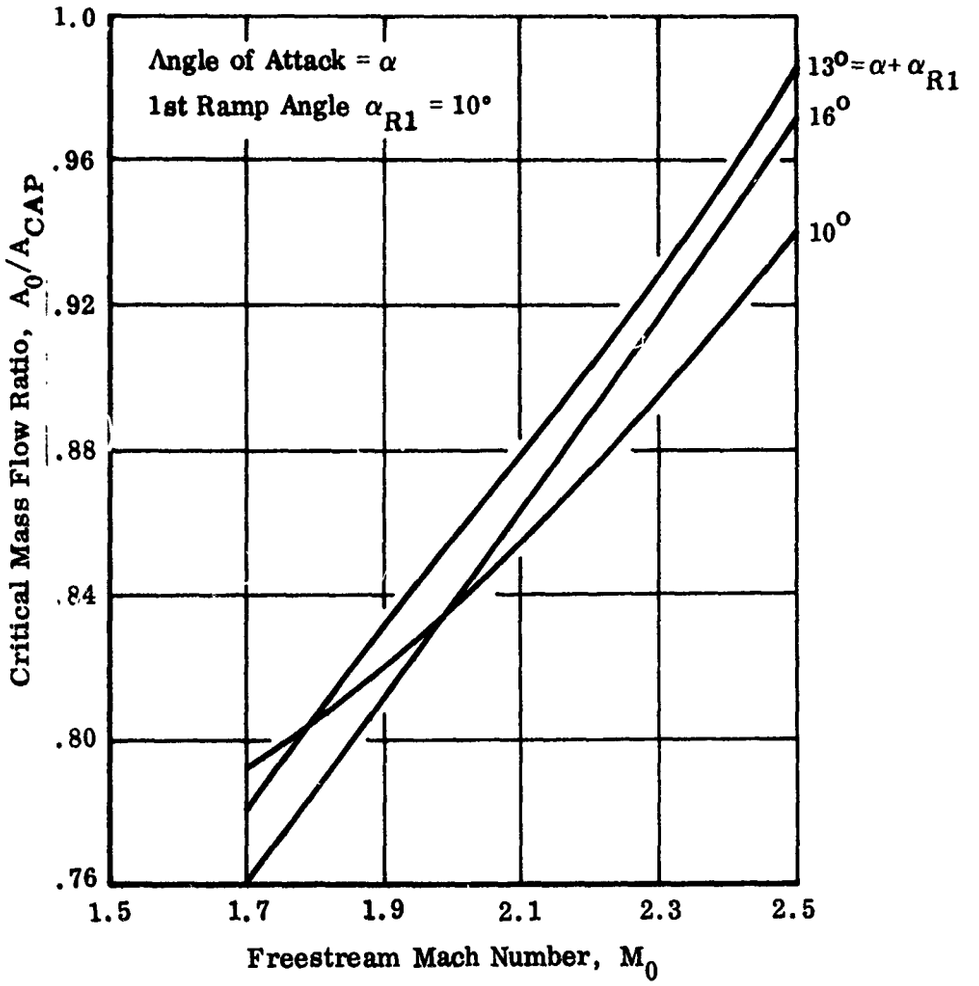

(e) $A_0/A_{CAP} = f(M_0, \alpha)$

Figure 19 Continued

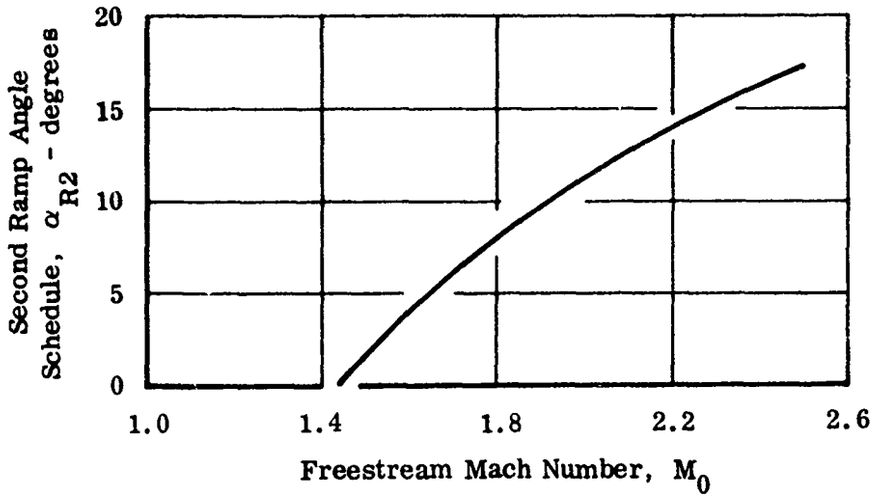

(f) $(\alpha_{R2})_{SCH} = f(M_0)$

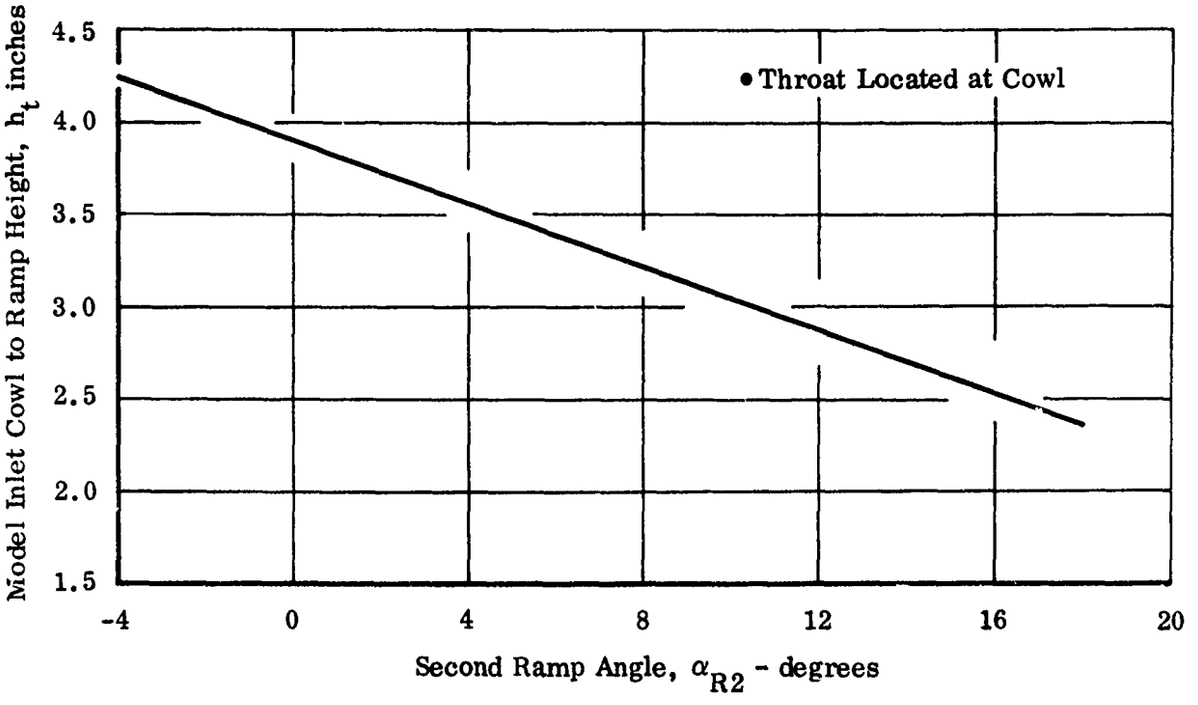

(g) $h_t = f(\alpha_{R2})$

Figure 19 Continued

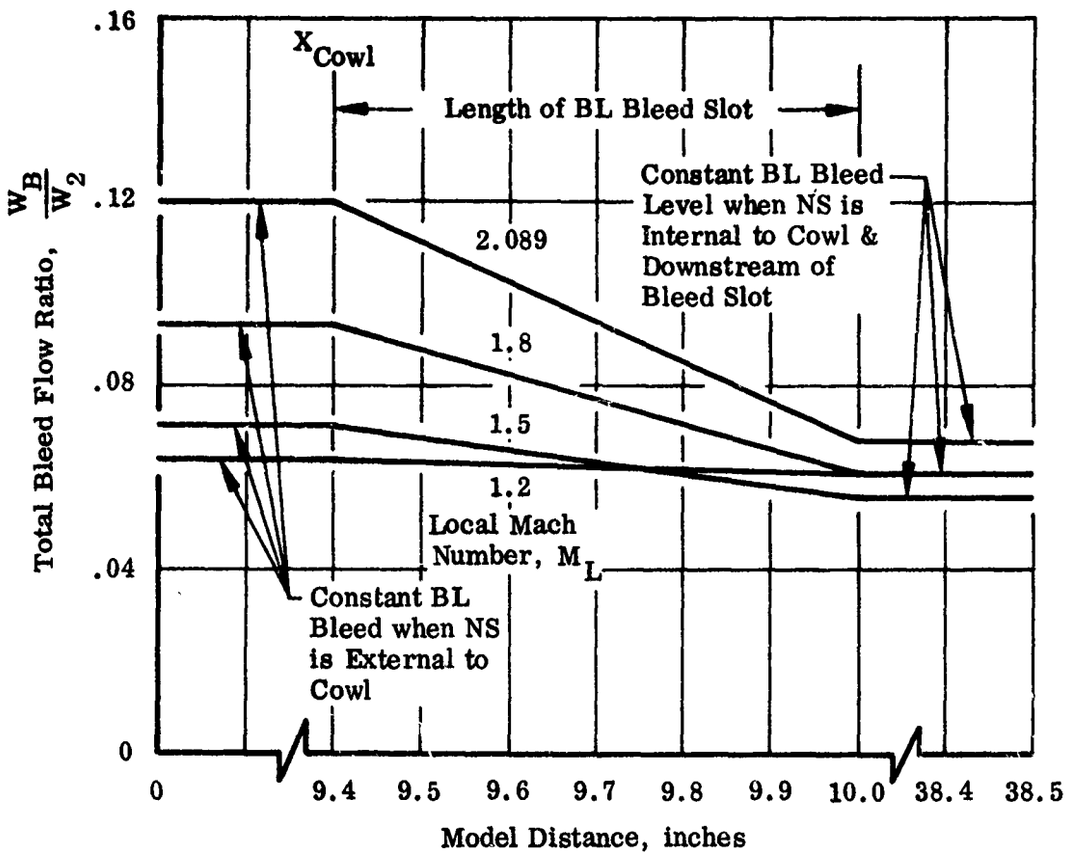

(h) $\frac{W_B}{W_2} = f(X, M_L)$

Figure 19 Continued

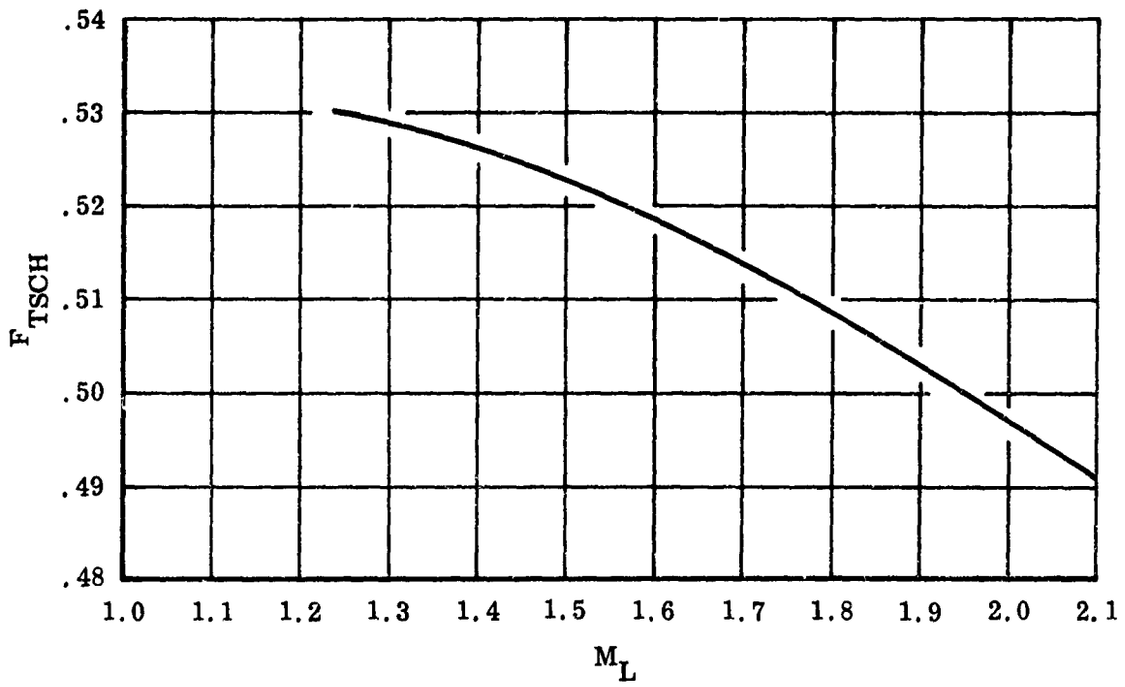

(i) $F_{TSCH} = f(M_L)$

Figure 19 Continued

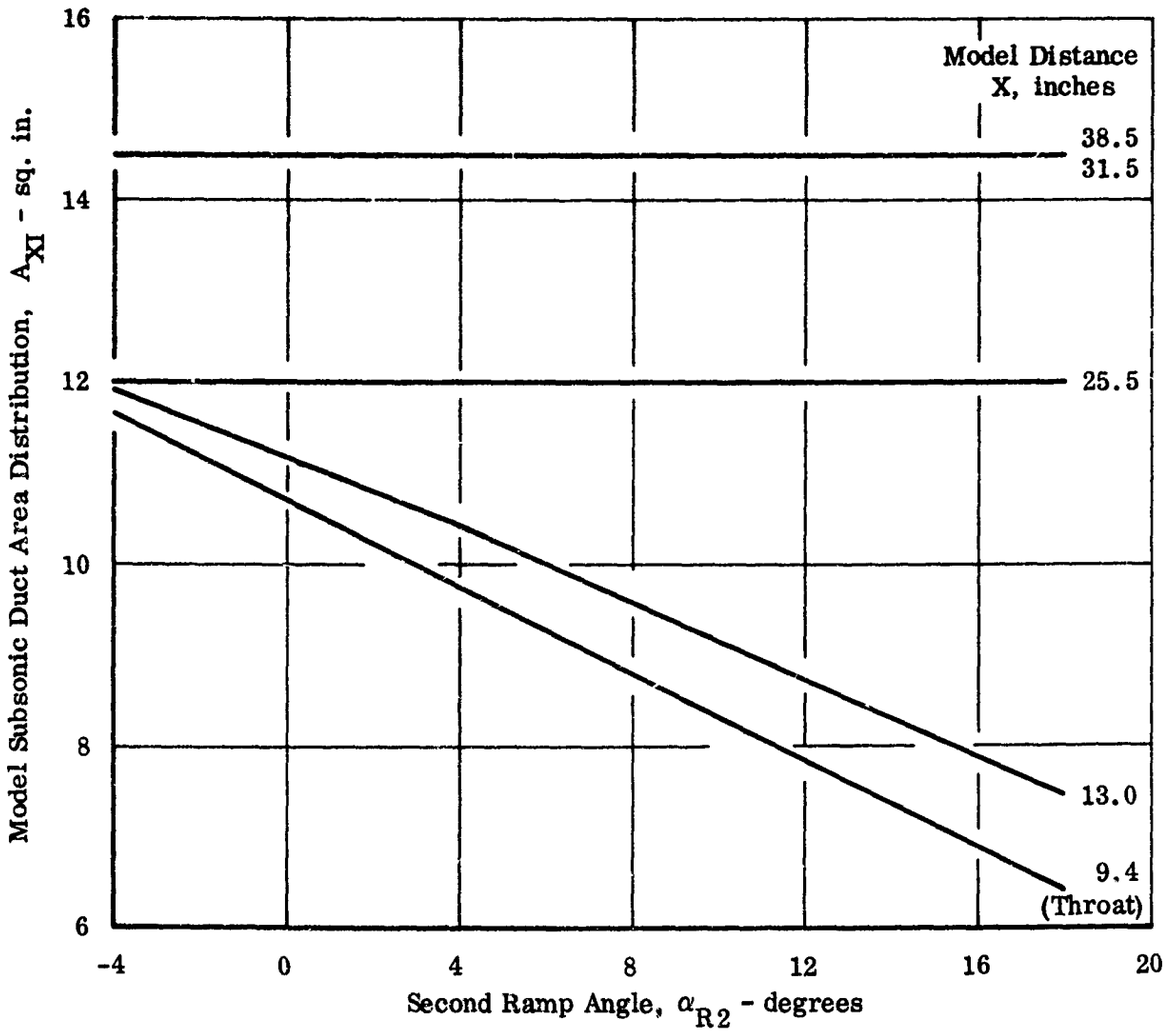

(j) $A_{XI} = f(\alpha_{R2}, X)$

Figure 19 Continued

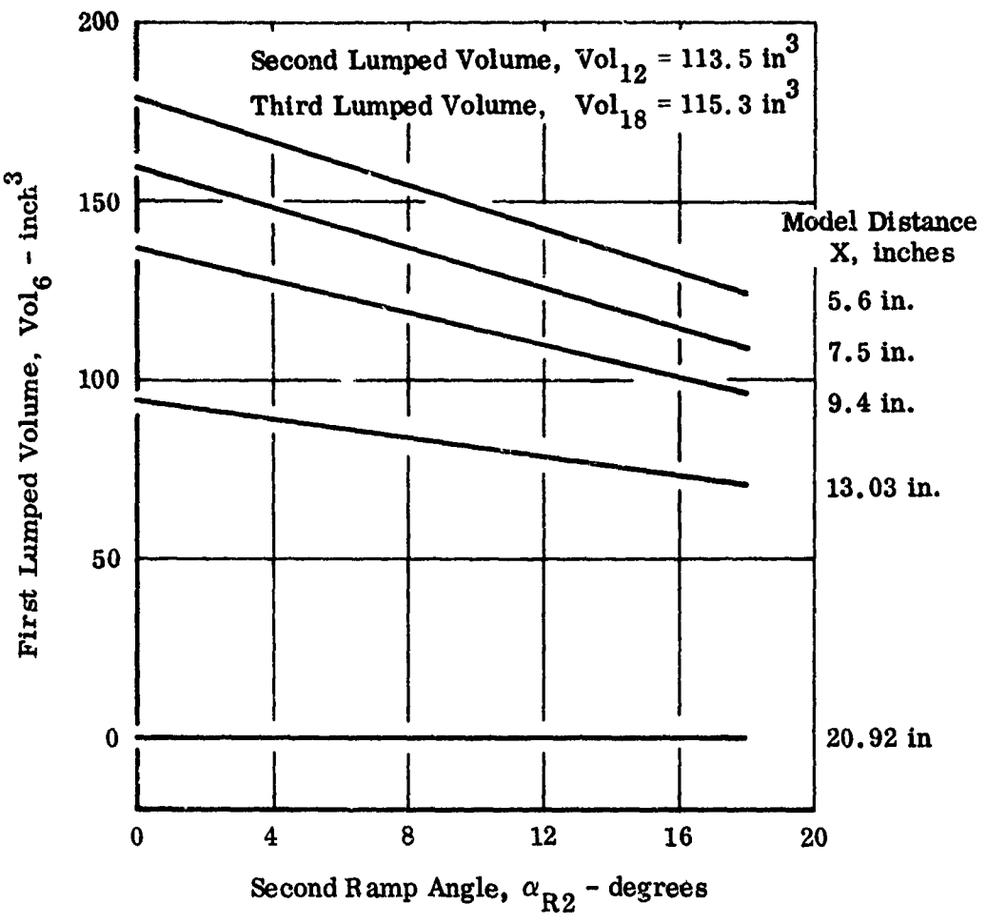

(k) $Vol_6 = f(\alpha_{R2}, X)$

Figure 19 Concluded

The Mach number behind the second shock (M_{XE}) is presented in Figure 19(b) as a function of M_L and α_{R2}. The total pressure recovery P_{TX}/P_{T0} is obtained similarly in two steps as shown in Figures 19(c) and 19(d). The critical mass flow ratio is presented in Figure 19(e) as a function of M_0 and $(\alpha + 10°)$.

Within the inlet operating speeds, a variable angle second ramp is required to maintain optimum performance as flight Mach number increases. Thus, some sort of a control mechanism sensitive to flight Mach number is required to accomplish this inlet geometry variation because the optimum geometry angles follow a definite Mach number schedule. This schedule, which gives optimum values of α_{R2} for maximum total pressure recovery (P_{TY}/P_{T0}) as a function of M_0 is shown in Figure 19(f). Although for this example α_{R2} stays constant since M_0 is constant, this schedule for α_{R2} must be followed, say, in an M_0 transient (i.e., gust) to avoid deterioration in inlet performance. An error signal $[(\alpha_{R2})_{SCH} - \alpha_{R2}]$ is generated by the ramp angle control logic for any deviations from the scheduled value and the control is set up to try to hold that value by reducing the error. The model inlet throat height defined as the perpendicular distance between the second ramp and the cowl lip (h_t) is shown in Figure 19(g) as a function of α_{R2}.

Figure 19(h) shows the changes in boundary layer bleed flow ratio (W_B/W_2) as a function of NS position and M_L. Ramp and throat slot bleeds are lumped together to simplify the calculations. Since the bleed flow rate is a function of the static pressure ratio at the slot, a higher constant value is used when the NS is external to the cowl (subsonic bleed) and a lower constant value is used when the NS is downstream of the slot (supersonic bleed). A linear variation in bleed flow between the above two constant values is assumed when the NS traverses the slot.

The bypass area is varied to control the shock position. A schedule for the throat flow function F_{TSCH} as a function of M_L is generated for this purpose [Figure 19(i)]. This flow function is calculated behind the NS when the shock is located at or slightly ahead of the throat at various operating conditions. This schedule essentially specifies the desired subsonic Mach number at the throat at various flight speeds. An error function ($F_{TSCH} - F_T$) is generated by the bypass area control logic for any deviation of the throat flow function, $F_T\left[W_T\sqrt{T_{TX}}/A_T\ P_{T6}\right]$ from the scheduled value F_{TSCH} when the NS is at a location other than the throat. This signal tends to close the bypass when the NS tends to travel too far downstream of the throat (highly supercritical operation resulting in unacceptable total pressure losses) in an attempt to drive it back

to the throat and, for the same reason, tends to open the bypass when the NS tends to travel too far upstream of the throat (highly subcritical operation).

Afterburner Blowout Transient (Model 1, Deck 2)

The dynamic response of the full-scale 2DE air induction system has been studied using the following example.

Transient:	A typical afterburner blowout transient (changes in engine corrected flow demand) is initiated at 1.0 second and lasts till 1.92 seconds.
Mach Number:	1.8
Altitude:	72,500 feet
Angle of Attack:	0

In this example the no-bypass no-control option of the program is exercised to simulate the 2DE air induction system. This is accomplished by assuming zero bypass area and neutralizing the bypass and ramp angle (α_{R2}) controls by inputting zero gains in the control logic. With no bypass, there is no means of controlling NS movement and all the excess flow is spilled subsonically at the cowl lip with the NS located at the proper standoff distance from the cowl to allow for the required spillage.

Discussion of Output Data. The afterburner blowout at 1 second [Figure 20(a)] causes engine exit air temperature to drop, thus rapidly decreasing pressure at engine exit and hence, an engine flow increase of about 10 percent before it is reduced to the original level at 1.9 seconds by reduction in nozzle area. Since there is no bypass, the engine demand W_{2E} [Figure 20(b)] is the same as diffuser exit flow W_2 [Figure 20(f)]. The effect of the transient on the NS is shown in Figure 20(e). Initially, the NS is located about 3 inches ahead of the cowl lip. The rapid increase in engine flow demand at 1.0 second causes depletion of the air in the lumped volumes (thus instantaneously reducing their total pressures) and, hence, a sucking effect on the NS resulting in downstream travel. The loss in duct pressure P_{T2} [Figure 20(d)] due to the initial sharp increase in engine flow demand is followed by a gain in pressure when the engine flow demand starts to decrease at 1.1 seconds. During the initial sharp rise of engine flow demand (10 percent within 40 milliseconds), the non-steady effect dominates since the pressure P_{T2} continues to drop, and the NS continues to move downstream for a short period (60 to 80 milliseconds), even after the Vol_{18} outflow W_2 reverses at 1.06 seconds.

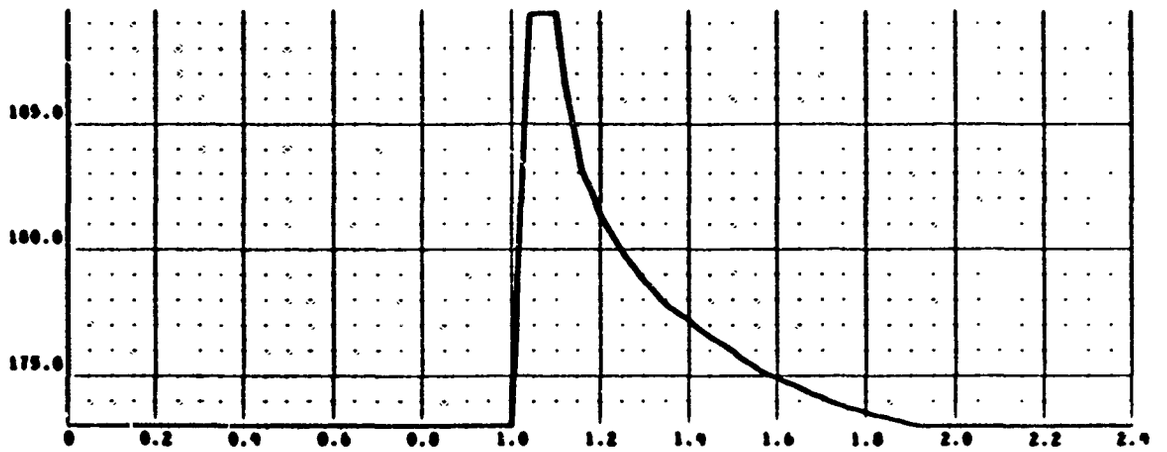

(a) Input Transient, W_{2EC} vs Time

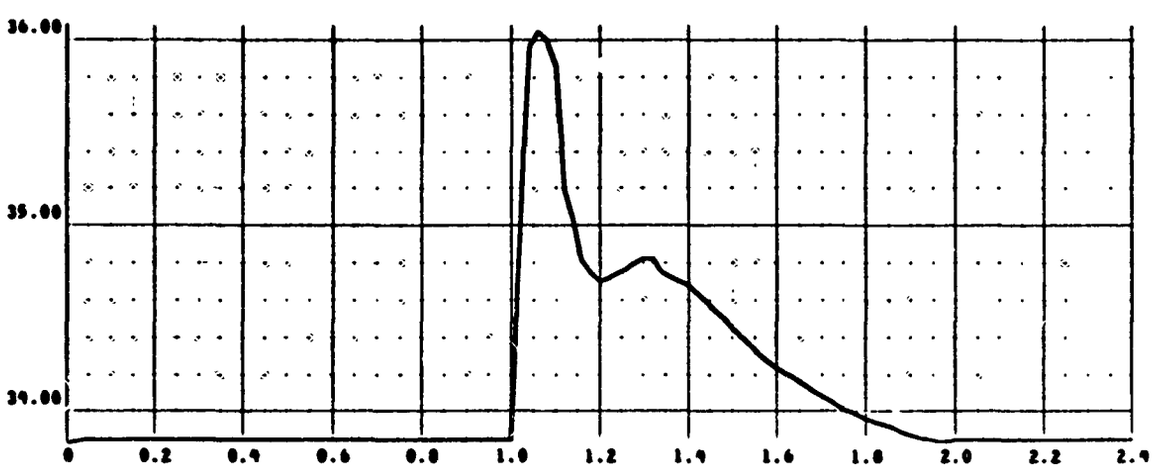

(b) W_{2E} (lbs/sec) vs Time

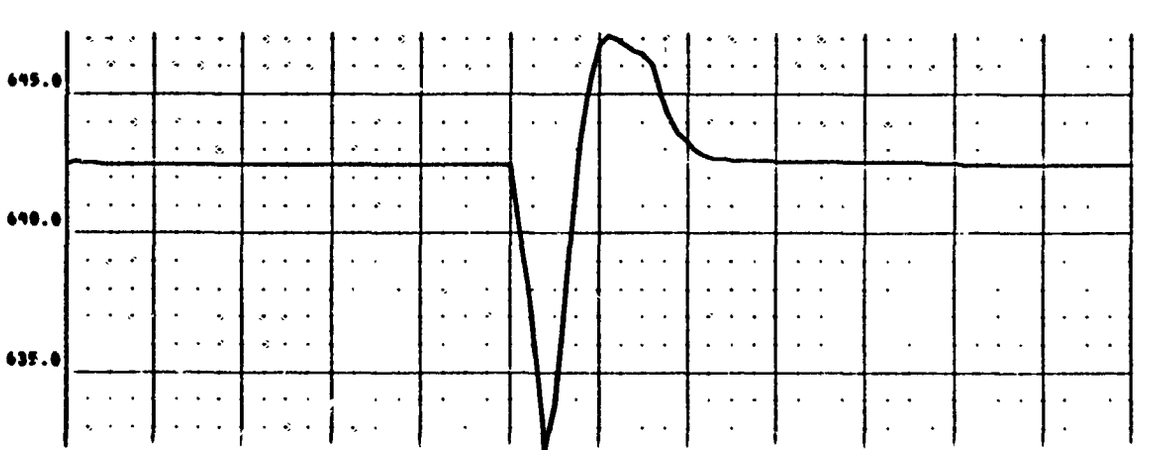

(c) T_{T2} (^{O}R) vs Time

Figure 20. 2DE Air Induction System Output Data - Afterburner Blowout (Model 1, Deck 2) $M_0 = 1.8$; H = 72500 ft; $\alpha = 0$

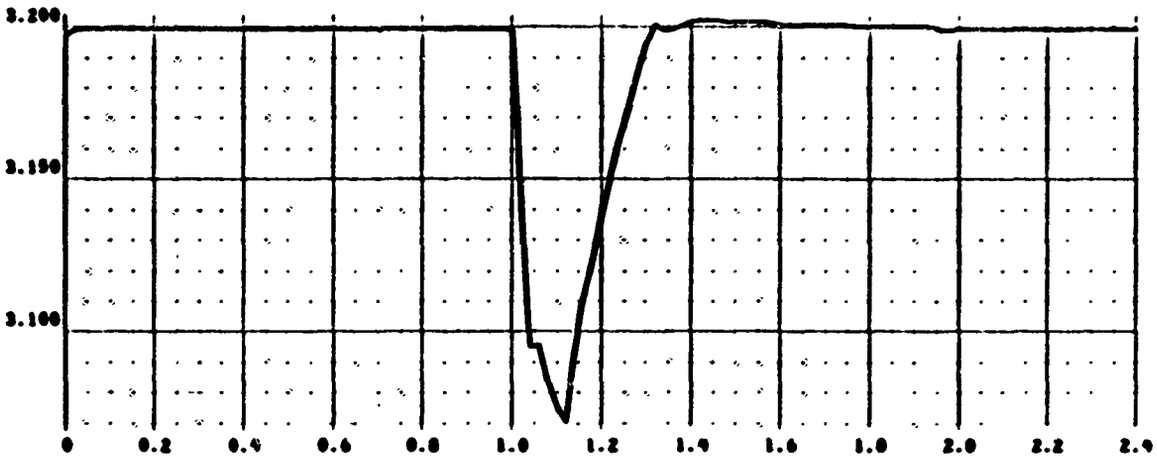

(d) P_{T2} (psi) vs Time

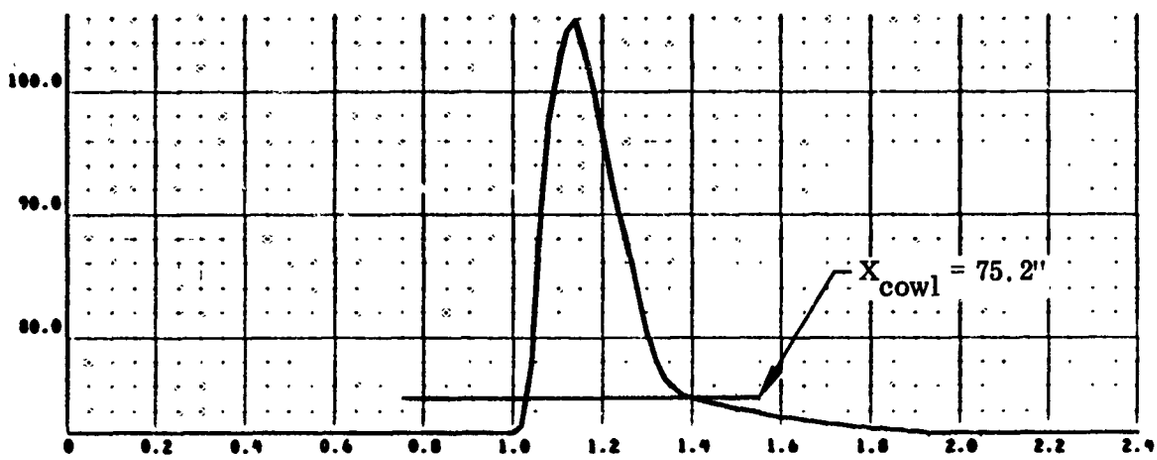

(e) X (in) vs Time

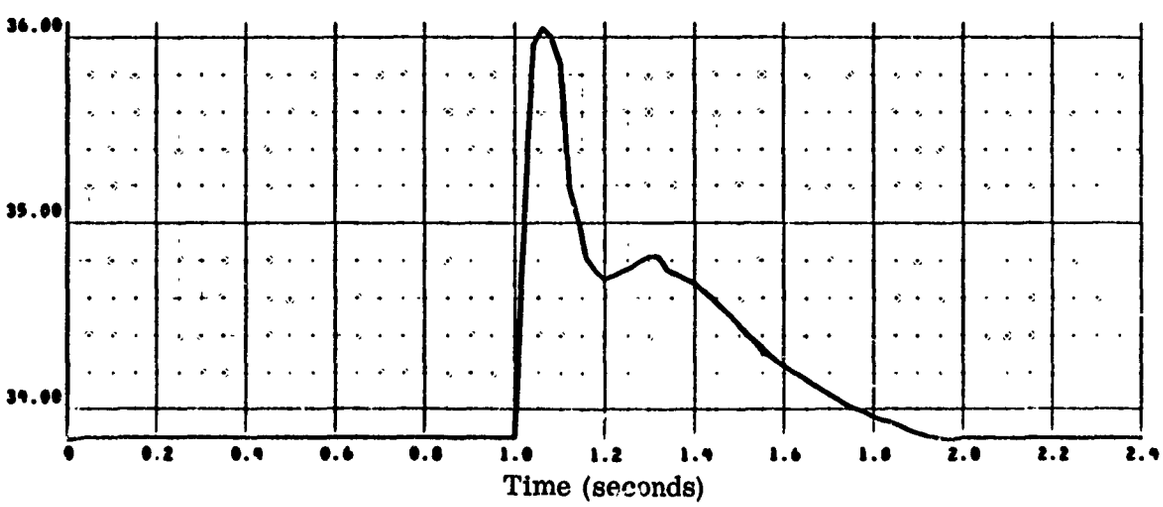

(f) W_2 (lbs/sec) vs Time

Figure 20 Concluded

The subsequent reduction in engine demand from 1.1 to 1.9 seconds is comparatively slow. At 1.14 seconds and 106 inches, the NS reverses direction and rapidly travels upstream until it reaches the cowl. The sudden change in slope (dx/dt) at the cowl (at 1.4 seconds) occurs because upstream of this point spillage flow effects are significant.

Angle of Attack Transient (Model 1, Deck 2)

The 2DE air induction system response to this transient is simulated at the following operating conditions.

Transient:	Angle of Attack. Initiated at 0.05 second as a ramp input at the typical rate of 24 degrees/second and lasting for 0.25 second.
Mach Number:	2.2
Altitude:	50,000 feet

The no-bypass no-controls option is again used for this example, along with the same input data as used for the previous example.

Discussion of Output Data. The input transient α changes through 6 degrees during the simulation run [Figure 21(a)]. The effect of this change on the properties P_{TX} and M_X upstream of the NS is shown in Figure 21(b) and 21(c) respectively. The overall change in P_{T2}, X, and T_{T2} as shown in Figures 21(d) to 21(f) is quite small. Due to the small overall change in properties during the simulation, the fluctuation in their values before initiation of and after termination of the transient is due to the exaggerated scale of the plots.

As the angle of attack changes, M_X and P_{TX} reduce and the NS moves upstream in response. This loss in P_{TX} is reflected in the P_{T2} curve [Figure 21(d)]. The T_{T2} level [Figure 21(f)] changes slightly during the transient but returns to its original value after the transient is over since the process is adiabatic.

As the NS travels upstream, the spillage flow W_{SP} increases as shown in Figure 21(g). The change in W_2 [Figure 21(h)] is seen to be directly proportional to changes in P_{T2} and T_{T2} since it is obtained from a constant value of corrected engine flow, W_{2EC}.

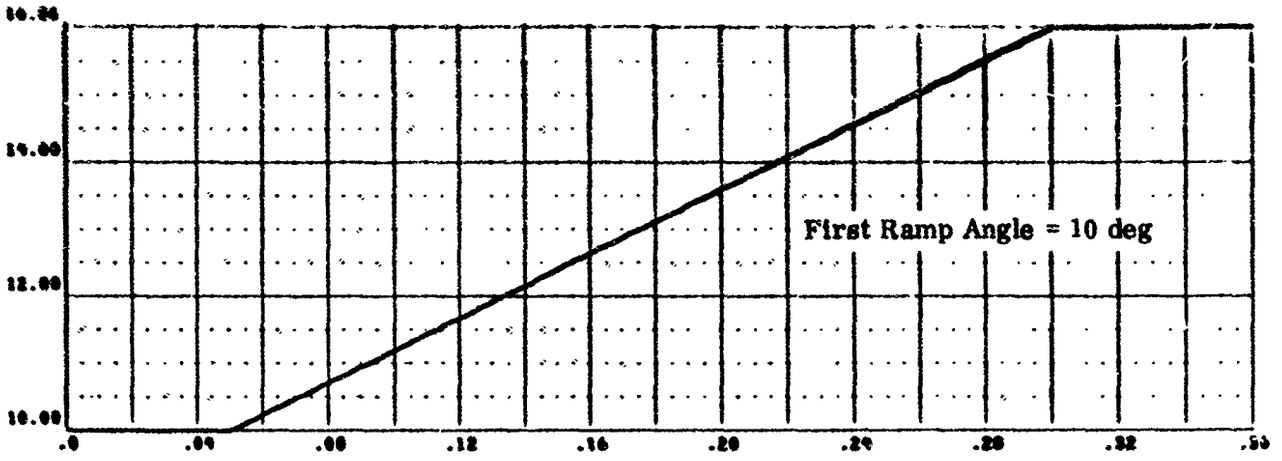

(a) Input Transient, Angle of Attack (α + 10 deg) vs Time

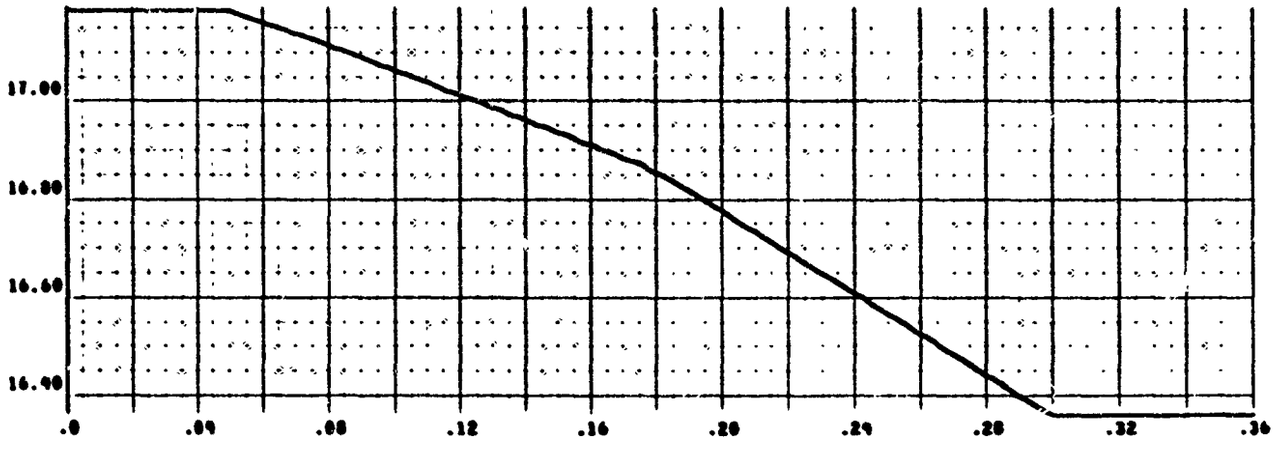

(b) P_{TX} (psi) vs Time

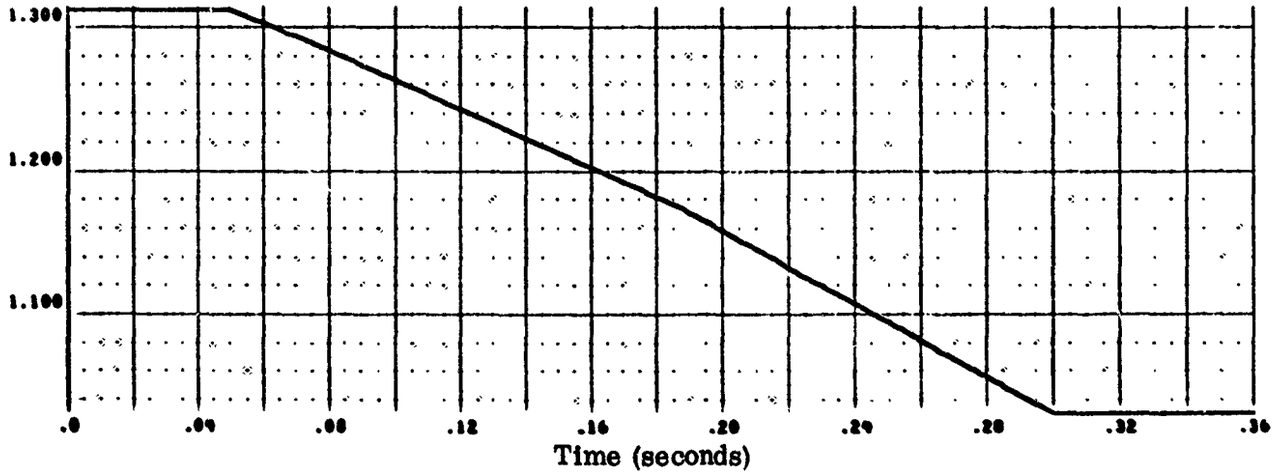

(c) M_X vs Time

Figure 21. 2DE Air Induction System Output Data - Angle of Attack (Model 1, Deck 2) M_0 = 2.2; H = 50000 ft

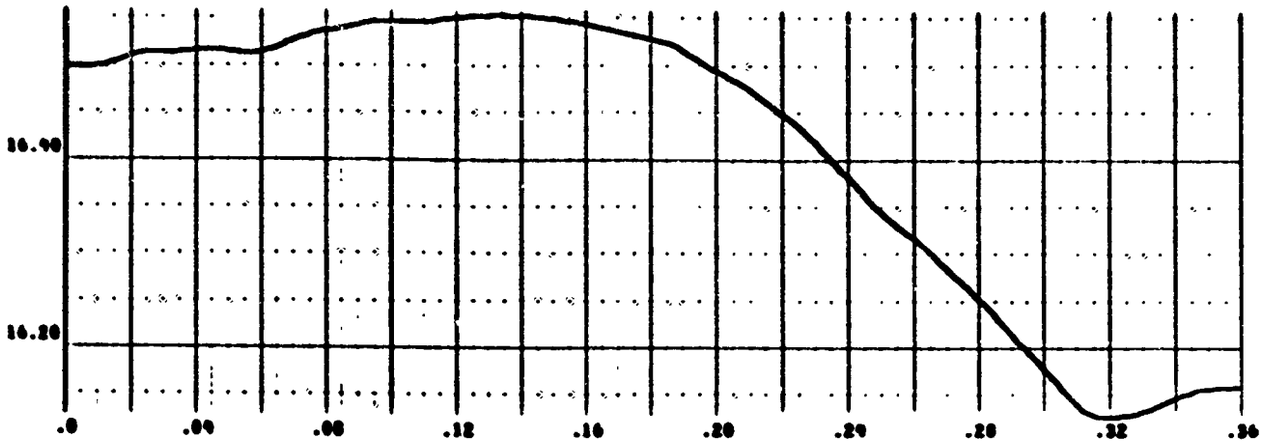

(d) P_{T2} (psi) vs Time

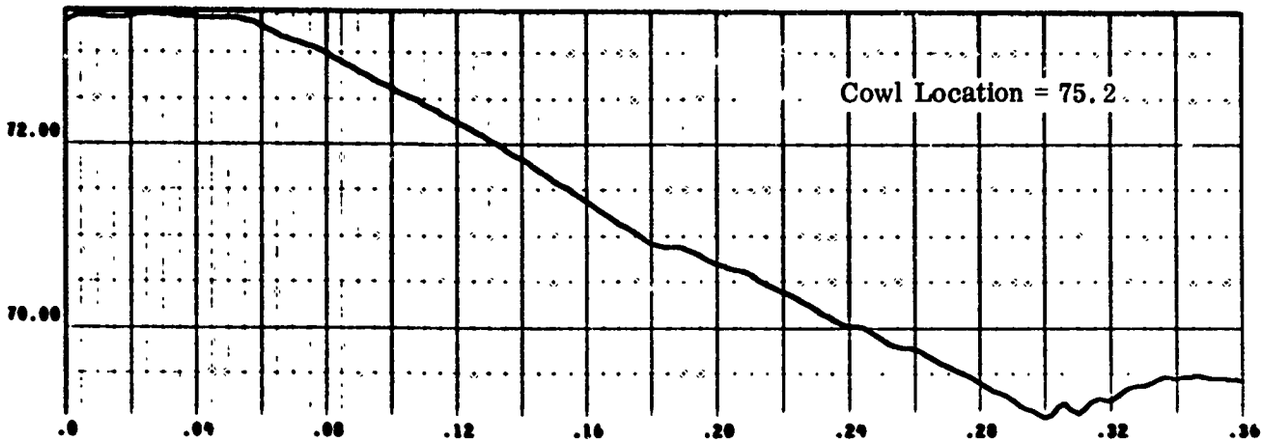

(e) X (in) vs Time

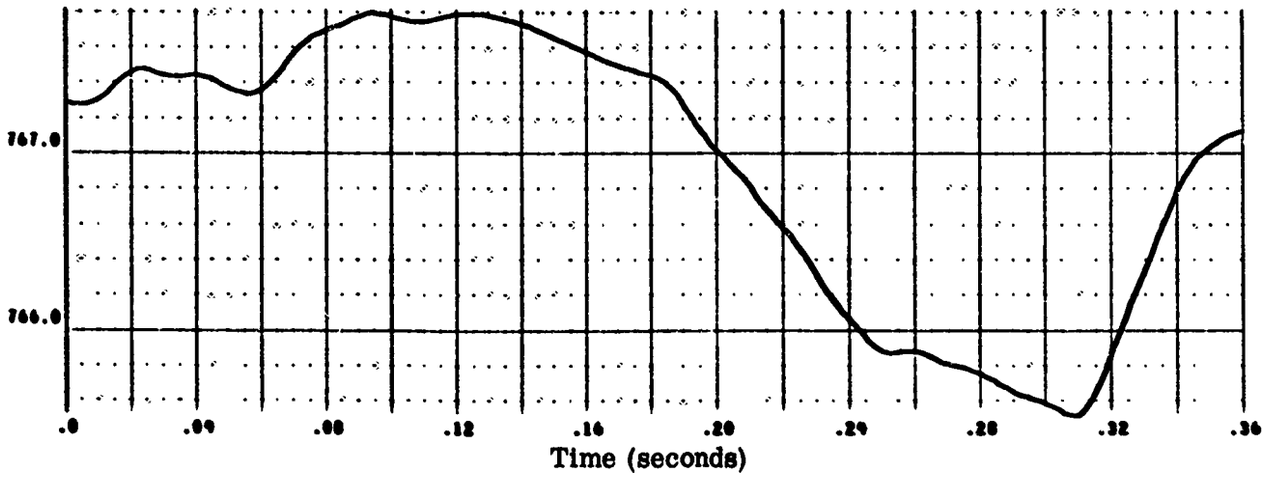

(f) T_{T2} (^{o}R) vs Time

Figure 21 Continued

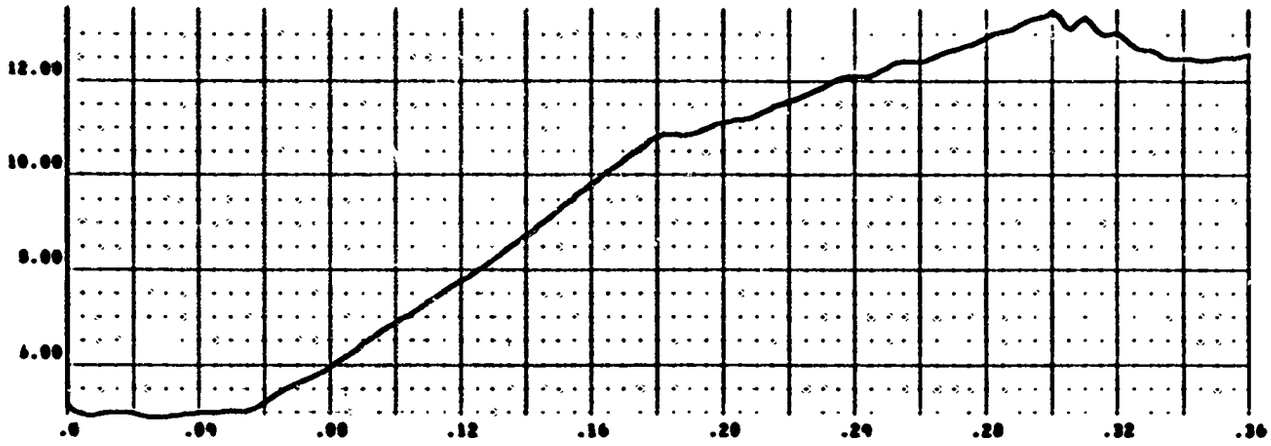

(g) W_{SP} (lbs/sec) vs Time

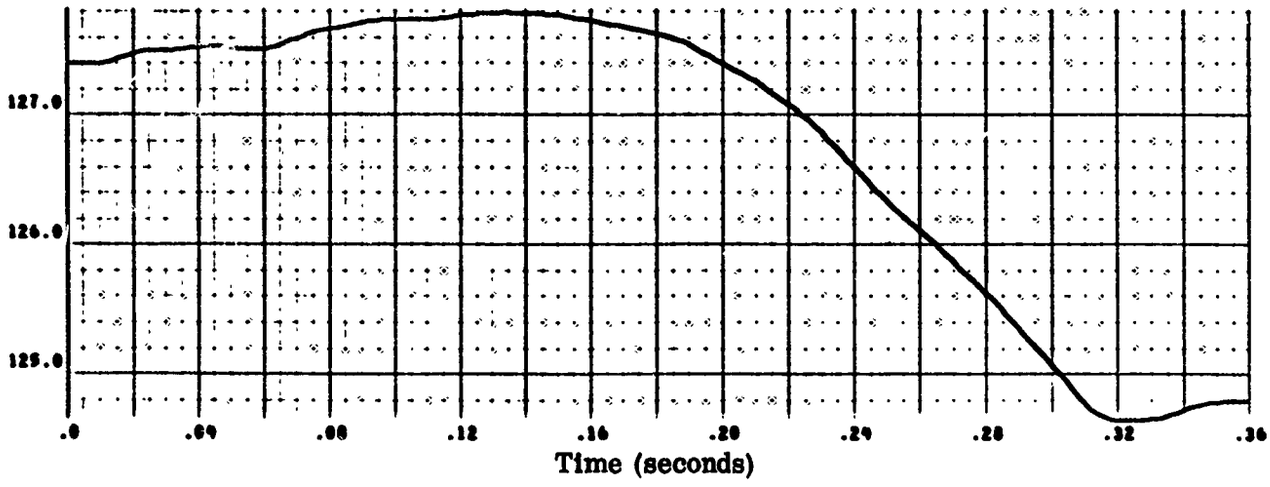

(h) W_2 (lbs/sec) vs Time

Figure 21 Concluded

Buzz Transient (Model 2, Deck 4)

The following example is used to simulate the buzz transient.

Transient:	Buzz
Mach Number:	2.5
Altitude:	50,000 feet
Angle of Attack:	0

At the design Mach number of 2.5, the inlet operates slightly subcritically with all the excess flow being spilled at the cowl lip. Buzz is initiated by triggering separation through program logic.

Discussion of Input Data. Additional input data curves required for this transient are presented in Figure 22. The approach used in developing these curves is similar to that followed for the 2DM air induction system except for the ΔA_{ET} curve [Figure 22(d)], where the maximum level of throat area blockage is reduced to 70 percent as compared to 93 percent at Mach 3 for the 2DM inlet. Reference 11, which compares XB-70 flight test data with simulation predictions of inlet unstart and buzz, indicates that model and flight tests for various inlets, including XB-70, have shown some variation in the magnitude of boundary layer separation as a function of the static pressure rise across the NS and, hence, the Mach number near the cowl. Since the latter decreases with decreasing M_0, there is a corresponding reduction in the separation level (and, hence, blockage) for the 2DE contract inlet operating at Mach 2.5 as compared to the 2DM inlet operating at Mach 3. The 70 percent level is based on XB-70 simulation input data available in Reference 11.

Discussion of Output Data. The output data for the buzz transient are presented in Figure 23. The key parameter P_{T12}/P_{T0} that triggers separation and attachment is shown in Figure 23(c). After the flow attaches at 0.37 second (when P_{T12}/P_{T0} drops below 0.315), the NS [Figure 23(a)] moves rapidly into the inlet to a highly supercritical location. Separation is triggered again when the NS emerges from the cowl since both the conditions [(1) that P_{T12}/P_{T0} be above 0.519 and (2) NS be upstream of the cowl] are satisfied at this point. The reason why separation is not triggered at 0.381 second when P_{T12}/P_{T0} initially rises to 0.519 (just after attachment has occurred) is because the NS is downstream of the cowl at that time.

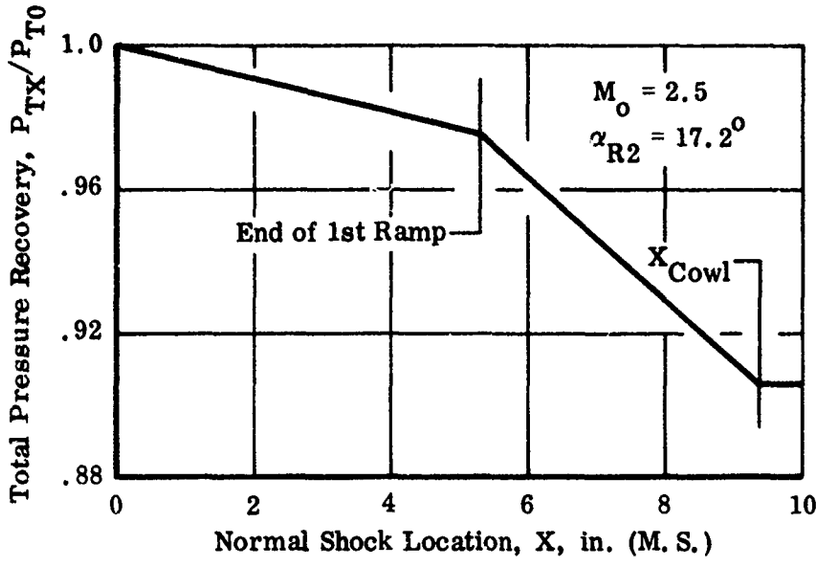

(a) $P_{TX}/P_{T0} = f(X)$

Figure 22. 2DE Air Induction System Additional Input Data for Buzz Model

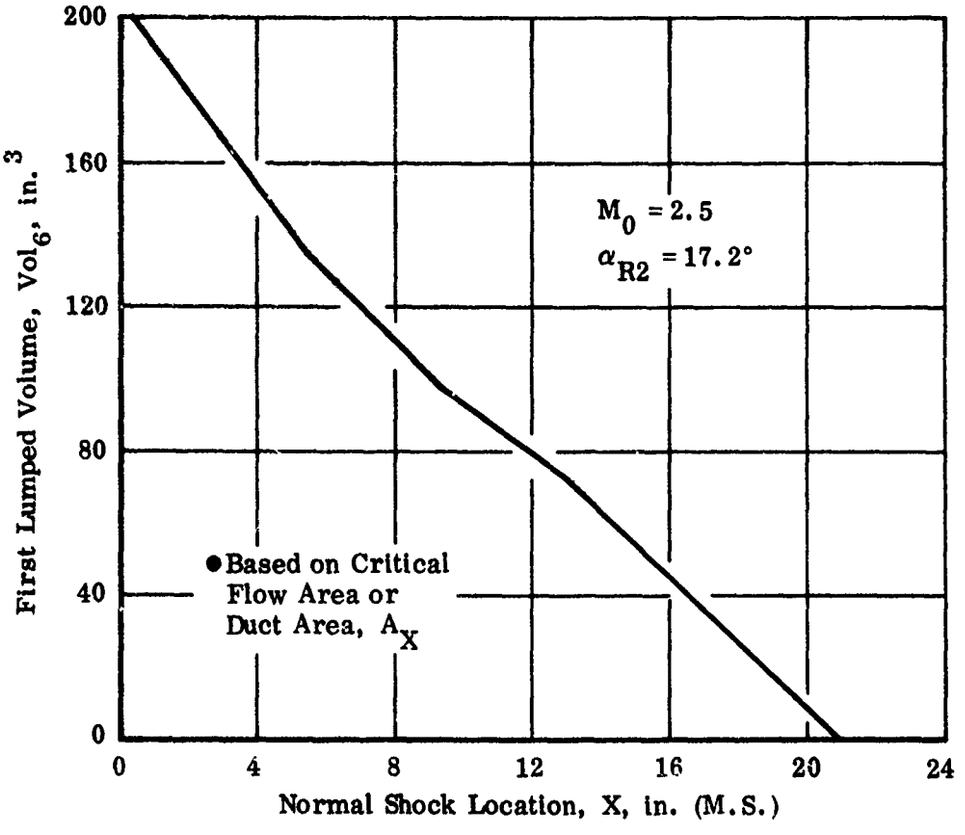

(b) $Vol_6 = f(X)$

Figure 22 Continued

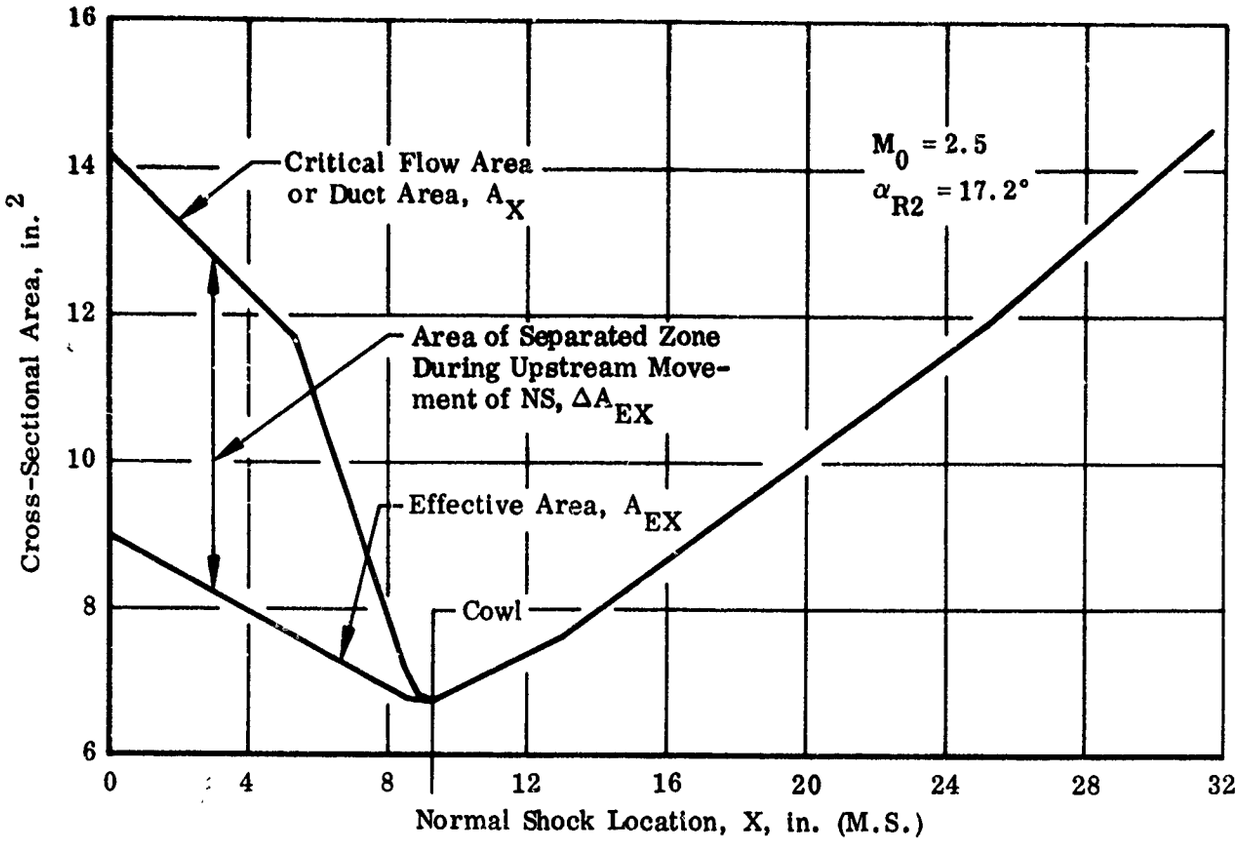

(c) Various Flow Areas as Function of X

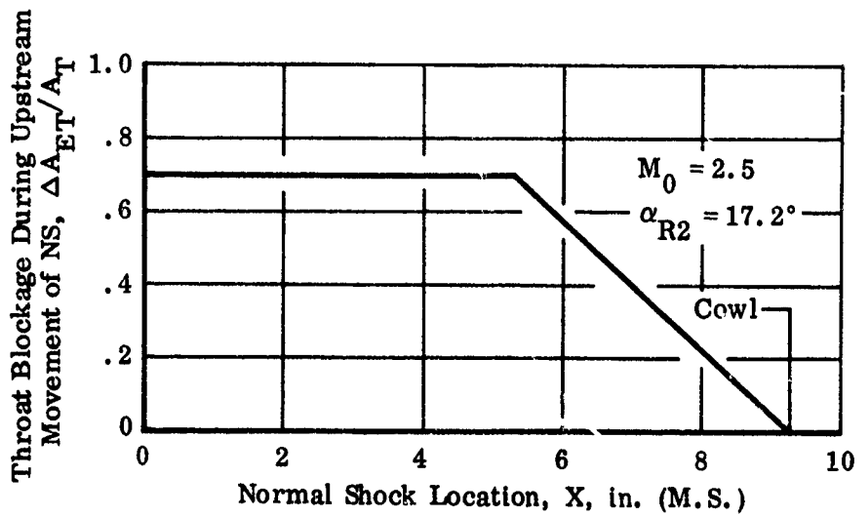

(d) $\Delta A_{ET}/A_T = f(X)$

Figure 22 Concluded

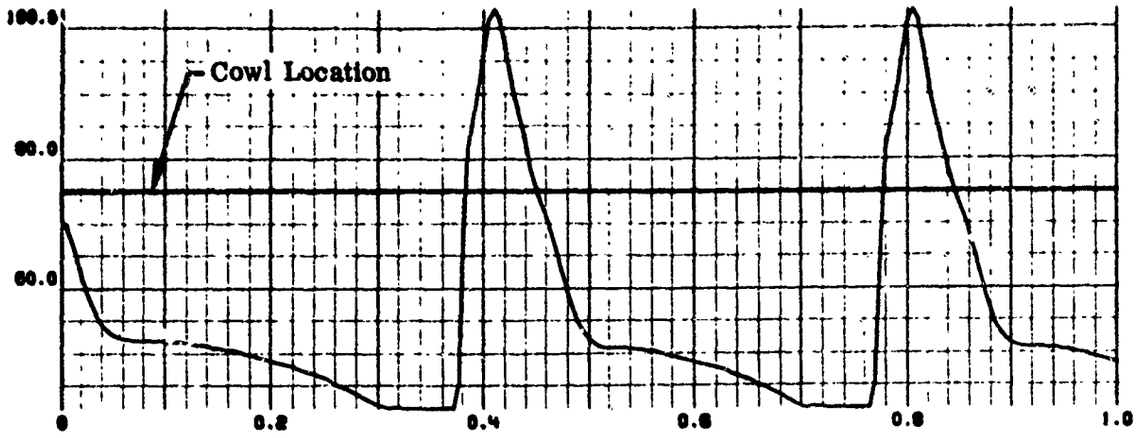

(a) X (in) vs Time

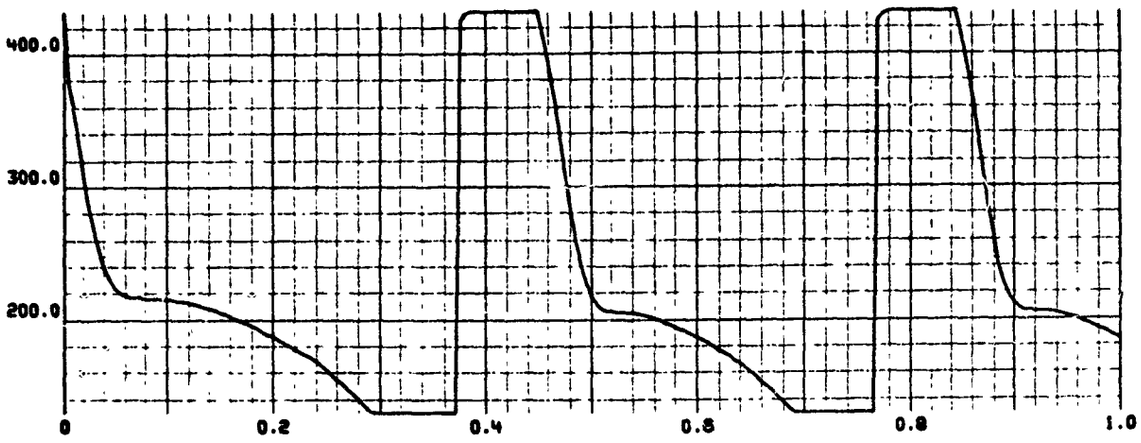

(b) A_{ET} (in^2) vs Time

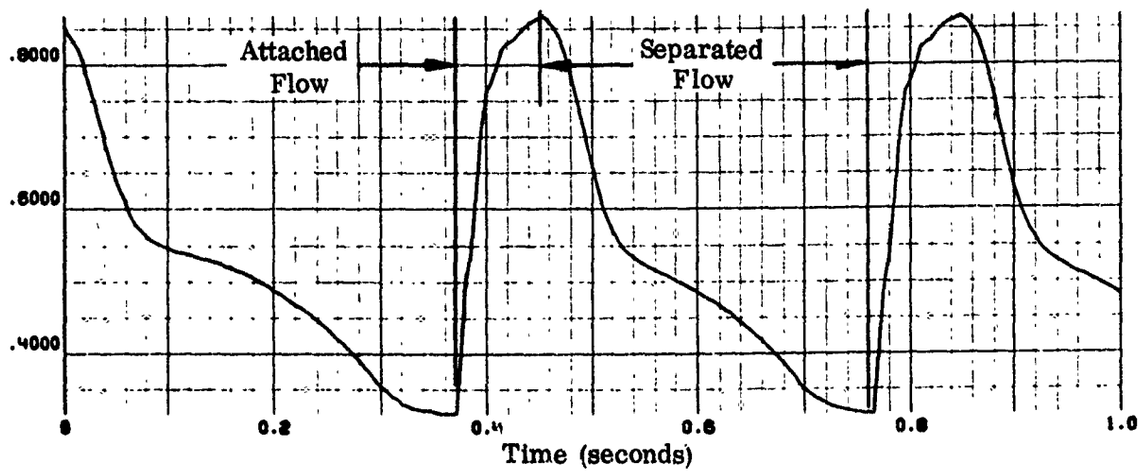

(c) P_{T12}/P_{T0} vs Time

Figure 23. 2DE Air Induction System Output Data - Buzz Transient (Model 2, Deck 4) M_0 = 2.5; H = 50000 ft; α = 0

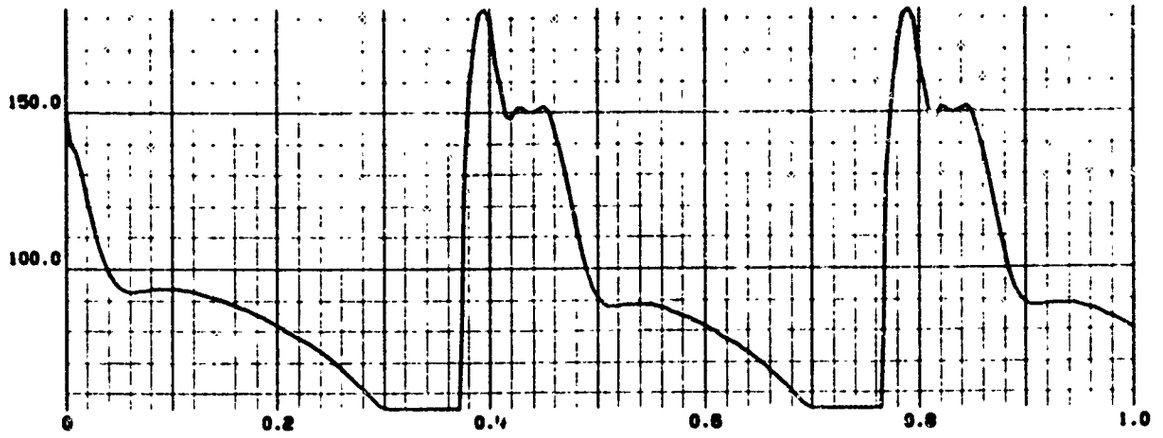

(d) W_8 (lbs/sec) vs Time

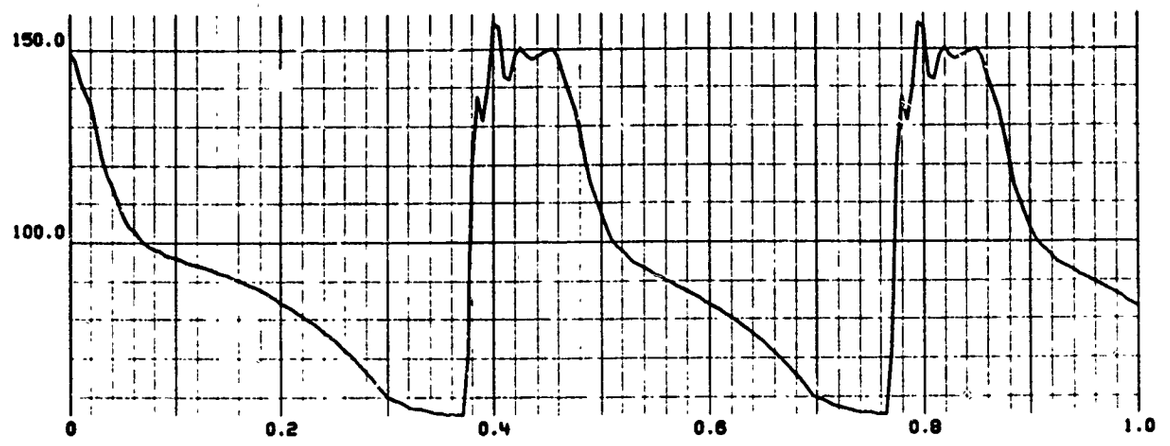

(e) W_{14} (lbs/sec) vs Time

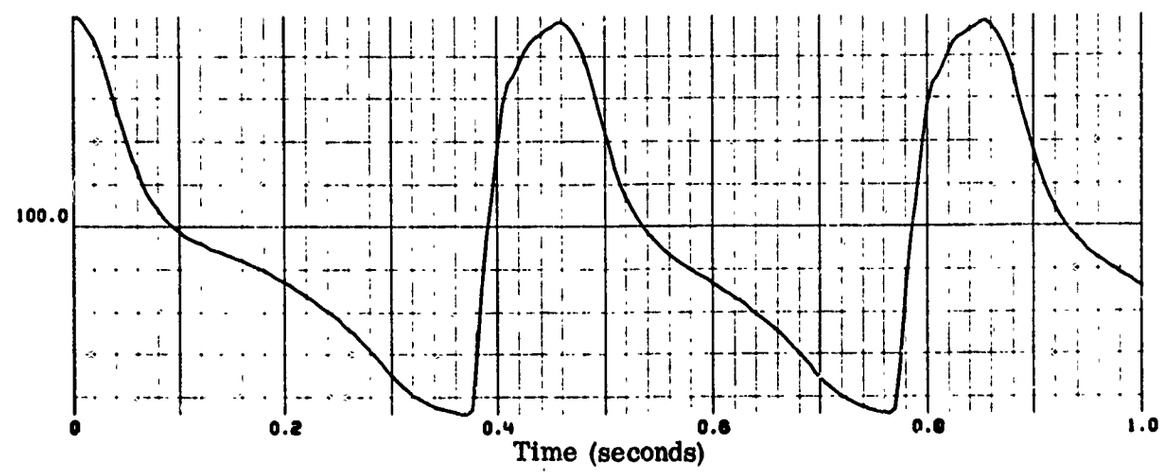

(f) W_2 (lbs/sec) vs Time

Figure 23 Continued

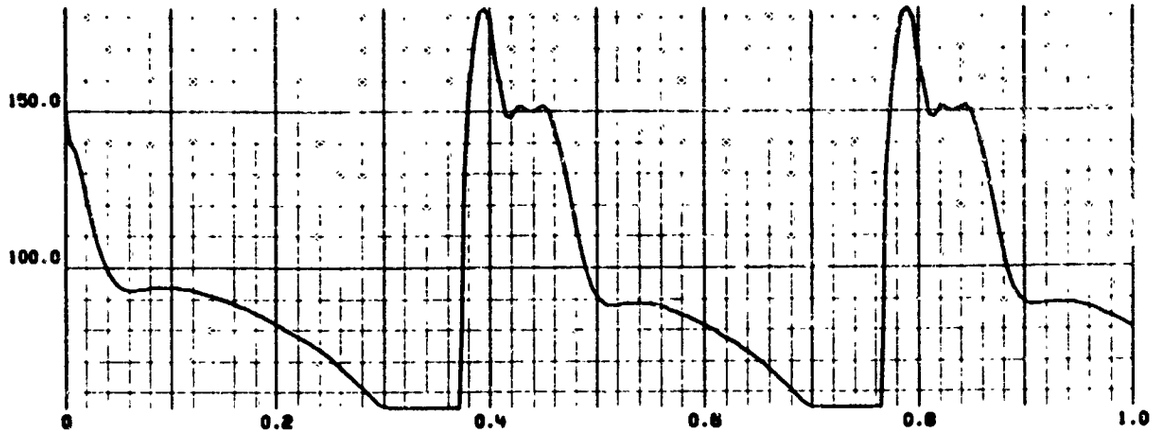

(d) W_8 (lbs/sec) vs Time

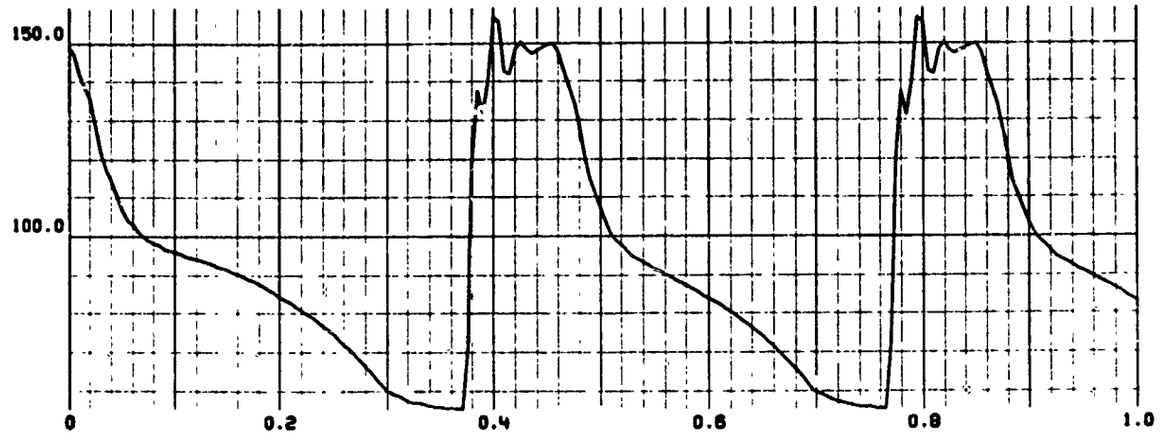

(e) W_{14} (lbs/sec) vs Time

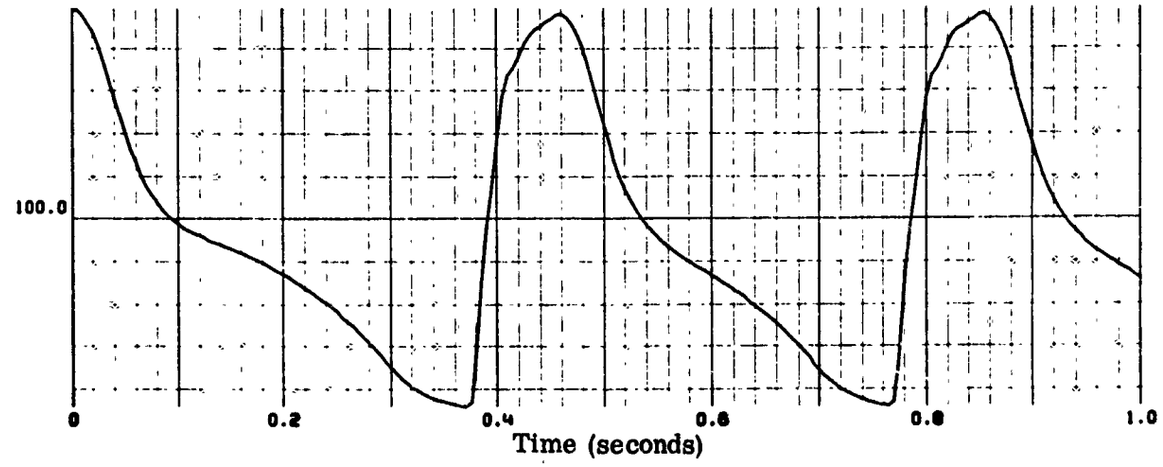

(f) W_2 (lbs/sec) vs Time

Figure 23 Continued

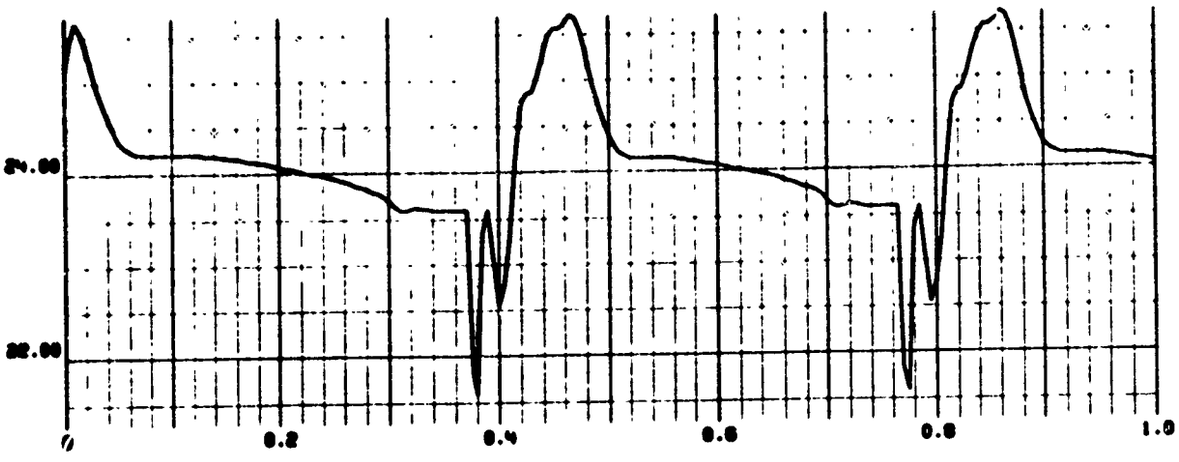

(g) P_{T6} (psi) vs Time

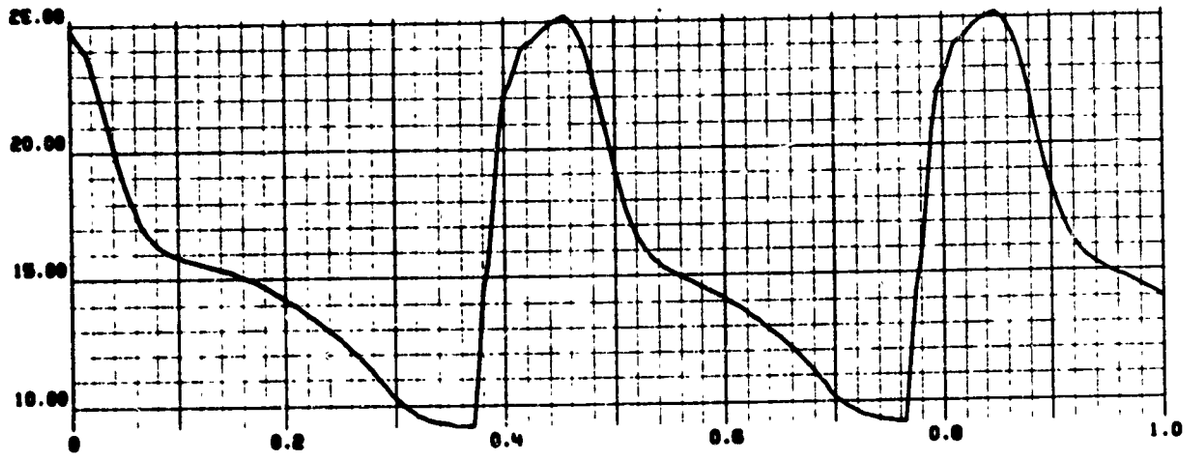

(h) P_{T5} (psi) vs Time

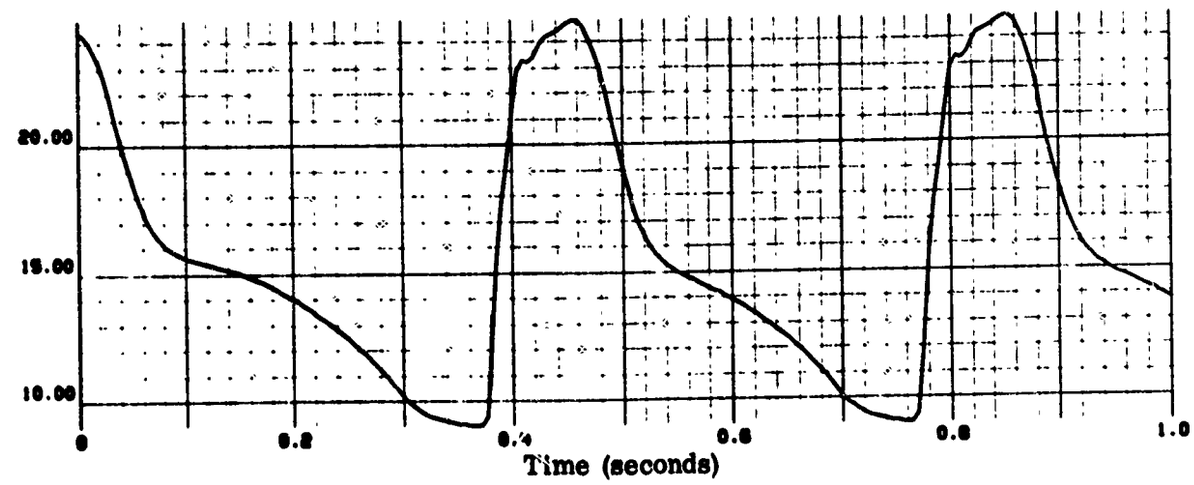

(i) P_{T2} (psi) vs Time

Figure 23 Continued

(j) T_{T6} (^{O}R) vs Time

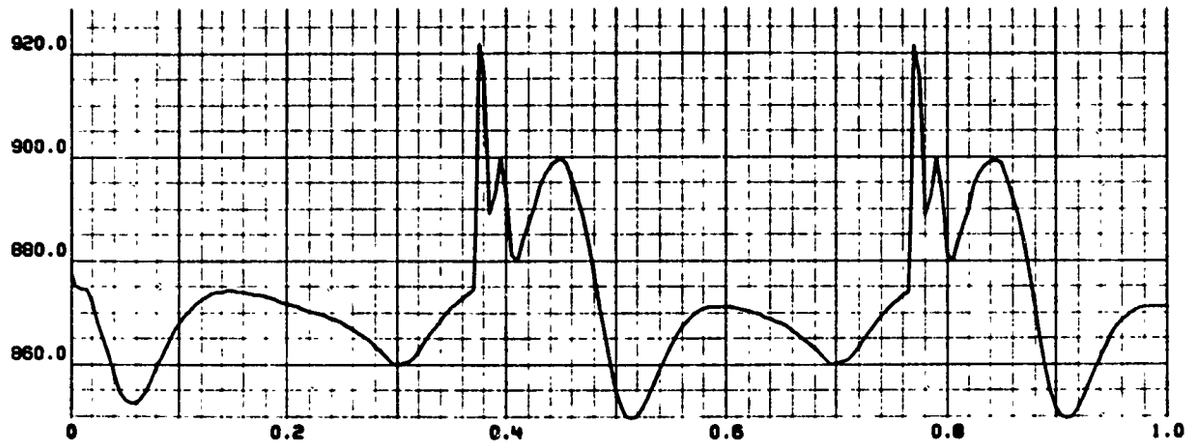

(k) T_{T12} (^{O}R) vs Time

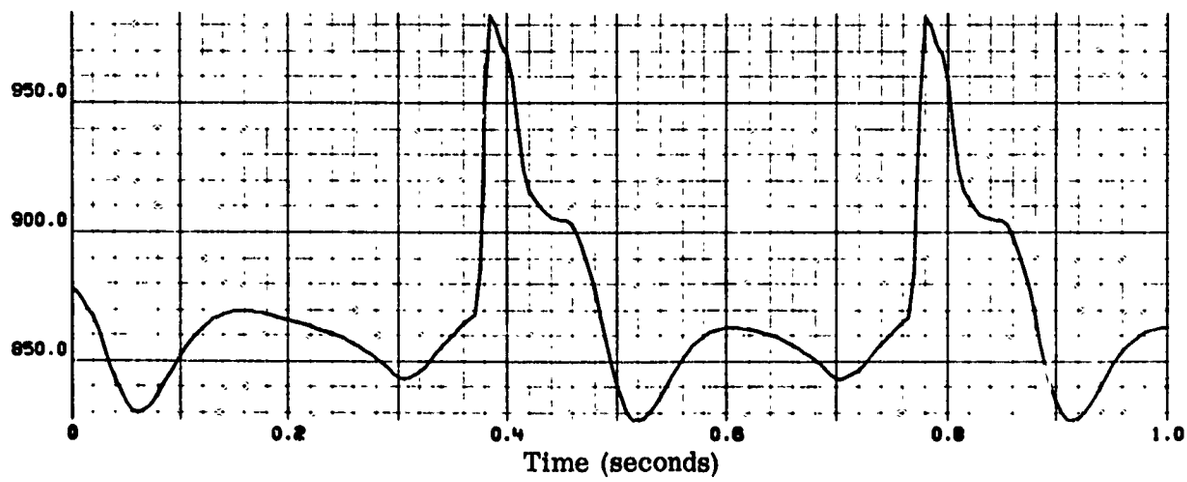

(l) T_{T2} (^{O}R) vs Time

Figure 23 Concluded

The NS upstream travel rate [Figure 23(a)] for the 2DE inlet is slower than the 2DM inlet and the buzz frequency is lower; 2.5 cps compared to 7 cps for the full scale 2DM inlet. The total pressure P_{T2} and total temperature T_{T2} amplitudes of 16 psi and 150°R during buzz are shown in Figure 23(k) and 23(l) respectively.

Hammershock Transient (Model 3, Deck 6)

The dynamic response of the 2DE air induction system to a hammershock transient has been studied at the following conditions.

Transient:	100 percent airflow cutoff in 0.01 second
Mach Number:	2.5
Altitude:	50,000 feet
Angle of Attack:	0

The basic input data are the same as that used for the buzz transient.

Discussion of Output Data. The output data are presented in Figure 24. Since no bypass is assumed, engine demand is the same as diffuser supply ($W_2 = W_{2E}$) and both reduce to zero within 10 milliseconds after flow cutoff at 0.01 second [Figures 24(a) and 24(f)]. Although P_{T12} [(Figure 24(h)], as expected, lags behind P_{T2} [Figure 24(i)], by about 3 milliseconds, P_{T6} [Figure 24(g)] actually leads P_{T12} by about 2 milliseconds. The reason for this is that in the 2DE inlet input data the boundary layer bleed curve [W_B/W_2, Figure 19(h)] is input as a function of W_2 [Figure 24(f)]. The resulting rapid reduction in instantaneous bleed outflow from Vol_6 (about 20 pounds/second at initiation of hammershock) to zero within 10 milliseconds causes Vol_6 total pressure P_{T6} to rise somewhat, immediately after the hammershock is initiated, before dropping rapidly due to the subsequent massive increase in instantaneous spillage outflow. The reason why this small initial increase in P_{T6} does not occur for the 2DM air induction system [Figure 18(g)] is because the 2DM bleed curve [Figure 13(l)] is input as a function of W_0 which stays constant during the hammershock.

During the hammershock the subsonic duct experiences a maximum pressure of 1.22 times the freestream total pressure at 0.033 second [Figure 24(c)].

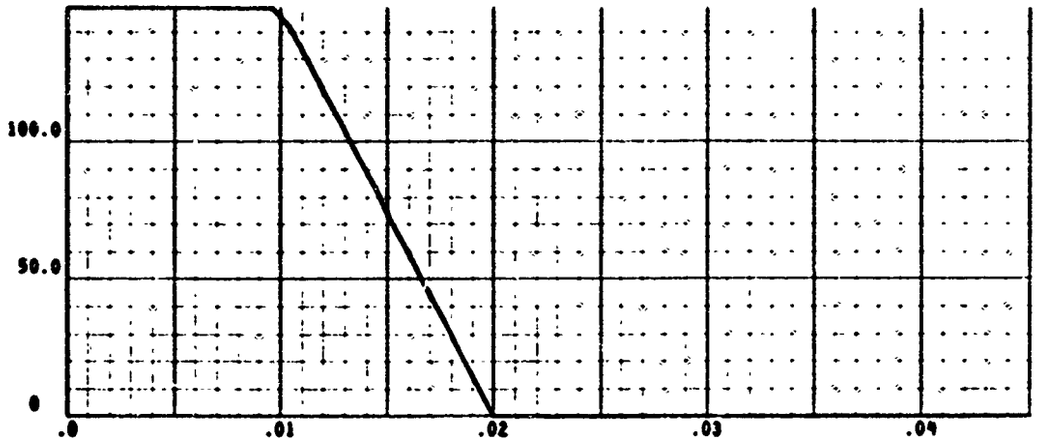

(a) Input Transient, W_{2E} (lbs/sec) vs Time

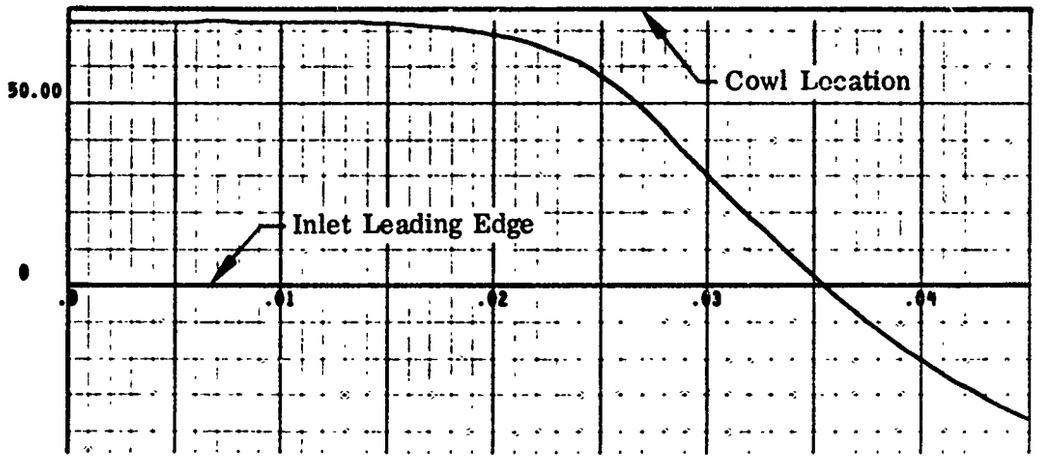

(b) X (in) vs Time

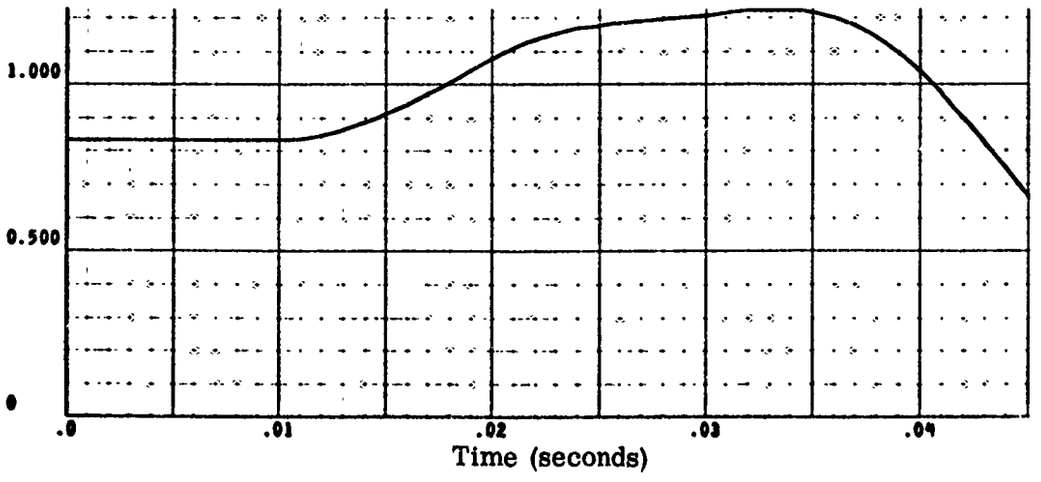

(c) P_{T2}/P_{T0} vs Time

Figure 24. 2DE Air Induction System Output Data - Hammershock Transient (Model 3, Deck 6) $M_0 = 2.5$; H = 50000 ft; $\alpha = 0$

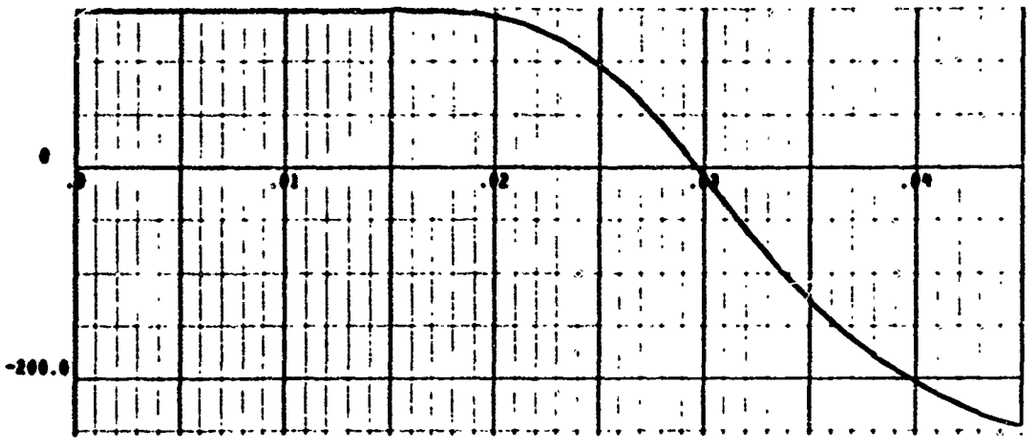

(d) W_8 (lbs/sec) vs Time

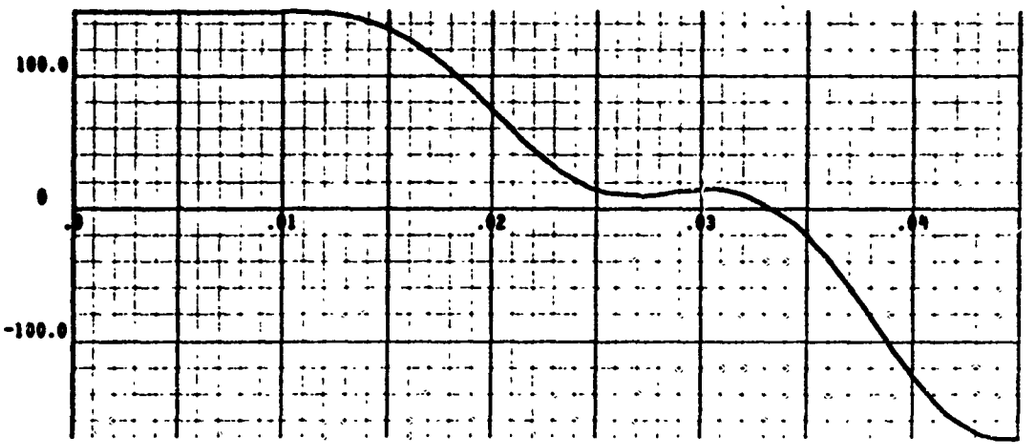

(e) W_{14} (lbs/sec) vs Time

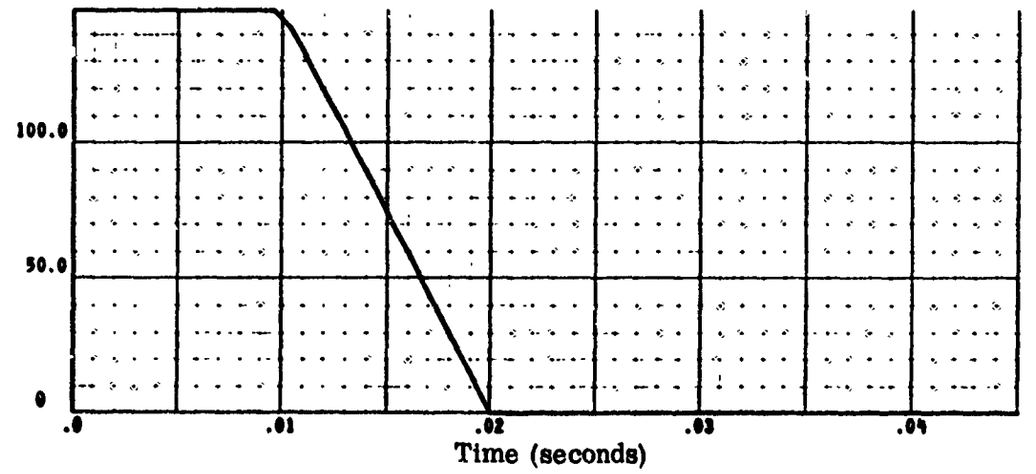

(f) W_2 (lbs/sec) vs Time

Figure 24 Continued

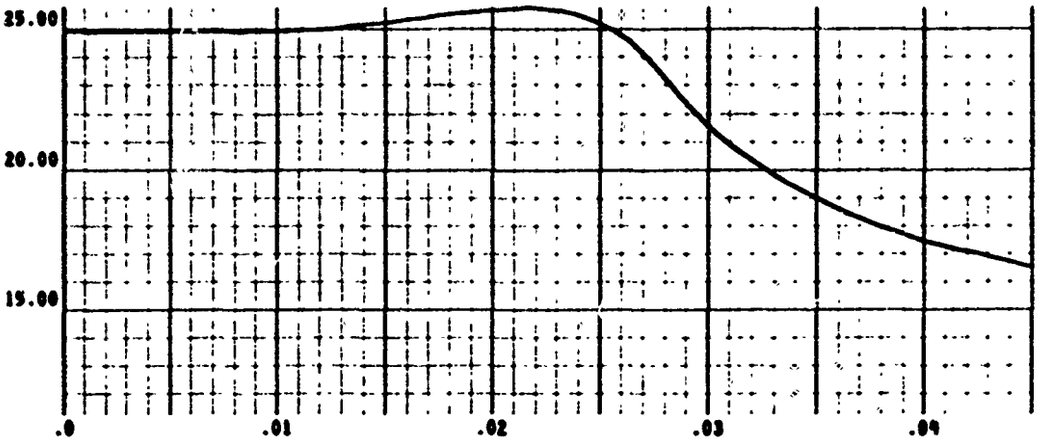

(g) P_{T6} (psi) vs Time

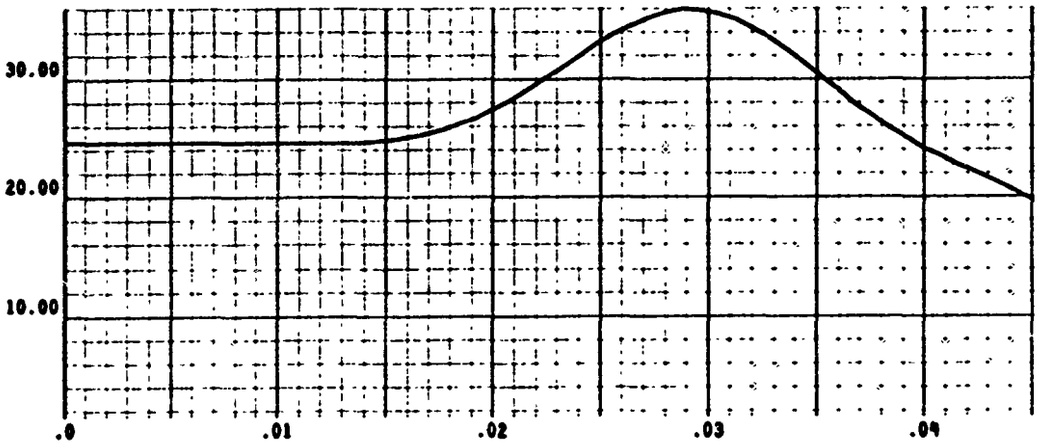

(h) P_{T12} (psi) vs Time

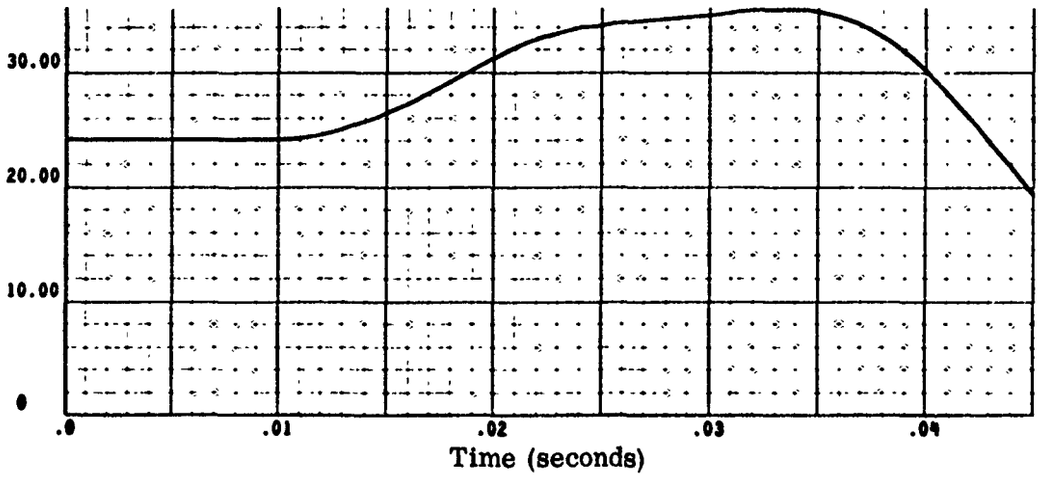

(i) P_{T2} (psi) vs Time

Figure 24 Continued

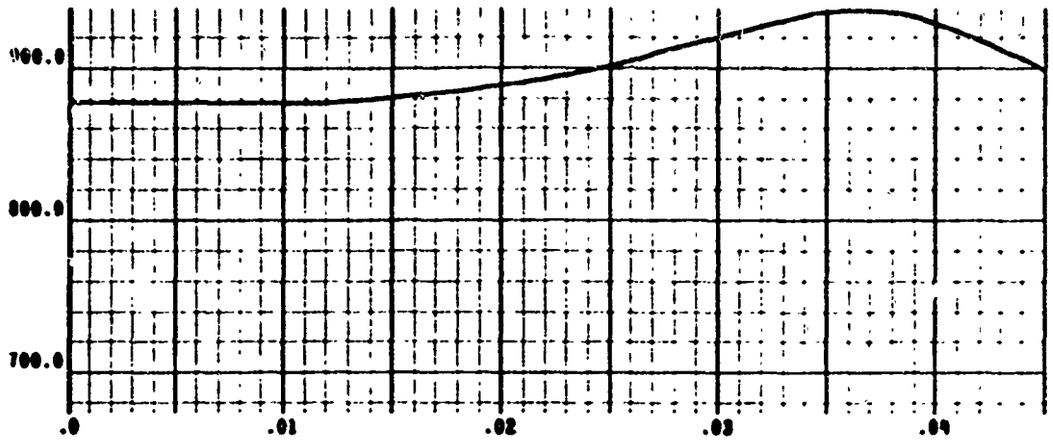

(j) T_{T6} (^{O}R) vs Time

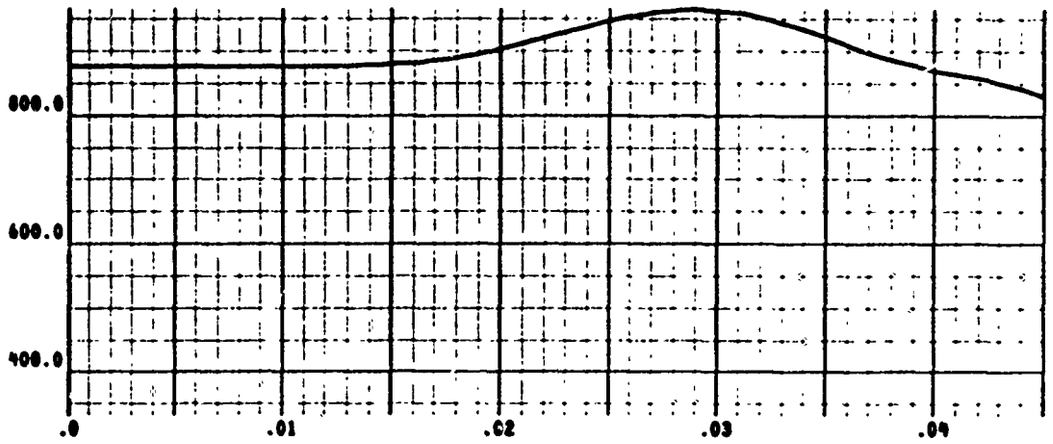

(k) T_{T12} (^{O}R) vs Time

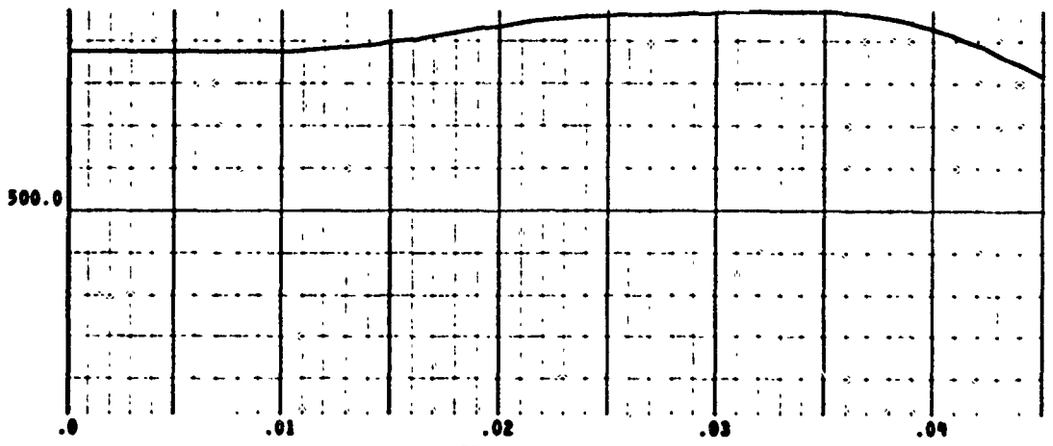

(l) T_{T2} (^{O}R) vs Time

Figure 24 Concluded

SECTION V

HAMMERSHOCK SIMULATION COMPARISONS

Hammershock simulation and test data available on the North American Rockwell (NAR) XB-70 and F108 air induction systems are compared with corresponding simulation runs, using Model 3. A full-scale XB-70 air induction system hammershock simulation at Mach 3 (Reference 12) is first compared with a corresponding Model 3 simulation run using XB-70 data available from NAR (References 13 and 14). This is followed with a comparison of Mach 3.1 hammershock test data on the NAR F108 wing tunnel model, with Model 3 simulated output using F108 input data, available in Reference 15. The results are discussed below.

NAR XB-70 INLET SIMULATION VS MODEL 3 SIMULATION

This comparison, using the full-scale XB-70 air induction system, is based on the following operating conditions.

Transient:	100 percent airflow cut-off in 1 millisecond
Mach Number:	3.0
Freestream Pressure:	.251 psi
Freestream Temperature:	373.5°R
Angle of Attack:	0

The output data obtained from the Model 3 simulation run is presented in Figure 25. Figure 25 (a) shows the hammershock input transient which is initiated at .01 second with 100 percent cutoff in engine airflow within 1 millisecond.

Figure 25 (c) shows the comparison in air induction system pressure recovery (P_{T2}/P_{T0}) between Model 3 and the NAR model. The latter is based on the "moving hammershock" approach, with the volume between the hammershock and the engine face treated as a single lump. The model locates a hammershock (HS) slightly forward of the compressor face at initiation of the transient. The lumped volume between this shock front and the engine face is the control volume, which increases as the HS moves upstream. Upon initiation of the transient, the instantaneous outflow from the control volume is drastically reduced as compared to the instantaneous inflow. The

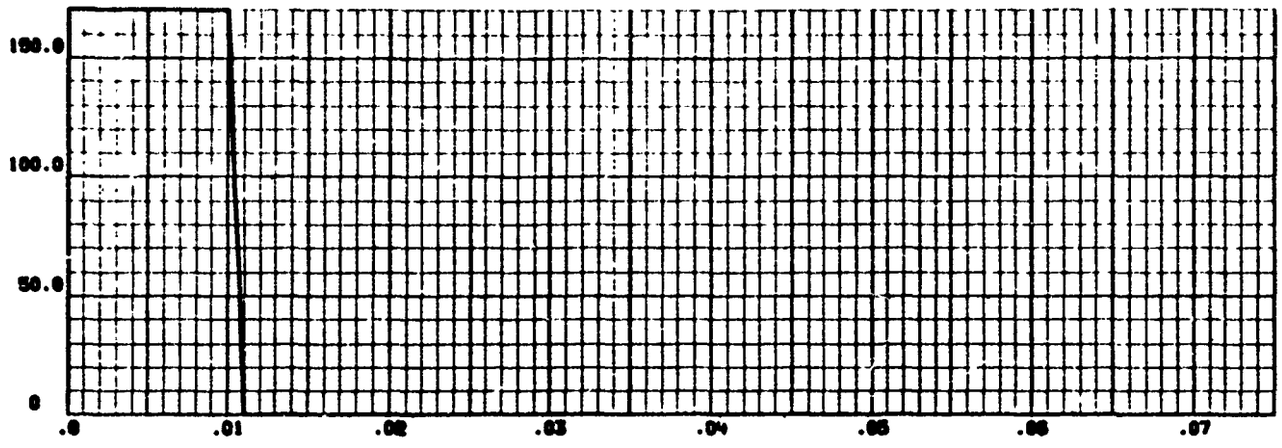

(a) Input Transient, W_2 (lbs/sec) vs Time

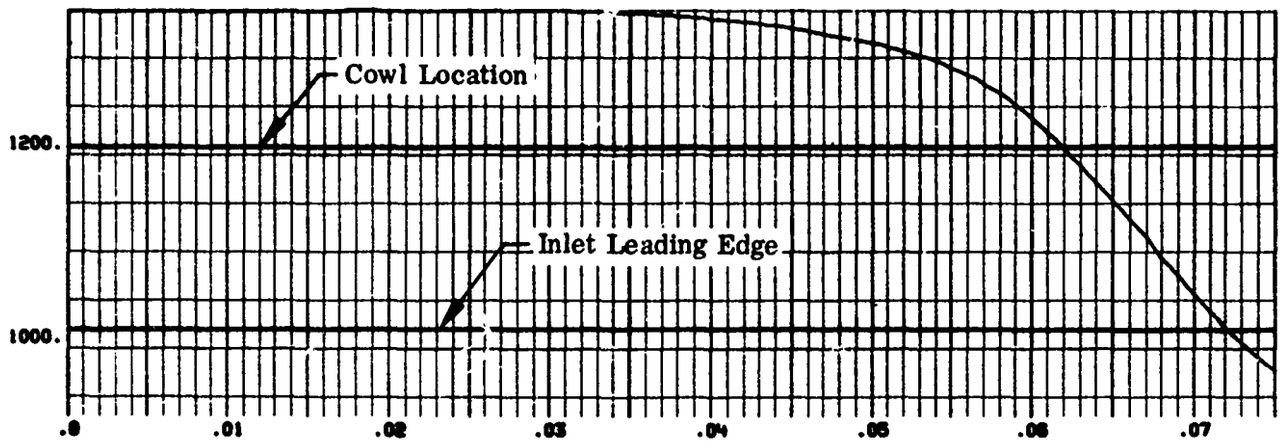

(b) X (in) vs Time

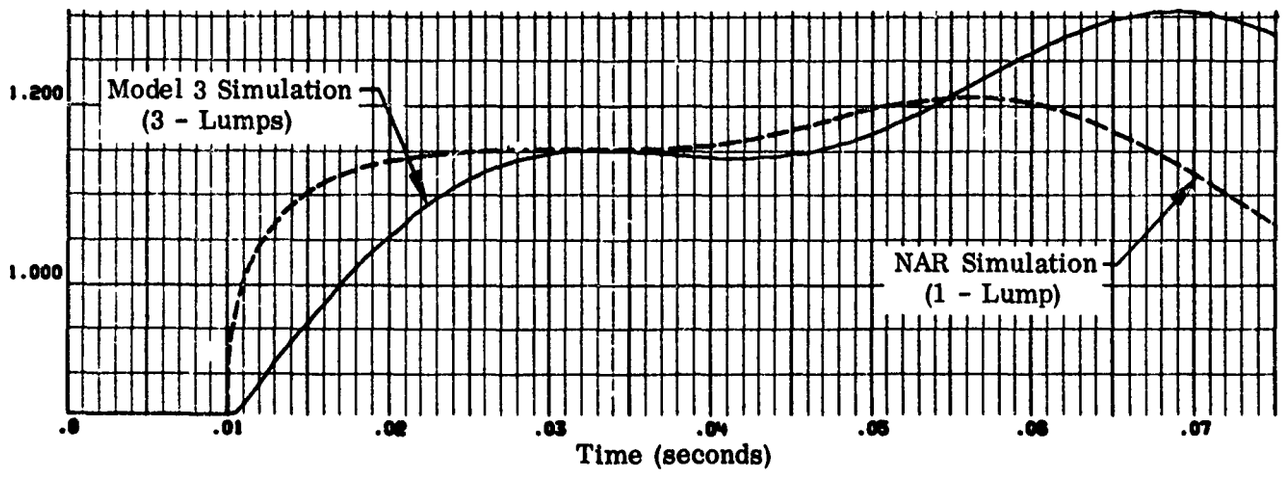

(c) P_{T2}/P_{T0} vs Time

Figure 25. Hammershock Simulation Comparison - NAR vs Model 3 - XB-70 Full Scale Inlet; $M_0 = 3$; $P_0 = .251$ psi; $T_0 = 373.5^\circ$ R; $\alpha = 0$

instantaneous control volume pressure rises, and the HS moves upstream at a velocity required to satisfy the instantaneous pressures across the HS. Since this is a single lump model, the control volume between the HS and the engine face is very small at initiation of the transient, and grows to include the whole subsonic diffuser when the HS reaches the cowl. On the other hand, Model 3 assumes a constant 'lumped' volume (Vol_{18}) near the compressor face. Thus, initially when the NAR control volume is much smaller than the constant Vol_{18}, the instantaneous P_{T2} within the NAR volume increases much more rapidly than within the Model 3 volume, as can be seen in Figure 25(c). This rate, however, drops off for the NAR model, since its control volume continues to increase during the transient, and may include the whole subsonic duct near the end of the simulation run. Both curves level off for about 3 milliseconds at .032 second and then rise again to the maximum values of 1.3 at .069 second for Model 3, and to 1.21 at .056 second for the NAR model

Due to unavailability of output data from the NAR model (other than P_{T2}/P_{T0}), comparison of parameters other than P_{T2}/P_{T0} was not possible.

NAR F108 INLET TEST VERSUS MODEL 3 SIMULATION

This comparison, using the NAR F108 inlet wind tunnel model (Reference 15) is based on the following example.

Transient:	100 percent airflow cutoff in 2.5 milliseconds
Mach Number:	3.1
Wind Tunnel	
Total Pressure:	14.7 psi
Total Temperature:	610°R
Angle of Attack:	0

Figure 26 shows the comparison between the F108 inlet model test and the Model 3 simulation. The latter compares well with the test results. It should be noted, however, that the test is in itself a simulation, since flow is completely cut off by a plug and, hence, it does not portray the response to an actual engine stall transient, where initial rapid cutoff in compressor flow leads to flow reversal and, finally, some positive flow while the engine windmills.

The complete simulation run is presented in Figure 27. The transient is initiated at .072 second, with flow demand completely cut off 2.5 milliseconds later [Figure 27(a)]. The instantaneous total pressures P_{T6}, P_{T12} and P_{T2} are shown in

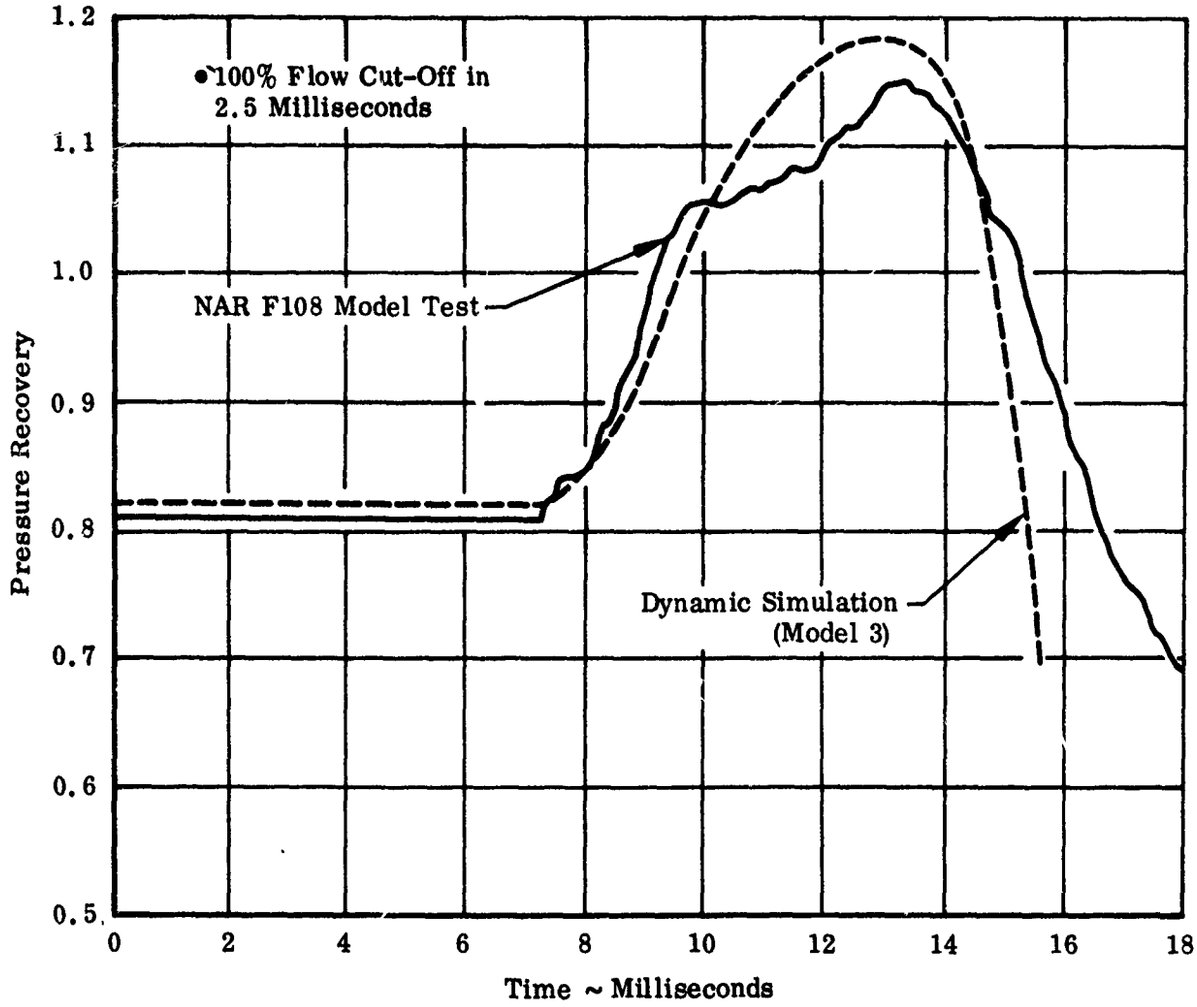

Figure 26. Hammershock Test vs Simulation Comparison - NAR F108 Wind Tunnel Model vs Model 3; $M_0 = 3.1$; $\alpha = 0$

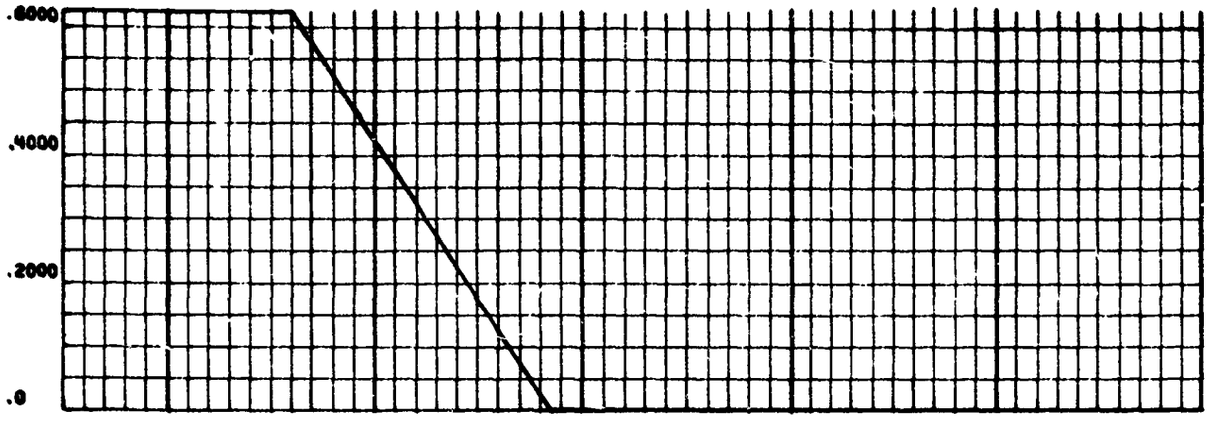

(a) Input Transient, W_{2E} (lbs/sec) vs Time

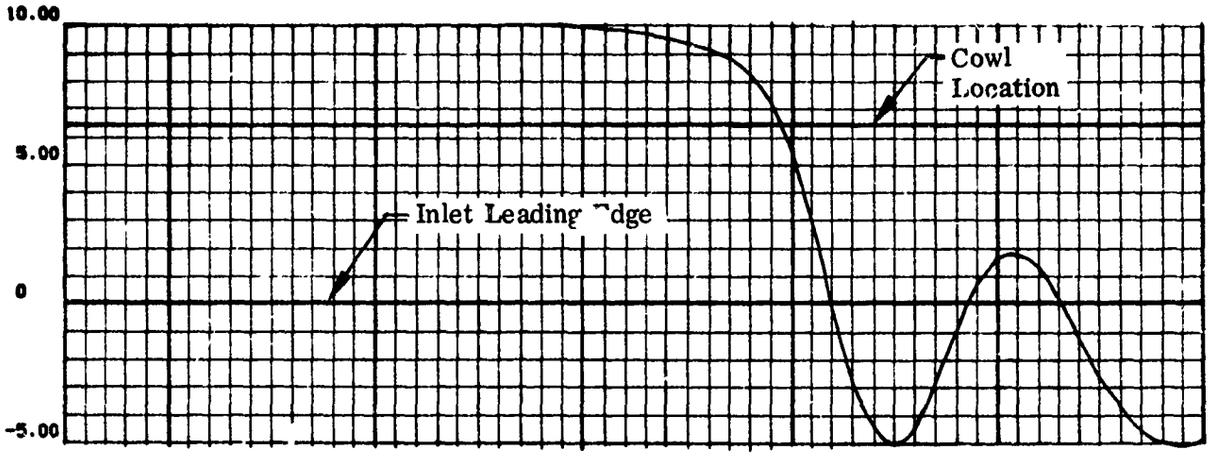

(b) X (in) vs Time

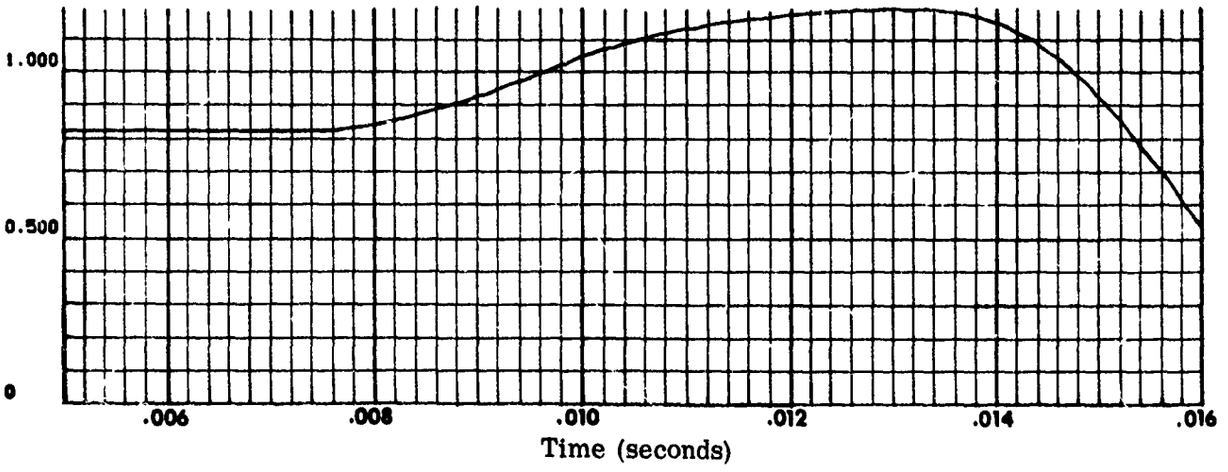

(c) P_{T2}/P_{T0} vs Time

Figure 27. Hammershock Simulation - F108 Wind Tunnel Model; $M_0 = 3.1$; $\alpha = 0$

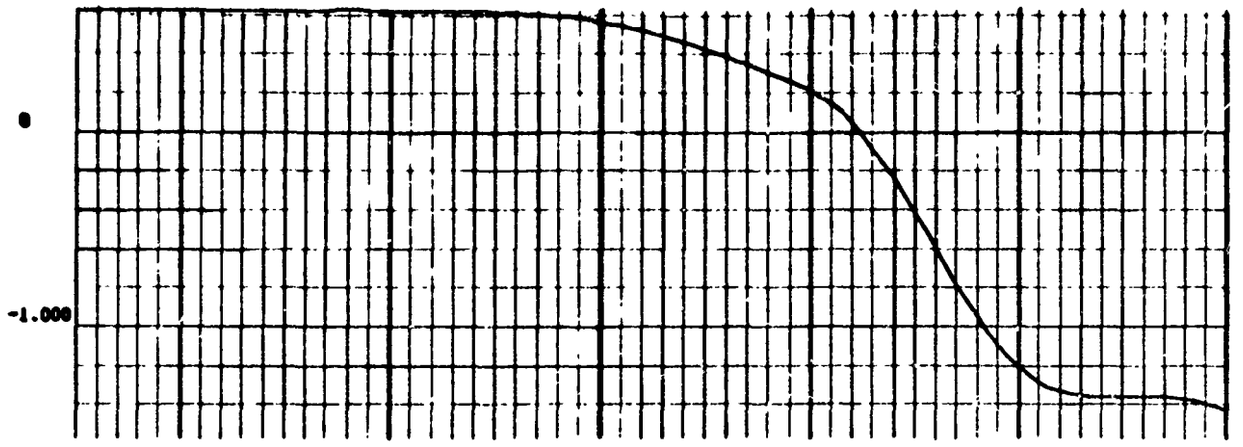

(d) W_8 (lbs/sec) vs Time

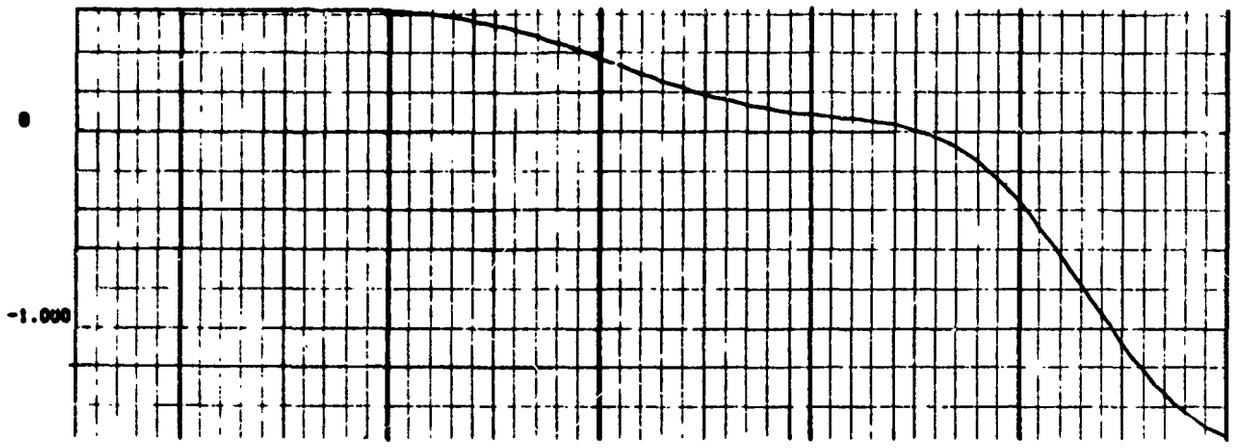

(e) W_{14} (lbs/sec) vs Time

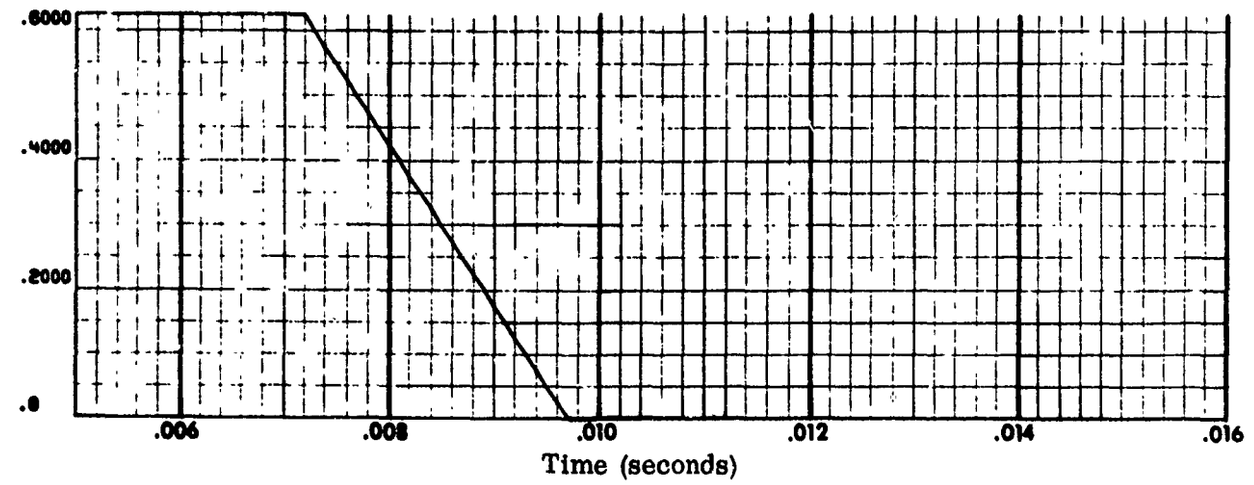

(f) W_2 (lbs/sec) vs Time

Figure 27 Continued

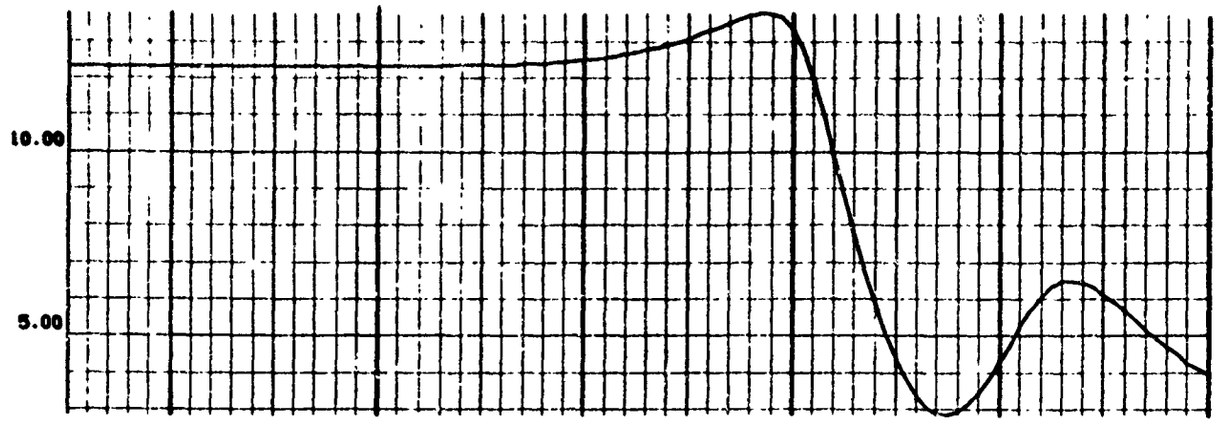

(g) P_{T6} (psi) vs Time

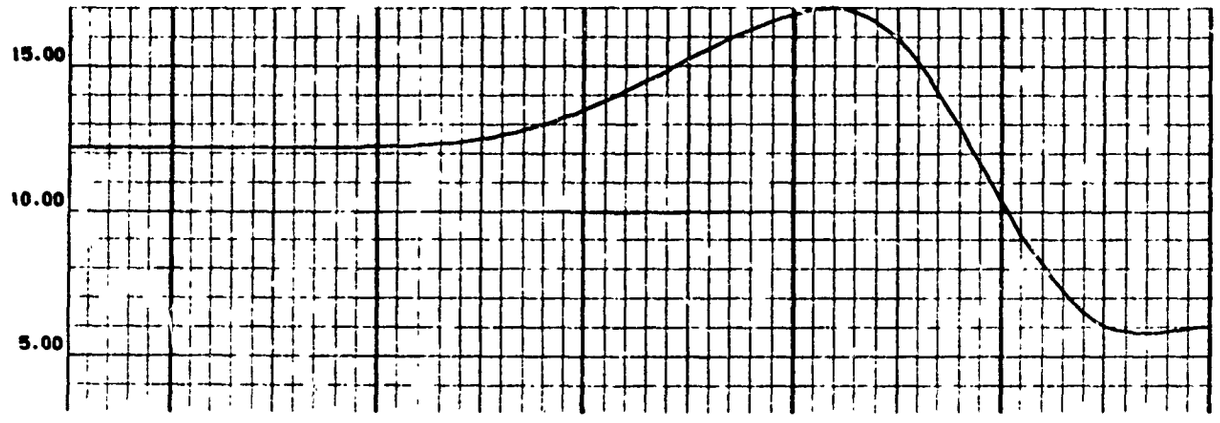

(h) P_{T12} (psi) vs Time

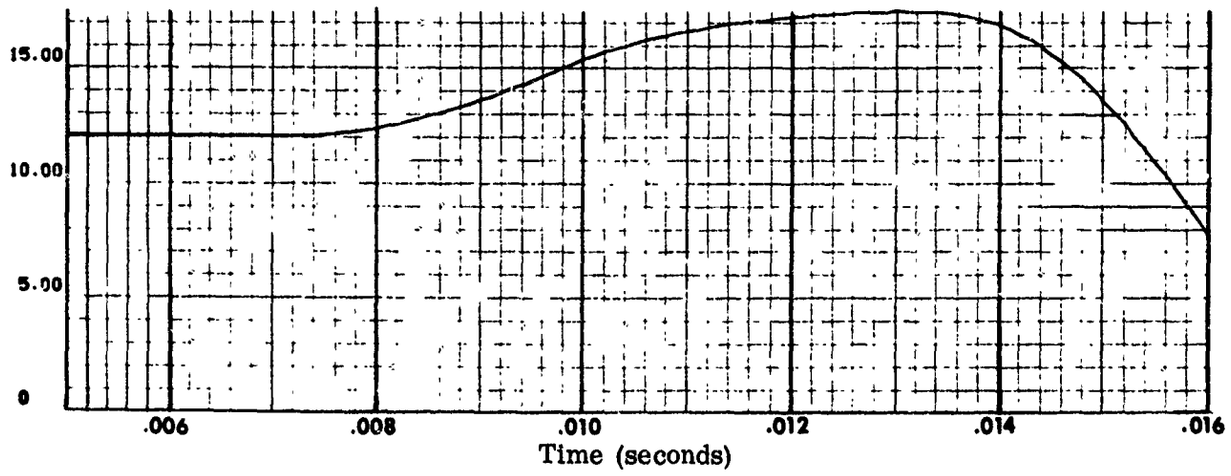

(i) P_{T2} (psi) vs Time

Figure 27 Continued

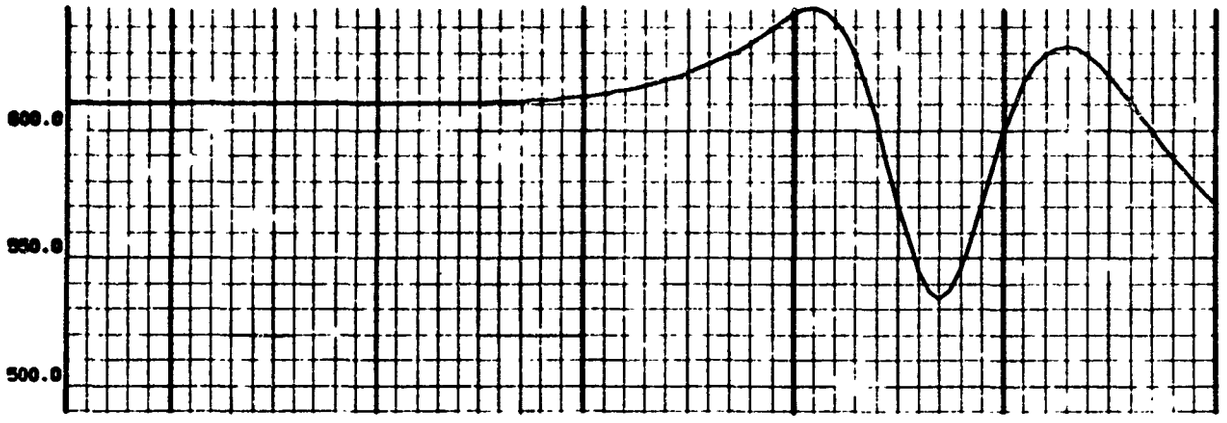

(j) T_{T6} (^{o}R) vs Time

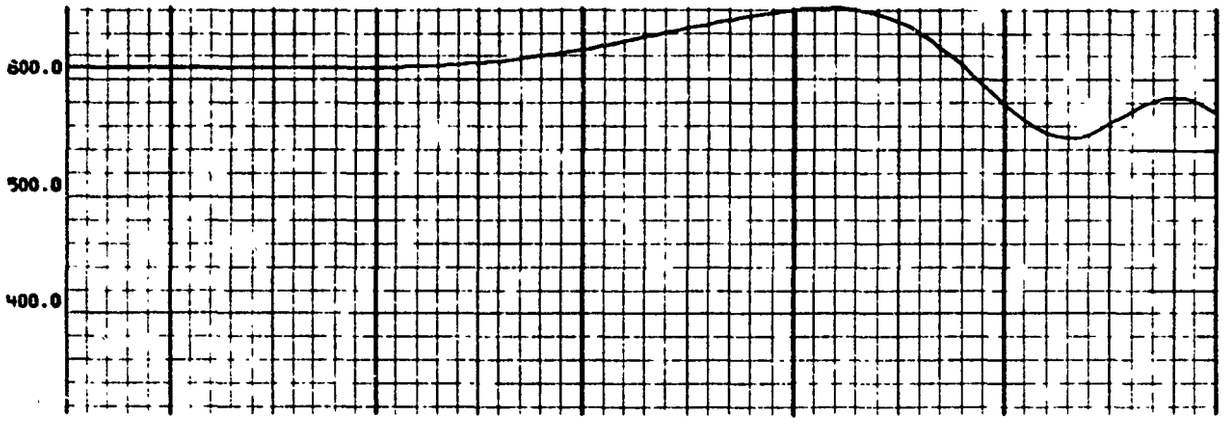

(k) T_{T12} (^{o}R) vs Time

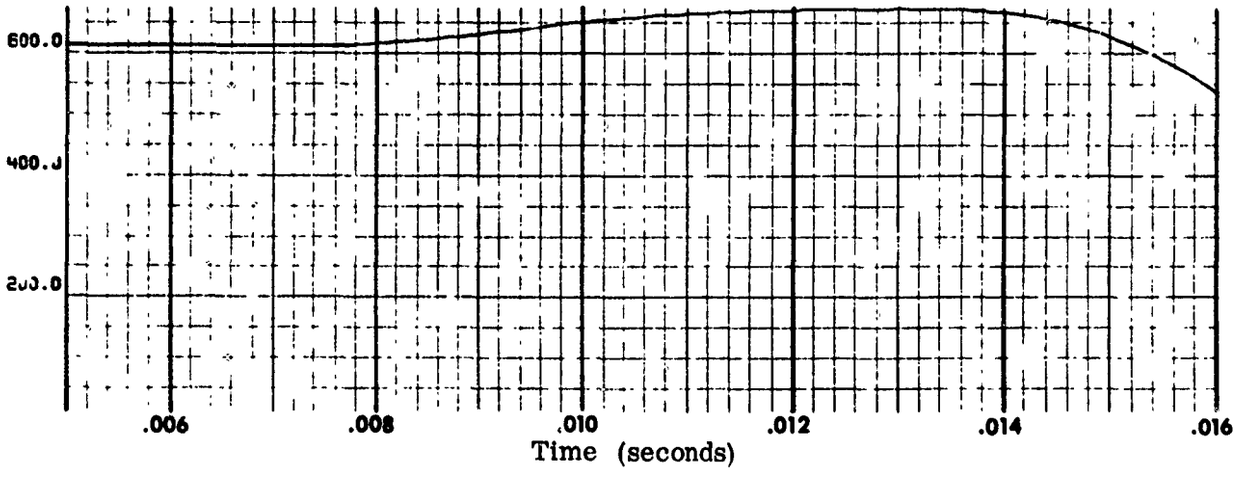

(l) T_{T2} (^{o}R) vs Time

Figure 27 Concluded

Figures 27(g), 27(h), and 27(i). It can be seen that P_{T6} starts to respond about 2.2 milliseconds after the transient has been initiated, and since this pressure affects NS movement, the latter also starts moving at about the same time [Figure 27(b)]. The oscillations in X and P_{T6} near the end of the simulation run tend to damp out fairly fast. Final steady state conditions calculated by Model 3 will indicate total pressure recovery behind the NS of .3 (which is the pressure recovery behind a normal shock at Mach 3.1) with the NS located three to four inches upstream of the inlet leading edge.

REFERENCES

1. Amin, N.F., "Air Induction System Dynamic Simulation User's Manual," NOR-71-210, September 1971.
2. Marvin, I.E., and Winkeljohan, A.A., "Propulsion System Modeling and Integrated Controls Optimization," Technical Report AFAPL-TR-67-149, November 1967.
3. Kaplan, E.H., "Catalog of Transients Causing Propulsion System Instability," Technical Report AFAPL-TR-68-142, Part II, December 1968.
4. Martin, A.W., "Propulsion System Dynamic Simulation Theory and Equations," North American Rockwell Report No. NA-67-384, 17 April 1967.
5. Mays, R.A., "Inlet Dynamics and Compressor Surge," AIAA Paper No. 69-484, June 1969.
6. Wasserbauer, J.F., and Willoh, R.G., "Experimental and Analytical Investigation of the Dynamic Response of a Supersonic Mixed Compression Inlet," AIAA Paper No. 68-651, June 1968.
7. Bronwell, A., "Advanced Mathematics in Physics and Engineering," pp. 414-417, McGraw-Hill Book Company, New York, 1953.
8. Ferri, A. and Nucci, L.M., "The Origin of Aerodynamic Instability of Supersonic Inlets at Subcritical Conditions," NACA RM L50K30, January 1951.
9. Trimpi, R.L., "An Analysis of Buzzing in Supersonic Ram Jets by a Modified One-Dimensional Non-Stationary Wave Theory," NACA RM L52A18, March 1952.
10. Nussdorfer, T.J., "Some Observations of Shock Induced Turbulent Separation on Supersonic Diffusers," NACA Report RM E51L26, May 1954.
11. Martin, A.W. and Beaulieu, W.D., "XB-70 Flight Test Data Comparisons with Simulation Predictions of Inlet Unstart and Buzz," NASA CR-1631, June 1970.
12. Martin, A.W., "Propulsion System Dynamic Simulation Data (U)," North American Report No. NA-67-387, 17 April 1967 (CONFIDENTIAL).

13. Martin, A.W. and Wong, H.W., "Propulsion System Dynamic Simulation - User's Manual," North American Report No. NA-67-385, 17 April 1967.

14. Randall, L.M., "The XB-70A Air Induction System," AIAA Paper No. 66-634, June 1966.

15. Martin, A.W. and Kostin, L.C., "Propulsion System Dynamic Test Results (U)," North American Report No. NA-67-386, 17 April 1967 (CONFIDENTIAL).

16. Zimmerman, D.I., Eschweiler, J.C. and Wallace, H.W., "An Improved Analytical Model for Predicting the Transient Performance of an Inlet/Engine System," McDonnell Aircraft Report No. MDC 70-020, June 1970.

17. Moeckel, W.E., "Approximate Method for Predicting Form and Location of Detached Shock Waves Ahead of Plane or Axially Symmetric Bodies," NACA TN 1921, July 1949.

APPENDIX I

DERIVATION OF THE LUMPED VOLUME TOTAL TEMPERATURE AND PRESSURE RATE EQUATIONS

APPENDIX I

DERIVATION OF THE LUMPED VOLUME TOTAL TEMPERATURE AND PRESSURE RATE EQUATIONS

In the 'lumped parameter' concept, the air induction system subsonic duct is divided into a series of lumped volumes. The volume nearest to the diffuser throat has a moving upstream boundary (the normal shock) and a fixed downstream boundary. The remaining lumped volumes have fixed boundaries. The instantaneous total temperatures and pressures within each of these volumes are obtained during the simulation run by numerically integrating the corresponding rate equations. These rate equations are derived by applying the one-dimensional unsteady continuity and energy equations in conjunction with the equation of state to each 'lumped' volume. The procedure adopted here in developing these rate equations is, first, to derive from basic principles, the one-dimensional unsteady energy equation for a control volume with a moving upstream boundary and a fixed downstream boundary, and then to apply the 'lumped' volume concept to this energy equation for developing the rate equations. The final forms in which these equations are used in the air induction system dynamic simulation computer program are obtained through some algebraic manipulation.

Total Temperature Rate Equation

The approach used in deriving the basic unsteady energy equation [Equation (5) in this Appendix] for a control volume with a moving upstream boundary (the normal shock) and a fixed downstream boundary follows Reference 16. It is included here in the original form except for some changes in nomenclature.

The time-dependent energy equation states that the rate of energy accumulation in an adiabatic control volume without shaft work is equivalent to the net flux of energy through its boundaries, lessened or increased by the rate of work done at the surfaces of the volume. The figure below portrays the situation. The control volume (CV) extends from a moving control surface to a fixed end boundary. In this portrayal, translation of the moving surface lags the fluid motion. However, the derivation applies to any control surface speed relative to fluid speed.

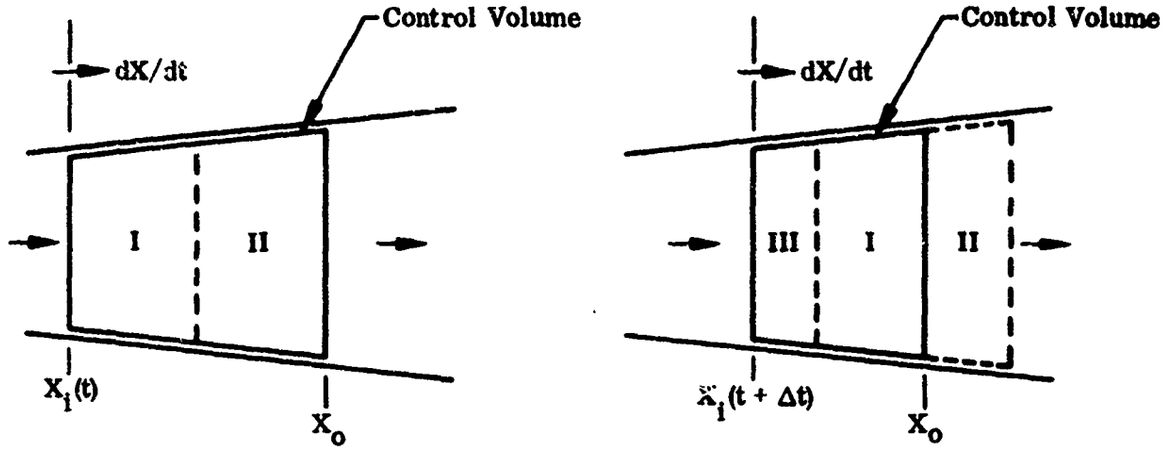

Time = t

Time = t + Δt

The energy contained by the system of fluid present in the control volume at time t is $E_{I_t} + E_{II_t}$. Since energy can be added to an adiabatic system in the form of work only, and since energy must be conserved:

$$(E_{I_{t+\Delta t}} + E_{II_{t+\Delta t}}) - (E_{I_t} + E_{II_t}) - dW = 0 \qquad (1)$$

At time t the control volume contains the fluid encompassed in Regions I and II. At t + Δt the fluid Regions I and III occupy the newly formed control volume. Therefore, during the same time interval Δt, the energy change for the control volume is:

$$E_{CV_{t+\Delta t}} - E_{CV_t} = (E_{I_{t+\Delta t}} + E_{III_{t+\Delta t}}) - (E_{I_t} + E_{II_t}) \qquad (2)$$

Combining Equations (1) and (2) gives:

$$dE_{CV} - E_{III_{t+\Delta t}} + E_{II_{t+\Delta t}} - dW = 0 \qquad (3)$$

where

$$dE_{CV} = E_{CV_{t+\Delta t}} - E_{CV_t}$$

The energy contained in the control volume is made up of internal energy (e), kinetic energy ($u^2/2g$), and potential energy, the latter assumed to be negligible.

Thus, from the calculus

$$\frac{dE_{cv}}{dt} = \frac{E_{cv\,t+\Delta t} - E_{cv\,t}}{\Delta t \to 0 \quad \Delta t} = \frac{d}{dt}\int_{X_i(t)}^{X_o} (e + u^2/2g)\rho_S A\,dX \tag{4}$$

where X_i and X_o denote the control volume entrance and exit stations, respectively.

Similarly, the energy flux across the boundaries is made up of internal and kinetic energy, so that the time derivative form of Equation (3) can be written as:

$$\frac{d}{dt}\int_{X_i(t)}^{X_o} (e + u^2/2g)\rho_S A\,dX - \rho_{Si} A_i \left(u_i - \frac{dX}{dt}\right)(e_i + u_i^2/2g) + \rho_{So} A_o u_o (e_o + u_o^2/2g) - d\mathring{W}/dt = 0 \tag{5}$$

Equation (5) is the basic unsteady energy equation for a control volume with a moving boundary.

Now the work performed on the control volume is assumed to occur only at the upstream and downstream flow boundaries and consists of flow work. At the two boundaries the fluid exerts pressure P_S on the control volume and enters the upstream moving boundary at $\left(u_i - \frac{dX}{dt}\right)$ ft/sec with respect to it and leaves the fixed boundary at u_o ft/sec. The flow work performed on the control volume is, therefore,

$$\left(\frac{d\mathring{W}}{dt}\right)_{\text{moving boundary}\,(X_i)} = P_{Si} A_i \left(u_i - \frac{dX}{dt}\right) = \frac{P_{Si}}{\rho_{Si}}\left[A_i \rho_{Si}\left(u_i - \frac{dX}{dt}\right)\right] \tag{6}$$

The expression $\left[A_i \rho_{Si}\left(u_i - \frac{dX}{dt}\right)\right]$ is the flow (W_i) entering the control volume, thus,

$$\left(\frac{d\mathring{W}}{dt}\right)_{\text{moving boundary}\,(X_i)} = \frac{P_{Si}}{\rho_{Si}} W_i \tag{7}$$

and, similarly,

$$\left(\frac{d\mathring{W}}{dt}\right)_{\text{fixed boundary}\,(X_o)} = -\frac{P_{So}}{\rho_{So}} W_o \tag{8}$$

Therefore, the net work performed on the control volume is,

$$\frac{dW}{dt} = \frac{P_{Si}}{\rho_{Si}} W_i - \frac{P_{So}}{\rho_{So}} W_o \qquad (9)$$

Now substituting Equation (9) into Equation (5) we obtain,

$$\frac{d}{dt}\int_{X_i(t)}^{X_o} \left(e + \frac{u^2}{2g}\right)\rho_S A\, dx + W_o\left(e_o + \frac{u_o^2}{2g}\right) - W_i\left(e_i + \frac{u_i^2}{2g}\right)$$

$$= \frac{P_{Si}}{\rho_{Si}} W_i - \frac{P_{So}}{\rho_{So}} W_o$$

or

$$\frac{d}{dt}\int_{X_i(t)}^{X_o} \left(e + \frac{u^2}{2g}\right)\rho_S A\, dx = \left[W_i\left(e_i + \frac{P_{Si}}{\rho_{Si}}\right) + W_i\frac{u_i^2}{2g}\right] - \left[W_o\left(e_o + \frac{P_{So}}{\rho_{So}}\right) + W_o\frac{u_o^2}{2g}\right]$$

$$= W_i\left(h_{Si} + \frac{u_i^2}{2g}\right) - W_o\left(h_{So} + \frac{u_o^2}{2g}\right) \qquad (10)$$

where the enthalpy $h_S = e + \frac{P_S}{\rho_S}$

or

$$\frac{d}{dt}\int_{X_i(t)}^{X_o} \left(e + \frac{u^2}{2g}\right)\rho_S A\, dx = W_i C_p T_{Ti} - W_o C_p T_{To} \qquad (11)$$

where

$$h_S + \frac{u^2}{2g} = h_T = C_p T_T$$

In order to evaluate the integral of the energy in the control volume accurately, the axial distribution of fluid properties through the volume must be known. This distribution cannot be obtained by the present theory. To overcome this deficiency, the 'lumped' volume concept is introduced. In this concept it is assumed that the lumped

instantaneous flow properties correspond to the instantaneous average properties of the entire control volume. Defining the control volume properties in this manner provides the equality:

$$\frac{d}{dt}\int_{X_i(t)}^{X_o}\left(e+\frac{u^2}{2g}\right)\rho_s A\,dx = \frac{d}{dt}\left[\left(e_c+\frac{u_c^2}{2g}\right)m_c\right] \tag{12}$$

where subscript c refers to the properties (i.e., energy, mass) within the 'lumped' control volume.

Thus,

$$\begin{aligned}\frac{d}{dt}\left[\left(e_c+\frac{u_c^2}{2g}\right)m_c\right] &= \frac{d}{dt}\left[\left(h_{Sc}+\frac{u_c^2}{2g}\right)m_c-\frac{P_{Sc}}{\rho_{Sc}}m_c\right]\\ &= \frac{d}{dt}\left(m_c C_p T_{Tc}-P_{Sc}V_c\right)\\ &= \frac{d}{dt}\left(m_c C_p T_{Tc}\right)-\frac{d}{dt}\left(P_{Sc}V_c\right).\end{aligned} \tag{13}$$

Applying the unsteady continuity equation which states that the mass accumulation $\left(\frac{dm_c}{dt}\right)$ within the control volume is equal to the net flux of fluid through its boundaries we get

$$\frac{dm_c}{dt} = W_i - W_c$$

or

$$m_c = \int(W_i - W_o)\,dt. \tag{14}$$

Substituting Equation (14) in Equation (13) we get

$$\frac{d}{dt}\left[\left(e_c+\frac{u_c^2}{2g}\right)m_c\right] = \frac{d}{dt}\left[C_p T_{Tc}\int(W_i-W_o)\,dt\right]-\frac{d}{dt}\left(P_{Sc}V_c\right) \tag{15}$$

instantaneous flow properties correspond to the instantaneous average properties of the entire control volume. Defining the control volume properties in this manner provides the equality:

$$\frac{d}{dt}\int_{X_i(t)}^{X_o}\left(e+\frac{u^2}{2g}\right)\rho_s A\,dx = \frac{d}{dt}\left[\left(e_c+\frac{u_c^2}{2g}\right)m_c\right] \tag{12}$$

where subscript c refers to the properties (i.e., energy, mass) within the 'lumped' control volume.

Thus,

$$\begin{aligned}\frac{d}{dt}\left[\left(e_c+\frac{u_c^2}{2g}\right)m_c\right] &= \frac{d}{dt}\left[\left(h_{sc}+\frac{u_c^2}{2g}\right)m_c-\frac{P_{sc}}{\rho_{sc}}m_c\right]\\ &= \frac{d}{dt}\left(m_c C_p T_{Tc}-P_{sc}V_c\right)\\ &= \frac{d}{dt}\left(m_c C_p T_{Tc}\right)-\frac{d}{dt}\left(P_{sc}V_c\right).\end{aligned} \tag{13}$$

Applying the unsteady continuity equation which states that the mass accumulation $\left(\frac{dm_c}{dt}\right)$ within the control volume is equal to the net flux of fluid through its boundaries we get

$$\frac{dm_c}{dt} = W_i - W_c$$

or

$$m_c = \int(W_i - W_o)\,dt. \tag{14}$$

Substituting Equation (14) in Equation (13) we get

$$\frac{d}{dt}\left[\left(e_c+\frac{u_c^2}{2g}\right)m_c\right] = \frac{d}{dt}\left[C_p T_{Tc}\int(W_i-W_o)\,dt\right]-\frac{d}{dt}\left(P_{sc}V_c\right) \tag{15}$$

Then Equation (11) can be written as

$$\frac{d}{dt}\left[C_p T_{Tc} \int (W_i - W_o)\, dt\right] - \frac{d}{dt}(P_{Sc} V_c) = C_p (W_i T_{Ti} - W_c T_{Tc}). \quad (16)$$

It is assumed that Cp is constant over the range of temperatures under consideration.

Now the flow work term on LHS of Equation (16) is

$$\frac{d}{dt}(P_{Sc} V_c) = \frac{d}{dt}(m_c R T_{Sc}) = \frac{d}{dt}\left[R T_{Sc} \int (W_i - W_o)\, dt\right]$$

$$= \frac{dT_{Sc}}{dt} R \int (W_i - W_o)\, dt + R T_{Sc} (W_i - W_o). \quad (17)$$

Substituting this in Equation (16) and performing the indicated derivative of the first expression on LHS of Equation (16) we get

$$C_p \left[\frac{dT_{Tc}}{dt} \int (W_i - W_c)\, dt + T_{Tc} (W_i - W_c)\right] - \frac{dT_{Sc}}{dt} R \int (W_i - W_o)\, dt$$

$$- R T_{Sc} (W_i - W_o) = C_p (W_i T_{Ti} - W_o T_{Tc}). \quad (18)$$

To eliminate the static temperature derivative, it is assumed that

$$\frac{dT_{Sc}}{dt} = \frac{T_{Sc}}{T_{Tc}} \frac{dT_{Tc}}{dt}. \quad (19)$$

This assumption is permissible for moderate subsonic flow velocities.

Substituting Equation (19) in Equation (18) and simplifying, we get

$$\frac{dT_{Tc}}{dt} \int (W_i - W_o)\, dt \left[C_p - R \frac{T_{Sc}}{T_{Tc}}\right] = C_p (W_i T_{Ti} - W_o T_{Tc})$$

$$+ (W_i - W_o)\left[R T_{Sc} - C_p T_{Tc}\right]. \quad (20)$$

Now

$$m_c = \int (W_i - W_o)\, dt = \rho_{Sc} V_c = \frac{P_{Sc} V_c}{R T_{Sc}}. \tag{21}$$

Substituting Equation (21) into Equation (20) and rearranging

$$\frac{dT_{Tc}}{dt} = \frac{c_p (W_i T_{Ti} - W_o T_{To}) + (W_i - W_o)\left[R T_{Sc} - c_p T_{Tc}\right]}{\frac{P_{Sc} V_c}{R T_{Sc}} \left[c_p - R \frac{T_{Sc}}{T_{Tc}} \right]}$$

$$= \frac{c_p \left[(W_i T_{Ti} - W_o T_{To}) + (W_o - W_i) T_{Tc} \left(1 - \frac{R}{c_p} \frac{T_{Sc}}{T_{Tc}}\right)\right]}{c_p \frac{P_{Sc} V_c}{R T_{Sc}} \left[1 - \frac{R}{c_p} \frac{T_{Sc}}{T_{Tc}} \right]} \tag{22}$$

Let

$$c' = \left[1 - \frac{R}{c_p} \frac{T_{Sc}}{T_{Tc}} \right] \tag{23}$$

and

$$z = \left[\frac{P_{Sc}}{P_{Tc}} \cdot \frac{T_{Tc}}{T_{Sc}} \right] \tag{24}$$

and

$$c = c' z \tag{25}$$

Substituting Equations (23), (24) and (25) into Equation (22) simplifies it to

$$\frac{dT_{Tc}}{dt} = \frac{R T_{Tc}}{c V_c P_{Tc}} \left[(W_i T_{Ti} - W_o T_{To}) + c' T_{Tc} (W_o - W_i) \right]$$

or,

$$\frac{dT_{Tc}}{dt} = \frac{R T_{Tc}}{c V_c P_{Tc}} (W_i T_{Ti} - W_o T_{To}) + \frac{R T_{Tc}^2}{z V_c P_{Tc}} (W_o - W_i) \tag{26}$$

Total Pressure Rate Equation

This equation is derived by applying the equation of state to the fluid within the control volume

$$P_{Sc}\, V_c = m_c\, R\, T_{Sc}$$

or

$$P_{Sc} = R\, \frac{m_c\, T_{Sc}}{V_c}\,. \tag{27}$$

Differentiating this with respect to time t, we get

$$\frac{dP_{Sc}}{dt} = R\left[\frac{V_c\, \frac{d(m_c\, T_{Sc})}{dt} - m_c\, T_{Sc}\, \frac{dV_c}{dt}}{V_c^2}\right]$$

or,

$$\frac{dP_{Sc}}{dt} = R\left[\frac{T_{Sc}}{V_c}\frac{dm_c}{dt} + \frac{m_c}{V_c}\frac{dT_{Sc}}{dt} - \frac{m_c\, T_{Sc}}{V_c^2}\frac{dV_c}{dt}\right]. \tag{28}$$

Now substituting

the continuity equation $$\frac{dm_c}{dt} = W_i - W_o \tag{29}$$

and the assumption $$\frac{dP_{Sc}}{dt} = \frac{P_{Sc}}{P_{Tc}}\left(\frac{dP_{Tc}}{dt}\right) \tag{30}$$

into Equation (28) we get

$$\frac{dP_{Tc}}{dt} = \frac{P_{Tc}}{P_{Sc}}\,\frac{R\, m_c\, T_{Sc}}{V_c}\left[\frac{W_i - W_o}{m_c} + \frac{1}{T_{Sc}}\frac{dT_{Sc}}{dt} - \frac{1}{V_c}\frac{dV_c}{dt}\right]. \tag{31}$$

Now substituting $$m_c = \rho_{Sc} V_c = \frac{P_{Sc} V_c}{R T_{Sc}}$$

and the assumption $$\frac{dT_{Sc}}{dt} = \frac{T_{Sc}}{T_{Tc}} \frac{dT_{Sc}}{dt}$$

into Equation (31) and rearranging yields,

$$\frac{dP_{Tc}}{dt} = \frac{R T_{Sc} P_{Tc}}{P_{Sc} V_c} (W_i - W_o) + \frac{P_{Tc}}{T_{Tc}} \frac{dT_{Tc}}{dt} - \frac{P_{Tc}}{V_c} \frac{dV_c}{dt}, \quad (32)$$

From Equation (24) $$\frac{T_{Sc}}{P_{Sc}} = \frac{T_{Tc}}{P_{Tc} z}.$$

Substituting this in the first term on the RHS of Equation (32) we get

$$\frac{dP_{Tc}}{dt} = \frac{R T_{Tc}}{V_c z} (W_i - W_o) + \frac{P_{Tc}}{T_{Tc}} \frac{dT_{Tc}}{dt} - \frac{P_{Tc}}{V_c} \frac{dV_c}{dt}. \quad (33)$$

Form of Total Temperature and Total Pressure Rate Equations Used in Computer Program

Through algebraic manipulation an alternative form of these equations, more suitable for use in the air induction system dynamic simulation computer program, is obtained as follows: Multiplying Equation (33) throughout by $\frac{T_{Tc}}{P_{Tc}}$ and rearranging, we get,

$$\frac{R T_{Tc}^2}{z V_c P_{Tc}} (W_o - W_i) = \frac{dT_{Tc}}{dt} - \frac{T_{Tc}}{V_c} \frac{dV_c}{dt} - \frac{T_{Tc}}{P_{Tc}} \frac{dP_{Tc}}{dt} \quad (34)$$

From this the total temperature rate $\frac{dT_{Tc}}{dt}$ is,

$$\frac{dT_{Tc}}{dt} = \frac{R T_{Tc}^2}{2 V_c P_{Tc}} (W_o - W_i) + \frac{T_{Tc}}{P_{Tc}} \frac{dP_{Tc}}{dt} + \frac{T_{Tc}}{V_c} \frac{dV_c}{dt} \quad (35)$$

Now Equation (26) can be rearranged as follows:

$$\frac{R T_{Tc}^2}{2 V_c P_{Tc}} (W_o - W_i) = \frac{dT_{Tc}}{dt} - \frac{R T_{Tc}}{c V_c P_{Tc}} (W_i T_{Ti} - W_o T_{To}) \quad (36)$$

Combining Equations (34) and (36), simplifying, and substituting C' Z for C [Equation (25)], we get

$$\frac{R T_{Tc}}{c' 2 V_c P_{Tc}} (W_i T_{Ti} - W_o T_{To}) - \frac{T_{Tc}}{V_c} \frac{dV_c}{dt} - \frac{T_{Tc}}{P_{Tc}} \frac{dP_{Tc}}{dt} = 0 \quad (37)$$

From this the total pressure rate $\frac{dP_{Tc}}{dt}$ is

$$\frac{dP_{Tc}}{dt} = \frac{R}{c' 2 V_c} (W_i T_{Ti} - W_o T_{To}) - \frac{P_{Tc}}{V_c} \frac{dV_c}{dt} \quad (38)$$

Thus, the final dimensionally consistent form of the total temperature and total pressure rate Equations [(35) and (38), respectively] in the computer program, is:

$$\frac{dT_{Tc}}{dt} = \dot{T}_{Tc} = \frac{T_{Tc}}{P_{Tc}} \left[\frac{12 R T_{Tc}}{2 V_c} (W_o - W_i) + \dot{P}_{Tc} - \frac{P_{Tc} A_x \dot{X}}{V_c} \right] \quad (39)$$

$$\frac{dP_{Tc}}{dt} = \dot{P}_{Tc} = \frac{12 R}{c' 2 V_c} (W_i T_{Ti} - W_o T_{To}) + \frac{P_{Tc} A_x \dot{X}}{V_c} \quad (40)$$

for P in psi, T in °R, W in lb/sec, V in cubic inch, t in seconds and R in ft lb/lb °R.

Note that the signs of the last expressions on the RHS of the Equations (39) and (40) have been reversed since $\frac{dV_c}{dt}$ is negative when $\dot{X}$ is positive (NS movement towards compressor face).

APPENDIX II

DERIVATION OF THE EQUATION FOR THE RATE OF CHANGE OF FLOW ACROSS FIXED LUMPED VOLUME BOUNDARY

APPENDIX II

DERIVATION OF THE EQUATION FOR THE RATE OF CHANGE OF FLOW ACROSS FIXED LUMPED VOLUME BOUNDARY

In the "lumped parameter" concept, the air induction system subsonic duct is divided into three lumped volumes. The volume near the throat (Vol_6) has a moving upstream boundary and a fixed downstream boundary and the remaining two volumes (Vol_{12} and Vol_{18}) have fixed boundaries.

To calculate the rate of change of flow rate ($\dot{W}_8$ and $\dot{W}_{14}$) at each of the two fixed boundaries the total subsonic duct is divided into two equal volumes, each volume containing a fixed boundary (Stations 8 and 14), from the previous three volumes (Figure 3). The rate of change of flow rate at these boundaries is then determined by calculating the rate of change of momentum within each volume due to the instantaneous net imbalanced force acting on it during transient conditions. For this calculation, both the volumes are frozen at their NS-at-throat value during the transient.

The equation for the rate of change of flow rate ($\dot{W}_8$) is derived in this Appendix. Exactly the same procedure applies in deriving the rate of change of flow rate ($\dot{W}_{14}$).

The momentum control volume is shown in Figure 28, in which the duct volume of interest (Vol_6 plus one-half Vol_{12}) is represented as an equivalent constant area (A_8) volume of length ℓ_1, defined by

$$\ell_1 \equiv \frac{Vol_6 + 1/2\, Vol_{12}}{A_8} \tag{1}$$

Applying the unsteady momentum equation to the constant area momentum control volume with the assumption that P_{S6} and P_{S12} act at the entrance and exit of the control volume respectively, we get,

$$\frac{d}{dt}\int_C^{\ell_1} \frac{W}{g}\, dx + \rho_{12} A_8 u_{12}^2 - \rho_6 A_8 u_6^2 = A_8 \left[P_{S6} - \left(P_{S12} + \frac{\Delta P_L}{2}\right)\right] \tag{2}$$

where the steady state duct pressure loss ($P_{T6} - P_{T12}$) is defined as $\frac{\Delta P_L}{2}$.

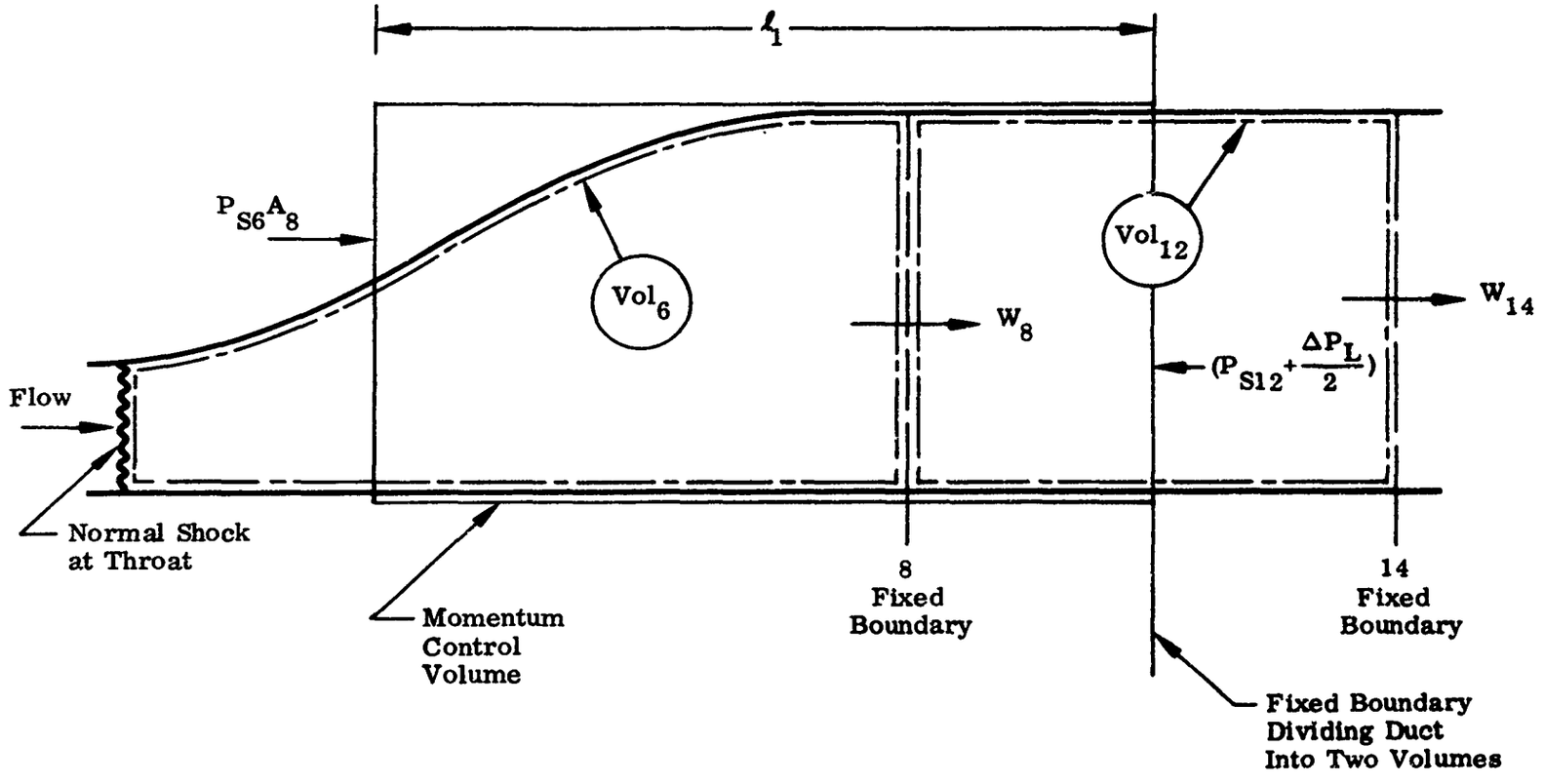

Figure 28. Momentum Control Volume Schematic

For subsonic duct flow, assuming that the velocity heads are relatively small compared to the static pressures, it is permissible to assume that the entering and exiting momentum terms are equal. Thus, Equation (2) can be written as,

$$\frac{d}{dt}\int_0^{\ell_1} \frac{W}{g}\,dx = A_8\left[P_{S6} - P_{S12} - \frac{\Delta P_L}{2}\right] \tag{3}$$

Further, again due to the relative magnitudes of the velocity heads relative to the static pressures, the dynamic pressures at the entrance and exit stations are assumed to be equal. Thus, in terms of P_{T6} and P_{T12}, Equation (3) can be written as

$$\frac{d}{dt}\int_0^{\ell_1} \frac{W}{g}\,dx = A_8\left[P_{T6} - P_{T12} - \frac{\Delta P_L}{2}\right] \tag{4}$$

In order to evaluate the integral of the LHS of Equation (4) accurately, the instantaneous axial distribution of flow rate (W) through the volume must be known. Since it is not possible to obtain this distribution using the current approach, to overcome this problem, the "lumped" volume concept is introduced. In this concept it is assumed that the lumped instantaneous weight flow corresponds to the instantaneous average weight flow of the entire momentum control volume, where the instantaneous average weight flow is

$$W_8 = \frac{g}{\ell_1}\int_0^{\ell_1} \frac{W}{g}\,dx$$

or

$$\int_0^{\ell_1} \frac{W}{g}\,dx = \frac{\ell_1 W_8}{g} \tag{5}$$

Substituting Equation (5) into Equation (4), we get

$$\frac{\ell_1}{g}\frac{dW_8}{dt} = A_8\left[P_{T6} - P_{T12} - \frac{\Delta P_L}{2}\right] \tag{6}$$

so that the equation for the rate of change of flow rate ($\dot{W}_8$) across the fixed boundary Station 8 is

$$\frac{dW_8}{dt} = \dot{W}_8 = \frac{1}{I_1}\left[P_{T6} - P_{T12} - \frac{\Delta P_L}{2}\right] \tag{7}$$

where the dynamic impedance constant, I_1, is defined as

$$I_1 \equiv \frac{l_1}{g A_8} \tag{8}$$

The equation for rate of change of flow rate ($\dot{W}_{14}$) across the fixed boundary Station 14, is also obtained using the same procedure and is given by,

$$\frac{d W_{14}}{dt} = \dot{W}_{14} = \frac{1}{I_2}\left[P_{T12} - P_{T18} - \frac{\Delta P_L}{2}\right] \tag{9}$$

where

$$I_2 = \frac{l_2}{g A_{14}} \tag{10}$$

APPENDIX III

MOECKEL'S MODEL FOR SHOCK STAND-OFF/SPILLAGE FLOW CALCULATIONS

APPENDIX III

MOECKEL'S MODEL FOR SHOCK STAND-OFF/SPILLAGE FLOW CALCULATIONS

Moeckel's continuity method (Reference 17) has been used in the dynamic models to calculate the expelled bow shock position ahead of the inlet cowl. Moeckel derives expressions for both plane and axially symmetric bodies and then applies the theory to two-dimensional and axisymmetric inlets. The theory as applied to 2D inlets is of interest here and is summarized below.

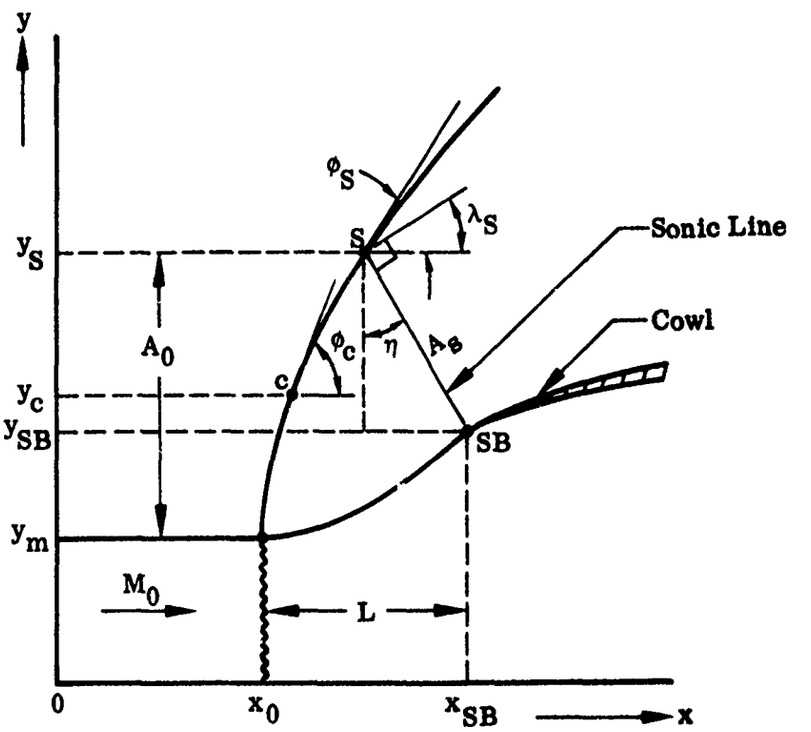

The above figure shows Moeckel's representation of the inlet bow shock. The subscripts used in the text are defined below.

- c Centroid of streamtube passing through sonic line
- m Freestream location of stagnation streamline
- S Sonic point of detached shock

APPENDIX III

MOECKEL'S MODEL FOR SHOCK STAND-OFF/SPILLAGE FLOW CALCULATIONS

Moeckel's continuity method (Reference 17) has been used in the dynamic models to calculate the expelled bow shock position ahead of the inlet cowl. Moeckel derives expressions for both plane and axially symmetric bodies and then applies the theory to two-dimensional and axisymmetric inlets. The theory as applied to 2D inlets is of interest here and is summarized below.

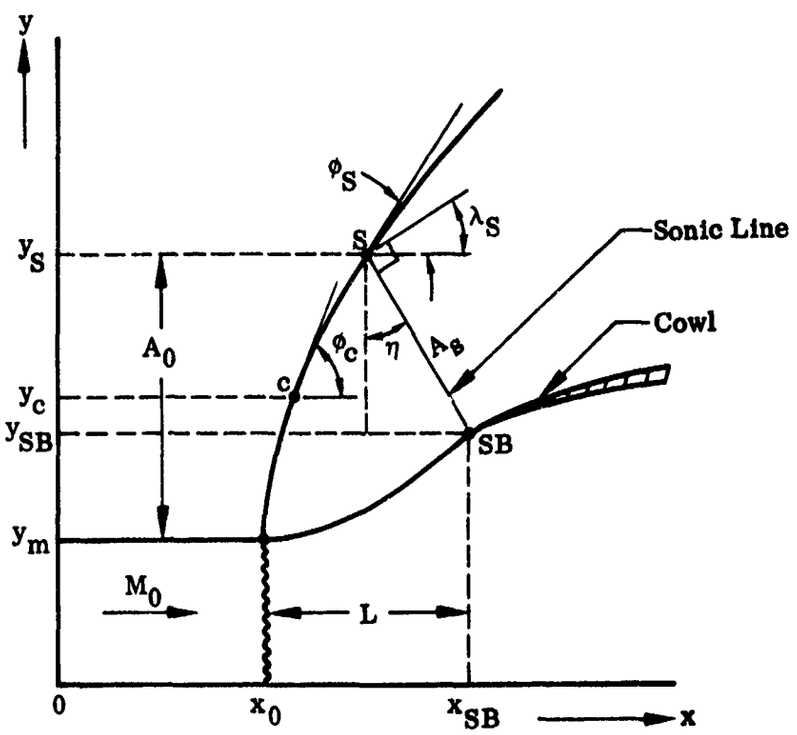

The above figure shows Moeckel's representation of the inlet bow shock. The subscripts used in the text are defined below.

- c Centroid of streamtube passing through sonic line
- m Freestream location of stagnation streamline
- S Sonic point of detached shock

SB Sonic point of body

s Conditions along sonic line

0 Freestream conditions

The coordinate y_m defines the location of the stagnation streamline that separates the mass entering the inlet (y_m) from that spilling subsonically outside the inlet ($y_{SB} - y_m$). For 2D inlets, the spillage is defined as $\tau = 1 - (y_m/y_{SB})$. Moeckel's continuity method establishes a relationship between this spillage and the NS stand-off distance (L) using the following procedure.

Assumed Form of Detached Shock Wave

This method assumes that

(a) the form of the detached shock from y_m to the sonic point S is a hyperbola. Thus, for a given M_0, the angles ϕ_S and λ_S for sonic velocity behind the shock are immediately known;

(b) the sonic curve between the detached shock and the cowl lip is a straight line and normal to the deflected streamline at S (i.e., $\eta = \lambda_S$).

For the 2D inlet, the following equation for the shock location $\left(\frac{L}{y_{SB}}\right)$ is developed from the hyperbolic equation of the shock wave in terms of $\left(\frac{y_S}{y_{SB}}\right)$, $\left(\frac{y_m}{y_{SB}}\right)$ and η.

$$\frac{L}{y_{SB}} = \frac{y_S}{y_{SB}}(C + \tan\eta) - C\frac{y_m}{y_{SB}} - \tan\eta \qquad (1)$$

where

$$C = \beta\left(\beta\tan\phi_S - \sqrt{\beta^2\tan^2\phi_S - 1}\right) \qquad (2)$$

C is known since the cotangent of the Mach angle $\beta = \sqrt{M_0^2 - 1}$ and ϕ_S are known quantities for any given freestream Mach number. β enters into the hyperbolic shock equation since typically detached shocks are asymptotic to the freestream Mach lines at large distances from their foremost point.

Application of the Continuity Equation

To determine the quantity y_S/y_{SB}, the continuity equation is applied to the fluid that passes through the sonic line by using an appropriate average value of the stagnation pressure distribution immediately behind the hyperbolic shock. This average

value $(P_s)_c$ is assumed to exist at the streamline which represents the mass centroid of the fluid passing through the sonic line. For plane flow, this streamline enters the shock at $y_c = (y_S - y_m)/2$.

The continuity equation for 2D flow between the sonic flow area (A_s) and the freestream area (A_0) of the stream tube can then be written as

$$\frac{A_s}{A_o} = \frac{\rho_o u_o}{(\rho_s u_s)_c} = \left(\frac{P_o}{P_s}\right)_c \left[\frac{\rho_o u_o}{(\rho u)^*}\right] \equiv B \tag{3}$$

where B is a function of the freestream Mach number only.

Independently, from inlet and shock geometry, A_s/A_0 may be written as

$$\frac{A_s}{A_o} = \frac{Y_S - Y_{SB}}{(Y_S - Y_m)\cos\eta} \tag{4}$$

Now for plane flow, η is assumed equal to λ_S so that,

$$\frac{A_s}{A_o} = \frac{Y_S - Y_{SB}}{(Y_S - Y_{SB})\cos\lambda_S} = B \tag{5}$$

or

$$\frac{Y_S}{Y_{SB}} = \frac{1 - \frac{Y_m}{Y_{SB}} B\cos\lambda_S}{1 - B\cos\lambda_S} \tag{6}$$

Substituting this value into Equation (1) gives the final equation in terms of the subsonic spillage.

$$\frac{L}{Y_{SB}} = \left(1 - \frac{Y_m}{Y_{SB}}\right)\left(\frac{C + B\sin\lambda_S}{1 - B\cos\lambda_S}\right) \tag{7}$$

Equation (7) can be written as

$$\frac{L}{Y_{SB}} = K_{SP}\left(1 - \frac{Y_m}{Y_{SB}}\right) \tag{8}$$

where

$$K_{SP} = \frac{C + B\sin\lambda_S}{1 - B\cos\lambda_S} = f(M_o) \tag{9}$$

In applying Equation (8) to the 2DE and 2DM inlets described in detail in Volume I of this report, it can be written as

$$\frac{L}{h_t} = K_{SP} \frac{W_{SP}}{W_o} \tag{10}$$

with the freestream Mach number as used in Moeckel now becoming the relevant local Mach number upstream of the detached shock.

Values of K_{SP} as a function of local Mach number (M_L) are used as program input for calculating either the shock stand-off distance or the subsonic spillage.

UNCLASSIFIED

Security Classification

DOCUMENT CONTROL DATA - R & D

(Security classification of title, body of abstract and indexing annotation must be entered when the overall report is classified)

1 ORIGINATING ACTIVITY (Corporate author)

NORTHROP CORPORATION, Aircraft Division
3901 West Broadway
Hawthorne, California 90250

2a. REPORT SECURITY CLASSIFICATION

Unclassified

2b. GROUP

3 REPORT TITLE

Supersonic Inlet Investigation,
Volume II, Air Induction System Dynamic Simulation Model

4 DESCRIPTIVE NOTES (Type of report and inclusive dates)

R&D Final Report - 1 May 1969 to 1 May 1971

5 AUTHOR(S) (First name, middle initial, last name)

Nasim F. Amin
Gordon R. Hall

6. REPORT DATE	7a. TOTAL NO. OF PAGES	7b. NO OF REFS
September 1971	174	17

8a. CONTRACT OR GRANT NO	9a. ORIGINATOR'S REPORT NUMBER(S)
F33615-69-C-1699 b. PROJECT NO 1476 c. Task No. 147602 d.	NOR 71-120 Volume II 9b. OTHER REPORT NO(S) (Any other numbers that may be assigned this report) AFFDL-TR-71-121, Volume II

10 DISTRIBUTION STATEMENT

Distribution limited to U.S. Government agencies only; this report contains information on test and evaluation of military hardware; September 1971; other requests for this document must be referred to Air Force Flight Dynamics Laboratory (FXM), Wright-Patterson AFB, Ohio 45433.

11 SUPPLEMENTARY NOTES	12. SPONSORING MILITARY ACTIVITY
	Air Force Flight Dynamics Laboratory AFFDL/FXM Wright-Patterson AFB, Ohio 45433

13 ABSTRACT

A one-dimensional mathematical dynamic simulation model for predicting the transient behavior of air induction systems for advanced tactical aircraft operating in the supersonic portion of the flight spectrum is discussed. As a part of the simulation model, control system logic is included to provide control system design criteria necessary to maintain air induction system response to selected input disturbances within prescribed limits. The model is applicable to both external and mixed compression inlets operating at supersonic conditions. The "lumped parameter" concept is used in simulating the dynamic response of the subsonic duct downstream of the terminal shock, with the duct divided into three lumps. CDC 6600 digital computer programs have been generated for each of three submodels (i.e., Standard, Buzz, and Hammershock models). Numerous sample simulation runs are presented and discussed in detail. Limited comparison of simulation results to available test data show good agreement.

DD FORM 1 NOV 68 1473

UNCLASSIFIED

Security Classification

14 KEY WORDS	LINK A		LINK B		LINK C	
	ROLE	WT	ROLE	WT	ROLE	WT
Air Induction System Dynamic Simulation/ Air Induction System Transient Phenomena						